

**PRESSURE-REGULATED MEMBRANE TRAFFIC AND ION  
TRANSPORT IN URINARY BLADDER EPITHELIUM**

by

Edward Chi Yu Wang

BS in Microbiology, University of Washington, 1997

Submitted to the Graduate Faculty of  
School of Medicine in partial fulfillment  
of the requirements for the degree of

Doctor of Philosophy

University of Pittsburgh

2004

UNIVERSITY OF PITTSBURGH

SCHOOL OF MEDICINE

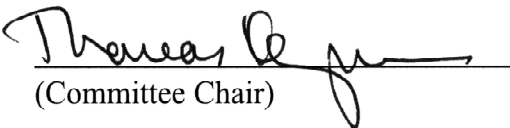
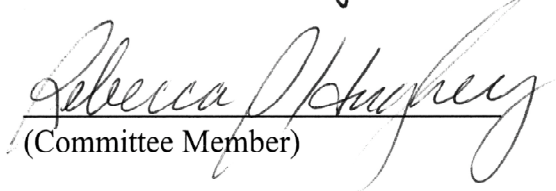
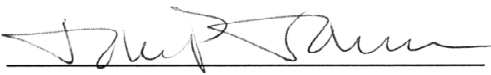
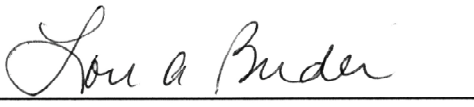
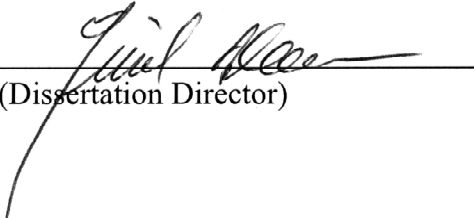
This dissertation was presented

by

Edward Chi Yu Wang

It was defended on January 30<sup>th</sup>, 2004

and approved by

Signature	Printed Name	Date Signed
 (Committee Chair)	<u>Dr. Thomas Kleyman, M.D.</u>	<u>2/5/04</u>
 (Committee Member)	<u>Dr. Rebecca Hughey, Ph.D.</u>	<u>2/5/04</u>
 (Committee Member)	<u>Dr. John Johnson, M.D.</u>	<u>2/5/04</u>
 (Committee Member)	<u>Dr. Lori Birder, Ph.D.</u>	<u>2/5/04</u>
 (Dissertation Director)	<u>Dr. Gerard Apodaca, Ph.D.</u>	<u>2-5-04</u>



**PRESSURE-REGULATED MEMBRANE TRAFFIC AND ION  
TRANSPORT IN URINARY BLADDER EPITHELIUM**

Edward Chi Yu Wang, Ph.D.

University of Pittsburgh, 2004

Mechanical forces affect many cellular functions. How cells respond to mechanical stimuli and how the stimuli are transduced into cellular signals are important questions in cell biology. To this end, the effects of hydrostatic pressure (filling) on bladder uroepithelium were examined by exposing isolated pieces of uroepithelium to hydrostatic pressure in modified Ussing chambers, thus mimicking the filling process of rabbit urinary bladders. Filling had profound effects on both ion and membrane transport in the uroepithelium. Membrane distention activated mechanosensitive ion channels, stimulating  $\text{Na}^+$  absorption across the umbrella cells via epithelial  $\text{Na}^+$  channels,  $\text{K}^+$  secretion via nonselective cation channels, and  $\text{Cl}^-$  secretion via  $\text{Cl}^-$  channels. In addition to elevated ion transport, pressure also stimulated discoidal vesicle exocytosis in umbrella cells, resulting in ~55% increase in apical surface area of the umbrella cells. Exocytosis in these cells also increased the amount of uroplakin III at the apical surface by 67%, and caused release of secretory proteins into the bladder lumen. One pressure-sensing mechanism that could regulate umbrella cell exocytosis is ATP and purinergic receptor signaling. Significant amounts of ATP were released from the uroepithelium during filling. However, when the serosal surface of the uroepithelium was treated with the ATPase apyrase or hexokinase, or incubated with the purinergic receptor antagonist PPADS, pressure-activated exocytosis was blocked. More importantly, filling-induced exocytosis was blocked when  $\text{P2X}_2$  or  $\text{P2X}_3$  receptors were absent from mice bladders. The exocytic events were mediated by  $\text{Ca}^{2+}$ , cAMP, and PKA-dependent mechanisms. In addition to exocytosis, hydrostatic pressure induced endocytosis of 100% of a biotinylated membrane pool within 5 minutes of stimulation. The

endocytosed membrane was delivered to lysosome and degraded by a leupeptin-sensitive pathway. The endocytic event could be activated by the purinergic receptor agonist ATP $\beta$ S, indicating that filling-induced endocytosis may depend on purinergic receptor signaling as well. These results have shed light on how hydrostatic pressure regulates ion and membrane transport in uroepithelial cells and may provide insights to how other mechanosensitive cell types respond to external forces.

# TABLE OF CONTENTS

<b>INTRODUCTION</b> .....	1
<b>I. OVERVIEW OF THE URINARY BLADDER</b> .....	2
A. Anatomy.....	3
B. Bladder innervation.....	4
C. Urine storage and elimination.....	5
<b>II. URINARY BLADDER EPITHELIUM</b> .....	5
A. What are epithelial tissues?.....	6
1. Development and maintenance of the permeability barrier.....	6
2. Regulation of epithelial cell permeability.....	7
a. Paracellular permeability.....	7
b. Transcellular permeability.....	8
B. Uroepithelium.....	8
1. Umbrella cells.....	10
2. Uroplakins.....	11
3. Barrier function of the uroepithelium.....	12
4. Factors that regulate uroepithelial permeability.....	13
a. Tight junctions.....	13
b. Ion channels.....	14
C. Accommodative changes of the bladder uroepithelium.....	15
D. Hydrostatic pressure-induced exocytosis in bladder.....	15
<b>III. MECHANOTRANSDUCTION AND REGULATION OF MEMBRANE TRAFFIC</b>	
A. Cytoskeleton.....	17
B. Mechnosensitive ion channels.....	18
C. Integrin receptors.....	19
D. Tyrosine kinases.....	20
E. Adenosine triphosphate.....	21

F. Purinoceptors.....	22
1. Purinergic receptors.....	22
2. Adenosine receptors.....	23
G. Secondary messenger cascades.....	24
<b>IV. GOALS OF THE DISSERTATION.....</b>	<b>26</b>
<b><i>CHAPTER 1 - Analysis of hydrostatic pressure-induced changes in umbrella cell surface area.....</i></b>	<b><i>27</i></b>
<b>ABSTRACT.....</b>	<b>27</b>
<b>INTRODUCTION.....</b>	<b>28</b>
<b>RESULTS.....</b>	<b>31</b>
<b>DISCUSSION.....</b>	<b>36</b>
<b><i>CHAPTER 2 - Hydrostatic pressure-regulated exocytosis/endocytosis in bladder umbrella cells.....</i></b>	<b><i>38</i></b>
<b>ABSTRACT.....</b>	<b>38</b>
<b>INTRODUCTION.....</b>	<b>40</b>
<b>RESULTS.....</b>	<b>43</b>
<b>DISCUSSION.....</b>	<b>64</b>
<b><i>CHAPTER 3 - Hydrostatic pressure-regulated ion transport in bladder uroepithelium.....</i></b>	<b><i>71</i></b>
<b>ABSTRACT.....</b>	<b>71</b>
<b>INTRODUCTION.....</b>	<b>72</b>
<b>RESULTS.....</b>	<b>75</b>
<b>DISCUSSION.....</b>	<b>92</b>
<b><i>CHAPTER 4 - ATP and P2X receptor-dependent membrane traffic in bladder umbrella cells.....</i></b>	<b><i>98</i></b>
<b>ABSTRACT.....</b>	<b>98</b>
<b>INTRODUCTION.....</b>	<b>100</b>
<b>RESULTS.....</b>	<b>103</b>
<b>DISCUSSION.....</b>	<b>126</b>
<b><i>SUMMARY AND CONCLUSIONS.....</i></b>	<b><i>138</i></b>
<b><i>APPENDICES.....</i></b>	<b><i>153</i></b>
<b>APPENDIX A – Materials and Methods.....</b>	<b>154</b>
<b>APPENDIX B – Abbreviations.....</b>	<b>180</b>

***BIBLIOGRAPHY***.....183

## LIST OF FIGURES

<b>Figure I-1</b>	Cross-section of the bladder.....	2
<b>Figure I-2</b>	Detrusor of the bladder wall.....	3
<b>Figure I-3</b>	Bladder innervation.....	4
<b>Figure 1-1</b>	Pressure chamber.....	31
<b>Figure 1-2</b>	Effect of pressure on changes in capacitance.....	32
<b>Figure 1-3</b>	Ultrastructural analysis of control tissue or tissue exposed to hydrostatic pressure.....	34
<b>Figure 2-1</b>	Capacitance changes in response to hydrostatic pressure.....	43
<b>Figure 2-2</b>	Morphological analysis of control and pressure-stimulated umbrella cells.....	45
<b>Figure 2-3</b>	Stereological analysis of umbrella cells and determination of vesicle/membrane continuity.....	48
<b>Figure 2-4</b>	Uroplakin III localization and pressure-induced increases in cell surface uroplakin III expression and metabolically labeled protein secretion.....	51
<b>Figure 2-5</b>	Effect of pressure on endocytosis.....	55
<b>Figure 2-6</b>	Role of cAMP and PKA in the filling response.....	60
<b>Figure 2-7</b>	Effects of altering cytoplasmic Ca <sup>2+</sup> on changes in membrane capacitance.....	62
<b>Figure 3-1</b>	Hydrostatic pressure-induced changes in short-circuit current, conductance, and membrane capacitance.....	76
<b>Figure 3-2</b>	Characterization of uroepithelial Na <sup>+</sup> transport in the presence of amiloride and in Na <sup>+</sup> -free Krebs solution.....	78
<b>Figure 3-3</b>	Characterization of <sup>22</sup> Na <sup>+</sup> flux and Na <sup>+</sup> transport in the presence of ouabain.....	80
<b>Figure 3-4</b>	Effects of Na <sup>+</sup> , Cl <sup>-</sup> -free Krebs solution, Ba <sup>2+</sup> , and ouabain on hydrostatic pressure-activated ion secretion.....	82

<b>Figure 3-5</b>	Effects of charybdotoxin, $Gd^{3+}$ and, amiloride on hydrostatic pressure-activated $K^+$ secretion.....	86
<b>Figure 3-6</b>	Hydrostatic pressure-induced transport of $Cs^+$ in nystatin-permeabilized uroepithelium.....	89
<b>Figure 3-7</b>	Model for hydrostatic pressure-induced ion transport in bladder umbrella cells.....	93
<b>Figure 4-1</b>	Pressure-activated ATP release from the mucosal membrane is via vesicular and connexin hemichannel-dependent pathways.....	105
<b>Figure 4-2</b>	Pressure-activated ATP release from the serosal membrane is via vesicular and connexin hemichannel-dependent pathways.....	106
<b>Figure 4-3</b>	ATP release from vesicular compartments is not the result of pressure-induced cell damage.....	107
<b>Figure 4-4</b>	ATP stimulates umbrella cell exocytosis.....	109
<b>Figure 4-5</b>	Mucosal ATPases have no effect on pressure-induced exocytosis.....	111
<b>Figure 4-6</b>	P2X receptors can modulate pressure-induced exocytosis.....	112
<b>Figure 4-7</b>	P2X <sub>2</sub> and P2X <sub>3</sub> receptors modulate pressure-induced membrane traffic.....	116
<b>Figure 4-8</b>	Characterization of the P2X <sub>2</sub> and P2X <sub>3</sub> antisera by Western blotting.....	117
<b>Figure 4-9</b>	Localization of P2X <sub>2</sub> receptor in the uroepithelium.....	118
<b>Figure 4-10</b>	Localization of P2X <sub>3</sub> receptor in the uroepithelium.....	119
<b>Figure 4-11</b>	Localization of P2X <sub>3</sub> receptor in the rabbit uroepithelium.....	120
<b>Figure 4-12</b>	ATP[ $\beta$ S stimulates endocytosis in bladder umbrella cells.....	122
<b>Figure 4-13</b>	Role of $Ca^{2+}$ on purinergic receptor-mediated exocytosis in umbrella cells.....	124
<b>Figure 4-14</b>	Effect of H89 on purinergic receptor-mediated exocytosis in umbrella cells...	125
<b>Figure 4-15</b>	Model for ATP and purinergic receptor-regulated exocytosis / endocytosis in bladder umbrella cells.....	127
<b>Figure A-1</b>	Mounting of tissue in pressure chamber.....	157
<b>Figure A-2</b>	Equivalent circuit of bladder epithelium.....	162
<b>Figure A-3</b>	Voltage response of rabbit bladder epithelium to square current pulse.....	165

## LIST OF TABLES

<b>Table 3-1</b>	Effects of channel inhibitors on $K^+$ conductance.....	83
<b>Table 3-2</b>	Effects of hydrostatic pressure on $^{86}Rb^+$ flux.....	83
<b>Table 3-3</b>	Effects of hydrostatic pressure on $^{36}Cl^-$ flux.....	91
<b>Table 4-1</b>	Effects of purinergic receptor agonists and antagonists on membrane capacitance.....	114
<b>Table 4-2</b>	P2X receptor pharmacology.....	115



# INTRODUCTION

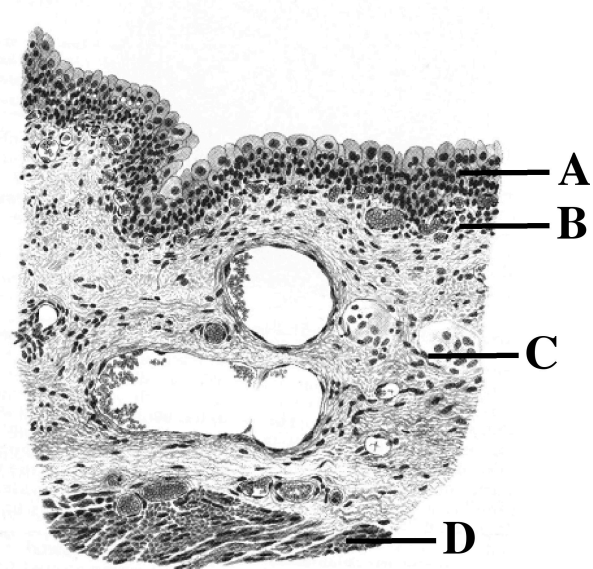
All cells are exposed to mechanical and chemical stimuli. Examples of mechanical stimuli include hydrostatic pressure, shear stress, twisting, compression, and vibration, while examples of chemical stimuli include hormones, the action of ecto-enzymes, and chemical messengers such as adenosine triphosphate (ATP). A fundamental question in cell biology is how cells respond to these external influences and how they are then translated into biochemical signals that lead to adaptation. One organ system that serves as a good model for understanding how cells react to mechanical and chemical forces is the urinary bladder, which experiences variations in hydrostatic pressure as the result of fluctuations in urine volume. Furthermore, the release of chemical agonists and antagonists from bladder tissues such as nerves, muscle, or the epithelium can affect the cell biology of uroepithelial cells via modulation of ion channels and membrane receptors. The following will be an overview on the biology of the mammalian urinary bladder and an examination of the effects of external cues (mechanical and chemical) on the adaptive response of the bladder and other mechanosensitive cell types.

## I. Overview of the urinary bladder

Historically, the urinary bladder has been compared to a plastic sac that functions as an isolated short-term storage site for urine. By performing the storage function, the sanitary condition of an animal's living area is improved, and controlled micturation serves as a mechanism of territorial identification for some animals (96, 128). However several studies, both past and present, indicate that the bladder can also alter the ion and protein composition of the kidney-generated urine.

Structurally, the mammalian bladder is a hollow, tetrahedron-shaped muscular sphere, with the wall of the sphere comprising of several layers (from the outside to the inside): the muscularis, submucosa, lamina propria, and the epithelium (Figure I-1) (23, 128, 177).

Intermeshed within the above structures is a circulatory, sensory, motor-sensory, and immune system. On top of the lamina propria lies a layer of epithelial cells, also known as the uroepithelium or the urothelium, and covers the entire inner surface of the sphere (128). The luminal surface of the uroepithelium is covered by mucin glycoproteins and glycosaminoglycans (GAG) (128, 250). Under normal conditions, the uroepithelium serves as a dynamic barrier that responds to changes in urine volume by altering the membrane biology of the epithelial cells



Bloom and Fawcett, 1994

Figure I-1. Cross-section of the bladder. (A) Epithelium. (B) Lamina propria. (C) Submucosa. (D) Muscularis.

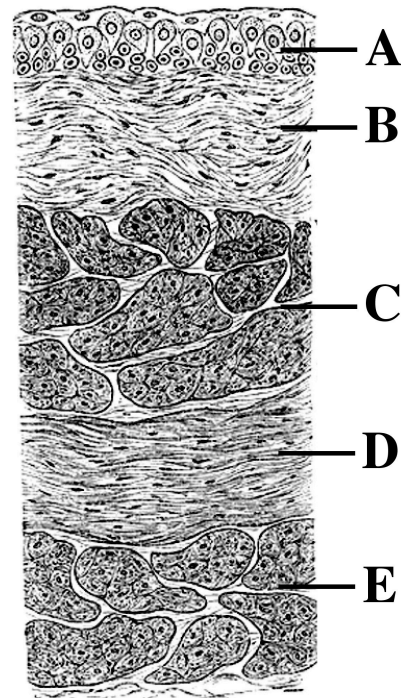
(212). Damage to the uroepithelium results in loss of barrier function, leading to inflammation, pain, and urgency to void (123, 124).

## A. Anatomy

The human urinary bladder is generally described as having two functional units: (1) a reservoir (body) that stores the urine, and (2) an outlet (neck) that gates the flow of urine (47). The reservoir of the bladder can be further divided into three sections: the trigone, the equatorial region, and the dome. The trigone forms the base of the bladder body that lies immediately above the bladder outlet and is where the urine enters via the ureters from the kidney. The equatorial region is the central and the largest portion of the bladder body, and the dome is located at the rear of the bladder toward the curved region opposite the outlet region.

The bladder wall consists of three smooth muscular layers: the outer longitudinal, middle circular, and the inner longitudinal (Figure I-2) (80, 177). The smooth muscle

layers are known as the detrusor. The detrusor muscles are oriented in three directions and thicken toward the neck of the bladder. Surrounding the neck of the bladder, the detrusor muscle is also known as the bundle of Heiss (177). Functionally, the detrusor muscle is responsible for increasing bladder pressure to initiate voiding. A band of smooth muscle known as the internal sphincter is thought to surround the neck of the bladder. The internal sphincter is widely



Gray, 2000

Figure I-2. Detrusor of the bladder wall. (A) Uroepithelium. (B) Submucosa. (C) Inner layer of longitudinal muscle layer. (D) Middle circular muscle fiber. (E) Outer layer of longitudinal muscle fibers.

accepted as an anatomical structure that regulates passage of urine through the neck region. However, a ring of musculature does not exist around the outlet of the bladder (177). Instead, the interureteric ridge, which forms the base of the trigone, acts as a final barrier to urine release (177). The interureteric ridge is a blend of smooth muscle between the neck region and the beginning of the urethra (177). During voiding, the muscles of the outlet relax and the bladder smooth muscles contract, raising intravesical pressure and inducing urine flow.

## B. Bladder innervation

The changes in the smooth muscular tone of the bladder are coordinated by two sets of nerves (parasympathetic and sympathetic) emerging from the sacral and thoracolumbar levels of the spinal cord (Figure I-3) (47, 177, 231). The sacral parasympathetic nerves innervate the detrusor muscle and stimulate bladder wall muscle contraction to initiate voiding by providing excitatory cholinergic and purinergic signals to the bladder (47). The thoracolumbar sympathetic nerves

release inhibitory signals to the bladder neck and urethra to facilitate urine storage. In addition to control of

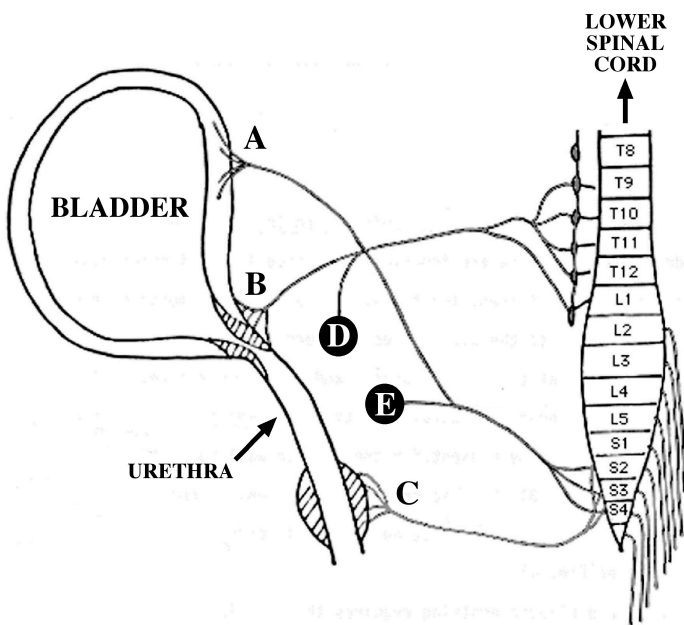


*Figure I-3. Bladder innervation. (A) Sacral parasympathetic neurons from the sacral cord (S2-4) innervate the detrusor muscle of the bladder and the vascular supply to the pelvic genital organs. (B) Thoracolumbar sympathetic neurons (T9-L1) innervate the bladder neck, vas deferens, seminal vesicles, and prostate. (C) Somatic neurons innervate the external urethral sphincter and the external anal sphincter. (D) vas deferens, seminal vesicles, and prostate. (E) Vascular supply to pelvis genital organs.*

Williamson-Kirkland, 1980

muscular tone by the autonomic nervous system, afferent nerves that innervate the bladder may respond to change in urine composition and differences in chemical composition due to release of nitric oxide (NO), ATP, and prostaglandins from the uroepithelial cells (47). The afferent nerves are located in the serosal and muscle layers and in between adjacent uroepithelial cells (5, 73). Changes in urine volume, which could result in alteration in chemical composition (e.g. release of NO, ATP, and prostaglandin) surrounding the afferent nerves could lead to changes in biology of the uroepithelium.

### **C. Urine storage and elimination**

The most important feature of the bladder is its ability to store and eliminate a variable volume of urine. This is partly dependent on the cross talk between the musculature of the bladder and the underlying nervous innervations. During the urine-filling phase, afferent nerve activities are increased, contributing to lowered tension of the smooth muscles surrounding the reservoir of the bladder. However, as intravesical (lumen) pressure increases steadily and rises above a threshold level, the micturition (voiding) reflex is initiated. The voiding mechanism involves activation of the parasympathetic input to the bladder reservoir and inhibition of the sympathetic inputs to the urethra leading to contraction of smooth muscle and expulsion of urine.

## **II. Urinary bladder epithelium**

The main function of the bladder epithelium is to provide a barrier against the toxic substances generated by the kidney even in the face of cyclical fluctuations in urine volume. This ability to isolate the urine from the underlining serosa is dependent on the uroepithelium, which is

composed of a sheet of highly specialized superficial cells. It is the special properties of these epithelial cells that allow the bladder to perform its main barrier function. The following sections will give a simple overview of the general characteristics of epithelial tissues and then an overview of the bladder epithelium.

## **A. What are epithelial tissues?**

Epithelial tissues are comprised of cells that cover the exterior surfaces of body and line both the internal closed cavities of the body and those body tubes that communicate with the exterior environment (180). Epithelial cells are found in many organ systems, including the gut, blood vessels, and the urogenital tract. In these different organ systems, epithelial tissues may serve different purposes including formation of an almost impervious barrier, as in the epidermis or urinary bladder. Epithelial cells may have secretory and absorptive functions, as in the intestines, or they may provide a transport system through cell-surface cilia that move particulates and mucus, as in the trachea and bronchi of the lung. Depending on the morphology and the surface specialization of the epithelial tissues, different epithelia are able to fulfill the functional demands that are placed upon them.

### **1. Development and maintenance of the epithelium**

Epithelial cells form barriers that separate biological compartments and regulate homeostasis by controlling ion and solute transport between these compartments (241). By forming a barrier, the membrane of the epithelial cell is exposed to different environments. The plasma membrane facing the lumen or the exterior of the organ is called the apical or the mucosal domain, and the membrane facing the underlying connective tissue is called the basolateral or the serosal domain.

Each domain is comprised of a distinct set of proteins, which regulate ion and solute transport across the epithelium. Differences in the distributions of membrane proteins between apical and basolateral plasma membrane domains are maintained by protein sorting from intracellular compartments and selective retention in the membrane. Protein delivery to either the apical or the basolateral membrane domain is determined by various factors including sorting signals found within the amino acid sequence of the protein or the result of post-translational modifications such as *N*-linked or *O*-linked glycosylation or acylation (165).

To maintain the polarized distribution of the lipid and proteins that are unique to either domain of the epithelial cell, tight junctions, a belt-like structure encircles the apex of the cell to form the apical junction complex (156). The tight junctions also serve as the contact point between adjacent epithelial cells. The presence of these specialized intercellular proteins provides an immovable fence to prevent mixing of apical and basolateral lipid and membrane proteins that are unique to their respective membrane domains.

## **2. Regulation of epithelial cell permeability**

### **a. Paracellular permeability**

In addition to maintenance of polarized lipid and protein distribution in epithelial cells, tight junctions regulate epithelial cell permeability by formation of pores between cells. Tight junctions are composed of a dense network of cytoplasmic proteins, cytoskeletal elements, and several transmembrane proteins. The cytoplasmic proteins include ZO-1, which links the tight junction associated transmembrane proteins to the actin cytoskeleton (152). Transmembrane proteins include junctional-associated membrane protein 1 (151), IG8 antigen (163), and occludin and claudins (71, 72). Depending on the epithelia (leaky or tight), differences in pore

sizes determined by the tight junction proteins can regulate solute movement across the tight junction (156).

### **b. Transcellular permeability**

The second determinant of cell permeability is the ability of epithelial cells to regulate movement of substances across cells, also known as the transcellular pathway. Movement of substances across the cell membrane can be mediated by several mechanisms. For example, transport of ions can be via primary (energy dependent) or secondary (energy independent) ion channels localized to the apical and basolateral membrane domains. Varying the number of ion channels and transporters on the plasma membrane can regulate the movement of small substances, such as ions and amino acids. Other substances, such as proteins (e.g. immunoglobulin A) can be transported across cells via membrane-bound vesicles. These vesicles are formed when areas of the plasma membrane undergo invagination and pinch off. Once the vesicles are formed, the internalized protein can be recycled back to the membrane of origin, the vesicle content can be delivered to the lysosome for degradation, or the internalized protein can be delivered to the opposing membrane by a process known as transcytosis. Altering the rate of transcytosis can modulate transcellular passage of large proteins. This may depend on external cues and regulatory molecules.

## **B. Uroepithelium**

The uroepithelium is a highly specialized epithelial tissue. No other epithelium has yet been identified which can satisfactorily substitute for the bladder epithelium as a barrier between tissue fluids and urine. By acting as a tight barrier, the uroepithelium isolates the hypertonic



urine, which in some animals may be 2 to 4 times the tonicity of blood plasma (96). In addition, urea and creatinine concentrations in urine may be 100 times the concentration of blood plasma, and sulphate and phosphate ions 60 and 30 times more, respectively (96). Therefore, not only does the barrier function of the uroepithelium prevent equilibration of electrolytes, which can lead to dehydration, the uroepithelium prevents dissipation of the chemical gradient generated by the kidney (96).

The uroepithelium is of endodermal origin. It is composed of multiple cell layers, with three morphologically distinct cell types. Sitting above the connective tissue attached to a thin layer of basal lamina are the basal cells. The basal cells are cuboidal or columnar, with a diameter of 5-10  $\mu\text{m}$ . When examined by light microscopy, the basal cell cytoplasm is highly basophilic, and when viewed by electron microscopy appears electron dense. Previous studies indicate that basal cells are germinal in nature. They elongate above the basal layer to give rise to intermediate cells (96).

Intermediate cells are derived from basal cells (96). They are approximately 20  $\mu\text{m}$  in diameter, and their cytoplasm appears less basophilic (96, 128). One distinguishing feature of the intermediate cell nearest the umbrella cells is the presence of a population of large (>200 nm) cytoplasmic vesicles (212). Currently, the functions of these cytoplasmic vesicles are unknown. However, the vesicles do not appear to play a role in modulation of membrane surface area in intermediate cells (212). In contrast, similar cytoplasmic vesicles are also found in the superficial umbrella cells that form the mucosal surface of the uroepithelium (96, 128, 213). Numerous studies have been performed that describe the morphology and function of the umbrella cells (96, 120, 128, 134, 135, 201, 212, 225). The following sections will summarize those findings.

## **1. Umbrella cells**

These large, hexagonal cells cover the urinary surface of the uroepithelium (96). When examined by transmission electron microscopy (TEM), the shape of these superficial cells loosely resembles an umbrella, thus the name umbrella cells. Depending on the degree of bladder fullness, umbrella cells can range from ~50  $\mu\text{m}$  in diameter in empty bladders to greater than 120  $\mu\text{m}$  in distended bladders (128). The umbrella cells are attached to one another by tight junctions, adherens junctions, and desmosomes. One hallmark of umbrella cells is the morphology of the apical surface (the surface that interfaces with urine). The entire apical surface is covered with scalloped areas of membrane called plaques that compose from 70-90% of the surface, with the remaining 10-30% of the membrane occupied by “hinge” regions (175). When the apical membrane is examined by electron microscopy the outer leaflet appears twice as thick as the inner leaflet, thus the term asymmetric unit membrane (AUM) (94, 120, 128, 234). Together, the AUM and the tight junction complexes provide an impenetrable barrier against the toxic materials found in the urine.

Another feature of the superficial umbrella cell is the presence of a large population of cytoplasmic vesicles. Depending on the animal species, the morphology of the vesicles can appear fusiform (in mouse bladder) or discoidal (in rabbit bladder) (94, 175). The vesicles are localized near the vicinity of the apical plasma membrane and express unique transmembrane proteins called uroplakins (to be discussed below). Because the protein composition of the vesicles is similar to the apical plasma membrane, these cytoplasmic vesicles may play an important role in the bladder accommodative response without compromising the barrier function of the bladder. This is thought to occur by trafficking of the vesicles to and from the

apical plasma membrane (95, 175). In addition, the vesicles may serve as specialized carriers for delivery and retrieval of membrane proteins as well as release of secretory proteins (48).

## **2. Uroplakins**

As described above, the apical plasma membrane of umbrella cells is covered with scalloped-shaped plaques that are separated by membrane domains called hinges (128). The plaques are composed of a paracrystalline array of subunits with center-to-center spacing of approximately 16 nm (128). Each subunit is composed of an inner and outer ring each having six protein particles, and together the particles form a twisted ribbon structure that protrudes from the lipid bilayer (223). The protein particles that make up the plaque subunits have been isolated and cloned (243). These proteins (uroplakins; UP) are transmembrane proteins, and there are at least five known members (UPIa, UPIb, UPII, UPIIIa, and UPIIIb). UPIa (27 kDa) and UPIb (28 kDa) have four transmembrane domains (128). UPII (15 kDa), UPIIIa (~47 kDa), and UPIIIb (~47 kDa) are type one transmembrane proteins (intracellular carboxy terminus) (128). Interestingly, UPIa associates with UPII and UPIb associates with UPIIIa or UPIIIb making up the inner and the outer ring of the plaque subunit (49, 237).

All five members of the UP family contain large extracellular domains, which contribute to the AUM morphology. The cytoplasmic domains of UPIa, UPIb, and UPII are minimal with the exception of UPIIIa and UPIIIb, that have a substantial hydrophilic tail of approximately 50 amino acids (49, 236). This has led to speculations that UPIIIa and UPIIIb may provide anchors for the plaque particles and may associate with the underlying cytoskeleton to facilitate changes in apical membrane structure.

In addition to the apical plasma membrane, UP are also present in the membrane of the cytoplasmic vesicles. The specific composition of the UP in the vesicles is not well characterized as that of the apical plasma membrane (212). However, similarities in the morphology of the vesicle membrane with that of the apical plasma membrane indicate that the vesicles may traffic to and from the membrane thus play an important role in modulating the membrane dynamics of the umbrella cells.

The areas of apical plasma membrane between adjacent plaques are the hinge regions (128). The protein and lipid composition of the hinge regions are not fully understood. However, a highly glycosylated (85 kDa) glycoprotein called urohingen is found in the hinge area (244). The function of the urohingen and the hinge regions is currently unknown, although the regions in between adjacent plaques must offer barrier protection against urine as well. Another speculation is that hinge regions may be the location of cytoplasmic vesicle insertion, but no direct evidence is available to support this speculation. Regardless, the hinge regions are likely to contain all other membrane proteins that are excluded from the plaque regions. Some of these proteins may include membrane receptors such as purinoceptors (P1 and P2), ion channels such as the epithelial sodium channel (ENaC), and the mucin-like glycoprotein MUC1, which have been localized to the apical surface of the umbrella cells (29, 97, 197).

### **3. Barrier function of the uroepithelium**

One of the major functions of the uroepithelium is to prevent the urine from invading the underlying connective tissues and musculature of the urinary bladder. This barrier function is reflected by the low permeability of paracellular and transcellular pathways in the uroepithelium. One method of assessing the paracellular and transcellular permeability is by measuring the

transepithelial resistance (TER), which is the ability of the epithelium to impede ion flow between epithelial cells and transport of ions across epithelial cells via channels or pumps. TER measurements can be made using Ussing chambers, where an isolated piece of uroepithelium is mounted between the chamber apparatus and modeled to an equivalent electrical circuit made up of capacitors and resistors (see Materials and Methods section for more detail). Using this method, the TER across isolated pieces of rabbit uroepithelium has been shown to reach as high as 75,000 – 135,000  $\Omega$ \*cm<sup>2</sup>, consistent with the relatively low levels of transcellular ion transport and paracellular ion flow (1). Although TER measures ion flow across all of the epithelial cell layers, in the uroepithelium the majority of resistance is provided by the apical membrane of the umbrella cell (37, 134, 138).

#### **4. Factors that regulate uroepithelial permeability**

##### **a. Tight junction**

In addition to plaques on the uroepithelial surface, tight junctions surrounding the umbrella cells are likely to play a major role in determination of paracellular permeability (77). In mice and rat bladders, occludin and claudin-4, -8, and -12 are reported in the umbrella cell tight junctions where claudins form continuous branching fibrils of transmembrane particles that completely encircle the apical aspect of the lateral surface of umbrella cells (1). This indicates that occludin and claudins may contribute to the high resistance phenotype of the umbrella cells by formation of size selective ion filter (215).

## **b. Ion channels**

The presence of ion channels on the apical and basolateral membrane of the umbrella cell is a major determinant of uroepithelial permeability. In contrast to tight junctions that can regulate paracellular movement of ions across the uroepithelium, ion channels on the apical and basolateral membranes of the umbrella cells regulate transcellular movement of ions. In rabbit uroepithelium, aldosterone increases the rate of sodium absorption (230). Sodium enters the umbrella cells via epithelial sodium channels localized on the apical plasma membrane and exits the umbrella cells via the basolateral membrane  $\text{Na}^+/\text{K}^+$  ATPase (137, 138). As sodium exits the cell via the  $\text{Na}^+/\text{K}^+$  ATPase, potassium is pumped into the cell generating a high intracellular potassium gradient (129). Potassium can exit the basolateral membrane of the umbrella cell through potassium selective channels driven by its high intracellular concentration (139).

In addition to the amiloride-sensitive epithelial sodium channel, Lewis and colleagues have also demonstrated that the apical membrane of the umbrella cell contain an amiloride-insensitive, cation-selective channel and a cation channel that partitions between the apical membrane and the mucosal solution (131, 133, 249). The basolateral membranes of the umbrella cells contain chloride channels, and  $\text{Na}^+/\text{H}^+$  and  $\text{Cl}^-/\text{HCO}_3^-$  exchangers. Aside from regulation of transcellular ion movement, additional functions of these ion channels are currently unknown, though the basolateral ion channels and exchangers may play important roles in cell volume regulation during osmotic stress (52). The apical sodium and nonselective cation channels described above may play important roles in mechanotransduction during the filling response.

### **C. Accommodative changes of the bladder uroepithelium**

Changes to the uroepithelium depend on the cyclical levels of urine volume. The uroepithelium can undergo dramatic changes in the overall tissue morphology. The umbrella cells can also undergo changes in cell biology such as initiation of biochemical signals that leads to alteration in membrane biology. The dynamic nature of the uroepithelium allows the bladder to accommodate various levels of urine volume. More important, the barrier function of the uroepithelium is maintained in the face of altered cell biology.

There are at least two ways for the uroepithelium to adapt to changes in urine volume. The first is simply unfolding of the mucosal surface, which is highly convoluted in the empty bladder (120, 201). Another adaptive response is changes in tissue morphology. As the urine volume increases, the intermediate and basal cells migrate laterally (96), and the superficial umbrella cells undergo a transition from roughly cuboidal in the empty bladder to squamous in the filled bladder (153). Alterations in the uroepithelial cells result in a thinner uroepithelium.

### **D. Hydrostatic pressure-induced exocytosis in bladder**

As urine volume increases, superficial umbrella cells undergo morphological changes. These changes could be explained by two different models. One model describes the folding and unfolding of the umbrella cell apical membrane as the only mechanism for accommodative response (120, 201). The other model supports the idea of hydrostatic pressure-induced exocytosis, where hydrostatic force (filling) stimulates the exocytosis of fusiform/discoidal vesicles in the umbrella cells leading to increased bladder surface area (95, 175). This latter model was based on several previous observations. First, morphological analysis revealed that umbrella cells from distended bladders contain much fewer vesicles than umbrella cells from

empty bladders (153). Second, isolated uroepithelium exposed to hypo-osmotic bathing buffer or increased hydrostatic pressure exerted against the tissue leads to significant increase in membrane capacitance (135). These data are consistent with exocytosis in the bladder umbrella cells. However, there is no direct correlation between discoidal vesicle exocytosis and increased surface area. Moreover, the modest change in response to hydrostatic pressure (17%; see (135)) and the difficulties in interpreting the results from osmotic stimuli (213) weaken the significance of exocytosis in response to hydrostatic pressure.

### **III. Mechanotransduction and regulation of membrane traffic in mechanosensitive cells**

Mechanical stimuli alter membrane traffic in many different cell types including astrocytes, fibroblasts, cardiac myocytes, endothelial cells, osteocytes, kidney epithelia, type II alveolar cells, and the hair cells in the inner ear (6). How mechanical stimuli are transduced into biochemical signals leading to changes in vesicular traffic is not well understood, and in the uroepithelium nothing is known. However, it is believed that the first step in mechanotransduction is the activation of a mechanosensor that is able to sense alterations in plasma membrane tension or changes in the underlying cytoskeleton. This initial signal is processed by downstream mechanotransducers and secondary messengers leading to changes in cellular events, such as endocytosis and exocytosis. Several different mechanosensors and mechanotransducers have been described (89, 184). Those that regulate membrane traffic include cytoskeleton, ion channels, integrins, tyrosine kinases, and signaling molecules such as ATP,  $\text{Ca}^{2+}$ , cAMP, and PKA (43, 89, 107, 147, 184, 185, 195). The following sections will provide a



brief overview of the role of these potential mechanosensors and mechanotransducers on membrane traffic in various mechanosensitive cell types.

## **A. Cytoskeleton**

Actin microfilaments, microtubules, and intermediate filaments are the chief components of cytoskeleton (6). Not only does the cytoskeleton uphold the structure of the cell, it also plays an important role in mechanotransduction. Deformation of the plasma membrane by mechanical forces is accompanied by a rapid reorganization of the cytoskeleton. Because the cytoskeleton is attached to the plasma membrane, alterations in the cytoskeleton can affect membrane tension and thereby affect various cellular events, including endocytosis and exocytosis (6, 89, 107, 158). Changes in the cytoskeleton can also affect membrane traffic through other mechanosensors such as integrins and stretch-activated ion channels. Since mechanosensors are attached to the actin cytoskeleton, disruption of this interaction can alter their activities (89). For example, disturbing the microfilament can influence the activity of stretch-activated ion channels in embryonic skeletal muscle (228). Alterations in cytoskeleton, which disrupt membrane tension can affect the activities of integrin receptors in capillary endothelial cells (45). Additionally, the cytoskeleton may regulate exocytosis by serving as a scaffold that coordinates the organization of endocytic and exocytic signaling complexes (107).

In the bladder, cytoskeleton may play an important role in pressure-induced exocytosis. In the umbrella cells, a dense network of intermediate filaments is observed in the vicinity of apical plasma membrane. When the bladder is empty, the intermediate filaments are arranged randomly throughout the cytoplasm. However, upon filling the intermediate filaments reorganize and align into a parallel-like arrangement beneath the apical surface. As the intermediate

filaments reorganize, the discoidal/fusiform vesicles move into close proximity with the membrane to allow for interaction with tethering and/or docking proteins to initiate fusion. Lewis and de Moura have shown that treating the uroepithelium with the actin-disrupting agent cytochalasin B inhibits osmotic pressure-induced capacitance increase, and colchicines, a microtubule disrupting agent, causes a more rapid increase in osmotic-induced capacitance (135). These data indicate that the cytoskeleton in umbrella cells may play an important role in exocytosis.

## **B. Mechanosensitive ion channels**

Mechanically sensitive ion channels, such as stretch-activated ion channels, are known to play important roles in signal transduction for different cell types (6, 89). Several classes of these ion channels have been described, including nonselective cation channels, some of which conduct  $\text{Ca}^{2+}$  and can induce  $\text{Ca}^{2+}$  release from intracellular stores (89, 90). Increased intracellular  $\text{Ca}^{2+}$  triggers exocytosis in many cell types (32). Entry of  $\text{Ca}^{2+}$  through plasma membrane channels can also regulate endocytosis (198). In the hair cells of the inner ear, a nonselective cation channel plays important roles in mechanotransduction (103). Bending of the stereocilia activates a nonselective cation channel that depolarizes the cell. This results in activation of a voltage-sensitive  $\text{Ca}^{2+}$  channel that raises intracellular  $\text{Ca}^{2+}$ , which in turn stimulates synaptic vesicle exocytosis (6, 67, 103). In the rat atrium, secretion of atrial natriuretic factor (ANF) is blocked by gadolinium, a rare earth metal that inhibits many stretch-activated nonselective cation channels (121). Recently, vanilloid receptor (VR1), a capsaicin-gated ion channel expressed by nociceptive primary afferent neurons was identified in the bladder (20). In mice bladders lacking VR1, ATP release was diminished, indicating that VR1 receptors may modulate ATP secretion

(21). Another vanilloid receptor-like protein, vanilloid receptor-related osmotically activated channel (VR-OAC), may have functional roles in sensing osmotic stretch (144). However, whether VR-OAC plays any role in secretion is unknown.

In addition to VR1 receptor/channel expression in the bladder, other mechanosensitive ion channels exist in the bladder uroepithelium that can conduct  $\text{Cl}^-$ ,  $\text{K}^+$ , and  $\text{Na}^+$  (224). Whether these ion channels play any role in pressure-sensitive membrane traffic in umbrella cells is unknown. However, Ferguson, *et al.* have suggested that the amiloride sensitive epithelial  $\text{Na}^+$  channels may modulate ATP release from the uroepithelium (62), which, in turn, plays an important role in modulating umbrella cell exocytosis (see Chapter 4). Other ion channels, including the ATP-gated P2X purinergic receptors (to be discussed below), which are nonselective cation channels that can increase intracellular  $\text{Ca}^{2+}$ , may have important functional roles in mechanotransduction in the bladder. More details on the mechanosensory role of ion channels in the bladder uroepithelium will be presented in Chapter 3 and 4.

### **C. Integrin receptors**

Integrins are another class of mechanosensors. They are made up of two receptor subunits,  $\alpha$  and  $\beta$ , which together links extracellular matrix molecules to the intracellular actin cytoskeleton (107). There are several ways in which integrin receptors can modulate exocytic events. The  $\alpha$ -subunit forms interactions with several intracellular molecules, including the cytoskeletal associated proteins talin and  $\alpha$ -actinin (6). The  $\beta$ -subunit also interacts with focal adhesion kinase, which in turn associates with other molecules including pp60<sup>src</sup>, Fyn, Grb2, and phosphatidylinositol-3 kinase (31, 107). These molecules can regulate the Rho family of GTPases, including Rho, Rac, and CDC-42 (31, 107). Disruption of these small GTPases has

been shown to interfere with activities such as organization of the actin cytoskeleton, endocytosis, and exocytosis.

When integrin receptors activities are disrupted, mechanosensory transduction is inhibited (6). In frog skeletal muscle, treatment with short amino acid peptides Arg-Gly-Asp (RGD peptide in single-letter amino acid code) uncouples integrin receptors from the extracellular matrix (34). As a result, stretch-induced release of neurotransmitters from the motor nerve terminal is blocked. RGD peptide treatment can also inhibit production of platelet-derived growth factor from smooth muscle cells exposed to mechanical stretch (34). In the bladder epithelium, nothing is known about the role of integrin receptors in mechanotransduction. The functional role of integrins in the accommodative responses of the uroepithelium is an area that remains to be explored.

#### **D. Tyrosine kinases**

Receptor and nonreceptor tyrosine kinases may play important roles in mechanotransduction (147, 184, 185). As their names indicate, receptor tyrosine kinases have transmembrane domains, whereas nonreceptor tyrosine kinases are anchored to the plasma membrane via amino-terminal myristoylation. One possibility that tyrosine kinases may transduce mechanical stimuli into biochemical signals is via conformational changes. In cardiac myocytes, mechanical stretch stimulates tyrosine kinase phosphorylation and elevation in intracellular  $\text{Ca}^{2+}$  (185). The tyrosine kinase inhibitor lavendustin A inhibits stretch-induced ANF secretion (209). In addition, stretch-activated secretion of vascular permeability factor in mesangial cells is inhibited by tyrosine kinase inhibitors genistein and herbimycin A (84). These data indicate that tyrosine kinases are

important regulators of stretch-sensitive secretory events and may be important in mechanosensitive cell types such as bladder epithelial cells.

## **E. Adenosine triphosphate**

Adenosine triphosphate (ATP) is an important biological molecule that is present in high concentration in the cell cytoplasm (~3-5 mM) (168). Not only is it an energy source for all cells, it is known to play an important role in mechanotransduction where it can modulate exocytosis in several cell systems (42, 89). In mechanosensitive cells, ATP can be released under physiological conditions (79). Once it is released, it has been demonstrated to stimulate exocytic events such as surfactant release by alveolar type II lung cells (179). ATP can also stimulate mucin secretion from goblet cells isolated from canine tracheal epithelium (46). In addition, exogenous ATP has been shown to stimulate membrane trafficking in brown adipocytes via purinergic receptor activation (170). In contrast, ATP can also modulate several types of ion channels. In hippocampal neuroblastoma cells, ATP can evoke two excitatory responses, opening of a receptor-operated nonselective cation channel and a Na<sup>+</sup> channel (57). Activation of nonselective cation channels may increase intracellular Ca<sup>2+</sup>, leading to membrane traffic.

ATP released from the bladder uroepithelium may also play an important role in mechanotransduction. There is growing evidence that the uroepithelium may communicate bladder fullness to the nervous system via ATP signaling pathways (39, 41). ATP released from the uroepithelial cells, nerves, and the bladder detrusor may activate the afferent nerve terminals to signal the state of bladder fullness to the central nervous system (62, 118, 221). ATP may also modulate umbrella cell membrane trafficking during filling (see Chapter 4). One of the goals of

this dissertation is to examine the effect of ATP signaling on membrane trafficking in umbrella cells. More on this topic will be discussed in Chapter 4 of this dissertation.

## **F. Purinoceptors**

### **1. Purinergic receptors**

There are two classes of purinoceptors, P1 and P2. P1 receptors are known as adenosine receptors (see below), and P2 receptors are purinergic receptors (30). There are two distinct P2 receptor families: the P2X ligand-gated nonselective cation channel that has been reported to be similar in structure to the subunits of the epithelial sodium channel (193), and the P2Y receptors, which are seven-transmembrane domain receptors coupled to heterotrimeric G-proteins (28). In the P2X receptor family eight P2X receptor isoforms (P2X<sub>1-7</sub> and P2X<sub>M</sub>) have been described and at least six P2Y receptors (P2Y<sub>1</sub>, P2Y<sub>2</sub>, P2Y<sub>4</sub>, P2Y<sub>6</sub>, P2Y<sub>11</sub>, and P2Y<sub>12</sub>) are molecularly distinct entities that can elicit functional responses (29, 167, 193). Both P2 receptors have a wide range of functions, including platelet recruitment, bone formation, fluid and electrolyte secretion in the colon and gallbladder, and membrane trafficking. As a result, they are ubiquitously expressed in a variety of cell types (30). Activation of P2 receptors by mechanical stimuli can lead to various downstream effects in cells. One common consequence of P2X and P2Y receptor activation is increases in cytosolic Ca<sup>2+</sup>, which can stimulate exocytosis (193). Because P2X receptors are nonselective cation channels they can directly mediate Ca<sup>2+</sup> entry into the cell (193). P2Y receptors act to raise Ca<sup>2+</sup> indirectly by coupling through G-proteins to modulate adenylate cyclases, which generate cAMP and phospholipases, which generate diacylglycerol and inositol 1,4,5-triphosphate (IP<sub>3</sub>). In turn, IP<sub>3</sub> binds to IP<sub>3</sub> receptors and stimulates increased cytosolic Ca<sup>2+</sup> (193).

Several P2X receptors, including P2X<sub>2</sub>, P2X<sub>3</sub>, P2X<sub>4</sub>, and P2X<sub>5</sub> receptors have been localized to the serosal surfaces of uroepithelial cells (58, 61, 125). These receptors, along with ATP, may play an important role in sensing bladder fullness (28). This regulatory function is in accordance with the hypothesis proposed by Burnstock and Williams where membrane distension leads to ATP release from uroepithelial cells, which then acts on P2X<sub>3</sub> receptors on the subepithelial sensory nerves to transmit biochemical signals to the central nervous system to convey information on bladder distension and pain (28, 30). When P2X receptors are blocked by antagonists, sensory nerve activities are inhibited (162). Similarly, in the absence of P2X<sub>3</sub> receptors in bladders of knockout mice, sensory nerve firing is decreased. (39) In addition to sensory function and detection of bladder fullness, P2X receptors may also modulate discoidal/fusiform vesicle trafficking in the umbrella cells during the urine-filling process (see Chapter 4). P2Y receptors may be involved in umbrella cell membrane trafficking as well. These observations indicate that purinergic receptors are important regulators of normal bladder function. They may modulate important accommodative responses during the urine-filling process.

## **2. Adenosine receptors**

The second class of purinoceptors that may play an important role in membrane trafficking is adenosine (P1) receptors. There are four different adenosine receptors, denoted A<sub>1</sub>, A<sub>2A</sub>, A<sub>2B</sub>, and A<sub>3</sub> (66). Similar to P2Y receptors, all four members of the P1 receptors have seven-transmembrane domains and are coupled to G-proteins (66). Depending on the P1 receptor isoforms, activation of adenosine receptors by its physiological agonist adenosine can have stimulatory or inhibitory effects. A<sub>1</sub> and A<sub>3</sub> receptors are coupled to G<sub>i</sub>-proteins, and A<sub>2A</sub> and A<sub>2B</sub> receptors are coupled to G<sub>s</sub>-proteins (66). Stimulatory effects of P1 receptors include

degranulation of mast cells and stimulation of sensory nerve activities (66). Inhibitory effects include reduced glomerular filtration and inhibition of platelet aggregation (66). In the bladder umbrella cells, the precise role of P1 receptors in pressure-induced exocytosis is currently unknown. However, in experiments where isolated pieces of uroepithelium are treated with adenosine membrane capacitance increased (245). Addition of isoform-specific P1 receptor agonists (CCPA, CGS, and IB-MECA) also stimulated capacitance increase (Yu, *et al.*; personal communication) (245). These data indicates that P1 receptors may also modulate membrane trafficking in mechanosensitive cells.

### **G. Secondary messenger cascades**

Mechanical stimulation can trigger elevation in intracellular  $\text{Ca}^{2+}$  in many cells, including cardiac and smooth muscle cells, fibroblasts, osteoblasts, endothelial cells, neurons, and epithelial cells (89). Changes in intracellular  $\text{Ca}^{2+}$  concentration can affect most regulated secretory events (17). In hair cells, mechanically-activated exocytosis of neurotransmitter-containing vesicles is dependent on increases in intracellular  $\text{Ca}^{2+}$  concentration (103). Stretch-induced ANF secretion from isolated rat atrium also requires the activity of  $\text{Ca}^{2+}$  channels and is blocked by  $\text{Ca}^{2+}$  channel inhibitors (114). Increases in intracellular  $\text{Ca}^{2+}$  can result from a combination of several mechanisms, including release of  $\text{Ca}^{2+}$  from intracellular stores, such as the endoplasmic reticulum, influx of  $\text{Ca}^{2+}$  from the extracellular environment through  $\text{Ca}^{2+}$  channels, and/or decreased efflux of  $\text{Ca}^{2+}$  from the cell (89). In bladder uroepithelial cells, pressure-induced exocytosis is dependent on both intra- and extracellular  $\text{Ca}^{2+}$ . Altering the intracellular  $\text{Ca}^{2+}$  concentration of the uroepithelial cells has profound effects on umbrella cell



membrane trafficking. The role of  $\text{Ca}^{2+}$  in pressure-induced exocytosis will be discussed further in Chapter 2 and 4.

In addition to  $\text{Ca}^{2+}$ , the secondary messenger cyclic adenosine monophosphate (cAMP) is also an important modulator of pressure-induced exocytosis. Mechanical stretch stimulates production of cAMP in some cell types including the endothelial cells, erythrocytes, lymphoma cells, fibroblasts, cardiac myocytes, and bladder umbrella cells (see Chapter 2) (228). Agents that raise cAMP (e.g. forskolin) can have significant effects on cellular functions. For example, transcytosis and apical secretion in Madin-Darby canine kidney (MDCK) cells are stimulated through cAMP-dependent signaling pathways. H89, an inhibitor of protein kinase A (PKA) and the downstream target of cAMP, blocks apical secretion in MDCK cells. Similarly, in lymphoma cells, osmotic stretch stimulates significant increases in intracellular cAMP and cell surface area. In bladder umbrella cells, cAMP and PKA are important regulators of pressure-induced exocytosis (see Chapter 2). These studies indicate that cAMP and PKA have intimate roles in many cellular events, including volume regulation and membrane trafficking.

One important regulator of vesicle trafficking is Rab GTPases. Rab GTPases have defined roles in the tethering/docking of vesicles to their target compartment leading to membrane fusion, and have also been implicated in cargo selection, vesicle budding, and organelle motility (247). One important Rab GTPase is Rab27a, where it has been implicated in melanosome traffic and exocytosis of lytic granules in cytotoxic T-cells (194). In preliminary studies, the Rab27a isoform, Rab27b, is identified in the bladder and expressed in the umbrella cell layer (7). The regulatory role of Rab27b on fusiform/discoidal vesicle exocytosis may be analogous to the regulation of melanosome trafficking by Rab27a. The localization and functional role of Rab27b in bladder umbrella cells are currently unknown.

## **IV. Goals of the dissertation**

Pressure-induced membrane trafficking in the bladder umbrella cells is a complex event that involves mechanotransducers and many signaling molecules that are currently poorly understood. One reason for this lack of understanding is the absence of an experimental model that mimics the urine-filling process in the bladder. To this end my first goal was to develop a new system in the Ussing chamber to duplicate the pressure-induced filling responses of the bladder uroepithelium. Using this Ussing chamber setup, the second goal was to examine the effect of hydrostatic pressure on vesicle trafficking in bladder umbrella cells and identify the signaling molecules involved in modulating pressure-induced membrane trafficking. To understand how mechanical stimuli, such as hydrostatic pressure, are transduced into biochemical signals my last goal was to identify mechanotransducers in the bladder, such as pressure-activated ion channels and membrane receptors, and examine the possible roles that these mechanotransducers play in pressure-induced membrane trafficking in bladder umbrella cells. The following chapters and sections will demonstrate the methodology and the results of my research to understand these unknown aspects of the urinary bladder.

# CHAPTER 1

## **Analysis of hydrostatic pressure-induced changes in umbrella cell surface area\***

### ***ABSTRACT***

All cells experience and respond to external mechanical stimuli including shear stress, compression, and hydrostatic pressure. Cellular responses can include changes in exocytic and endocytic traffic. An excellent system to study how extracellular forces govern membrane trafficking events is the bladder umbrella cells, which line the inner surface of the mammalian urinary bladder. It is hypothesized that umbrella cells modulate their apical plasma membrane surface area in response to hydrostatic pressure. Understanding the mechanics of this process is hampered by the lack of a suitable model system. I describe a pressure chamber that allows one to increase hydrostatic pressure in a physiological manner while using capacitance to monitor real-time changes in the apical surface area of the umbrella cell. It is demonstrated that application of hydrostatic pressure results in an increase in umbrella cell apical surface area and a change in the morphology of umbrella cells from roughly cuboidal to squamous. This system will be useful in further dissecting the mechanotransduction pathways involved in cell shape change and regulation of exocytic and endocytic traffic in umbrella cells.

\*Reprinted from *Methods*, (2003, volume 30, pg. 207-217), with permission by Elsevier Science

## ***INTRODUCTION***

All cells are subjected to external mechanical stimuli such as shear stress, twisting, compression, vibrations, and hydrostatic pressure (89). Cellular responses to these forces include changes in their rate of division, death, differentiation, movement, signal transduction, gene expression, secretion, and endocytosis (14, 15, 43, 45, 54, 89, 158, 184). Understanding how cells respond to mechanical stimuli and the cellular signals that mediate these responses are universal questions in cell biology. One organ that provides an excellent model system to study these biological phenomena is the urinary bladder, which is subjected to variations in hydrostatic force as a result of cyclical changes in luminal volume.

The inner surface of the bladder is lined by an epithelium, the uroepithelium that forms the interface between the urine and the underlying submucosa and muscularis of the bladder wall (96). The uroepithelium also acts as a barrier that maintains the ionic and solute composition of the urine and prevents pathogens and toxic metabolites of urine from entering the underlying tissue (164). The uroepithelium is stratified and is composed of three cell types including basal cells, intermediate cells, and umbrella cells. Basal cells form a single layer that contacts the underlying capillary bed and connective tissue and these cells serve as precursors for the other cell types. Intermediate cells form a layer on top of the basal cell layer that is one to six cell layers thick. These cells rapidly differentiate into umbrella cells when the luminal umbrella cell layer is damaged (123, 161). The outer umbrella cell layer interfaces with urine and forms the primary barrier, which includes a layer of mucin glycoproteins and glycosaminoglycans that may prevent bacterial attachment (172, 173), tight junctions that form a tight seal between adjacent cells (137, 139), and an apical plasma membrane with low permeability to urea and water (164).

The uroepithelium undergoes a dramatic transition during bladder filling. In filled bladders the uroepithelium appears thinner (96), apparently the result of intermediate and basal cells being pushed laterally to accommodate the increased urine volume. Furthermore, the umbrella cells change shape from roughly cuboidal to squamous, and there is a significant increase in their apical surface area (96, 134, 135, 214). The latter is thought to be the result of hydrostatic pressure-induced fusion of discoidal/fusiform vesicles with the apical surface of the umbrella cells (134, 135, 214), which allows the cells to maintain their barrier function while accommodating increased urine volume. The increase in apical surface area is modulated by hydrostatic pressure-induced endocytosis that in combination with vesicle exocytosis balances the change in apical surface area (214). Basolateral surface area is unchanged during filling (214). The mechanotransduction pathways involved in the regulation of exocytosis and endocytosis in these cells are largely unexplored, although the cytoskeleton and cAMP are likely to play a role (134, 135, 214).

To increase our understanding of how mechanical forces alter umbrella cell surface area, it was necessary to develop a system that allows one to mechanically stimulate the uroepithelium in a physiologically relevant manner. Previously developed techniques used to mimic bladder filling included the instillation of buffer into the catheterized bladders of anesthetized rats (4). While this method allows for examination of the tissue *in situ*, it is difficult to assess real-time changes in surface area or to perform biochemical experiments. Alternatively, uroepithelial tissue, mounted in Ussing chambers, was exposed to increased hydrostatic pressure by raising the buffer level in the mucosal hemichamber (facing the apical surface of the umbrella cells) and lowering the buffer level in the serosal hemichamber (facing the basolateral surface of the umbrella cells and underlying intermediate and basal cells) (135). This technique is relatively

physiological, but the increase in hydrostatic pressure was small (135). Other techniques used were mechanical stimulation of the uroepithelium by placing isolated tissue in hypotonic medium (which induces cell swelling) and membrane “punching” (134, 135). The latter technique involves rapidly raising then lowering the fluid level in the mucosal hemichamber several times. Cell swelling does result in large changes in membrane surface area, while punching does not (134, 135).

An ideal feature of any system is that it should be amenable to continuous monitoring of surface area changes. One attractive characteristic of the Ussing chamber system is that area changes can be monitored in real-time by measuring changes in capacitance (132, 139). As described below, membrane capacitance is an electrical parameter directly proportional to surface area (where  $1 \mu\text{F} \approx 1 \text{ cm}^2$  of tissue area) (132, 139). In fact, in the Ussing chamber experiments described above, increased hydrostatic pressure was accompanied by a modest 15% increase in capacitance (134, 135). An alternative technique to measure changes in umbrella cell surface area is stereology, a statistical analysis that allows one to calculate three-dimensional parameters (volume and surface area) from two-dimensional tissue sections (102). Although this technique allows for an unbiased estimate of umbrella cell apical and basolateral surface area (214), it is performed on fixed tissue (which precludes real-time monitoring) and is laborious and time consuming. I have developed a new Ussing chamber system that allows for the application of physiologically relevant pressures across the mucosal surface of isolated uroepithelium, while allowing for the simultaneous monitoring of tissue capacitance (214). Real-time analysis of hydrostatic pressure-induced changes in the surface area of umbrella cells is now possible and is providing insight into the mechanotransduction pathways involved in surface area modulation in these cells

## RESULTS

### *Hydrostatic pressure induces an increase in the surface area of umbrella cells*

A newly designed pressure chamber (Figure 1-1, see Materials and Methods) was used to increase hydrostatic pressure across the mucosal surface of isolated rabbit bladder epithelium. In the mammalian bladder, pressure rises in a biphasic manner as the organ fills with urine. The first rise occurs rapidly and then pressure remains relatively constant for an extended period. This extended phase is called the storage phase, and in rabbit bladders it can last for upward of 5 hours, with an average pressure of ~8 cmH<sub>2</sub>O. The storage phase is followed by the micturation phase, which is characterized by a rapid rise in bladder pressure punctuated by spikes in pressure as the smooth muscle undergoes contractions.

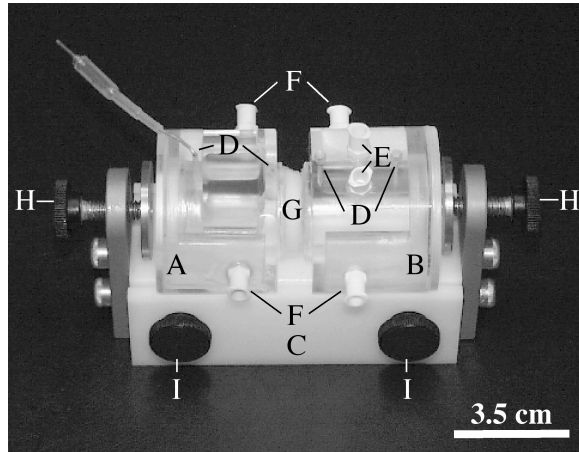


*Figure 1-1. Pressure chamber. A, serosal hemichamber; B, mucosal hemichamber; C, chamber base; D, electrode ports; E, Luer ports; F, water jacket ports; G, tissue; H, outside-edge thumb screws; I, parallel alignment thumb screws.*

In this system the extended storage phase of the bladder filling process was reproduced by increasing the back pressure to 8 cmH<sub>2</sub>O either rapidly (within 30 seconds) or slowly (by filling the chamber at a rate of 0.1 ml/min), and then closing off the pressure chamber. The increased pressure was accompanied by a large increase in capacitance (Figure 1-2A). In samples where the pressure was increased rapidly the capacitance quickly increased by ~20 % in the first 10 minutes and then gradually peaked at ~50% above starting levels after 300 minutes (Figure 1-2A). When the chamber was filled more gradually, the increase was slower (especially at early time points), but achieved the same overall increase in capacitance of ~50% (Figure 1-2B) (In

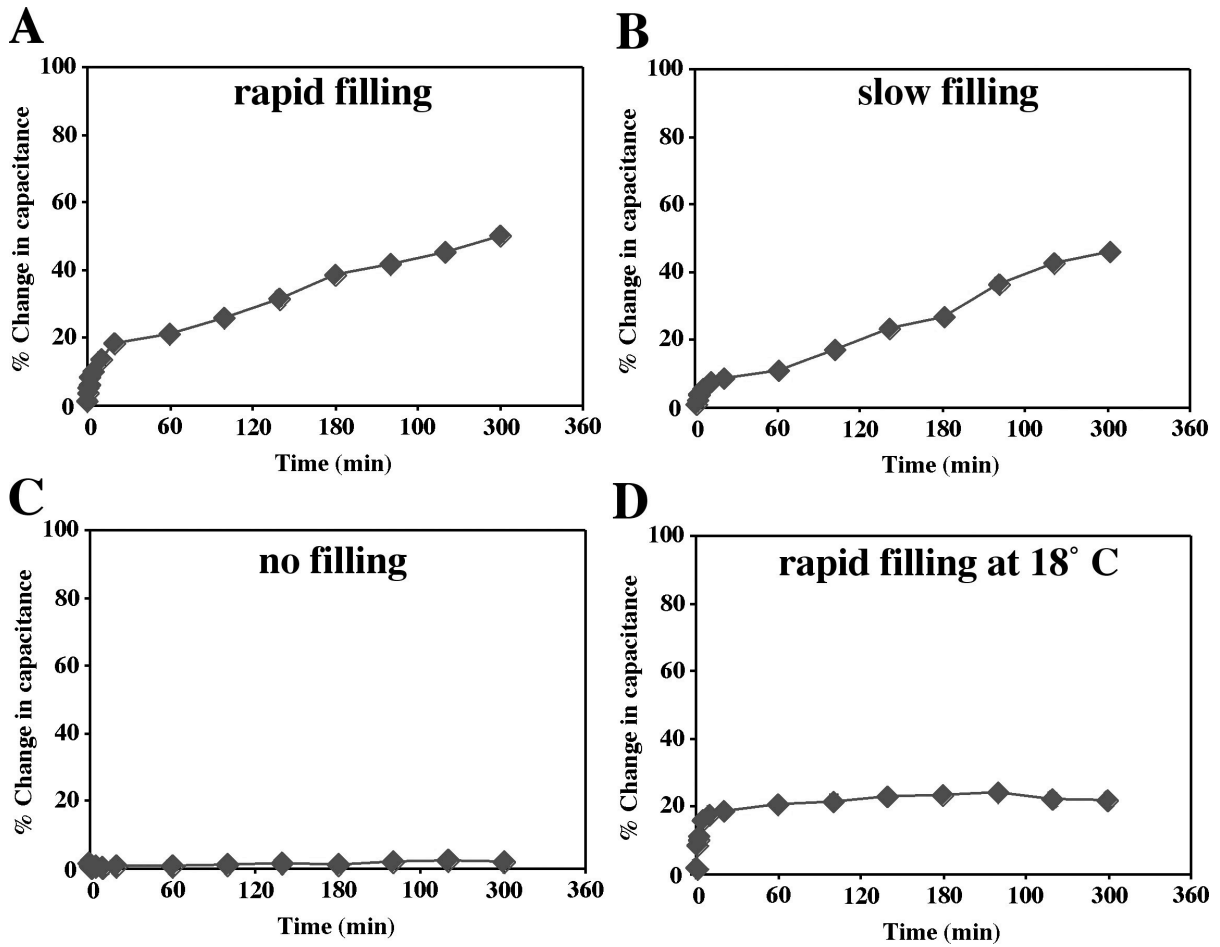


Figure 1-2. Effect of pressure on changes in capacitance. (A) Changes in capacitance following rapid filling. (B) Changes in capacitance following slow filling. (C) Changes in capacitance in the absence of filling. (D) Changes in capacitance in tissue incubated at 18°C. Data are means  $\pm$  SEM. In most cases the error is smaller than the symbol.



subsequent experiments, the rapid filling method was used as it was quick and reliable, and the overall change was similar to that achieved with the slower filling method). Using stereological methods, I confirmed that the apical surface area of umbrella cells has indeed increased by 50% after a 5 hour exposure to increased hydrostatic pressure in the chamber, while basolateral surface area was not significantly changed under these same conditions (214). To confirm that changes in capacitance were due to changes in pressure and did not simply reflect time of incubation in the chamber, I measured capacitance on tissue that was mounted in the pressure chamber but was not exposed to increased hydrostatic pressure. Under these conditions there was no change in capacitance (Figure 1-2C). Furthermore, I observed that hydrostatic pressure-induced increases in capacitance were significantly inhibited by incubation at 18°C (Figure 1-2D), a temperature that slows many membrane trafficking events including steps in the biosynthetic and endocytic pathways (13, 83, 105).

***Increased pressure is accompanied by changes in the morphology of the epithelium***

As described above, a well-known feature of the bladder epithelium is that it undergoes a significant morphological change during bladder filling. During filling, the thickness of the epithelium decreases and the umbrella cells change shape from roughly cuboidal to squamous (96). A similar transition occurred in bladder epithelium exposed to hydrostatic pressure in the pressure chambers. Control tissue not exposed to hydrostatic pressure is shown in Figure 1-3A. The umbrella cells were roughly cuboidal in shape and often exhibited portions of cytoplasm that extended downward into the underlying intermediate cell layer (Figure 1-3A). The surface of these cells was somewhat folded and numerous discoidal vesicles were present throughout the

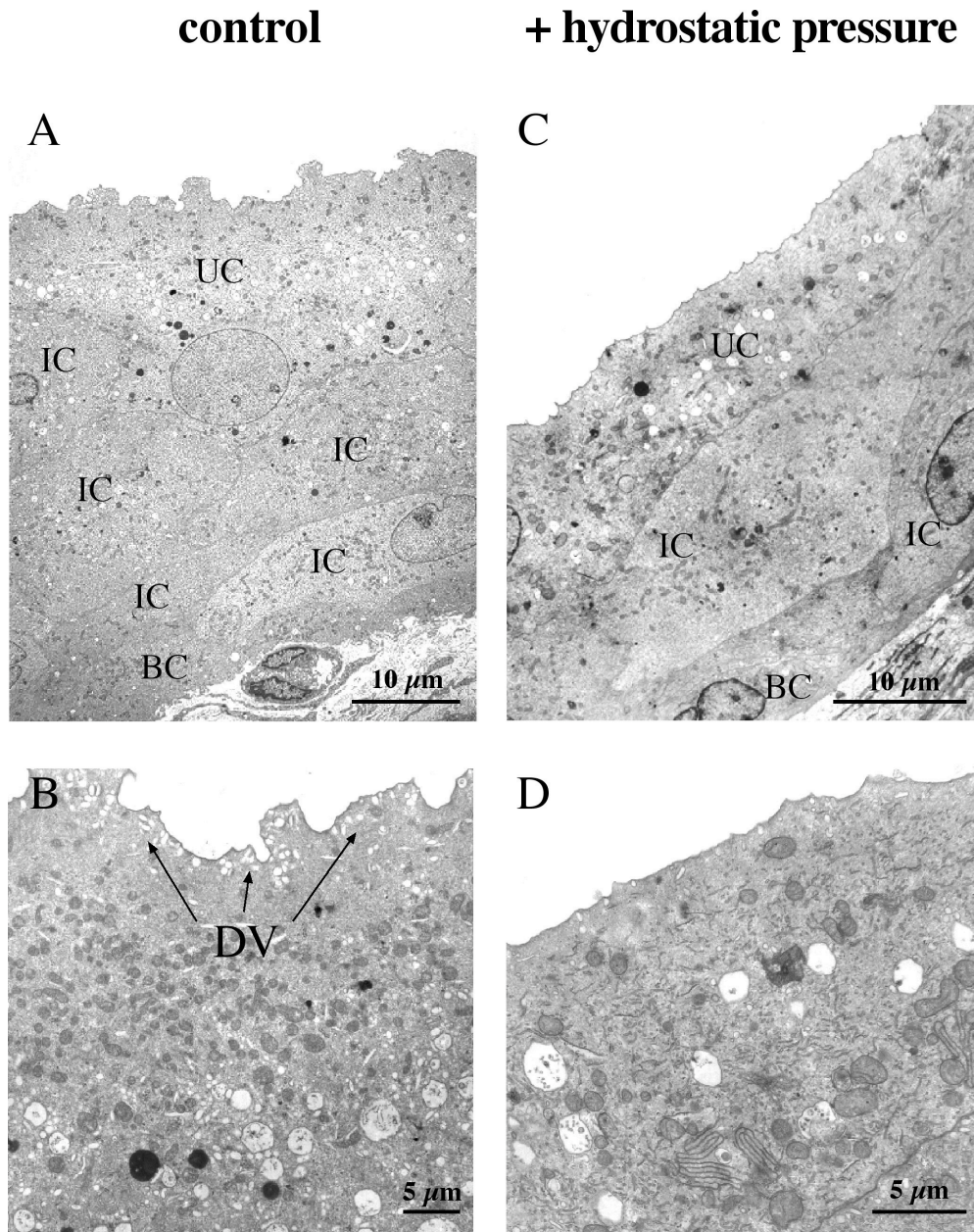


*Figure 1-3. Ultrastructural analysis of control tissue or tissue exposed to hydrostatic pressure. (A, B) Tissue was placed in chamber and incubated for 5 h in the absence of pressure. A low-magnification view of the uroepithelium (A) and higher-magnification view of umbrella cell cytoplasm (B) are shown. (C, D) Tissue was mounted in the chamber and incubated in the presence of hydrostatic pressure for 5 h. A low-magnification view of the uroepithelium (C) and higher-magnification view of umbrella cell cytoplasm (D) are shown. BC, basal cell; DV, examples of discoidal vesicles; IC, intermediate cell; UC, umbrella cell.*

apical cytoplasm of the cells, but were concentrated underneath the apical surface (Figure 1-3B). This morphology is typical of umbrella cells observed in contracted bladders (96).

In contrast to control cells, umbrella cells subjected to 5 hours of increased hydrostatic pressure underwent a significant change in morphology (Figure 1-3C). The depth of the cell was reduced with a concomitant increase in cell length; it was no longer possible to fit the umbrella cells within the frame of the electron microscope. In addition to these changes, the apical and basal surfaces were flattened and retained only a small degree of membrane folding. Another striking feature of the 5 h pressure-stimulated samples was a large decrease in the number of discoidal vesicles below the apical surface of the cell (Figure 1-3D).

## ***DISCUSSION***

Mechanical stimuli alter exocytic and endocytic traffic in many cell types including endothelial cells, myocytes, kidney epithelia, type II alveolar cells, osteocytes, and the hair cells in the inner ear (6). How mechanical stimuli are sensed and how they are transduced into downstream changes in vesicular traffic are not well understood. The cytoskeleton, stretch-activated channels, increased cytoplasmic  $\text{Ca}^{2+}$ , integrins, phospholipases, tyrosine kinases, ATP, and cAMP have been implicated in these events (6). Until recently, little was known about the mechanotransduction pathways involved in discoidal vesicle exocytosis, although a function for the actin and microtubule cytoskeleton was proposed some years ago (134, 135).

Our understanding of umbrella cell biology was hampered by the lack of a suitable system to mimic bladder filling. In this chapter I described a pressure chamber that allows for application of physiological pressures across the mucosal surface of isolated rabbit uroepithelium. Importantly, the chamber design allows one to monitor real-time changes in cell surface area. As previously described, raising hydrostatic pressure, either rapidly or slowly, was sufficient to induce increases in the apical surface area of the umbrella cells, as monitored by capacitance (see Materials and Methods). This increase in apical surface area was confirmed by a stereological analysis of surface area changes in umbrella cells exposed to hydrostatic pressure (see Chapter 2). Changes in capacitance were not observed if pressure was not increased. When tissue was incubated at 18°C with increased pressure there was an initial rapid rise in capacitance, but then the capacitance plateaued and failed to increase. Apparently, the early events occur even at reduced temperatures. After 5 hours of increased pressure, the cells adopted a squamous morphology and exhibited a substantial decrease in the number of discoidal vesicles in the cytoplasm. This morphological change in the uroepithelium after 5-hour of pressure was

consistent with an earlier study that examined umbrella cells in expanded bladders (153). These data demonstrated that the pressure-induced morphological transition in umbrella cells occurs within the pressure chamber system, confirming the physiological relevance of our system.

The signaling pathways that regulate pressure-induced membrane trafficking in umbrella cell are unknown. An important use of this pressure chamber system will be to study the regulatory molecules and signaling pathways that are involved in the umbrella cell response to pressure. In the next chapter, pressure-induced membrane trafficking (exocytosis and endocytosis) will be further examined and the roles of various signaling molecules during increased hydrostatic pressure will be evaluated.

## CHAPTER 2

### Hydrostatic pressure-regulated exocytosis / endocytosis in bladder umbrella cells\*

#### *ABSTRACT*

The epithelium of the urinary bladder must maintain a highly impermeable barrier despite large variations in urine volume during bladder filling and voiding. To study how the epithelium accommodates these volume changes, bladder tissue was mounted in modified Ussing chambers and exposed to hydrostatic pressure. Stimulating the tissue with hydrostatic pressure for 5 h resulted in a 50% increase in luminal surface area ( $\sim 2900 \mu\text{m}^2$  to  $\sim 4300 \mu\text{m}^2$ ), exocytosis of a population of discoidal vesicles located in the apical cytoplasm of the superficial umbrella cells, and release of secretory proteins. Surprisingly, exposure to increased pressure also induced endocytosis of apical membrane and 100% of biotin-labeled membrane was internalized within 5 min after pressure induction. The endocytosed membrane was delivered to lysosomes and degraded by a leupeptin-sensitive pathway. Lastly, the exocytic events were mediated, in part, by a cyclic adenosine monophosphate, protein kinase A, and calcium-dependent process. These were shown by increased membrane capacitance in the presence of adenylate cyclase agonists, inhibition in pressure-induced capacitance increases in the presence of protein kinase inhibitor H89, and alterations in membrane capacitance in the presence of intracellular calcium modulators. The results indicate that pressure modulates mucosal surface area by coordinating

both exocytosis and endocytosis at the apical membrane of umbrella cells and provide insight into the mechanism of how mechanical forces regulate membrane traffic in non-excitabile cells.

\*Reprinted from *Molecular Biology of the cell*, (2002, volume 13, pg. 830-846), with permission by the American Society for Cell Biology

## ***INTRODUCTION***

The plasma membrane forms the interface between the cell and its extracellular environment and in response to external stimuli coordinates changes in cellular function. The size and function of this organelle is regulated by the processes of endocytosis and exocytosis. Exocytosis is involved in the cell surface delivery and secretion of newly synthesized and recycled molecules while endocytosis is required for the internalization and recovery of exocytosed membrane. In spite of the growing body of literature describing the effects of mechanical force on exocytosis (38, 51, 122, 185, 186, 202, 232, 238), much less is known about how mechanical stimuli affect endocytosis, although membrane tension may play an important role in this process (6, 44, 64, 101, 158, 176).

One cell type that may provide additional insight into these phenomena is the specialized umbrella cell that lines the mucosal surface of the bladder and forms the barrier between the urine and the underlying tissue. This barrier must be maintained in spite of dramatic changes in luminal urine volume during filling and voiding. The bladder accommodates these changes in large part by macroscopic and microscopic folding and unfolding of the mucosal surface. Furthermore, it is hypothesized that during filling the umbrella cells recruit a sub-apical pool of cytoplasmic vesicles (which are either fusiform or discoidal shaped) to fuse with the apical membrane thereby increasing the mucosal surface area (95, 175). The evidence for vesicle insertion is largely based on two observations. First, a morphometric analysis showed that umbrella cells from full bladders contained significantly fewer vesicles than those from contracted bladders (153), and second, osmotic or mechanical stimulus resulted in increased tissue capacitance, a measure of membrane surface area (135). However, a study that correlates pressure-activated changes in apical and/or basolateral surface area with changes in vesicle



dynamics has yet to be performed. In addition, the underlying mechanism that regulates exocytosis in these cells is largely unexplored, although the cytoskeleton is likely to play a role in this process (135).

Upon voiding, the extra surface membrane is believed to be endocytosed which replenishes the population of cytoplasmic vesicles, followed by a re-folding of the umbrella cell membrane and mucosal surface in preparation for the next filling cycle (153, 175). The exact role of endocytosis in these cells is unclear. The increases in capacitance observed after osmotic or hydrostatic stimulus were partially reversed by removal of hydrostatic pressure (134). In addition, some studies showed that when fluid phase markers were added to the bladder lumen, the markers were detected in vesicles after voiding (33, 95, 175), consistent with re-internalization of membrane. However, the uptake of marker was modest, indicating that the vesicle membrane may not be derived from the apical surface. Other investigators failed to demonstrate uptake of horseradish peroxidase (HRP) or HRP-labeled lectin into vesicles during bladder contraction but instead observed marker in multivesicular bodies and lysosomes (4). Thus, the role that endocytosis plays in apical surface modulation of umbrella cells is currently not understood. Moreover, the effects of mechanical stimuli on endocytosis remain poorly characterized in this or other cell types (6).

Based on results presented in this chapter, I propose an alternative model of vesicle trafficking and surface area modulation in umbrella cells. Initially upon filling, there was little change in the apical or basolateral surface area. However, continued exposure to pressure induced large increases in apical surface area in combination with a decrease in vesicle surface area. The increase in apical surface area coincided with a significant increase in surface expression of uroplakin III, a membrane/vesicle protein, and secretion of <sup>35</sup>S-labeled proteins. In

contrast to the current model, pressure-induced vesicle fusion was accompanied by a simultaneous apical membrane endocytosis, and the internalized membrane was delivered to lysosomes. Lastly, the exocytic, but not the endocytic events were modulated, in part, by a cyclic adenosine monophosphate (cAMP), protein kinase A (PKA)-dependant mechanism. Both intracellular and extracellular calcium were also required for pressure-induced membrane trafficking in umbrella cells. These data indicate that in addition to activating exocytosis, filling also induces endocytosis and the balance of these events governs the size of the umbrella cell apical plasma membrane.

## RESULTS

### *Hydrostatic pressure-regulated changes in umbrella cell apical surface area*

It has been argued that unfolding of the membrane is sufficient to accommodate the increases in urine volume during filling (120, 201). Therefore, my first goal was to determine whether filling resulted in changes in the apical surface area of umbrella cells or simply caused unfolding of the membrane. To mimic the extended storage phase of the bladder I chose a method of stimulation that exposed the uroepithelium to a constant physiological pressure over relatively long periods of time. In rabbits this phase naturally lasts ~5 h (126) and the luminal pressure (~8 cmH<sub>2</sub>O) remains relatively constant (127).

Rabbit uroepithelium, which is comprised of umbrella, intermediate, and basal cell layers was stripped of underlying muscle tissue and mounted in modified Ussing chambers. The muscle tissue was removed to prevent unwanted contraction and ease of tissue manipulation (see Materials and Methods section). Following a period of equilibration, hydrostatic pressure was

applied to the mucosal chamber until a pressure of 8 cmH<sub>2</sub>O was generated and then maintained throughout the duration of the experiment (see Materials and Methods). To confirm that the tissue remained intact and retained its barrier function,

Transepithelial resistance (TER) was monitored throughout the experiment.

The initial TER ( $11,396 \pm 760 \Omega \cdot \text{cm}^2$ )

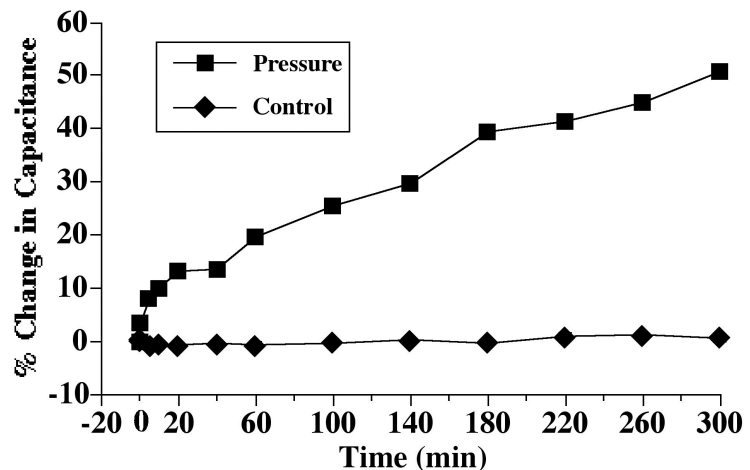
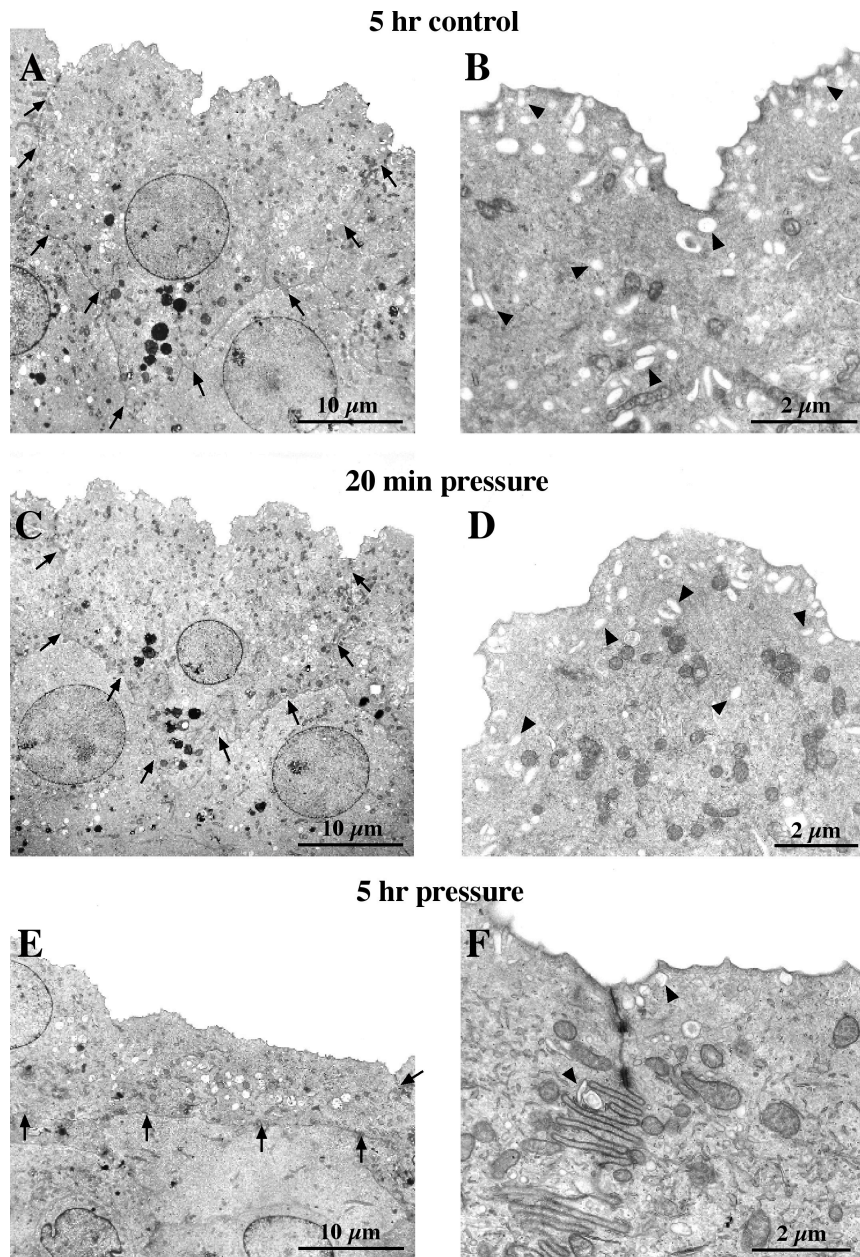


Figure 2-1. Capacitance changes in response to hydrostatic pressure. The change in capacitance of control tissues (no pressure stimulation) and tissues subjected to pressure is shown. Data is mean  $\pm$  SEM (n=5). The error bars are smaller than the symbols.

dipped following increased pressure, but rapidly recovered and at the end of the 5 h period TER was  $14,222 \pm 1,062 \Omega \cdot \text{cm}^2$ . The initial fall in TER likely reflects increased ion conductance as the short-circuit current (Isc) significantly increased upon application of pressure (see Chapter 3).

Changes in surface area were measured in real time by monitoring tissue capacitance. This electrophysiological parameter is directly proportional to surface area ( $1 \mu\text{F} \approx 1 \text{cm}^2$ ) and in bladder tissue is thought to primarily measure changes in the surface area of the apical plasma membrane of the umbrella cells (137). If surface unfolding was sufficient to accommodate the filling response, no changes in capacitance were expected. However, when tissue was stimulated the capacitance rapidly rose approximately 15% within the first 20 min followed by a slower increase to 50% after 5 h of stimulation (Figure 2-1 and Figure 1-2). This bi-phasic response in capacitance was similar to earlier studies that employed osmotic stretch (134, 135). Subjecting the tissue to increased pressure for longer than 5 h did not significantly increase the capacitance above 50% (data not shown).

As a control, the tissue was incubated in the chamber without the addition of hydrostatic pressure. Throughout the 5 h period of incubation the capacitance of the control tissue was unchanged, confirming that incubation in the chamber was not sufficient to elicit changes in surface area (Figure 2-1). Tissue pretreated with cycloheximide followed by pressure stimulation exhibited an initial rise in capacitance of ~25% that remained unchanged for the 5 h period of increased pressure (data not shown) indicating that protein synthesis was important during the later stages of filling. In summary, the data indicated that my method of stimulus was effective for increasing apical surface area and were inconsistent with the hypothesis that surface



*Figure 2-2. Morphological analysis of control and pressure-stimulated umbrella cells. Cells were mounted in modified Ussing chambers and incubated for 5 h without pressure (A and B), or stimulated with pressure for 20 min (C and D) or 5 h (E and F), fixed, and processed for TEM. (A, C, and E) Low-magnification views of representative umbrella cells from each experimental condition. The arrows delineate the borders of the cells. (B, D, and F) Higher magnification views of the apical portion of each umbrella cell. Representative discoidal vesicles are marked by arrowheads.*

unfolding is the only mechanism responsible for accommodating increased urine volume (120, 201).

### ***Morphological changes in pressure-stimulated uroepithelium***

The morphological changes that accompanied pressure treatment were also examined. Tissue was mounted in the chambers and subjected to pressure for either 20 min or 5 h, or was incubated without stimulus as a control. The tissue was subsequently fixed and examined by transmission electron microscopy (TEM). In control tissue (no pressure), the umbrella cells were roughly cuboidal in shape and often exhibited portions of cytoplasm that extended downward into the underlying intermediate cell layer (Figure 2-2A). This morphology is typical of umbrella cells observed in contracted bladders (96). Both the apical and the basolateral surfaces exhibited some degree of folding, although there was considerable variation among the cells. When viewed at higher magnification, numerous discoidal vesicles were commonly observed throughout the cytoplasm but appeared to be concentrated in the apical region of the cell just beneath the plasma membrane (Figure 2-2B). There were no observable differences between cells incubated without pressure for 20 min or 5 hours.

When the cells were exposed to increased pressure for 20 min, very few morphological changes were observed relative to controls. The majority of the cells retained a cuboidal-like shape and exhibited a similar degree of apical and basolateral surface folding (Figure 2-2C). Similar to controls, higher magnification images of these cells revealed an abundance of discoidal vesicles present in the cytoplasm just below the apical membrane (Figure 2-2D), although the relative abundance of vesicles localized in the center of the cell appeared to be

diminished. This change in distribution may represent a shuttling of vesicles to the apical membrane during the initial period of filling in order to prime the vesicles for fusion.

In contrast to control cells, or to those subjected to increased pressure for 20 min, umbrella cells exposed to 5 h of pressure underwent dramatic changes in morphology (Figure 2-2E). The depth of the cell was drastically reduced with a concomitant increase in cell length. In addition to these changes, the apical and basal surfaces were flattened and retained only a small degree of membrane folding. Some cells exhibited an exaggerated folding of the lateral membrane (Figure 2-2F), which is also observed in expanded bladders (153). Another striking feature of the 5 h stimulated samples was the paucity of discoidal vesicles in the cytoplasm (Figure 2-2F). This morphological change in the uroepithelium after 5 h of stimulation was consistent with an earlier study that examined umbrella cells in expanded bladders (153). These data not only confirmed the physiological nature of my system, but also demonstrated that the filling-induced morphological transition in umbrella cells required a considerable amount of time to occur.

### ***Quantification of changes in apical, basolateral, and vesicle surface area in response to pressure***

Changes in apical surface area as determined by capacitance are only estimates and do not provide any information about the source of added membrane. Further, some of these changes in capacitance may reflect alterations in basolateral surface area. Therefore, an alternative experimental method to quantify changes in apical, basolateral, and vesicle surface area was sought. To do this, I analyzed the tissue by stereology, a statistical analysis that calculates 3-



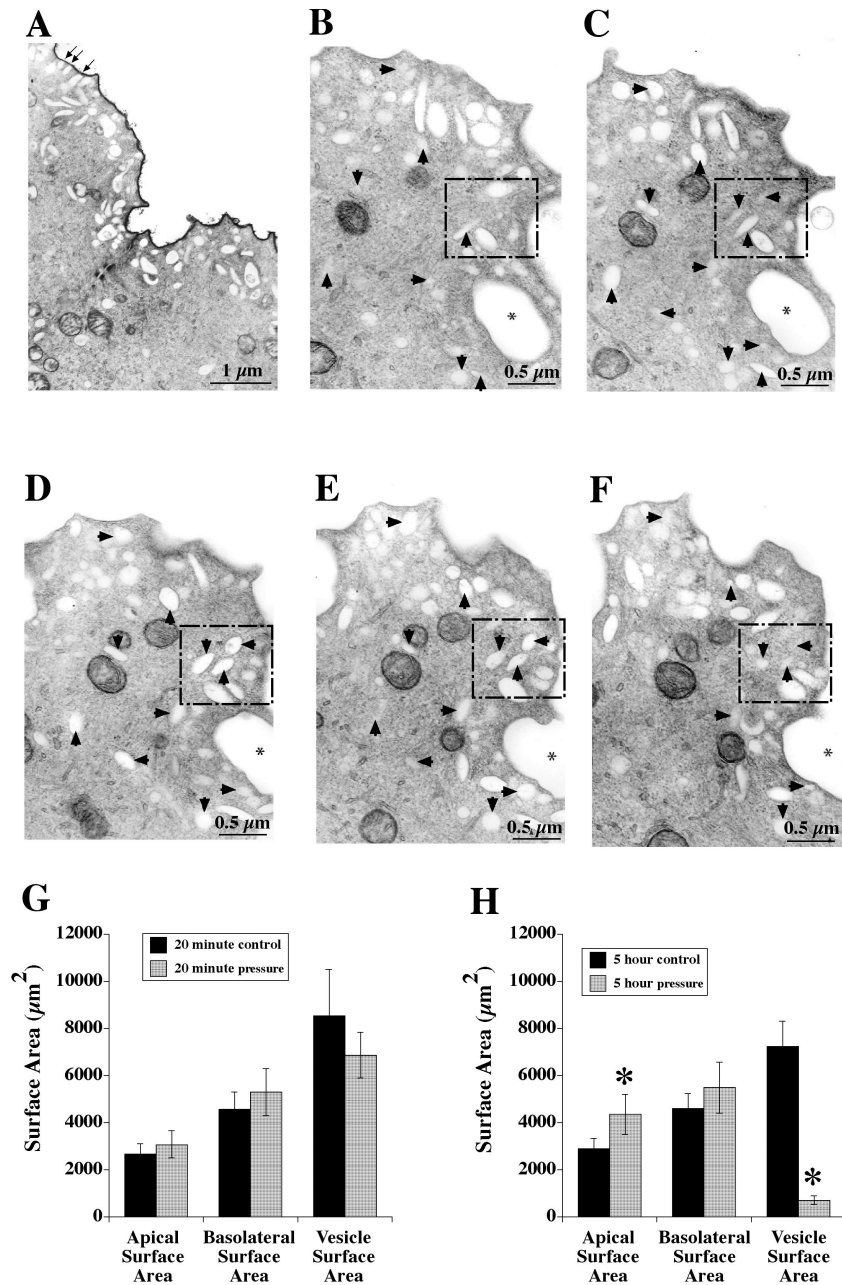


*Figure 2-3. Stereological analysis of umbrella cells and determination of vesicle/membrane continuity.* (A) Mounted bladder tissue was fixed in the presence of 0.01% (wt/vol) ruthenium red and processed for TEM. Arrows point to discoidal vesicles that are in proximity, but not continuous with the apical membrane. (B-F) Serial sections of an umbrella cell reveal the discontinuity of vesicles with each other and the plasma membrane. Arrowheads depict individual discoidal vesicles as they appear and disappear within the sections. The dashed box surrounds an area of clustered discoidal vesicle that remain distinct from one another in all sections. A large plasma membrane-associated vesicle is marked with an asterisk. Uroepithelium was incubated in chambers for 20 min with pressure or without (G) or for 5 h with pressure or without pressure (H). The apical, basolateral, and vesicle surface area were determined. Shown is mean  $\pm$  SEM (n=50). Values that are significantly different (p<0.05) from matched control values are marked with an asterisk.



dimensional geometric parameters (volume and surface area) based on multiple 2-dimensional images (tissue sections) (81).

First, it was necessary to demonstrate that a stereological analysis could accurately distinguish between the apical membrane and the vesicular membrane pools. Indeed it has been argued that many of the vesicular structures observed by TEM are actually continuations of the plasma membrane that only appear to be separate structures based on the plane of the cross section (120). Obviously, this visual artifact would render my stereological analysis ineffective for measuring changes in surface area of either membrane pool. Therefore, to confirm that the vesicular structures observed by TEM are distinct from the plasma membrane, bladder tissue was incubated for 20 min without stimulus and then fixed in the presence of ruthenium red, a membrane impermeant stain used to distinguish between the plasma membrane (including its invaginations) and structures that are distinct from the plasma membrane (92). In tissue that was incubated with ruthenium red, none of the vesicles acquired the stain (Figure 2-3A), including those vesicles that closely abutted the plasma membrane (arrows). These data clearly demonstrated that the vesicular structures represent a distinct pool of membrane that is not in continuity with the apical surface.

It has also been proposed that the vesicles are not distinct from one another but instead form a large interconnected network of tubular canals (120). To confirm that the vesicles are individual and distinct intracellular structures, bladder tissue was mounted in the chambers for 20 min without stimulation, fixed, and processed for TEM. The tissue was serial sectioned and the sections were ordered successively to allow tracking of individual vesicles as they appeared and disappeared within the cytoplasm of a single cell. Figures 2-3B to 2-3F displays an example of 5 TEM micrographs taken from the apical portion of an umbrella cell. Each arrowhead tracks an

individual vesicle as it appears and then fades from view. Analysis of many areas where vesicles were clustered together (dashed box), showed no fusion of individual vesicles. In addition, all vesicular structures remained separate from the plasma membrane in all sections examined with the exception of occasional infoldings of the plasma membrane that appeared as much larger vacuolar structures. An example of the latter is marked by the asterisks in Figures 2-3B and 2-3C. Taken together, these results confirm that the vesicles are individual, intracellular structures that are distinct from the apical surface.

Next, I quantified the apical, basolateral, and vesicle surface areas of the umbrella cells in 20 min and 5 h control samples, or tissue that had been exposed to increased hydrostatic pressure for 20 min or 5 h. In 20 min control samples, the average apical cell surface area was  $\sim 2700 \mu\text{m}^2$ , the basolateral surface area was measured at  $\sim 4600 \mu\text{m}^2$  and the vesicles occupied  $\sim 8500 \mu\text{m}^2$  of surface area (Figure 2-3G). Thus the surface area of the vesicles in control conditions was more than 3 times the surface area of the apical membrane. These results clearly indicated that the cells possess a tremendous reserve capacity to increase apical surface area via the fusion of vesicles with the apical membrane. Relative to controls, the samples exposed to mechanical stimulus for 20 min exhibited no significant changes in any of the 3 parameters. These data were consistent with the morphological observations described above but were inconsistent with the capacitance data (see Chapter 2 Discussion).

After 5 h of pressure treatment, the apical surface area was increased approximately 50% over the matched control ( $\sim 2900 \mu\text{m}^2$  to  $\sim 4300 \mu\text{m}^2$ ) with no significant change in basolateral surface area (Figure 2-3H). These results were consistent with the capacitance data and indicated that a considerable amount of membrane was added to the apical surface in response to increased pressure. However, when the changes in vesicle surface area were quantified after 5 h of pressure

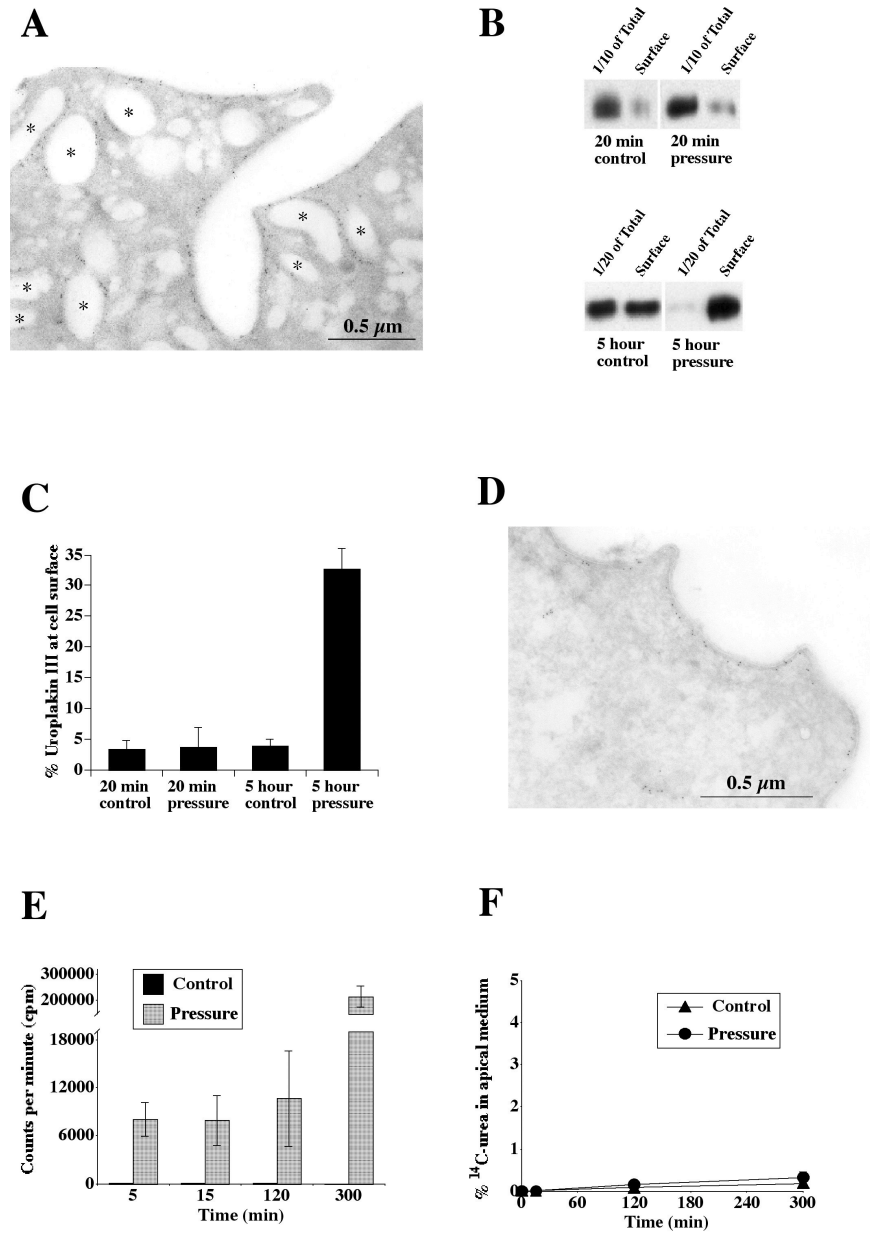


*Figure 2-4. Uroplakin III localization and pressure-induced increases in cell surface uroplakin III expression and metabolically labeled protein secretion. (A) Ultrathin cryosections of 5 h control tissue labeled with anti-uroplakin III antibody and secondary antibody conjugated to 5 nm gold. Asterisks denote examples of uroplakin III-positive vesicles. (B) Representative Western blots of total and cell surface uroplakin III expression in control or pressure-stimulated samples. (C) Quantification of relative expression of cell-associated uroplakin III at the apical surface for each condition. Shown is mean  $\pm$  SEM (n=5). (D) Samples were pressure-stimulated for 5 h and labeled with anti-uroplakin III antibody and secondary antibody conjugated to 5 nm gold. (E) Cells were pulsed with [ $^{35}$ S] cysteine/methionine, chased for 1 h, and stimulated with pressure or incubated without pressure for 5, 15, 120, or 300 min. Shown is average cpm present in apical medium at each time point  $\pm$  SEM (n=3). (F) Percentage of basally added [ $^{14}$ C]-urea that appeared in the apical medium after 0, 15, 120, or 300 min of pressure stimulation or absence of pressure. Shown is mean  $\pm$  SEM (n=3).*

treatment, it was found that the surface area of the vesicles decreased from  $\sim 7200 \mu\text{m}^2$  to less than  $1000 \mu\text{m}^2$  (Figure 2-3H). This revealed that the increase in apical surface area ( $\sim 1400 \mu\text{m}^2$ ) accounted for only a small fraction of the decrease in vesicle surface area ( $\sim 6200 \mu\text{m}^2$ ), indicating that an additional cellular event was occurring during the pressure response.

***Hydrostatic pressure increases cell surface expression of uroplakin III and induces apical secretion of metabolically-labeled proteins***

One prediction of the vesicle fusion model is that exposure to increased hydrostatic pressure will result in the delivery and incorporation of vesicle cargo into the apical membrane. A cargo molecule that can be utilized for this purpose is uroplakin III (UPIII), a 47 kD transmembrane component of both the apical membrane plaques and discoidal vesicles (Figure 2-4A) (143, 236). I demonstrated that UPIII was associated with the plasma membrane and discoidal vesicles of rabbit tissue by immunogold labeling with a UPIII antibody (Figure 2-4A).

To test the hypothesis that the discoidal vesicles were contributing to the increase in apical surface area, bladder tissue was left undisturbed or was subjected to increased pressure for either 20 min or 5 h. The cell surface was biotinylated, the cells were lysed and the biotinylated fraction was recovered with streptavidin beads. The amount of UPIII at the cell surface relative to the total cellular UPIII was determined by Western blot (Figure 2-4B). In control conditions, less than 5% of the total UPIII pool was present on the apical surface (Figure 2-4C). This is consistent with the large amount of surface area present in the vesicles relative to the apical membrane. This value remained unchanged after 20 min of stimulation. In contrast, after 5 h of stimulation, the fraction of UPIII at the cell surface increased to  $\sim 32\%$ , and the absolute amount at the surface increased  $\sim 67 \pm 18\%$  above that observed in controls. This latter value is consistent

with vesicle fusion and delivery of UPIII to the apical surface. In support of this, immunogold labeling demonstrated that UPIII was found at the plasma membrane in pressure-stimulated tissue (Figure 2-4D). As noted in Figure 2-2F, there was a significant decrease in the number of discoidal vesicles.

Also evident from the Western blot analysis was that the total cell expression of UPIII was considerably lower after 5 h of stimulation than in control. This effect was not simply due to a conformational change in the protein, as blotting for total cell surface proteins with streptavidin-HRP yielded a similar decrease in signal (see Figure 2-5E). This result indicated that a significant portion of the apical membrane including UPIII was being degraded during stimulation and is consistent with the decrease in vesicles observed both in this study and that of Minsky and Chlapowski (153).

To confirm that exocytosis was occurring throughout the 5-hour pressure period, secretion of metabolically-labeled proteins was measured over time. Unlike proteins anchored to the membrane, secreted proteins are not efficiently re-internalized after reaching the apical surface and thus provide an alternative way to detect exocytosis. Growth hormone, a secretory protein, has previously been localized to discoidal/fusiform vesicles (113). Tissue was radiolabeled with  $^{35}\text{S}$ -cysteine/methionine for 30 min and chased for 1 hour to label secretory proteins. The tissue was then stimulated for 5, 15, 120 or 300 min or incubated without pressure as a control and the amount of radioactivity in the apical medium was determined. In control tissue, the radioactivity detected in the apical medium was <100 counts per min (cpm) regardless of the duration of incubation indicating that little secretion occurred under these conditions (Figure 2-4E). In contrast, within 5 min of stimulation the apical cpm measured  $7,980 \pm 2100$  and this amount increased to  $214,687 \pm 40,252$  cpm after 5 h. This secretion was completely

blocked by adding 10  $\mu\text{g/ml}$  brefeldin A (data not shown), demonstrating a bona fide membrane trafficking event rather than non-specific release.

Hydrostatic pressure also stimulated significant release of secretory proteins into the basolateral chamber (data not shown). To further ensure that the apical secretion I observed was not the result of paracellular diffusion of secretory proteins from the basolateral to apical chamber,  $^{14}\text{C}$ -urea was added to the basolateral chamber and the appearance of radioactivity in the apical chamber was determined in control or stimulated tissue. In either case the amount of  $^{14}\text{C}$ -urea that crossed the cells was  $<0.4\%$  after 5 h of stimulation, demonstrating that the integrity of the umbrella cell layer was not compromised (Figure 2-4F). Apical to basolateral diffusion of  $^{14}\text{C}$ -urea was also determined and was not significantly different from basolateral to apical diffusion (data not shown). If the umbrella cell layer was disrupted by pressure stimuli, increased  $^{14}\text{C}$ -urea flux would occur via paracellular pathways. Taken together, these results confirmed that hydrostatic pressure induces a rapid and continual secretion of protein and that this secretion represents a genuine exocytic event.

### ***Hydrostatic pressure induces endocytosis at the apical surface of umbrella cells***

The stereological analysis revealed that after 5 h of exposure to hydrostatic pressure the increase in apical surface area accounted for only a small fraction of the loss in vesicle surface area. Furthermore, the biochemical data indicated that UPIII was degraded during the 5 h of stretch. Therefore, I hypothesized that membrane added to the apical surface during pressure stimulation was being endocytosed and degraded.

To test whether increased pressure induced endocytosis, the tissue was mounted in the modified Ussing chambers and the apical cell surface was biotinylated at  $4^\circ\text{C}$  with sulfo-*N*-

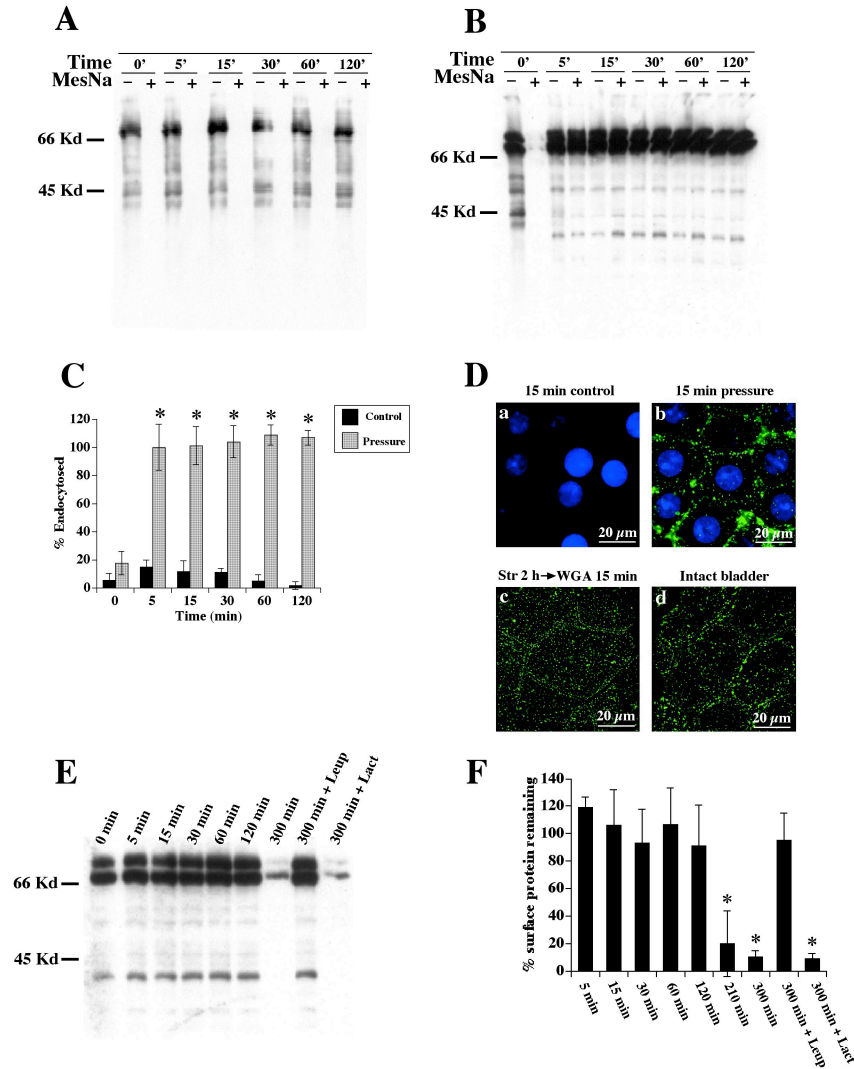


**Figure 2-5. Effect of pressure on endocytosis.** Surface of umbrella cells were biotinylated and incubated for 0, 5, 15, 30, 60, or 120 min without pressure (A) or with pressure (B). MESNA-protected biotinylated proteins were isolated and Western blots were probed with streptavidin-HRP. Representative blot of control tissue (A) shows no visible endocytosis by the lack of signal in MESNA-treated lanes. Pressure-stimulated tissue (B) exhibits large MESNA-protected signal, indicating endocytosis. (C) Quantification of endocytosis in control and stimulated tissue. Shown is mean  $\pm$  SEM (n=5). Values that are significantly different (p<0.05) from matched control values are marked with an asterisk. (D) WGA-FITC was internalized for 15 min in control (no pressure) tissue (a) or pressure-stimulated (b) tissue. Surface-bound WGA-FITC was removed by incubation at 4 °C with *N*-acetyl glucosamine, and the samples were fixed, stained with 4,6-diamidino-2-phenylindole, and then examined by epifluorescence microscopy. A projection of digitally deconvoluted sections is shown. (Dc) Bladder cells were stimulated for 2 h with pressure, WGA-FITC was added to the chamber and the samples stimulated for an additional 15 min. Surface WGA-FITC was removed, the samples were fixed, and then examined in a confocal microscope. A projection of XY sections is shown. (Dd) WGA-FITC was added to an excised but otherwise intact bladder for 15 min. Surface WGA-FITC was removed, the samples were fixed, and then examined in a confocal microscope. A projection of multiple XY section is shown. (E) Apical surface proteins were biotinylated and the tissue was stimulated for 0-300 min. The cells were lysed and biotinylated proteins detected by probing Western blots with streptavidin-HRP. Treatment with 40  $\mu$ M leupeptin (Leup) prevented the degradation, whereas lactacystin (Lact) had no effect. (F) Quantification of apical membrane protein degradation upon pressure treatment. Values are relative to pressure-stimulated tissue biotinylated at t=0. Shown is mean  $\pm$  SEM (n=4). Values that are significantly different (p<0.5) from control (no pressure) tissue at t=0 are marked with an asterisk.

hydroxysuccinimide (NHS)-S-S-biotin to label surface proteins. Several protein species were biotinylated (Figure 2-5A). The major protein species was rabbit albumin, which migrated with a molecular weight in the 67-70 kDa range. Several smaller molecular weight species were also detected, one of which was confirmed to be UPIII by probing blots of biotinylated proteins with anti-UPIII antibodies (data not shown). Exposing the blot for longer periods of time also revealed that other protein species were biotinylated including proteins that migrated around 15, 27 and 28 kDa (data not shown), which are the molecular weights of uroplakins II, Ia and Ib, respectively (235). After biotinylation, the tissue was warmed and stimulated for 0-120 min or incubated for the same amount of time undisturbed as a control. The internalized biotin-labeled proteins were detected by treating cells with the membrane impermeant reducing agent MESNA (see Materials and Methods).

In control cells, the MESNA treatment removed essentially all of the biotin regardless of the duration of incubation (Figure 2-5A). This showed that little or no endocytosis occurred. In contrast, stimulated cells exhibited a large MESNA-protected signal after 5 min, demonstrating that a significant amount of the surface membrane was rapidly internalized (Figure 2-5B). The quantification of this and other blots indicated that nearly 100% of the labeled membrane was endocytosed within 5 min of stimulation (Figure 2-5C) and this value remained constant over a 2 h period of incubation. The latter data indicated that in the time frame examined, little recycling of biotinylated apical proteins occurred following endocytosis.

WGA-FITC, which binds to sialic acid and *N*-acetyl glucosamine-modified proteins and lipids on the apical surface of the umbrella cells (70), was used as an alternative marker of endocytosis. The lectin was included in the apical half of the Ussing chamber and the tissue was then stimulated for 15 min or incubated without stimulation for the same amount of time. After



the incubation, surface-bound WGA-FITC was removed with *N*-acetyl glucosamine treatment at 4°C and the internalization of WGA-FITC was determined by fluorescence microscopy. No uptake was observed in control (unstimulated) samples either after 15 min (Figure 2-5Da) or after 5 h (data not shown). Cells stimulated for 15 min exhibited a significant amount of fluorescence in punctate structures, consistent with uptake into vesicular structures (Figure 2-5Db). Confocal microscopy verified that the endocytic structures were localized to the apical cytoplasm of the umbrella cells and that no staining was observed in the intermediate cell layer. To assess whether endocytosis continued throughout the stimulation period, WGA-FITC was added to the apical chamber of the preparations 2 h or 5 h after the application of pressure. Uptake of WGA-FITC was observed under both conditions (the data for uptake after 2 h is shown in Figure 2-5Dc).

As final confirmation that hydrostatic pressure stimulates endocytosis in bladder umbrella cells I filled excised but otherwise intact bladders with buffer containing WGA-FITC for 15 min at 37°C. The mucosal surface was treated to remove cell surface lectin, fixed, and then imaged by immunofluorescence microscopy. Again, significant uptake of lectin was observed in the umbrella cell population (Figure 2-5Dd). The latter observation is consistent with earlier experiments that showed uptake of fluid-phase markers in bladders that were emptied and then filled with fluid-phase marker (95, 175). Although these original observations were taken as evidence of uptake following voiding, filling the bladder mechanically stimulates the tissue, and the internalization previously observed is likely to be the pressure-regulated endocytosis described in this study.

### *The endocytosed membrane is delivered to lysosomes*

Having established that hydrostatic pressure induced apical membrane endocytosis, I next examined the hypothesis that internalized membrane was being degraded. Accordingly, the kinetics of degradation was determined by biotinylating the cell surface at 4°C and subsequently exposing the tissue to increased pressure for 5 to 300 min. After each time point, the tissue was lysed, the cohort of biotinylated proteins was isolated and the proteins were separated by SDS-PAGE, transferred to membranes and probed with streptavidin-HRP (Figure 2-5E). The fraction of protein remaining after each time point relative to the starting amount was quantified (Figure 2-5F). The total amount of biotinylated proteins remained constant for up to 120 min of stimulation. However, by 210 min there was a significant decrease in protein to ~20% of the starting value and by 300 min the protein levels were reduced to ~9% (Figure 2-5F). This result was consistent with my earlier experiment with UPIII and indicated that the apical membrane proteins were being degraded.

Two mechanisms can account for degradation within cells; delivery to lysosomes or proteasomes. To discriminate between the two pathways, the apical cell surface was biotinylated at 4°C, and the tissue was mechanically stimulated for 5 h in the presence of 40 µM leupeptin to block lysosomal degradation (106). Consistent with lysosomal delivery, incubation with leupeptin inhibited the degradation that was observed in cells stimulated without the drug treatment (Figure 2-5E and 2-5F). In order to rule out the possibility of proteasomal-mediated degradation, uroepithelial cells were treated with 10 µM lactacystin to inhibit proteasome function (60). Lactacystin treatment had no effect on the degradation of apical membrane proteins (Figure 2-5F), confirming that degradation was via a lysosomal-mediated pathway.

These data supported our hypothesis that the internalized membrane was delivered to lysosomes where it was degraded.

### ***The filling response is a cAMP-mediated event***

In other mechanically sensitive tissues, mechanical stimulation is associated with elevated levels of the second messenger cAMP (182, 188, 227). To ascertain the role of cAMP in the uroepithelium, I measured intracellular levels of cAMP in control and pressure-stimulated tissue over time. Mechanically stimulating the tissue caused the intracellular levels of cAMP to rise more than 2-fold within 15 min (Figure 2-6A). These levels remained elevated throughout the 5-h period of stimulation, implicating cAMP in the pressure response. To test the effects of elevating cAMP in the umbrella cells, I incubated the tissue with 10  $\mu$ M forskolin and 500  $\mu$ M 3-isobutyl-1-methylxanthine (IBMX) to raise intracellular cAMP levels. Unexpectedly, an unusually large increase of 120% in capacitance was observed over a 5 h period, versus the 50% change observed with pressure stimulation alone (Figure 2-6B). Incubating the tissue with 8-Br-cAMP, a membrane permeant analog of cAMP, induced a similar effect as forskolin/IBMX (data not shown) and treatment with di-deoxy forskolin, a nonfunctional forskolin analog, had no effect on capacitance (data not shown). I also explored the effect on capacitance when forskolin was added to pressure-stimulated tissue. The response was similar to control tissue treated with forskolin but the net rise in capacitance was slightly greater (~140% versus ~120%). The above data demonstrated that cAMP dramatically altered membrane trafficking at the apical surface of umbrella cells.

A likely effector of cAMP is protein kinase A (PKA), the target of the H89 kinase inhibitor (68). In pressure stimulated tissue treated with H89, the capacitance initially rose ~20%

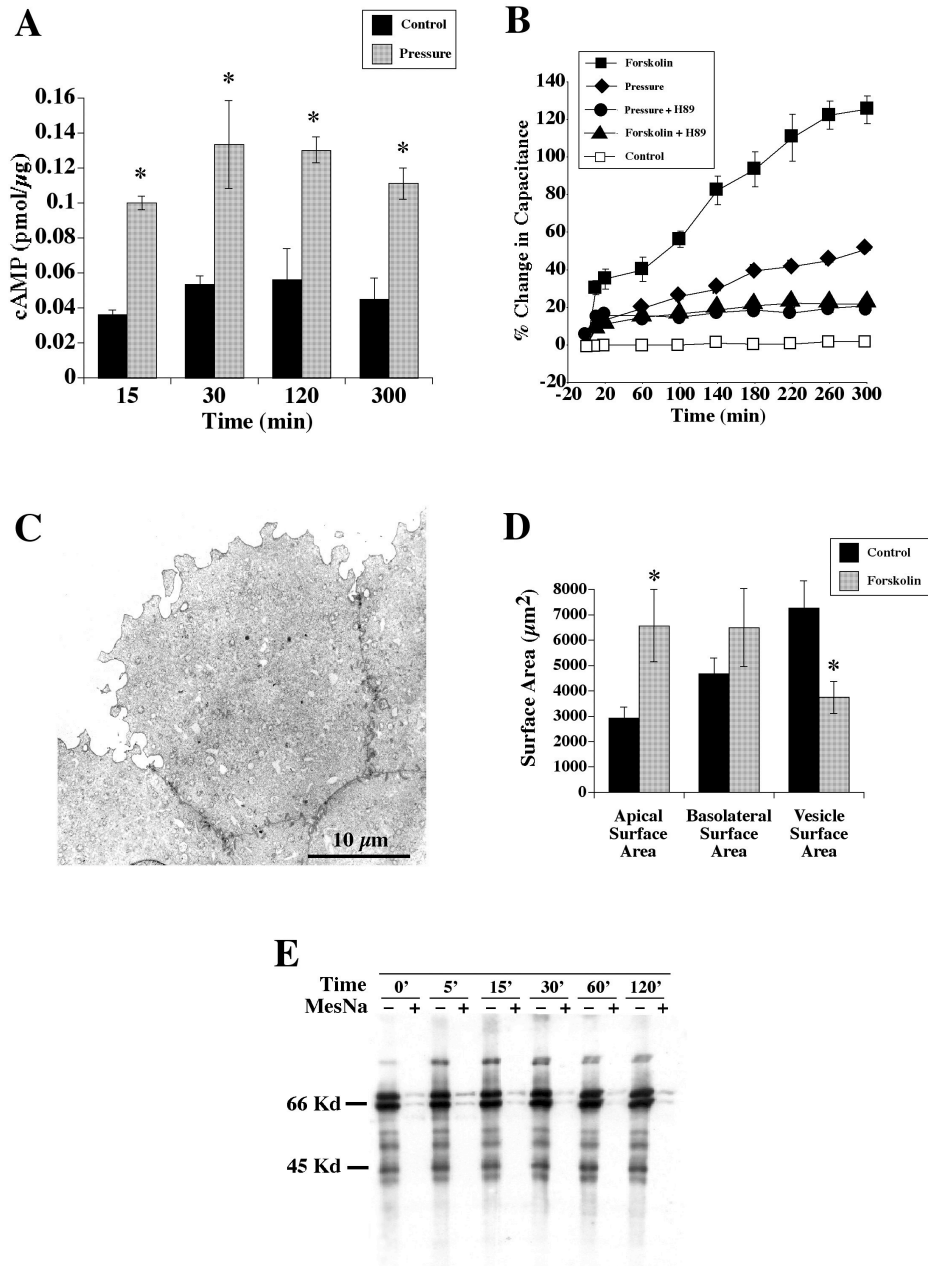


**Figure 2-6. Role of cAMP and PKA in the filling response.** (A) Intracellular levels of cAMP were measured in control cells (no pressure) and cells stimulated with pressure after 15, 30, 120, or 300 min. Shown is mean  $\pm$  SEM (n=4). Values that are significantly different ( $p < 0.05$ ) from matched control values are marked with an asterisk. (B) Effects of forskolin and H89 on capacitance. Cells were treated with 10  $\mu$ M forskolin/500  $\mu$ M IBMX without pressure, treated with forskolin/IBMX and 10  $\mu$ M H89, or stimulated in the presence of 10  $\mu$ M H89 alone. For comparison, the capacitance readings from Figure 1 of pressure-stimulated and non-stimulated, control cells are shown. Shown is mean  $\pm$  SEM (n=6). (C) Effects of forskolin/IBMX on umbrella cell morphology. Tissue was treated with forskolin/IBMX without pressure for 5 h and processed for TEM. (D) Changes in surface area resulting from forskolin/IBMX treatment. Tissue was treated with forskolin/IBMX and stereological analysis was performed as described. Control surface areas are shown for comparison, n=50. Values that are significantly different ( $p < 0.05$ ) from matched control values are marked with an asterisk. (E) Endocytosis was determined in forskolin/IBMX-treated cells. Shown is representative Western blot of internalized proteins after 0, 5, 15, 30, 60, or 120 min with or without MESNA treatment.

but failed to increase any further, implicating PKA as a possible effector of the filling response (Figure 2-6B). Moreover, the rise in capacitance observed after incubating the tissue in forskolin/IBMX was also significantly inhibited when the tissue was pretreated with H89. These findings underscored the importance of cAMP and PKA in the regulation of mucosal surface area and indicated that cAMP modulated, in part, the response of the umbrella cell to hydrostatic pressure.

The significant changes observed in capacitance when the tissue was incubated with forskolin/IBMX prompted me to examine the morphology of the umbrella cells after forskolin treatment and to assess the effect of these drugs on endocytosis. Accordingly, I treated undisturbed umbrella cells with forskolin/IBMX for 5 h and processed the tissue for TEM. Treatment with forskolin/IBMX (Figure 2-6C) elicited exaggerated convolutions in the apical cell membranes, supporting the large increases observed in capacitance. Stereological measurements confirmed the capacitance results (Figure 2-6D). The apical surface area of forskolin-treated cells increased to  $\sim 6,500 \mu\text{m}^2$ , more than double the apical surface area of an unstimulated umbrella cell. No significant changes in basolateral surface area were detected. There was a significant decrease in vesicle area that accompanied the forskolin/IBMX-induced fusion. However, unlike stimulated tissue a significant amount of vesicle area remained. Lastly, I measured the effects of forskolin/IBMX on endocytosis. The amount of MESNA-protected biotin remained constant over a 2 h time period, demonstrating that no endocytosis occurred (Figure 2-6E). This result indicated that forskolin may be modulating apical surface area by means of discoidal vesicle exocytosis without affecting apical membrane endocytosis.

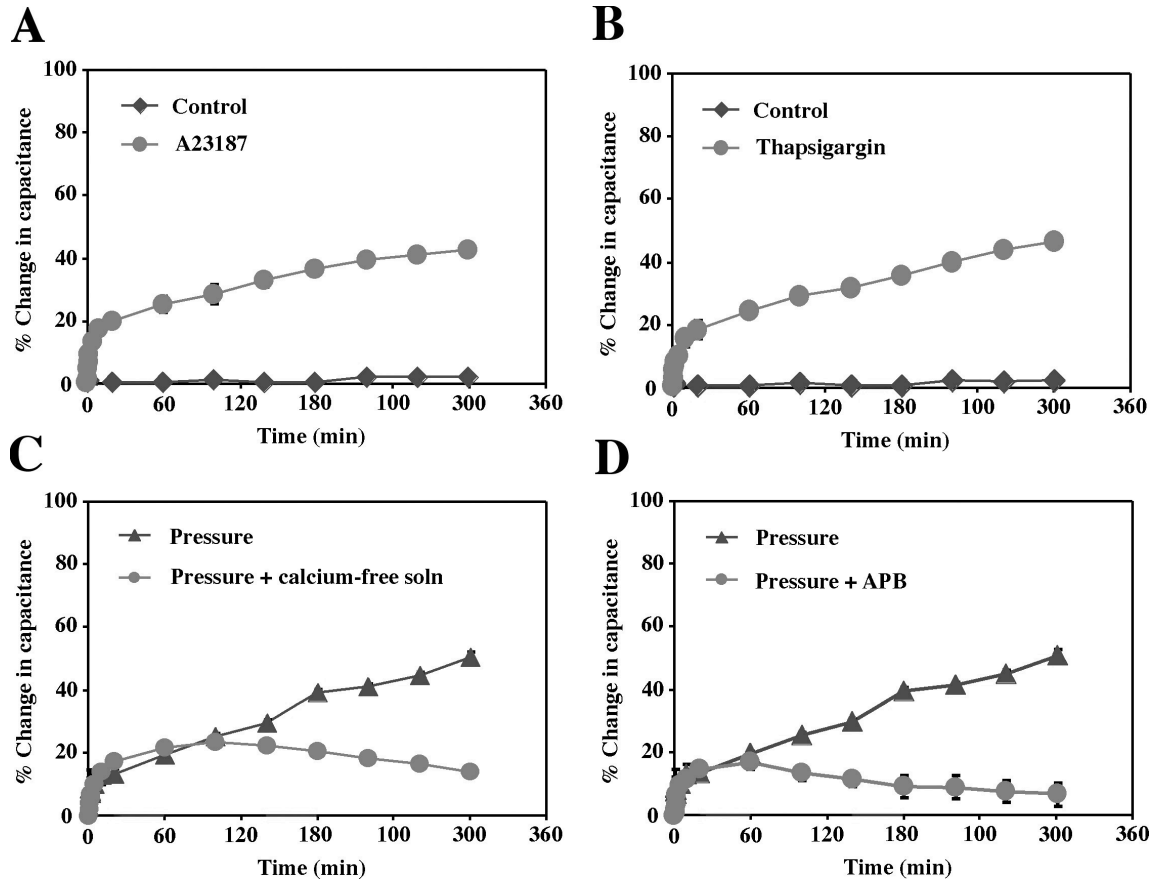


Figure 2-7. Effects of altering cytoplasmic  $Ca^{2+}$  on changes in membrane capacitance. (A) Bladder was mounted in the chamber and allowed to equilibrate, and at the zero time point 1  $\mu$ M A23187 was added to both hemichambers and the tissue was incubated in the absence of increased pressure. Control tissue was left untreated. Changes in capacitance were monitored over time. (B) Mounted bladder tissue was left untreated (control) or treated at the zero time point with 10  $\mu$ M thapsigargin (added to both hemichambers) in the absence of increased pressure. Changes in capacitance were monitored over time. (C) Following equilibration, the normal Krebs solution was isovolumetrically replaced with Krebs solution (control) or Krebs solution lacking  $Ca^{2+}$ . At  $t=0$ , hydrostatic pressure was increased and changes in capacitance were monitored over time. (D) Following equilibration, tissue was either left untreated (control) or pretreated for 15 min with 75  $\mu$ M APB (APB). At  $t=0$ , hydrostatic pressure was increased and changes in capacitance were monitored over time. Data are means  $\pm$  SEM (n=6).

### ***Hydrostatic pressure-induced changes in surface area is Ca<sup>2+</sup>-dependent***

Most regulated secretory events are governed by changes in cytoplasmic Ca<sup>2+</sup> (17). Increases in cytoplasmic Ca<sup>2+</sup> can result from opening of conductive pathways across the plasma membrane (e.g., opening of stretch-activated ion channels) or release of Ca<sup>2+</sup> from intracellular stores. To determine whether Ca<sup>2+</sup> was important in signaling hydrostatic pressure-induced changes in bladder umbrella cells the following experiments were performed.

Addition of 1 μM A23187, a Ca<sup>2+</sup> ionophore, to isolated rabbit uroepithelium caused a significant increase in membrane capacitance even in the absence of hydrostatic pressure (Figure 2-7A), indicating the presence of a Ca<sup>2+</sup>-sensitive pathway for stimulation of exocytosis in umbrella cells. Similarly, treatment with 10 μM thapsigargin, which raises cytoplasmic Ca<sup>2+</sup> by inhibiting Ca<sup>2+</sup> uptake via the ER-localized Ca<sup>2+</sup>-ATPase, also resulted in an increase in capacitance in these cells (Figure 2-7B). The hydrostatic pressure-induced changes in exocytosis were inhibited in cells treated with 75 μM 2-aminoethoxydiphenylborate (APB), which blocks IP<sub>3</sub>-induced Ca<sup>2+</sup> release from the ER, or cells in which Ca<sup>2+</sup> was removed from the extracellular Krebs solution (Figure 2-7C and 2-7D). In the latter case, the cells retained high TER. However, it was not possible to include the Ca<sup>2+</sup> chelator EGTA in the extracellular fluid, as it resulted in a rapid loss of TER.

## ***DISCUSSION***

### ***Hydrostatic pressure-induced changes in the apical surface area of umbrella cells***

The ability of the bladder to retain urine requires a barrier epithelium that can accommodate large variations in urine volume. At the cellular level this is likely accomplished by changes in umbrella cell architecture and surface area. The latter is thought to be modulated by discoidal vesicle exocytosis (134, 135, 153). The underlying intermediate and basal cell layers also undergo morphological transitions, but much less are known about their cellular biology (96).

The data presented in this chapter confirms that exposure to hydrostatic pressure increases the apical surface area of umbrella cells, and these changes are likely mediated by discoidal vesicles. Mechanical distention of the uroepithelium resulted in an ~50% increase in capacitance after a 5 h period of stimulation. This large change in capacitance is consistent with, but significantly greater than the previous observation that short-term mechanical bowing of the uroepithelium increased capacitance by ~18% (135). Furthermore, a stereological analysis confirmed that the apical surface area of the umbrella cells increased by 50%, while there was no statistically significant change in basolateral surface area. The stereological analysis also revealed that pressure stimulation was accompanied by a 4-fold decrease in vesicle surface area. These data concur with previous observations that the numerical density of discoidal vesicles was decreased in expanded versus contracted bladders (153). Biotinylation experiments demonstrated that both the relative and absolute amount of uroplakin III (UPIII) (a “cargo” molecule found in discoidal vesicles) at the cell surface significantly increased after 5 h of stimulation, consistent with discoidal vesicle fusion. Lastly, secretion of metabolically labeled proteins confirmed a rapid and significant apical secretion in pressure-stimulated tissue that increased over time. While exocytosis was observed shortly after stimulation, the majority of



exocytosis occurred between the 2 h and 5 h period. Although the above results are consistent with the fusion of discoidal vesicles during exposure to increased pressure, I cannot rule out that some of the observed changes in surface area were the result of other membranous organelles fusing with the apical surface of the umbrella cells.

Release of metabolically labeled secretory proteins was observed within 5 min of mechanical stimulation, indicating that hydrostatic pressure rapidly stimulated exocytosis in umbrella cells. Whether these early exocytic events result in a change in the apical surface area of these cells is unclear. I observed a small increase (~15%) in capacitance within the first 20 min of hydrostatic pressure stimulation. However, a stereological analysis showed no significant change in apical, basolateral, or vesicle surface area. Furthermore, the amount of UPIII at the cell surface was unchanged after 20 min of stimulation. Because hydrostatic pressure stimulates ion transport (see Chapter 3), the small capacitance change I observe may be insignificant (76). Alternatively, the area change may be too small to be detected by either stereology or biotinylation.

### ***Hydrostatic pressure stimulates apical endocytosis in umbrella cells***

In the classical model, vesicle endocytosis is proposed to occur only upon voiding (i.e. after release of pressure) (95, 175). The data in this chapter is inconsistent with this aspect of the model. Most notably, I observed that essentially all biotinylated apical membrane proteins, general markers of the apical plasma membrane, were endocytosed within 5 min of increased hydrostatic pressure. However, I cannot rule out that only a sub-population of apical membrane is biotinylated and that I am overestimating the amount of endocytosis. Moreover, I observed

uptake of WGA-FITC in stimulated preparations of isolated uroepithelium or upon filling excised but otherwise intact bladders.

Despite significant amounts of endocytosis, there was little apparent change in apical surface area during the first 20 min of stimulation thus indicating that the amount of endocytosis must have been balanced by roughly equivalent amounts of exocytosis. This rapid exocytosis could be a result of either recycled membrane or delivery of newly synthesized vesicle membrane. Because apical surface area increased over the longer time scale, the rate of exocytosis must ultimately outpace the rate of endocytosis. This is supported by the large increase in secretion between 2 h and 5 h of stimulation. Nonetheless, endocytosis continues throughout the entire period of stimulation as evidenced by uptake of WGA-FITC at 2 h and 5 h after applying hydrostatic pressure.

Although it may seem counterintuitive that exocytosis and endocytosis are occurring simultaneously during filling, these two processes occur constitutively and simultaneously in all cells, even under resting conditions (91, 160). Coupled exocytosis/endocytosis likely plays a key role in fine-tuning the changes in umbrella cell surface area as a result of exposure to hydrostatic pressure and/or other external stimuli (see Chapter 2 Discussion below). Furthermore, rapid endocytosis/exocytosis would provide the umbrella cells with a means of quickly replacing old or damaged surface plaques with new ones in preparation for imminent lumen expansion. In this regard, it has recently been shown that expression of UPIII, a major plaque constituent, is required for the maintenance of bladder barrier function (104). Finally, exocytosis decreases membrane tension (158), which is compensated for by endocytosis. Regardless of its function, endocytosis clearly represents a major pathway of membrane trafficking during filling and its specific functions and regulations will be addressed in future studies.

In the present analysis I have not directly examined the events that occur when hydrostatic pressure is released. Because filling increases apical surface area, this added membrane must be endocytosed at some point after voiding. Minsky and Chlapowski observed that within 10 min after voiding, the number of discoidal vesicles in the umbrella cells increased by ~2-fold compared with the number of vesicles in distended bladders (153). This implies that some vesicles are replenished within a short period of time following filling. The increased number of discoidal vesicles could reflect apical membrane internalization and/or rapid delivery of newly synthesized vesicles from the Golgi (95). This assembly of vesicles in the Golgi is likely to be significant. Only a small fraction of discoidal/fusiform vesicles are labeled by apically endocytosed fluid or membrane markers indicating that they are primarily involved in exocytic traffic (4, 95, 175). Moreover, from these data it is evident that the amount of internalized membrane would be insufficient to replenish the surface area of the discoidal vesicles lost during filling.

#### ***Endocytosed membrane is delivered to lysosomes***

Discoidal vesicles or discoidal vesicle-derived membrane was previously observed in multivesicular bodies as well as lysosomes (4, 175). However, the extent of apical membrane entry into this pathway and the role that filling played in this process was previously unknown. I observed that upon internalization biotin-labeled apical surface proteins were eventually degraded. This proteolytic event was prevented by the lysosomal enzyme inhibitor leupeptin, but not by the proteasome inhibitor lactacystin. This finding is consistent with the decrease in vesicles observed in this study and that described previously (153). However, degradation was not apparent until some time after 2 h of pressure stimulation. In other cell types degradation can

proceed as quickly as 15-20 min after internalization and delivery to lysosomes usually occurs within 30-45 min of endocytosis (82). It is possible that either the delivery of endocytosed membrane to late endosomes/lysosomes is slow in umbrella cells or that exposure to hydrostatic pressure up regulates a pathway that results in enhanced degradation of discoidal vesicles. The latter possibility would explain the sudden change in protein signal after 120 min of stimulation. Alternatively, there may be some recycling of vesicle membrane that escaped detection.

### ***Role of cAMP in pressure-regulated exocytosis***

In addition to elucidating the dynamics of membrane trafficking in response to hydrostatic pressure, I have also gained insight into one of the signal transduction pathways that may regulate these trafficking events. The data in this chapter indicate that a cAMP-PKA pathway plays a role in the filling response. Increased amounts of cAMP were observed in pressure stimulated tissue and elevating the intracellular concentration of cAMP in undisturbed umbrella cells with forskolin/IBMX resulted in a >100% increase in apical cell surface area. These events were blocked by treatment with the PKA antagonist H89. Importantly, pressure-regulated changes in membrane capacitance were significantly decreased by H89, further confirming that the cAMP-PKA pathway is required for vesicle exocytosis. These results are consistent with the recent observation that cultured uroepithelial cells or bladder explants secrete tissue-type plasminogen activator and urokinase in a cAMP-dependent fashion (48), although the study did not examine the effects of hydrostatic pressure on secretion. The results of my experimentation have additional significance because they indicate that the surface area of umbrella cells can be regulated by external stimuli independent of pressure. These stimuli could come in the form of growth factors, hormones, or neurotransmitters present in the blood or released by the bladder-

associated musculature and nerves. Interestingly, some afferent neuronal processes terminate within the uroepithelium and umbrella cells apparently express surface receptors for various neurotransmitters (19). As such, the apical surface area of umbrella cells may be regulated by mechanical as well as exocrine/paracrine stimuli.

The dramatic increases in umbrella cell surface area mediated by cAMP occurred in the apparent absence of endocytosis. This observation underscores the importance of endocytosis in regulating umbrella cell apical surface area. While pressure stimulated endocytosis of the apical membrane, treatment with forskolin/IBMX without mechanical stimulus had no effect on endocytosis but resulted in a greater increase in surface area. These observations indicate that the response to pressure may involve at least two levels of regulation, one of which that operates by modulating intracellular levels of cAMP and the other that utilizes another uncharacterized mechanism. Other cellular events rapidly triggered by mechanical stimuli include stimulation of stretch-activated channels, activation of the integrin-associated focal adhesion kinase, phosphoinositide turnover, and autocrine release of growth factors (218). Some or all of these mechanosensory mechanisms could play an important role in signaling exocytosis/endocytosis in umbrella cells.

### ***Role of $Ca^{2+}$ in pressure-regulated exocytosis***

In this study I found evidence that  $Ca^{2+}$  may also play an important role in regulating hydrostatic pressure-regulated exocytic traffic. Artificially raising cytoplasmic  $Ca^{2+}$  by addition of thapsigargin or A23187 was sufficient to stimulate increases in capacitance, even in the absence of hydrostatic pressure. This is consistent with recent observations that secretion in isolated umbrella cells can be stimulated by A23187 (48). Importantly, I show in this study that

hydrostatic pressure-induced changes were inhibited when extracellular  $\text{Ca}^{2+}$  was lowered or if cells were treated with APB. These results indicate that hydrostatic pressure-induced exocytosis is dependent on  $\text{Ca}^{2+}$  entering the cell from the extracellular milieu, as well as intracellular release of  $\text{Ca}^{2+}$  from  $\text{IP}_3$ -sensitive stores in the ER. Additional work is necessary to confirm these results and to identify the downstream effectors of  $\text{Ca}^{2+}$  that modulate exocytic traffic in these cells.

In summary, findings presented in this chapter further elucidate the poorly understood process of mucosal surface area regulation in the uroepithelium during the filling process. The data not only shed light on the membrane trafficking that occurs in these cells, but also provide insight into the intracellular signal cascade that is responsible for this trafficking. Moreover, I have uncovered an additional pathway for apical endocytosis that is modulated by mechanical force. This discovery broadens our understanding of the effects of mechanical stimuli on membrane traffic especially in regard to the pivotal function of endocytosis in balancing the exocytic response of the cell. The coordinated balance between these two plasma membrane events in umbrella cells is likely to play a similarly important role in other cell types that are responsive to mechanical forces. In the following chapters, I will examine and discuss other cellular events that are rapidly triggered by hydrostatic pressure, including stimulation of pressure-activated ion channels (Chapter 3) and activation of membrane receptors that play important roles in mechanotransduction (Chapter 4).

## CHAPTER 3

### Hydrostatic pressure-regulated ion transport in bladder uroepithelium\*

#### *ABSTRACT*

The effect of hydrostatic pressure on ion transport in the bladder uroepithelium was investigated. Isolated rabbit uroepithelium was mounted in modified Ussing chambers and mechanically stimulated by applying hydrostatic pressure across the mucosa. Increased hydrostatic pressure led to increased mucosal-to-serosal  $\text{Na}^+$  absorption across the uroepithelium via the amiloride-sensitive epithelial sodium channel. In addition to this previously characterized pathway for  $\text{Na}^+$  absorption, hydrostatic pressure also induced  $\text{Cl}^-$  and  $\text{K}^+$  secretion into the mucosal bathing solution under short-circuit conditions, which was confirmed by a net serosal-to-mucosal flux of  $^{36}\text{Cl}^-$  and  $^{86}\text{Rb}^+$ .  $\text{K}^+$  secretion was likely via a stretch-activated non-selective cation channel sensitive to 100  $\mu\text{M}$  amiloride, 10 mM tetraethylammonium, 3 mM  $\text{Ba}^{2+}$ , and 1 mM  $\text{Gd}^{3+}$ . Hydrostatic pressure-induced ion transport in the uroepithelium may play important roles in electrolyte homeostasis, volume regulation, and mechanosensory transduction.

\*Reprinted from *American Journal of Physiology – Renal Physiology*, (2003, volume 285, pg. F651-F663), with permission by the American Physiological Society

## ***INTRODUCTION***

Cells are exposed to an array of physical forces, including compression, shear stress, and hydrostatic pressure, which occurs when bodily fluids push against the epithelium that lines the tubes and sacs that form many of the body's organs (10). Changes in these forces can result in alterations in cellular structure, function, gene expression, and membrane traffic (6, 45, 89, 228). A common response of cells exposed to mechanical stimuli is activation of stretch-activated ion channels. The first such channel described in detail is the stretch-activated non-selective cation channel of chick embryonic skeletal muscle (183), which is cation selective but discriminates poorly between  $\text{Na}^+$  and  $\text{K}^+$ . Since these initial studies, stretch-activated  $\text{K}^+$ ,  $\text{Cl}^-$ , and non-selective cation channels have been identified in many cell types, including erythrocytes, oocytes, fibroblasts, aortic endothelium, heart cells, kidney cells, muscle cells, and epithelial cells (89).

In the urinary tract, where cells experience shear stress and hydrostatic pressure, mechanosensitive ion channels may play an important role in volume regulation and ion homeostasis. For example, a stretch-activated cation-selective channel is found in the apical membrane of proximal tubule cells. This channel is permeable to  $\text{Ca}^{2+}$ ,  $\text{K}^+$ , and  $\text{Na}^+$  and is not gated by membrane potential or cytosolic  $\text{Ca}^{2+}$  (63), but its activity is dependent on changes in extracellular osmolarity. Mechanical stimulation of this channel (e.g., by cell swelling) could lead to cell volume regulation. In renal cortical collecting ducts, changes in hydrostatic pressure may increase the open probability, or number, of stretch-sensitive epithelial  $\text{Na}^+$  channels (ENaC), enhancing the rate of  $\text{Na}^+$  reabsorption (189). Moreover, the rate of  $\text{K}^+$  secretion by large conductance maxi-K channels in cortical collecting ducts is also affected by variations in intraluminal flow rates (233).



The lower urinary tract is also subject to mechanical stimuli; hydrostatic pressure increases as the bladder fills and decreases during bladder emptying. The cell type most directly affected by these changes is the umbrella cell. These large polygonal cells constitute the innermost layer of the uroepithelium and the combination of an impermeable apical membrane and high resistance tight junctions form an effective barrier to solute and ion permeability. Umbrella cells respond to mechanical stimuli in a number of ways including increasing surface area as well as ion transport (61, 135, 141, 214). Membrane “punching”, performed by rapidly increasing then decreasing hydrostatic pressure across the mucosal surface of the bladder uroepithelium, leads to increased ion conductance after 10-30 min (135, 141). The observed rise in ion conductance is contributed by the amiloride-sensitive ENaC as well as by an amiloride-insensitive non-selective cation channel (133, 140). Alternatively, ENaC activity can be acutely stimulated by removing fluid from the serosal side of bladder tissue mounted in an Ussing chamber, thereby increasing hydrostatic pressure across the mucosal surface of the bladder. In addition to Na<sup>+</sup> absorption, a K<sup>+</sup> secretory pathway, sensitive to the K<sup>+</sup> channel blocker tetraethyl ammonium (TEA), has been identified in resting bladder tissue (62), but the nature of this secretory pathway and whether it is stimulated by hydrostatic pressure has not been defined.

The goal of this chapter was to examine the possibility that like the upper urinary tract hydrostatic pressure stimulates multiple ion transport pathways in bladder uroepithelium. Rabbit uroepithelium was mounted in modified Ussing chambers and was then subjected to cycles of increased hydrostatic pressure while monitoring changes in short circuit current (I<sub>sc</sub>) and ion conductance. I found that in addition to hydrostatic pressure-induced Na<sup>+</sup> absorption across the uroepithelium there was also, under short-circuit conditions, hydrostatic pressure-induced parallel electrogenic Cl<sup>-</sup> and K<sup>+</sup> secretion into the mucosal chamber. Na<sup>+</sup> absorption was via the

previously described amiloride-sensitive ENaC while  $K^+$  secretion was probably via a nonselective cation channel sensitive to 100  $\mu$ M amiloride, TEA,  $Ba^{2+}$ , and  $Gd^{3+}$ . These results provide additional evidence that besides retaining urine, the mammalian bladder epithelium might play an important role in electrolyte homeostasis.

## **RESULTS**

### ***Increasing hydrostatic pressure across the mucosal surface of the uroepithelium is accompanied by increases in ion transport***

Because of its rapid effect, reversibility, and physiological relevance we used an adaptation of the hydrostatic pressure method to mimic bladder filling and emptying (61, 135). Rabbit uroepithelium was mounted in a modified Ussing chamber that allowed hydrostatic pressure to be increased then decreased across the mucosal surface of the tissue. Under control conditions, the uroepithelium exhibited a small basal  $I_{sc}$  of  $0.94 \pm 0.03 \mu A \cdot cm^{-2}$  and a conductance of  $\sim 0.1 mS \cdot cm^{-2}$  ( $\sim 10,000 \Omega \cdot cm^2$ ) (Figure 3-1A). These are well within the range of previously reported values for  $I_{sc}$  and conductance in the bladder uroepithelium (128, 136-138). Increasing hydrostatic pressure across the mucosal surface of the tissue resulted in an almost instantaneous  $\sim 5$ -fold increase in  $I_{sc}$  from  $0.94 \pm 0.03 \mu A \cdot cm^{-2}$  to  $4.20 \pm 0.21 \mu A \cdot cm^{-2}$ , indicating active ion transport accompanied the mechanical stimulus. Hydrostatic pressure was also accompanied by a significant increase in conductance to  $\sim 0.2 - 0.3 mS \cdot cm^{-2}$  (arrows in Figure 3-1A). The increased values for  $I_{sc}$  and conductance remained relatively constant during the 5-min period of increased hydrostatic pressure, and this was true when the pressure remained elevated for up to 60 min (data not shown). The change in  $I_{sc}$  and conductance were rapidly reversible and returned to near control levels when the pressure was decreased (arrowheads in Figure 3-1A).

The changes in  $I_{sc}$  and conductance were highly reproducible and were seen when tissue was subjected to multiple cycles of raising then lowering the hydrostatic pressure head (Figure 3-1A). The change in  $I_{sc}$  at each pressure cycle was relatively constant, as was the basal  $I_{sc}$  value when the hydrostatic pressure was released. In contrast, the conductance values decreased during periods of increased hydrostatic pressure and during the intervening periods following the release

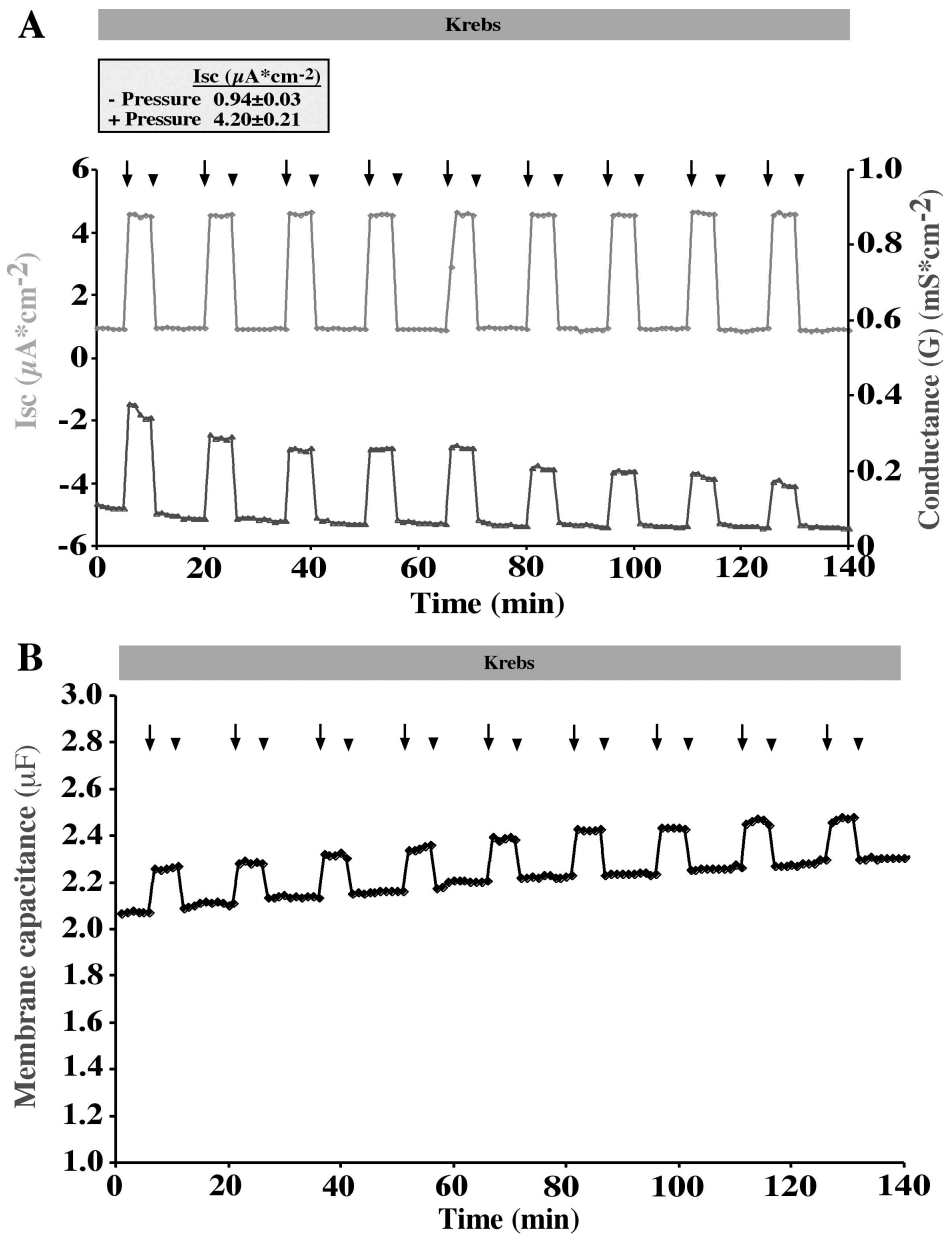


*Figure 3-1. Hydrostatic pressure-induced changes in Isc, conductance, and membrane capacitance. (A) Uroepithelium was mounted in modified Ussing chambers and equilibrated for 30 to 60 min. After the equilibration period, the tissue was subjected to increased hydrostatic pressure for 5 min (arrows) followed by release for 10 min (arrowheads). This experimental treatment was repeated nine times. A representative tracing is shown with Isc in upper trace (grey) and conductance in lower trace (black). The average Isc value before and after increased hydrostatic pressure is shown as mean  $\pm$  SEM (values are from six separate experiments). The grey bar above the graph indicates the bathing solution used during the experimental protocol. In this case it was Krebs solution. (B) Membrane capacitance was measured in Krebs solution. The start of the period of a 5-min increase in hydrostatic pressure are marked by arrows, while the start of the 10-min period of recovery are marked by arrowheads. Shown is a representative tracing from three separate experiments.*

of hydrostatic pressure, leading to a 50% reduction in conductance by the end of the experiment. The cyclical increase in hydrostatic pressure caused no apparent damage to the tissue as the conductance values returned to baseline levels immediately upon release of hydrostatic pressure and as noted, decreased as the experiment progressed. Furthermore, I have previously shown by transmission electron microscopy that epithelium exposed to hydrostatic pressure remains intact (see Chapter 1 and 2) and urea permeability remains low and unchanged (see Chapter 2).

Hydrostatic pressure induces increases in the apical, but not basolateral, surface area of umbrella cells (214). Because increases in surface area would result in an overestimation of changes in  $I_{sc}$  and conductance I measured hydrostatic pressure-induced changes in membrane capacitance, which are proportional to changes in surface area (where  $1 \mu\text{F} \approx 1 \text{cm}^2$  of surface area) (139). However, the cyclical increases in hydrostatic pressure were accompanied by only a small ( $\sim 10\%$ ) increase in capacitance (Figure 3-1B), indicating that the  $I_{sc}$  values ( $\mu\text{A}\cdot\text{cm}^{-2}$ ) and conductance values ( $\text{mS}\cdot\text{cm}^{-2}$ ) obtained for tissue exposed to hydrostatic pressure tissue shown in Figure 3-1A, and in the subsequent figures described below, are overestimated by  $\sim 10\%$ . Unfortunately, the system I routinely use for monitoring  $I_{sc}$  does not allow for the simultaneous measurement of  $I_{sc}$ , conductance, and capacitance. Similar changes in capacitance were obtained using impedance analysis that employed sinusoidal current waveforms (data not shown).

### ***Hydrostatic pressure increases $\text{Na}^+$ transport across the uroepithelium***

The mammalian bladders express ENaC, which transports sodium across the mucosal surface of the bladder (128, 137), and changes in hydrostatic pressure alter the  $\text{Na}^+$ -transporting properties of the uroepithelium in a highly specific and reproducible manner (61). To determine whether the hydrostatic pressure-induced changes in  $I_{sc}$  were the result of increased  $\text{Na}^+$  conductance by

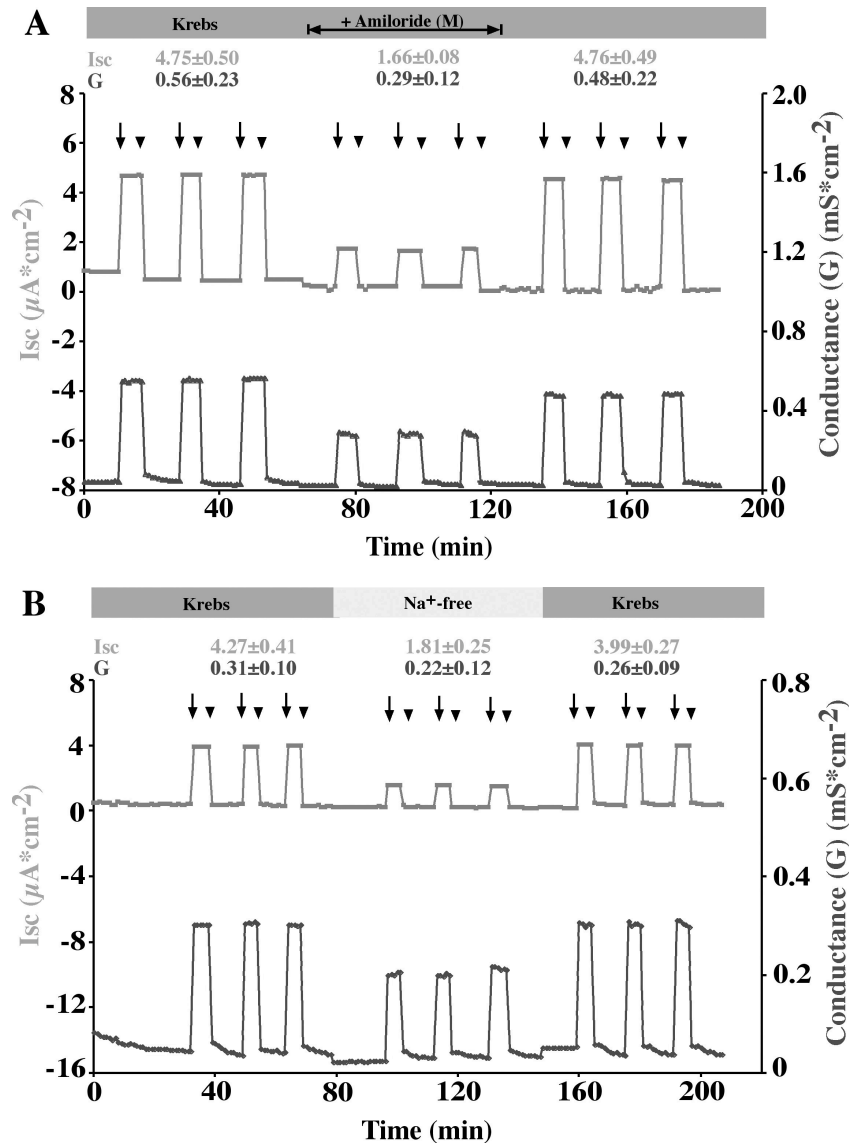


Figure 3-2. Characterization of uroepithelial  $\text{Na}^+$  transport in the presence of amiloride and in  $\text{Na}^+$ -free Krebs solution. (A) Isolated uroepithelium was mounted in Ussing chambers. Tissue was subjected to three cycles of raising (arrows) then lowering (arrowheads) hydrostatic pressure in control Krebs solution (indicated by a grey bar above the graph), followed by three cycles in the presence of  $10 \mu\text{M}$  amiloride added to mucosal Krebs solution (indicated by the horizontal double arrow). Amiloride was removed by isovolumetric replacement with Krebs solution and the tissue was subjected to an additional three cycles of increased and then decreased hydrostatic pressure. (B) Isolated uroepithelium was subjected to three cycles of increased then decreased hydrostatic pressure and the Krebs solution was then isovolumetrically replaced in the serosal and mucosal chambers with  $\text{Na}^+$ -free Krebs solution (indicated by the light grey bar above the graph). Following three more cycles of increased then decreased hydrostatic pressure, the  $\text{Na}^+$ -free Krebs solution was replaced with Krebs solution and then subjected to three additional cycles of increased then decreased hydrostatic pressure. In each panel a representative tracing is shown. Average values for Isc and conductance during the 5-min periods of increased hydrostatic pressure are shown above the graph and are the mean  $\pm$  SEM from 6 separate experiments.

ENaC I performed the following experiment. Ussing chamber-mounted tissue was first subjected to three cycles of increased then decreased hydrostatic pressure, which resulted in the expected changes in Isc and conductance (Figure 3-2A). Next, tissue was exposed to three cycles in the presence of the diuretic amiloride, which when used at 1-10  $\mu\text{M}$  acts as a specific blocker of ENaC (116, 117). When 10  $\mu\text{M}$  amiloride was added to the mucosal hemichamber hydrostatic pressure-induced Isc was reduced from  $4.75 \pm 0.50 \mu\text{A}\cdot\text{cm}^{-2}$  to  $1.66 \pm 0.08 \mu\text{A}\cdot\text{cm}^{-2}$ , an inhibition of  $\sim 65\%$  (Figure 3-2A). Similar levels of inhibition were observed when amiloride was used at 1  $\mu\text{M}$  (data not shown). When amiloride was isovolumetrically washed from the mucosal chamber with Krebs solution, followed by three cycles of increased then decreased hydrostatic pressure, the inhibitory effect of amiloride was reversed (Figure 3-2A).

To further confirm that increased  $\text{Na}^+$  transport accompanied increases in hydrostatic pressure, Krebs solution in both the mucosal and serosal chambers were isovolumetrically replaced with Krebs solution in which  $\text{Na}^+$  ions are substituted with the non-transportable cation TMA, generating nominally  $\text{Na}^+$ -free Krebs solution. The actual concentration of  $\text{Na}^+$  under these conditions was  $<10 \text{ mM}$  as measured by a  $\text{Na}^+$ -sensitive ion probe. Under these conditions the Isc was inhibited by  $\sim 58\%$  (Figure 3-2B), which was reversed when the modified Krebs solution was replaced with the regular Krebs solution (Figure 3-2B). Similar results were obtained when  $\text{Na}^+$  ions were replaced with NMDG, however, the level of Isc inhibition was  $\sim 87\%$  ( $3.61 \pm 0.01 \mu\text{A}\cdot\text{cm}^{-2}$  in Krebs solution and  $0.48 \pm 0.01 \mu\text{A}\cdot\text{cm}^{-2}$  in NMDG-Cl-containing Krebs solution).

The Isc observed in the presence of hydrostatic pressure was consistent with  $\text{Na}^+$  absorption. To confirm this observation, unidirectional  $^{22}\text{Na}^+$  flux studies were performed in the mucosal-to-serosal and serosal-to-mucosal directions both before and during application of

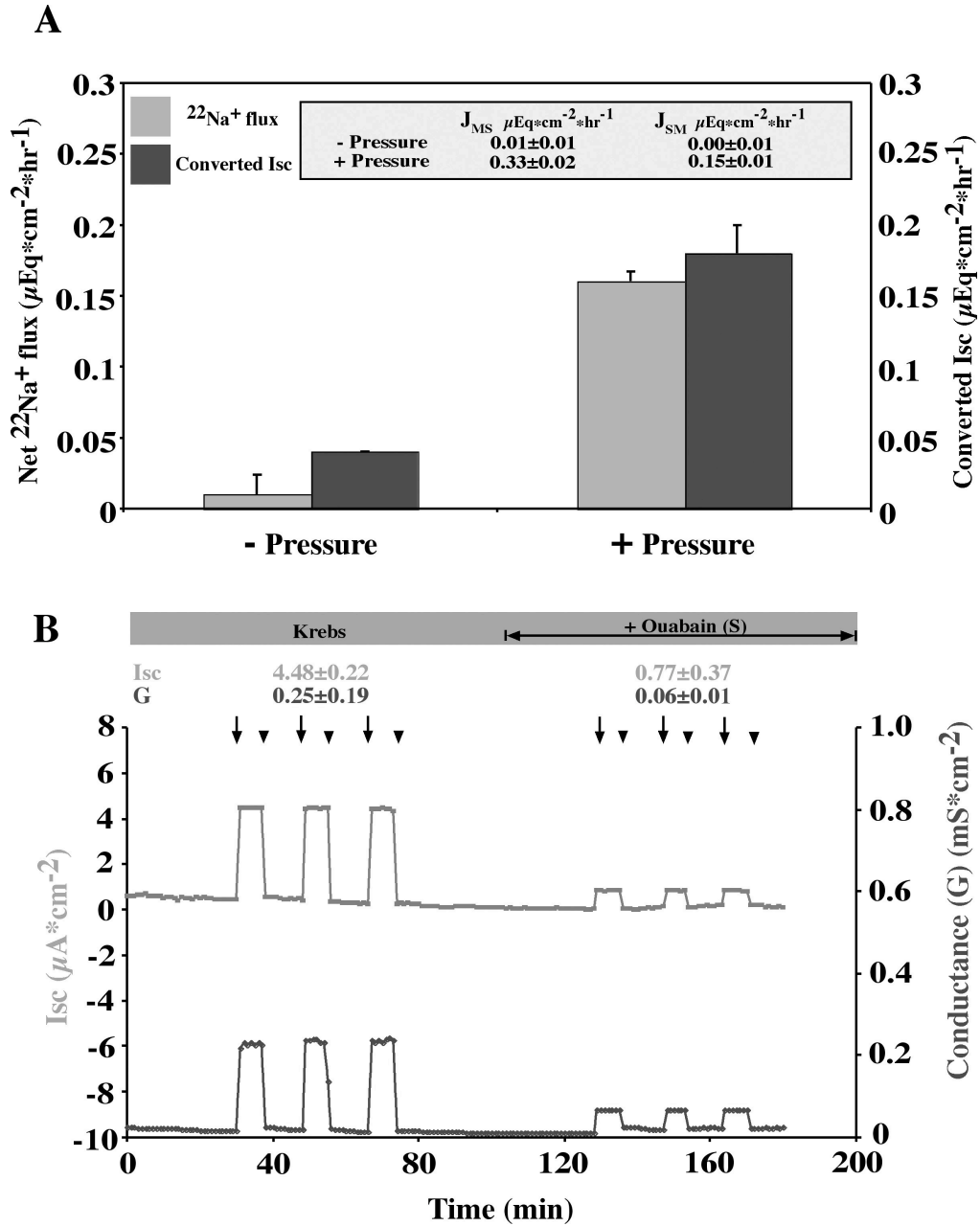


Figure. 3-3. Characterization of  $^{22}\text{Na}^+$  flux and  $\text{Na}^+$  transport in the presence of ouabain. (A) Net  $^{22}\text{Na}^+$  flux (grey bars) and Isc (black bars) were measured before and after increased hydrostatic pressure. Values for Isc were converted to  $\mu\text{Eq}\cdot\text{cm}^{-2}\cdot\text{h}^{-1}$ . There was no significant difference between net  $^{22}\text{Na}^+$  flux and converted Isc  $\pm$  pressure ( $p > 0.05$ ). (B) Uroepithelium was exposed to 3 cycles of increased then decreased hydrostatic pressure in Krebs solution, ouabain was added to the serosal chamber (indicated by the double arrow) and after 30 min the tissue was subjected to three additional cycles of increased then decreased hydrostatic pressure. A representative tracing is shown. Average values for Isc and conductance during the 5-min periods of increased hydrostatic pressure are shown above the graph and are the mean  $\pm$  SEM from 6 separate experiments.



hydrostatic pressure. The mucosal-to-serosal unidirectional flux ( $J_{MS}$ ) was  $0.01 \pm 0.01 \mu\text{Eq}\cdot\text{cm}^{-2}\cdot\text{hr}^{-1}$  prior to increasing pressure and  $0.33 \pm 0.02 \mu\text{Eq}\cdot\text{cm}^{-2}\cdot\text{hr}^{-1}$  after increasing pressure. In contrast, the serosal-to-mucosal unidirectional flux ( $J_{SM}$ ) was  $0.0 \pm 0.01 \mu\text{Eq}\cdot\text{cm}^{-2}\cdot\text{hr}^{-1}$  before pressure and  $0.15 \pm 0.01 \mu\text{Eq}\cdot\text{cm}^{-2}\cdot\text{hr}^{-1}$  after increasing pressure. In all experiments there was a net mucosal-to-serosal flux of  $\text{Na}^+$  in the presence of hydrostatic pressure equal to  $0.15 \pm 0.01 \mu\text{Eq}\cdot\text{cm}^{-2}\cdot\text{hr}^{-1}$  (Figure 3-3A). This value was not significantly different ( $p > 0.05$ ) from the measured  $I_{sc}$  in the presence of hydrostatic pressure, which when converted to chemical equivalent units was equal to  $0.17 \pm 0.02 \mu\text{Eq}\cdot\text{cm}^{-2}\cdot\text{hr}^{-1}$ .

The driving force for  $\text{Na}^+$  conductance across the bladder uroepithelium is the electrochemical gradient generated by the  $\text{Na}^+\text{-K}^+$  ATPase (53, 98), which favors the net absorption of  $\text{Na}^+$  across uroepithelium. The importance of this driving force in hydrostatic pressure-induced ion transport was assessed using ouabain, a selective inhibitor of the  $\text{Na}^+\text{-K}^+$  ATPase. When hydrostatic pressure was increased in the presence of 1 mM ouabain (added to the serosal hemichamber), the values for  $I_{sc}$  were reduced from  $4.48 \pm 0.22 \mu\text{A}\cdot\text{cm}^{-2}$  to  $0.77 \pm 0.37 \mu\text{A}\cdot\text{cm}^{-2}$  (Figure 3-3B), and conductance concomitantly decreased from  $0.25 \pm 0.19 \text{mS}\cdot\text{cm}^{-2}$  to  $0.06 \pm 0.01 \text{mS}\cdot\text{cm}^{-2}$ .

### ***K<sup>+</sup> is secreted into the mucosal hemichamber in response to hydrostatic pressure***

Previously, Ferguson and colleagues presented preliminary data that a  $\text{K}^+$  secretory pathway may exist in the umbrella cell (62). To determine whether  $\text{K}^+$  transport was elevated by hydrostatic pressure, the uroepithelium was exposed to hydrostatic pressure in Krebs solution in which  $\text{Na}^+$  and  $\text{Cl}^-$  were substituted with non-transportable ions to form nominally  $\text{Na}^+$ ,  $\text{Cl}^-$ -free Krebs

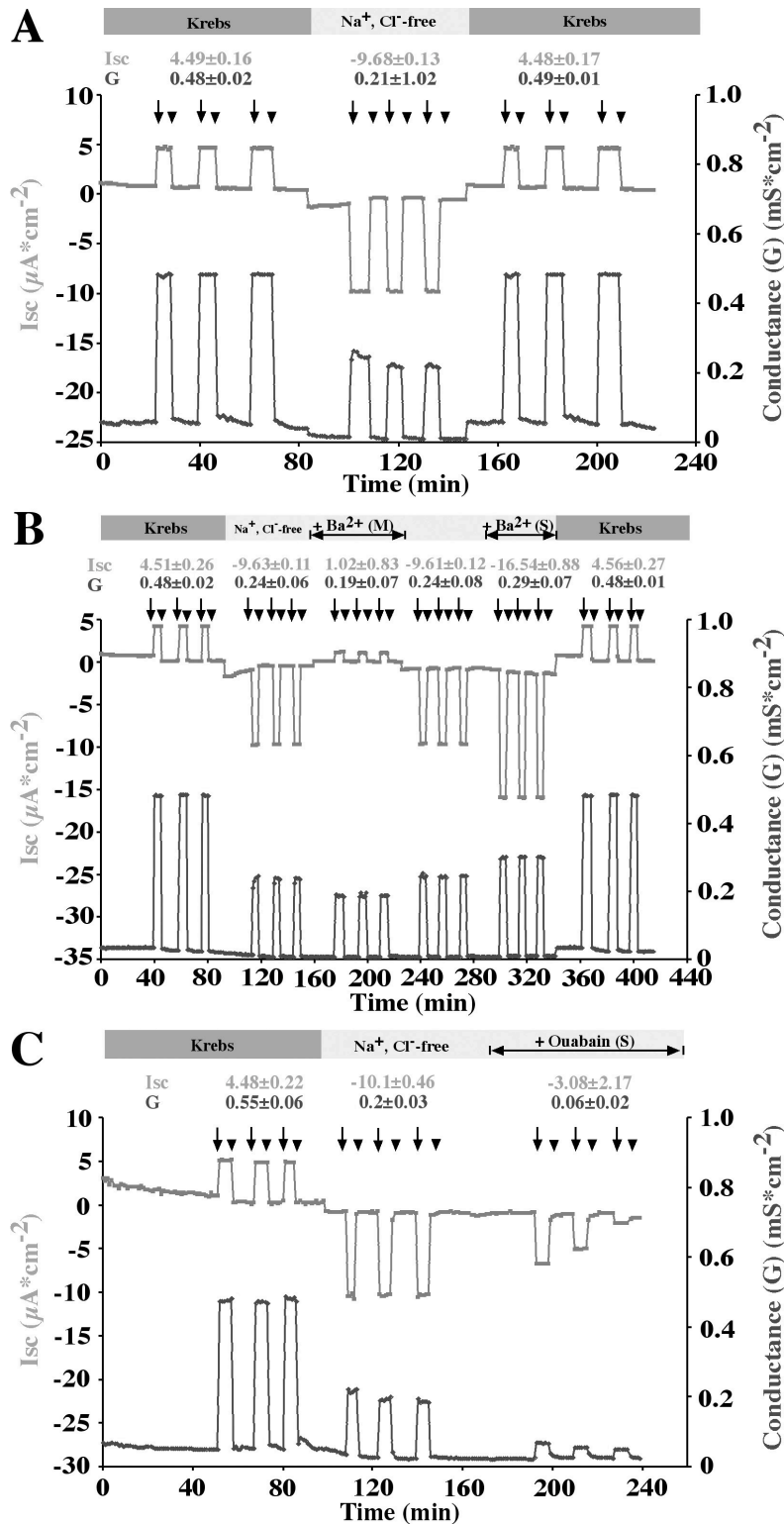


Figure 3-4. The effects of Na<sup>+</sup>, Cl<sup>-</sup>-free Krebs solution, Ba<sup>2+</sup>, and ouabain on hydrostatic pressure-activated ion secretion. (A) Isolated uroepithelium was subjected to three cycles of increased (arrow) then decreased (arrowhead) hydrostatic pressure in Krebs solution, three cycles in Na<sup>+</sup>, Cl<sup>-</sup>-free Krebs solution, and three cycles in Krebs solution. (B) Isolated uroepithelium was subjected to three cycles of increased then decreased hydrostatic pressure in Krebs solution, three cycles in Na<sup>+</sup>, Cl<sup>-</sup>-free Krebs solution, three cycles after addition of 3mM Ba<sup>2+</sup> to the mucosal chamber, three cycles in Na<sup>+</sup>, Cl<sup>-</sup>-free solution, three cycles after addition of Ba<sup>2+</sup> to the serosal chamber, and three cycles in Krebs solution. (C) Isolated uroepithelium was subjected to three cycles of increased then decreased hydrostatic pressure in Krebs solution, three cycles in Na<sup>+</sup>, Cl<sup>-</sup>-free Krebs solution, and three cycles after addition of ouabain to the serosal chamber. A representative tracing is shown for each panel. Average values for I<sub>sc</sub> and conductance during the 5-min periods of increased hydrostatic pressure are shown above the graph and are the mean ± SEM from 6 separate experiments.

**Table 3-1***Effects of channel inhibitors on K<sup>+</sup> conductance*

Drug	Block	[C] <sub>f</sub>	No treatment, μA/cm <sup>2</sup>	Mucosal treatment μA/cm <sup>2</sup>	Serosal treatment μA/cm <sup>2</sup>
Amiloride	NSC	100 μM	-9.11±0.94	-6.40±0.05*	
Ba <sup>2+</sup>	K channel	3 mM	-9.63±0.11	1.02±0.83*	-16.54±0.88*
TEA	K channel	10 mM	-9.73±0.05	2.63±0.02*	-19.25±0.07*
Gd <sup>3+</sup>	NSC	1 mM	-9.66±0.05	0.34±0.25*	-14.68±0.71*
CTX	BK or IK1	100 nM	-9.45±0.58	-9.42±0.61	-14.92±0.58*
Apamin	SK-type	100 nM	-9.89±0.27	-12.78±2.24*	-10.28±0.09*
Iberiotoxin	BK	20 nM	-9.49±0.44	-9.72±0.70	-9.43±1.03
Margatoxin	Kv1.3	10 nM	-10.0±0.33	-10.2±0.05	-10.3±0.04
Glibenclamide	ATP-sen. K <sup>+</sup>	50 μM	-10.1±0.32	-11.35±0.03*	-11.08±0.32*
Ouabain	Na <sup>+</sup> /K <sup>+</sup> ATPase	1 mM	-10.1±0.47		-3.08±2.17*

Values are means ± SEM; n ≥ 6 during increased hydrostatic pressure. Uroepithelium was mounted in modified Ussing chambers and subjected to cycles of increased and decreased hydrostatic pressure in Na<sup>+</sup>, Cl<sup>-</sup> free Krebs solution, and the effects of various channel inhibitors on pressure-activated short-circuit current (*I*<sub>sc</sub>) were assessed similar to the protocols used in Figs. 4 and 5. [C]<sub>f</sub>, final concentration; TEA, tetraethylammonium; CTX, charybdotoxin. \*Significantly different from no treatment (p<0.05).

**Table 3-2***Effects of hydrostatic pressure on <sup>86</sup>Rb<sup>+</sup> flux*

	Converted I <sub>sc</sub> , μeq·cm <sup>-2</sup> ·h <sup>-1</sup>	Measured <sup>86</sup> Rb <sup>+</sup> Flux		
		J <sub>MS</sub> , μeq·cm <sup>-2</sup> ·h <sup>-1</sup>	J <sub>SM</sub> , μeq·cm <sup>-2</sup> ·h <sup>-1</sup>	J <sub>net</sub> , μeq·cm <sup>-2</sup> ·h <sup>-1</sup>
<b>- Pressure</b>	<b>0.04±0.02</b>	<b>0.01±0.03</b>	<b>0.04±0.05</b>	<b>0.03±0.02</b>
<b>+ Pressure</b>	<b>0.18±0.01</b>	<b>0.09±0.03</b>	<b>0.46±0.06</b>	<b>0.37±0.03</b>

Values are mean ± SEM; n ≥ 3. <sup>86</sup>Rb<sup>+</sup> was added into the mucosal or the serosal Krebs solution, and the effects of pressure on <sup>86</sup>Rb<sup>+</sup> flux from mucosal-to-serosal (J<sub>MS</sub>) or serosal-to-mucosal (J<sub>SM</sub>) compartments were assessed. J<sub>net</sub>, J<sub>SM</sub>-J<sub>MS</sub>.

solution. In the modified Krebs solution a reversal in I<sub>sc</sub> was observed when the tissue was exposed to hydrostatic pressure (Figure 3-4A).

To test whether K<sup>+</sup> was secreted in response to hydrostatic pressure, Ba<sup>2+</sup> was added to either the mucosal or serosal Na<sup>+</sup>, Cl<sup>-</sup>-free Krebs solution during application of hydrostatic pressure (Figure 3-4B). Ba<sup>2+</sup> is a commonly used blocker of K<sup>+</sup> channels; however, it can block some non-selective cation channels as well (56, 75, 87, 248). Following three cycles of increased then decreased hydrostatic pressure in Krebs solution and three in Na<sup>+</sup>, Cl<sup>-</sup>-free Krebs solution, 3 mM Ba<sup>2+</sup> was added to the mucosal hemichamber. In the presence of mucosal Ba<sup>2+</sup> hydrostatic-pressure induced I<sub>sc</sub> was reduced from  $-9.63 \pm 0.11 \mu\text{A}\cdot\text{cm}^{-2}$  to  $1.02 \pm 0.83 \mu\text{A}\cdot\text{cm}^{-2}$  during increased pressure (Figure 3-4B). These inhibitory effects were reversed after isovolumetric washout of Ba<sup>2+</sup> with Na<sup>+</sup>, Cl<sup>-</sup>-free Krebs solution (Figure 3-4B). When Ba<sup>2+</sup> was added to the serosal medium, hydrostatic pressure led to an increase in I<sub>sc</sub> from  $-9.61 \pm 0.12 \mu\text{A}\cdot\text{cm}^{-2}$  to  $-16.54 \pm 0.88 \mu\text{A}\cdot\text{cm}^{-2}$  (Figure 3-4B). These effects were reversed when the cells were returned to normal Krebs solution. The mucosal and serosal effects of another K<sup>+</sup> channel blocker, 10 mM TEA, were also evaluated and I observed essentially identical effects to those observed with Ba<sup>2+</sup> (Table 3-1).

As additional evidence that hydrostatic pressure stimulated K<sup>+</sup> transport under short-circuit conditions I measured, in standard Krebs buffer, unidirectional flux of <sup>86</sup>Rb<sup>+</sup>, which is transported by both K<sup>+</sup> channels and non-selective cation channels (22, 35, 146, 205). Consistent with the results presented in Figure 4, there was a net serosal-to-mucosal flux of <sup>86</sup>Rb<sup>+</sup> in the presence of hydrostatic pressure equal to  $0.37 \pm 0.03 \mu\text{Eq}\cdot\text{cm}^{-2}\cdot\text{hr}^{-1}$  (Table 3-2). Essentially identical results were observed when <sup>86</sup>Rb<sup>+</sup> fluxes were performed in Na<sup>+</sup>, Cl<sup>-</sup>-free Krebs

solution (data not shown), indicating that the magnitude and direction of  $K^+$  transport was similar regardless of bathing solution.

As described above, the ion gradients generated by the  $Na^+/K^+$  ATPase provide the driving force for transport of  $Na^+$  and  $K^+$  across the uroepithelium. Isovolumetric washing with  $Na^+$ ,  $Cl^-$ -free Krebs solution is likely to leave some  $Na^+$  both outside and within the cell and this may have been sufficient to allow  $K^+$  entry via the  $Na^+/K^+$  ATPase. Alternatively, the  $K^+$  chemical gradient, generated by the high intracellular  $K^+$  pool coupled with a low extracellular  $K^+$  pool, may have been sufficient to drive hydrostatic-pressure induced  $K^+$  exit via mucosal  $K^+$  channels. To determine whether stretch-induced  $K^+$  secretion was dependent on the activity of the  $Na^+/K^+$  ATPase, uroepithelium was hydrostatically stimulated in the presence of 1 mM ouabain added to the  $Na^+$ ,  $Cl^-$ -free Krebs solution bathing the serosal hemichamber (Figure 3-4C). Ouabain effectively blocked the putative hydrostatic-pressure induced  $K^+$  secretion, the inhibition being greater during each subsequent pressure cycle (Figure 3-4C). This likely represents the depletion of intracellular  $K^+$  stores, which could not be replenished in the presence of ouabain. Treatment with ouabain also decreased the magnitude of the hydrostatic pressure-induced increase in conductance, consistent with a block in ion transport. These data indicated that  $K^+$  secretion was in fact dependent on basolateral  $K^+$  import by the  $Na^+/K^+$  ATPase.

To characterize further the putative  $K^+$  conductance pathway I used commercially available toxins and venoms that are selective for different classes of  $K^+$  channels. CTX, a scorpion venom that is selective for high and intermediate conductance  $Ca^{2+}$ -activated and some voltage-gated  $K^+$  channels, had little effect on hydrostatic pressure induced  $I_{sc}$  when added to the mucosal hemichamber ( $-9.45 \pm 0.58 \mu A \cdot cm^{-2}$  in  $Na^+$ ,  $Cl^-$ -free Krebs solution versus  $-9.42 \pm 0.61 \mu A \cdot cm^{-2}$  in  $Na^+$ ,  $Cl^-$ -free Krebs solution containing 100 nM CTX) (Figure 3-5A). When

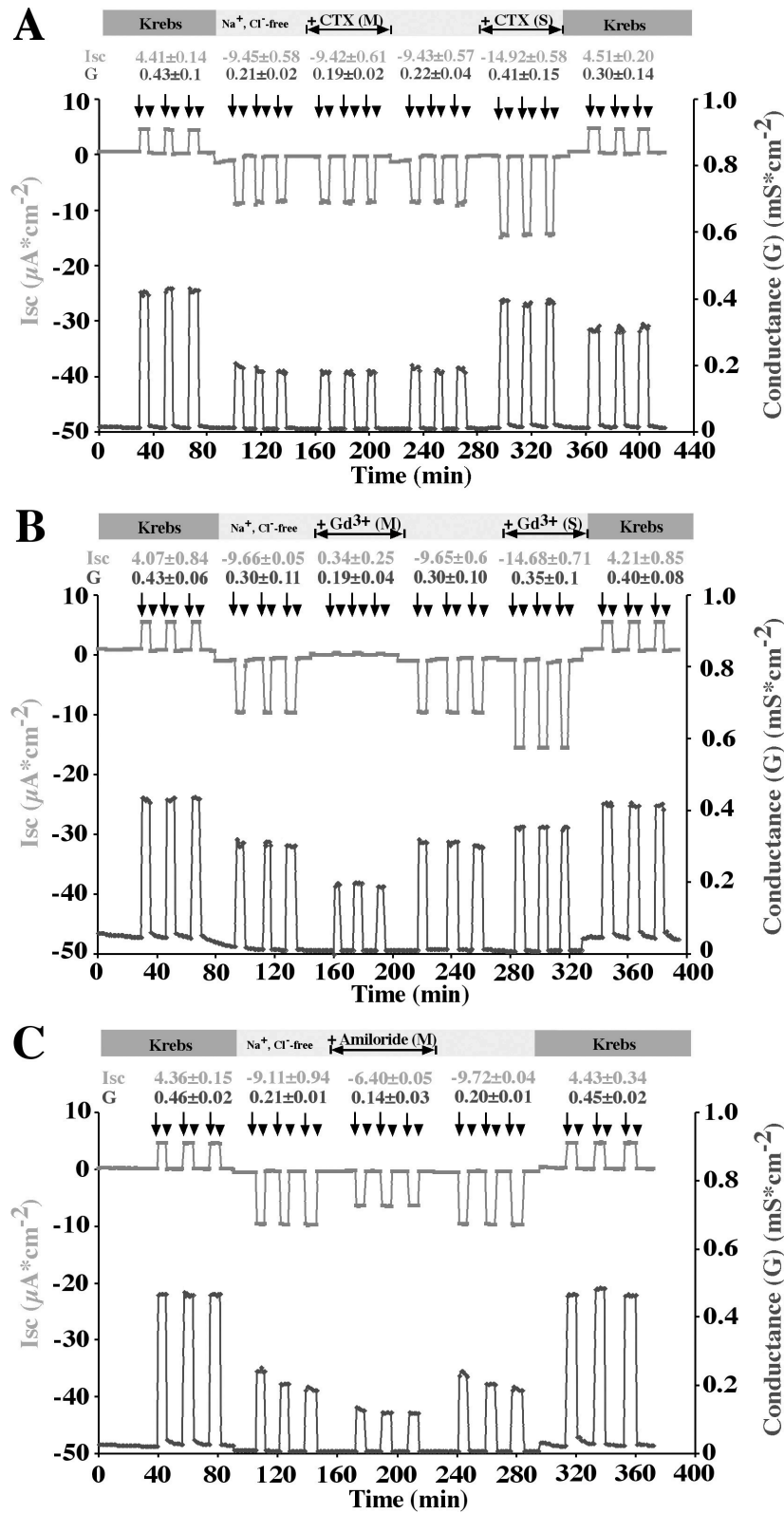


Figure. 3-5. The effects of CTX,  $Gd^{3+}$ , and amiloride on hydrostatic pressure-activated  $K^+$  secretion. (A) Isolated uroepithelium was subjected to three cycles of increased (arrows) then decreased (arrowheads) hydrostatic pressure in Krebs solution, three cycles in  $Na^+$ ,  $Cl^-$ -free Krebs solution, three cycles after addition of 100 nM CTX to the mucosal chamber, three cycles in  $Na^+$ ,  $Cl^-$ -free solution, three cycles after addition of 100 nM CTX to the serosal chamber, and three cycles in Krebs solution. (B) Isolated uroepithelium was subjected to three cycles of increased then decreased hydrostatic pressure in Krebs solution, three cycles in  $Na^+$ ,  $Cl^-$ -free Krebs solution, three cycles after addition of 1 mM  $Gd^{3+}$  to the mucosal chamber, three cycles in  $Na^+$ ,  $Cl^-$ -free solution, three cycles after addition of 1 mM  $Gd^{3+}$  to the serosal chamber, and three cycles in Krebs solution. (C) Isolated uroepithelium was subjected to three cycles of increased then decreased hydrostatic pressure in Krebs solution, three cycles in  $Na^+$ ,  $Cl^-$ -free Krebs solution, three cycles after addition of 100  $\mu$ M amiloride to the mucosal chamber, three cycles in  $Na^+$ ,  $Cl^-$ -free solution, and three cycles in Krebs solution. A representative tracing is shown for each panel. Average values for Isc and conductance during the 5-min periods of increased hydrostatic pressure are shown above the graph and are the mean  $\pm$  SEM from 6 separate experiments.

CTX was subsequently added to the serosal chamber, the level of  $K^+$  transport in the presence of hydrostatic pressure was augmented ( $-14.92 \pm 0.58 \mu A \cdot cm^{-2}$ ) in comparison to secretion in  $Na^+$ ,  $Cl^-$ -free Krebs solution ( $-9.43 \pm 0.57 \mu A \cdot cm^{-2}$ ) (Figure 3-5A). Other  $K^+$  channel blockers were tried as well. Addition of apamin, an inhibitor of the small conductance  $Ca^{2+}$ -activated  $K^+$  channels, to the mucosal hemichamber caused Isc to increase from  $-9.89 \pm 0.27 \mu A \cdot cm^{-2}$  to  $-12.78 \pm 2.24 \mu A \cdot cm^{-2}$  after applying hydrostatic pressure (Table 3-1). The addition of iberiotoxin, an inhibitor of the high conductance  $Ca^{2+}$ -activated  $K^+$  channel, and margatoxin, an inhibitor of some voltage-gated  $K^+$  channels, also had no inhibitory effect on hydrostatic pressure-induced  $K^+$  secretion (Table 3-1). Finally, glibenclamide, which blocks plasma membrane ATP-sensitive  $K^+$  channels (3), did not demonstrate any inhibitory effects but did marginally stimulate Isc (Table 3-1). These results indicated that hydrostatic pressure-induced  $K^+$  secretion from the mucosal surface of the tissue was not dependent on CTX-, iberiotoxin-, apamin-, margatoxin-, or glibenclamide-sensitive transport pathways.

### ***$K^+$ secretion is via a non-selective cation channel***

Since I was unable to find a selective  $K^+$  channel blocker that could inhibit the pressure-activated  $K^+$  secretion described above, I asked if the trivalent cation gadolinium ( $Gd^{3+}$ ) had any effect, as this is a general inhibitor of mechanosensitive ion channels (183). Following three cycles of hydrostatic pressure/relaxation in control Krebs solution and three in  $Na^+$ ,  $Cl^-$ -free Krebs solution, 1 mM  $Gd^{3+}$  was added to the mucosal  $Na^+$ ,  $Cl^-$ -free Krebs solution (Figure 3-5B). In the presence of  $Gd^{3+}$ , hydrostatic pressure-activated Isc was almost completely blocked ( $-9.66 \pm 0.05 \mu A \cdot cm^{-2}$  in  $Na^+$ ,  $Cl^-$ -free Krebs solution versus  $0.34 \pm 0.25 \mu A \cdot cm^{-2}$  in the presence of  $Gd^{3+}$ ) (Figure 3-5B). The addition of  $Gd^{3+}$  to the serosal hemichamber caused an increase in Isc from

$-9.65 \pm 0.06 \mu\text{A}\cdot\text{cm}^{-2}$  in  $\text{Na}^+$ ,  $\text{Cl}^-$ -free Krebs solution to  $-14.68 \pm 0.71 \mu\text{A}\cdot\text{cm}^{-2}$  in  $\text{Na}^+$ ,  $\text{Cl}^-$ -free Krebs solution containing  $\text{Gd}^{3+}$  (Figure 3-5B). These effects were reversible when the tissue was returned to control Krebs solution (Figure 3-5B). When used at high concentrations ( $\geq 100 \mu\text{M}$ ), amiloride inhibits several types of mechanically activated ion channels (78, 100, 181). In the presence of  $100 \mu\text{M}$  mucosal amiloride, hydrostatic pressure-activated Isc was blocked  $\sim 40\%$  when compared to stretch-activated Isc in  $\text{Na}^+$ ,  $\text{Cl}^-$ -free Krebs solution (Figure 3-5C). Similar levels of inhibition were observed with  $500 \mu\text{M}$  amiloride (data not shown). Addition of amiloride at  $100 \mu\text{M}$  did not potentiate the effects of  $\text{Gd}^{3+}$  or  $\text{Ba}^{2+}$  (data not shown).

The sensitivity of the  $\text{K}^+$  secretion pathway to  $\text{Gd}^{3+}$  and high concentrations of amiloride prompted me to explore the possibility that the transport pathway of my interest was a mechanosensitive non-selective cation channel. One characteristic of nonselective cation channels is their ability to conduct cesium ( $\text{Cs}^+$ ). Classical  $\text{K}^+$  channels do not conduct this ion (99). To test whether  $\text{Cs}^+$  could be transported across the mucosal membrane in a hydrostatic pressure dependent manner, we designed an experiment where regular Krebs solution was replaced with NMDG gluconate buffer in the mucosal chamber and  $\text{Cs}^+$  gluconate buffer in the serosal chamber, generating a  $\text{Cs}^+$  chemical gradient from the serosal to mucosal hemichamber. To move down this chemical gradient,  $\text{Cs}^+$  needs to cross the basolateral membranes of the umbrella cells and subsequently exit the apical membranes. Because there is no known pathway for  $\text{Cs}^+$  to enter the basolateral membrane of the umbrella cells, nystatin, an ionophore, was added to the serosal hemichamber to allow transport of  $\text{Cs}^+$  across the basolateral membrane of the umbrella cells. Exit of  $\text{Cs}^+$  from the umbrella cell apical membrane via nonselective cation channels was then monitored by Isc measurements.



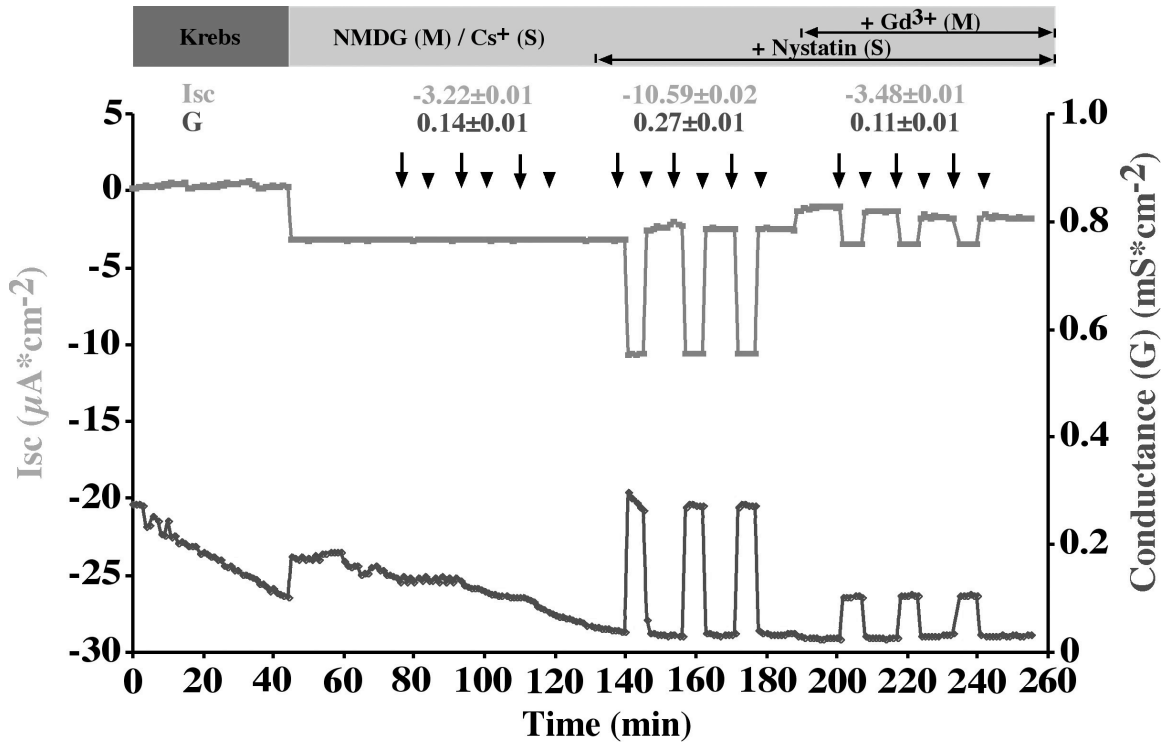


Figure 3-6. Hydrostatic pressure-induced transport of  $\text{Cs}^+$  in nystatin-permeabilized uroepithelium. Isolated uroepithelium was equilibrated in Krebs solutions and the Krebs solution was replaced by NMDG-gluconate buffer in the mucosal chamber and  $\text{Cs}^+$  gluconate buffer in the serosal chamber. Hydrostatic pressure was increased (arrows) and then decreased (arrowheads) three times. 2  $\mu\text{M}$  nystatin was added to the serosal chamber and the tissue was again subjected to three cycles of increased then decreased hydrostatic pressure. Finally, 1 mM  $\text{Gd}^{3+}$  was added to the mucosal chamber and three more cycles of increased then decreased hydrostatic pressure were performed. A representative tracing is shown. Average values for Isc and conductance during the 5-min periods of increased hydrostatic pressure are shown above the graph and are the mean  $\pm$  SEM from 6 separate experiments.

Following a period of equilibration, control Krebs solution was isovolumetrically replaced with mucosal NMDG gluconate buffer and serosal Cs<sup>+</sup> gluconate buffer. Other than Cs<sup>+</sup>, there were no transportable ions in these buffers. In the absence of nystatin, hydrostatic pressure had no effect on I<sub>sc</sub>, indicating that Cs<sup>+</sup> could not cross the basolateral membrane of the umbrella cells (Figure 3-6). In addition, there was no change in conductance, further indicating that changes in conductance were dependent in part on ion transport. However, after addition of nystatin to the serosal hemichamber a significant change in I<sub>sc</sub> was observed after application of hydrostatic pressure ( $-10.59 \pm 0.02 \mu\text{A}\cdot\text{cm}^{-2}$ ) that was similar in magnitude to the hydrostatic pressure-induced I<sub>sc</sub> observed in Na<sup>+</sup>, Cl<sup>-</sup>-free Krebs solution ( $\sim -9.5 - -9.11 \mu\text{A}\cdot\text{cm}^{-2}$ ) (Figure 3-4 and 3-5). Additionally, the transport of Cs<sup>+</sup> was accompanied by a significant, reversible increase in conductance, suggesting opening and closing of ion channels. As expected, the hydrostatic pressure-activated I<sub>sc</sub> was blocked when Gd<sup>3+</sup> was added to the mucosal hemichamber (Figure 3-6). These results indicated that hydrostatic pressure activated a nonselective cation channel in the apical membrane of the umbrella cells that was capable of conducting K<sup>+</sup>.

### ***Hydrostatic pressure induces Cl secretion into the mucosal hemichamber***

In Krebs solution, the net hydrostatic pressure-induced change in I<sub>sc</sub> was  $\sim 4 \mu\text{A}\cdot\text{cm}^{-2}$  (equivalent to  $\sim 0.15 \mu\text{Eq}\cdot\text{cm}^{-2}\cdot\text{h}^{-1}$ ) (Figure 3-1A), which was not significantly different from the net <sup>22</sup>Na<sup>+</sup> flux we measured ( $\sim 0.15 \mu\text{Eq}\cdot\text{cm}^{-2}\cdot\text{h}^{-1}$ ) (Figure 3-3A). However, the <sup>86</sup>Rb<sup>+</sup> flux experiments in Krebs solution (Table 3-2) and the experiments in Na<sup>+</sup>, Cl<sup>-</sup> - free Krebs solution indicated that hydrostatic pressure also induced an  $\sim 10 \mu\text{A}\cdot\text{cm}^{-2}$  (equal to a flux of  $\sim 0.4 \mu\text{Eq}\cdot\text{cm}^{-2}\cdot\text{h}^{-1}$ ) secretory K<sup>+</sup> current in the opposite direction. This prompted me to explore

whether pressure stimulated transport of an additional ion species that was of similar magnitude but opposite charge to the  $K^+$  current, thus masking the contribution of the  $K^+$  current to the net  $I_{sc}$ . Previous studies indicated that a pathway for  $Cl^-$  entry exists on the basolateral membrane of the bladder umbrella cells (140). To determine whether a pressure-sensitive pathway for  $Cl^-$  transport exists in these cells, the uroepithelium was exposed to hydrostatic pressure and unidirectional flux measurements were performed. These experiments confirmed that in standard Krebs solution and under short-circuit conditions there was a net serosal-to-mucosal flux of  $^{36}Cl^-$  in the presence of hydrostatic pressure equal to  $0.41 \pm 0.03 \mu Eq \cdot cm^{-2} \cdot hr^{-1}$  (Table 3-3). This value was not significantly different ( $p > 0.05$ ) from the net  $^{86}Rb^+$  flux in the presence of hydrostatic pressure, indicating that hydrostatic pressure induced electroneutral  $K^+$  and  $Cl^-$  transport under short circuit condition.

**Table 3-3**

*Effects of hydrostatic pressure on  $^{36}Cl^-$  flux*

	Converted $I_{sc}$ , $\mu eq \cdot cm^{-2} \cdot h^{-1}$	Measured $^{36}Cl^-$ Flux		
		$J_{MS}$ , $\mu eq \cdot cm^{-2} \cdot h^{-1}$	$J_{SM}$ , $\mu eq \cdot cm^{-2} \cdot h^{-1}$	$J_{net}$ , $\mu eq \cdot cm^{-2} \cdot h^{-1}$
<b>- Pressure</b>	<b>0.03±0.01</b>	<b>0.03±0.01</b>	<b>0.04±0.29</b>	<b>0.01±0.01</b>
<b>+ Pressure</b>	<b>0.16±0.02</b>	<b>0.10±0.13</b>	<b>0.51±0.31</b>	<b>0.41±0.03</b>

Values are means  $\pm$  SEM;  $n \geq 3$ .  $^{36}Cl^-$  was added into the mucosal or the serosal Krebs solution, and the effects of pressure on  $^{36}Cl^- J_{MS}$  or  $J_{SM}$  were assessed.

## ***DISCUSSION***

### ***Hydrostatic pressure stimulates Na<sup>+</sup> transport across the uroepithelium***

The bladder plays an active part in regulating the total Na<sup>+</sup>, Cl<sup>-</sup>, and K<sup>+</sup> content of the organism, a function mediated by ion transport across the apical surface of the umbrella cell (128). I observed that raising then lowering hydrostatic pressure, which mimics bladder filling and voiding, was accompanied by increased then decreased ion transport. Like previous reports, which employed membrane punching and small changes in hydrostatic pressure (61, 135), I observed that mechanical stimulation was accompanied by increased Na<sup>+</sup> absorption across the apical membrane of the umbrella cells (61, 62, 128, 129, 135-138). This was confirmed by demonstrating a net mucosal-to-serosal <sup>22</sup>Na<sup>+</sup> flux of ~0.15 μEq\*cm<sup>-2</sup>\*h<sup>-1</sup>. Furthermore, I observed a significant decrease in I<sub>sc</sub> when tissue was exposed to pressure in Na<sup>+</sup>-free Krebs solution, or when pressure was increased in the presence of ouabain, indicating that the ion gradients generated by the Na<sup>+</sup>-K<sup>+</sup> ATPase provided the driving force for Na<sup>+</sup> entry across the basolateral membrane of the umbrella cell (Figure 3-7). The sensitivity of this transport pathway to low concentrations of amiloride (1-10 μM), and previous localization of ENaC to the apical surface of the umbrella cell (197), were consistent with an absorptive Na<sup>+</sup> transport pathway mediated by ENaC (Figure 3-7).

### ***K<sup>+</sup> transport is elevated during hydrostatic pressure stimulation***

In addition to this Na<sup>+</sup> transport pathway, I also characterized a pressure-sensitive K<sup>+</sup> secretion pathway, which was revealed under short-circuit conditions when tissue was exposed to hydrostatic pressure in Na<sup>+</sup>, Cl<sup>-</sup>-free Krebs solution. This pathway was confirmed by measuring a net serosal-to-mucosal flux of <sup>86</sup>Rb<sup>+</sup> in standard Krebs solution. Mechanically-stimulated K<sup>+</sup>

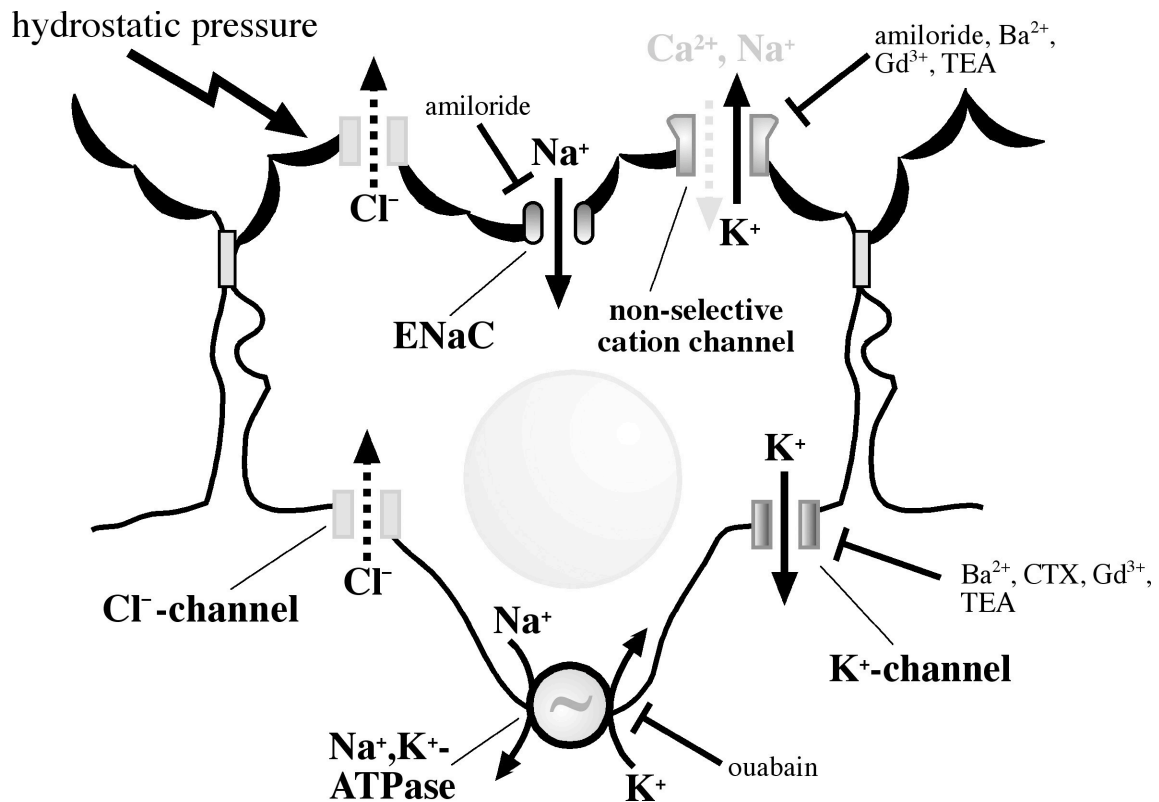


*Figure 3-7. Model for hydrostatic pressure-induced ion transport in bladder umbrella cells.* Increased hydrostatic pressure causes increased conductance of Na<sup>+</sup>, K<sup>+</sup>, and Cl<sup>-</sup>. Na<sup>+</sup> enters the cell via the amiloride-sensitive ENaC, driven by the favorable electrochemical gradient (low cell [Na<sup>+</sup>] and cell negative voltage), and exits the cell, in exchange for K<sup>+</sup>, via the ouabain-sensitive Na<sup>+</sup> - K<sup>+</sup> ATPase located at the basolateral surface of the cell. K<sup>+</sup> can exit the cell via basolaterally-localized K<sup>+</sup> leak channels (which are inhibited by Ba<sup>2+</sup>, CTX, Gd<sup>3+</sup>, and TEA), or under short-circuit conditions through an apically localized non-selective cation channel, which is inhibited by amiloride (≥ 100 μM), Ba<sup>2+</sup>, Gd<sup>3+</sup>, and TEA. The former may also conduct Ca<sup>2+</sup> and Na<sup>+</sup>, but this has not been directly demonstrated. The apical K<sup>+</sup> conductance is balanced by an electroneutral Cl<sup>-</sup> conductance, which may represent transport of Cl<sup>-</sup> through basolateral and then apical Cl<sup>-</sup> channels.

secretory pathways have been described in several cell types including marginal cells of the stria vascularis, gall bladder epithelial cells, epithelial cells of Reissner's membrane, apical membrane of rabbit cortical collecting tubule, and vestibular dark cells (207, 208, 219, 233, 242). In each of these cell types  $K^+$  is secreted via a large conductance  $K^+$  channel that is blocked by TEA and  $Ba^{2+}$ . The  $K^+$  conductance in the umbrella cells is also sensitive to these channel blockers. However, I found that CTX and iberiotoxin (both inhibitors of large-conductance  $K^+$  channels), or apamin or margatoxin had either no effect or a small effect on  $K^+$  secretion when added to the mucosal surface of the uroepithelium. In contrast,  $Ba^{2+}$ , TEA,  $Gd^{3+}$ , and CTX stimulated secretion when added to the serosal surface of the tissue. This likely reflects inhibition of basolateral  $K^+$  channels, which would enhance apical release of  $K^+$  when pressure was increased. The driving force for  $K^+$  secretion was apparently the ion gradients generated by the  $Na^+-K^+$  ATPase, as ouabain inhibited  $K^+$  secretion (Figure 3-7).

***Pressure-activated  $K^+$  transport is via nonselective cation channels***

The observation that  $Ba^{2+}$  and TEA can inhibit the activity of nonselective cation channels (87), prompted me to explore whether the  $K^+$  secretory pathway I observed was possibly via a mechanosensitive nonselective cation channel. Several observations indicated that this was the case. First,  $K^+$  secretion in the uroepithelium was inhibited by mucosal addition of  $Gd^{3+}$ , a blocker of both mechanosensitive ion channels and nonselective cation channels (36, 89, 159, 183). Second, I observed that high concentrations of amiloride, which block mechanosensitive non-selective cation channels (36), partially inhibited the  $K^+$  secretory pathway. Third, the  $Gd^{3+}$ -sensitive  $K^+$  secretory pathway also conducted  $Cs^+$ , a hallmark of a non-selective cation conductance pathway (99, 240). Based on these observations, I propose that hydrostatic pressure

may increase the activity of a mechanosensitive non-selective cation channel in the apical membrane of the umbrella cell (Figure 3-7).

A non-selective cation channel has previously been described in bladder uroepithelium (130, 249). This so-called “leak” channel is localized to the apical membrane of the umbrella cells, and is thought to be a degradation product of ENaC (133). Zweifelh and colleagues showed that the conductivity for  $K^+$  by the leak channel was significantly greater than that of  $Na^+$  or  $Cl^-$ . Despite the similarity in ion conductivity and localization between the leak channel and the putative nonselective cation channel that I described, there are notable differences between the two channels. First, the leak channel is unaffected by 10-100  $\mu M$  amiloride (130, 141, 249), whereas the non-selective cation channel I have characterized is partially inhibited by 100  $\mu M$  amiloride. Second, the amiloride-sensitive  $K^+$  conductance that is observed in this chapter is relatively stable (>10 min) during increased hydrostatic pressure and can be activated during multiple cycles of increased pressure and relaxation. This contrasts with the short residency time of the leak channel (~2 min) in the apical membrane of the umbrella cell (249). Third, the pressure-activated nonselective cation channel described in this chapter produced a secretory  $K^+$  current whereas Lewis and colleagues described an absorptive leak current. In fact, in the presence of  $Ba^{2+}$ , TEA, or  $Gd^{3+}$  I observe a small residual absorptive current that may represent leak channel activity.

### ***Hydrostatic pressure stimulates $Cl^-$ transport across the uroepithelium***

In addition to  $Na^+$  and  $K^+$  transport, increased hydrostatic pressure lead to increased  $Cl^-$  secretion under short-circuit conditions, which was of a similar magnitude to the  $K^+$  secretory pathway I described (Figure 3-7). Mechanically-sensitive  $Cl^-$  channels have been described in several other

tissues and cell types including Reissner's membrane, the stria vascularis, and cortical collecting duct (191, 206, 242); however, none have been described in bladder epithelium. Known pathways for  $\text{Cl}^-$  entry across the basolateral membrane of umbrella cells include  $\text{Cl}^-$  channels and  $\text{Cl}^-/\text{HCO}_3^-$  exchangers (128, 140). An apical pathway for  $\text{Cl}^-$  conductance has not been described in bladder epithelium, and I found that the  $\text{Cl}^-$  secretory pathway was insensitive to mucosal addition of DIDS, serosal addition of bumetanide, or mucosal addition of niflumic acid (unpublished observations) that are inhibitors of other known  $\text{Cl}^-$  conductance pathways (115, 145, 216). The nature of the  $\text{Cl}^-$  secretory pathway requires additional experimentation.

Finally, the relatively stable change in  $I_{sc}$  during increased pressure (see Figure 3-1), but the tendency for the conductance to fall during increased pressure and during the period between cycles of elevated pressure indicates that paracellular conductance and/or the magnitude of the different ion channel activities may be affected by pressure. These changes may also explain why mucosal addition of  $\text{Ba}^{2+}$  and  $\text{Gd}^+$  inhibited pressure-induced changes in the  $I_{sc}$  contributed by  $\text{K}^+$  secretion, but had less of an effect on changes in conductance (Figure 3-4B and 3-5B).

In summary, my findings further increase our understanding of the mechanically sensitive ion transport processes in the mammalian urinary bladder. My data indicate that in addition to the previously characterized  $\text{Na}^+$  absorption pathway, hydrostatic pressure also stimulates  $\text{Cl}^-$  and  $\text{K}^+$  secretion under short-circuit conditions. Although the bladder is generally thought to store urine and maintain the ion composition of the urine generated by the kidney, the ion transport pathways others and I have described indicate that the uroepithelium could alter the water and ion composition of the urine. Furthermore, absorption of ions from the urine (e.g.  $\text{Na}^+$ ) or secretion of ions into the urine (e.g.  $\text{K}^+$ ) may provide a means of regulating the electrolyte composition of the extracellular fluid. Finally, transport of  $\text{Cl}^-$ ,  $\text{K}^+$ , and  $\text{Na}^+$  during the urine-



filling process may also play an important role in sensory transduction and may couple changes in hydrostatic pressure to release of hormones such as ATP that would modulate other cellular functions as well as other processes such as neural-epithelial signaling (61, 62, 204).

## CHAPTER 4

### ATP and P2X receptor-dependent membrane traffic in bladder umbrella cells

#### *ABSTRACT*

ATP and purinergic receptor signaling have been implicated in mechanotransduction in the bladder uroepithelium. One downstream event of mechanotransduction is alteration in membrane trafficking. To investigate whether ATP and purinergic receptors can modulate changes in umbrella cell surface area ATP release from rabbit uroepithelium was measured. Upon increased pressure, levels of ATP in the mucosal media increased >1000 fold above background levels while basolateral release increased >10 fold. ATP release was blocked by 10 $\mu$ g/ml brefeldin A, an inhibitor of protein secretion, and 100 $\mu$ M anandamide, a connexin hemichannel blocker. To determine whether pressure-evoked ATP release played a role in signaling pressure-induced exocytosis, membrane capacitance (where 1 $\mu$ F  $\square$  1cm<sup>2</sup>) was measured. In control uroepithelium pressure stimulated an ~55% increase in capacitance. This increase was completely blocked by the addition of the ATPase apyrase or the purinergic receptor antagonist PPADS to the serosal bathing solution. No inhibition was observed when apyrase and PPADS were added mucosally. To determine whether P2X or P2Y receptors modulate changes in surface area, uroepithelium was incubated in the presence of purinergic receptor agonists. The P2X receptor agonists had the following rank potency on exocytosis: ATP $\square$ S > 2-MeSATP > ATP > BzATP >  $\square$ ,  $\square$ -MeATP

when added serosally, but UTP, a P2Y receptor agonist had no effect. Finally, umbrella cells from knockout mice lacking expression of P2X<sub>2</sub> or P2X<sub>3</sub> receptors failed to increase surface area when exposed to hydrostatic pressure. Instead, in the absence of P2X<sub>2</sub> receptors, pressure-induced endocytosis was stimulated. Treating the uroepithelium with ATP[S induced endocytosis of umbrella cell apical membrane and ~40% of biotin-labeled membrane was internalized within 5 minutes of ATP[S treatment. These results indicate that increased hydrostatic pressure stimulates vesicular and connexin hemichannel-dependent ATP release from the uroepithelium, and this may coordinate endocytosis and exocytosis via serosal P2X-dependent signaling pathways in bladder umbrella cells to modulate apical surface area.

## ***INTRODUCTION***

ATP is an important biological molecule, not only because it is the primary energy source for living cells, but also because it can act extracellularly to signal various cellular processes ranging from synaptic transmission and apoptosis to nociception and bladder contraction (168). As an energy source, ATP is abundant in the cell cytoplasm where it ranges from ~3-5 mM (168). While it is known that ATP is released under physiological conditions the exact mechanism for ATP release is still under debate. ATP may potentially be released from the cell via exocytosis of ATP-containing vesicles (24, 150, 168, 199), through connexin hemichannels (203), and possibly via the cystic fibrosis transmembrane conductance regulator (CFTR) (178, 192), although the latter may be an indirect mechanism (85, 229).

After ATP is released into the extracellular environment it can bind to cell-surface purinergic (P2) receptors. The P2 receptors are comprised of two different families, the ligand-gated ionotropic P2X receptors and the P2Y metabotropic heptahelical G-protein coupled receptors (30, 190). To date, eight distinct P2X receptors, named P2X<sub>1</sub>-P2X<sub>7</sub> and P2X<sub>M</sub>, have been identified at the molecular level (167). All P2X receptors bear a common topology, containing intracellular N- and C- termini, two transmembrane domains, and a large extracellular loop (167). The topology of the P2X receptor is similar to that of the epithelial sodium channel (ENaC) and inwardly rectifying potassium channel (IRK, ROMK) superfamily (167). All P2X receptors are permeable to small monovalent cations, although some have significant calcium or anion permeability (167). Similar to other ion channels, homo- or hetero-oligomeric assembly of several subunits of P2X receptor isoforms forms the functional P2X channel (167). However, the true stoichiometry of the channel is still unclear.

Functionally, P2X receptors play important roles in epithelial tissues. Upon binding of ATP ligand to P2X receptors present on the apical or basolateral membrane of airway epithelial cells, a transient increase in cytosolic  $\text{Ca}^{2+}$  and activation of  $\text{Ca}^{2+}$ -dependent protein kinase signaling is observed (171). This may stimulate  $\text{Cl}^-$  and fluid secretion and increase ciliary beat frequency (50, 110). In other epithelia, Lou and colleagues found that P2X receptors are expressed on the luminal and serosal membranes of pancreatic duct, where they stimulate  $\text{Cl}^-$  secretion and increase intracellular  $\text{Ca}^{2+}$  (148). In the renal epithelia, Insel and co-workers have shown that Madin-Darby canine kidney (MDCK) cells release ATP endogenously and continuously (108). The release of ATP provides a mechanism to modulate phosphatidylinositol signaling and turnover and cAMP production (239, 246). The downstream effect of this signaling pathway may inhibit  $\text{Na}^+$  absorption and arginine vasopressin (AVP)-induced water reabsorption (190).

Despite evidence suggesting important roles for P2X receptors in the airway, pancreatic, and the renal epithelium, there is limited data on the function of P2X receptors in the urinary bladder. P2X<sub>3</sub> receptors are found on a subpopulation of pelvic afferent fibers that innervate the bladder (221). Studies in knockout mice showed that when P2X<sub>3</sub> receptors are absent, the ability of the central nervous system to sense bladder filling is attenuated, implicating P2X<sub>3</sub> receptors on bladder afferents in nociception (221). Intriguingly, P2X<sub>2</sub> receptors have also been localized to the uroepithelium, and P2X<sub>4</sub> receptors are found to colocalize with the fine capillary network underlying the bladder epithelium. On the plasma membrane of the uroepithelial cells, including the umbrella cells, P2X<sub>2</sub>, P2X<sub>3</sub>, P2X<sub>4</sub>, and P2X<sub>5</sub> receptors are found (58, 61, 125). Despite the endogenous expression of many P2X receptor isoforms in the uroepithelial cells, their role is unknown, and the mechanism of ATP release from the uroepithelial cells remains unclear.

In this chapter, I examined the role of ATP and P2X receptors in the bladder umbrella cells. Upon increased pressure, ATP was released into the mucosal and serosal media and this stimulated umbrella cell exocytosis. ATP release was via exocytosis of ATP-containing vesicles and connexin hemichannels. Umbrella cell exocytosis was stimulated by activation of P2X receptors on the serosal membrane of uroepithelial cells and was dependent on  $\text{Ca}^{2+}$  and PKA-signaling. In addition to exocytosis, purinergic receptors on the serosal surface of the uroepithelium could modulate umbrella cell endocytosis. These results indicate that increased hydrostatic pressure stimulates ATP release from the uroepithelium, and this may coordinate endocytosis and exocytosis via serosal P2X-dependent signaling pathways to modulate luminal surface area.

## **RESULTS**

### ***Hydrostatic pressure stimulates ATP release from the mucosal and serosal surfaces of the uroepithelium***

Rabbit uroepithelium was isolated and exposed to increased hydrostatic pressure in modified Ussing chambers (see Materials and Methods). Consistent with earlier observations, mechanical distension of the uroepithelium triggers ATP release (62, 221). In control tissue preparations (without pressure stimulation), the levels of mucosal and serosal ATP remained similar to background (Figure 4-1A and 4-2A; BKG). In contrast, when the uroepithelium was subjected to increased pressure at  $t = 0$  (ATP measured immediately after addition of pressure), 3, 6, 10, 20, 30, 50, or 60 minutes the levels of ATP released into the mucosal (Figure 4-1A) and serosal (Figure 4-2A) bathing media were elevated. The amount of ATP released into the mucosal media was significantly greater than the amount released into the serosal media (compare scale; Figure 4-1A and 4-2A). The extracellular levels of ATP plateaued within 3 minutes post stimulus and remained elevated for at least 60 minutes (Figure 4-1A and 4-2A).

### ***Pressure-induced ATP release is via vesicular and connexin hemichannel dependent pathways***

The mechanism of ATP release from the uroepithelium is poorly understood. To determine whether pressure-induced ATP release is via vesicular or nonvesicular-dependent pathways the uroepithelium was mechanically stimulated in the presence of BFA, a fungal metabolite that has been shown to block secretion of various proteins in several cell lines and the bladder epithelium (48, 69, 149, 154). In the presence of BFA, pressure-induced ATP release from the mucosal membrane was inhibited >99% (Figure 4-1B), but very small amounts of ATP were still released during the periods of pressure stimulation (Figure 4-1B inset). A similar inhibitory effect was

observed on pressure-induced ATP release from the serosal membrane of the uroepithelium after BFA treatment (Figure 4-2B and 4-2B inset).

Hydrostatic pressure-induced ATP release was also inhibited after treating the uroepithelium with the connexin hemichannel blocker anandamide (86) (Figure 4-1C and 4-2C). In the presence of anandamide, mucosal ATP release from the uroepithelium was partially blocked (Figure 4-1C). Serosal release of ATP showed partial inhibition (Figure 4-2C). In contrast, treating the uroepithelium with glibenclamide, a blocker of adenosine triphosphate binding cassette (ABC) proteins such as CFTR and sulfonylurea receptor (65, 196), had no effect on mucosal (Figure 4-1D) or serosal (Figure 4-2D) ATP release, indicating that pressure-induced ATP release from the uroepithelium was independent of ABC proteins.

All cells exhibit high physiological concentrations of cytoplasmic ATP (168). If the structural integrity of the umbrella cell was disrupted by mechanical stimulus ATP would leak into the extracellular milieu. To demonstrate that our method of mechanical stimulus (hydrostatic pressure) did not damage the umbrella cell plasma membrane release of lactate dehydrogenase (LDH), a stable cytoplasmic enzyme, was monitored before and during exposure to pressure. In uroepithelium that was undisturbed, LDH levels in the mucosal and serosal bathing media were relatively low (<0.005% of total LDH in cell lysate) (Figure 4-3A). In pressure-stimulated tissues, the amount of LDH released into the mucosal or serosal bathing media remained low (<0.01% of total LDH in cell lysate) regardless of the duration of pressure stimulation (Figure 4-3A). The small percentages of extracellular LDH indicated that exposure to hydrostatic pressure did not cause significant plasma membrane damage. More importantly, estimated differences in the percentage of LDH and ATP release were greater than 9-fold, indicating that pressure-induced ATP release into the media was not a result of leakage due to membrane disruption.



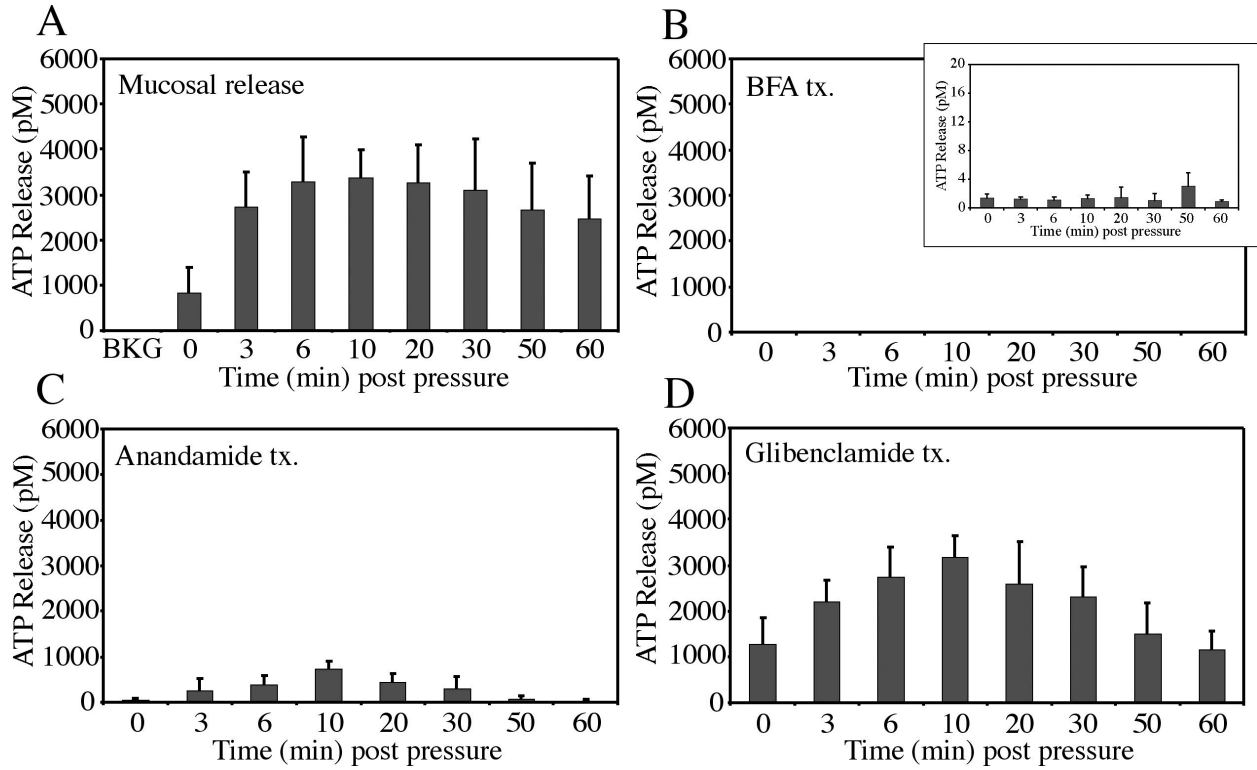


Figure 4-1. Pressure-activated ATP release from the mucosal membrane is via vesicular and connexin hemichannel-dependent pathways. (A) Pressure-induced release of ATP from mucosal membrane. Uroepithelium was pressure-stimulated for time = 0 (ATP measured immediately after addition of pressure), or after 3, 6, 10, 20, 30, 50, 60 minutes. Background (BKG) = control tissues (no pressure stimulation). (B) Effects of 10 $\mu$ g/ml BFA on pressure-induced ATP release. Uroepithelium was pretreated with BFA 10-15 minutes prior to pressure stimulation at t=0. Inset represents identical graph with reduced y-axis range. (C) Effects of 100 $\mu$ M anandamide on pressure-induced ATP release. (D) Effects of 100 $\mu$ M glibenclamide on pressure-induced ATP release.

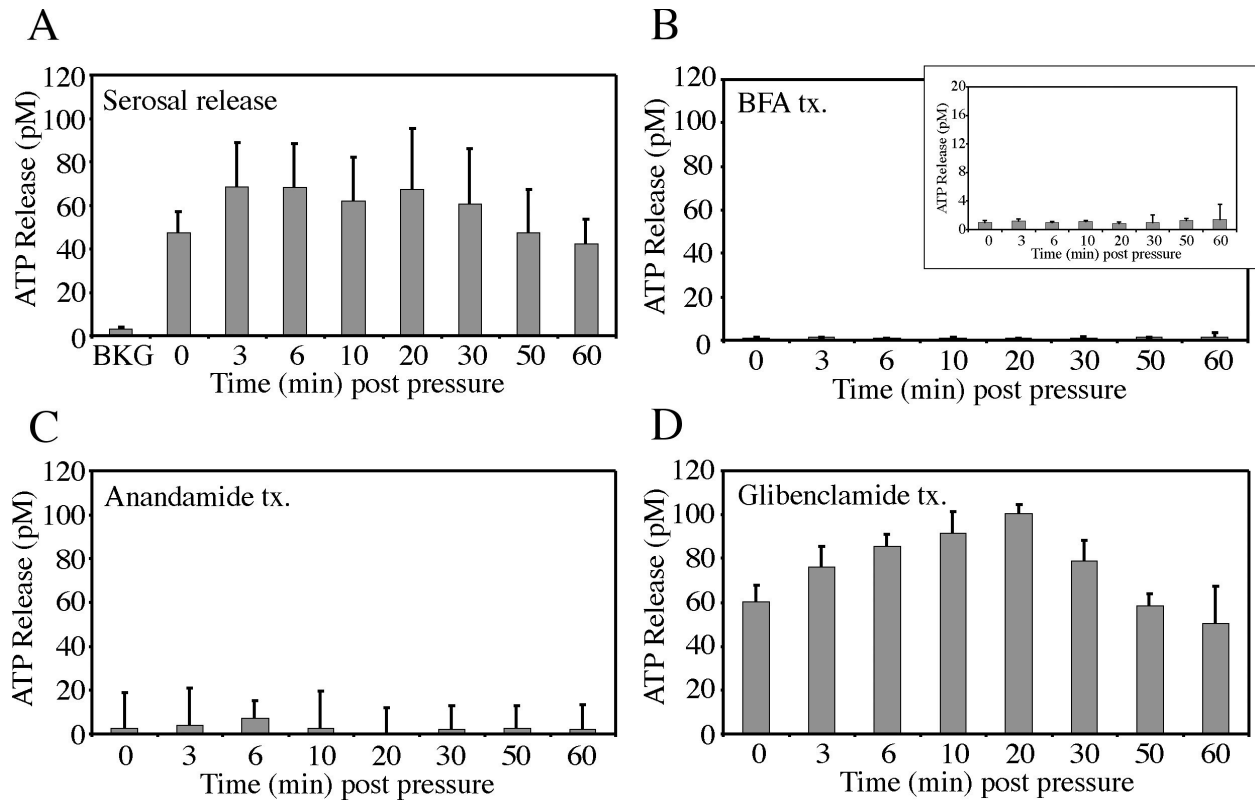
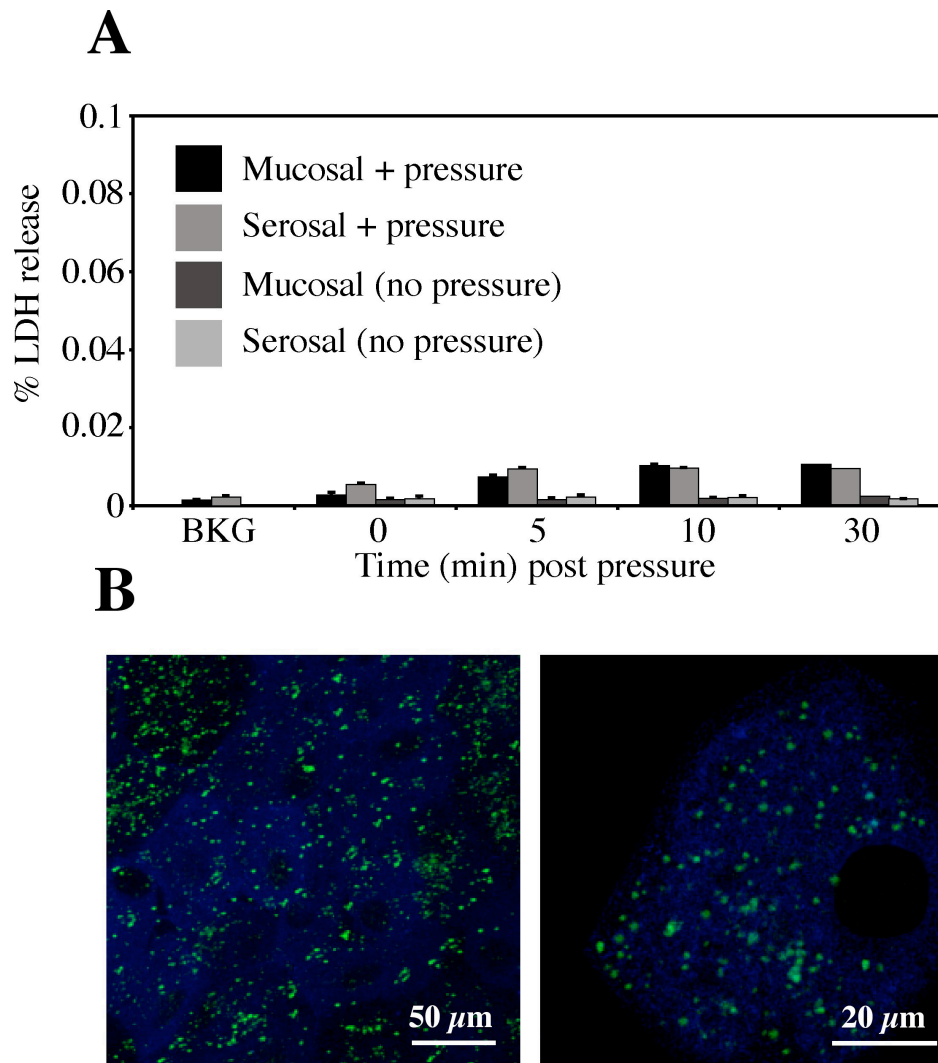


Figure 4-2. Pressure-activated ATP release from the serosal membrane is via vesicular and connexin hemichannel-dependent pathways. (A) Pressure-induced release of ATP from the serosal membrane. Uroepithelium was pressure-stimulated for time = 0 (ATP measured immediately after addition of pressure), or after 3, 6, 10, 20, 30, 50, 60 minutes. Background (BKG) = control tissues (no pressure stimulation). (B) Effects of 10 $\mu$ g/ml BFA on pressure-induced ATP release. Uroepithelium was pretreated with BFA 10-15 minutes prior to pressure stimulation at t=0. Inset represents identical graph with reduced y-axis range. (C) Effects of 100 $\mu$ M anandamide on pressure-induced ATP release. (D) Effects of 100 $\mu$ M glibenclamide on pressure-induced ATP release.



*Figure 4-3. ATP release from vesicular compartments is not the result of pressure-induced cell damage. (A) Effects of pressure on LDH release from the uroepithelium. LDH release from the mucosal or serosal membrane was measure at time = 0 (immediately after addition of pressure), 5, 10, or 30 minutes after pressure. (B) Localization of ATP in the bladder umbrella cells. Isolated uroepithelium was incubated with 5 $\mu$ M quinacrine for 30 minutes. After 30 minutes, the tissue was removed and FM4-64 prepared in ice-cold Krebs buffer was added onto the mucosal membrane and incubated for 30 minutes prior to imaging.*

To visualize ATP in the bladder umbrella cells, isolated uroepithelium was incubated with quinacrine, a membrane permeant fluorescence dye that interacts with ATP bound to peptide in large granular vesicles (24, 40). The cells were labeled with FM 4-64 to visualize the apical membrane of the umbrella cells. In the presence of quinacrine, large punctate staining patterns were observed in the umbrella cells, possibly exocytic vesicles (Figure 4-3B). The punctate staining patterns indicated that in umbrella cells ATP may be stored in vesicular structures.

### ***ATP stimulates umbrella cell exocytosis***

If ATP is an important regulator of umbrella cell exocytosis then addition of exogenous ATP or analogs of ATP in the absence of hydrostatic pressure should evoke exocytosis, whereas depletion of pressure-induced released ATP should inhibit exocytosis. To determine whether ATP can stimulate pressure-induced exocytosis in bladder umbrella cells uroepithelium was stimulated with exogenous ATP. In control tissues without ATP or pressure stimulation, there were no changes in membrane capacitance. When the tissue was treated with 50  $\mu$ M ATP added into the serosal bathing media there was ~50% increase in membrane capacitance after 5 hours (Figure 4-4A). In the presence of 50  $\mu$ M mucosal ATP, membrane capacitance increased by a small amount (~20%) (data not shown). Similarly, when the uroepithelium was treated with 50  $\mu$ M adenosine 5'-[ $\gamma$ -thio]triphosphate (ATP $\gamma$ S), a nonhydrolyzable analog of ATP added into the serosal bathing solution, there was ~60% increase in membrane capacitance after 5 hours (Figure 4-4B). When 50  $\mu$ M ATP $\gamma$ S was added into the mucosal media there were no changes in membrane capacitance after 5 hours (data not shown). To determine the optimal concentration of ATP $\gamma$ S required to illicit the maximal increase in membrane capacitance a dose response curve

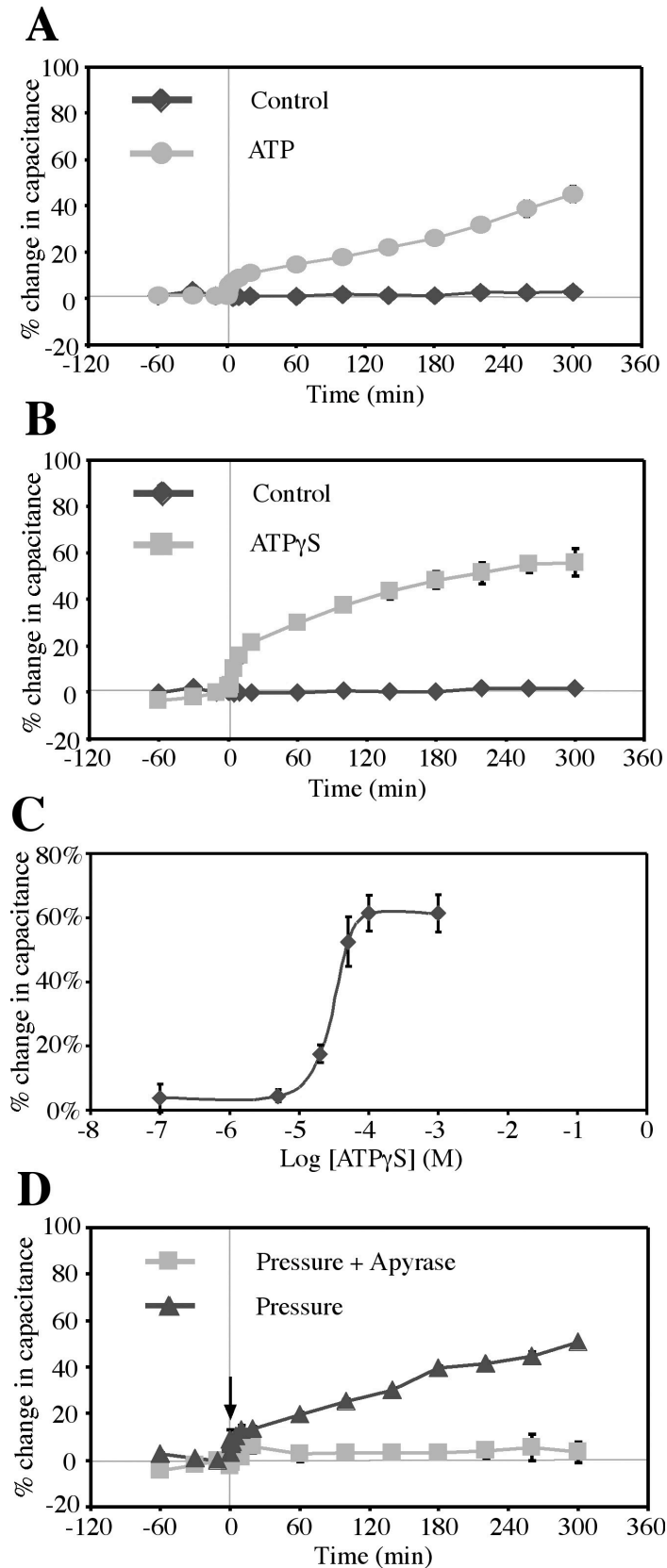


Figure 4-4. ATP stimulates umbrella cell exocytosis. (A) Effect of serosal ATP on capacitance in control tissues (no pressure). (B) Effects of serosal ATP $\gamma$ S on capacitance in control tissues. (C) Functional characterization of ATP $\gamma$ S. Uroepithelium was stimulated with different concentrations of ATP $\gamma$ S and membrane capacitance monitored. Maximal capacitance responses were plotted with the concentration of ATP $\gamma$ S applied. (D) Effects of 0.4 U/ml serosal apyrase on capacitance in stimulated tissues. Arrow indicates pressure stimulation. Data is mean  $\pm$  SEM (n=6).

for ATP $\beta$ S was generated. The minimal concentration of ATP $\beta$ S that could maximally stimulate capacitance increase was ~50  $\mu$ M (Figure 4-4C). This concentration was used in all subsequent pharmacology experiments unless stated otherwise.

If pressure-induced release of ATP from the uroepithelium could stimulate exocytosis, then depletion of extracellular ATP should block exocytosis. To test this, uroepithelium was incubated in the presence of apyrase, a membrane-impermeant exonucleotidase that breaks down extracellular ATP (157, 168). In control tissues without apyrase treatment, membrane capacitance increased ~55% after 5 hours of pressure stimulation (Figure 4-4D). When apyrase was added into the serosal bathing media, pressure-induced increases in membrane capacitance were blocked (Figure 4-4D). Addition of an alternative ATPase, hexokinase, also showed inhibitory effects on pressure-induced exocytosis when added into the serosal bathing solution (data not shown). If apyrase or hexokinase was added into the mucosal bathing solution, no inhibitory effect on membrane capacitance was observed upon pressure stimulation (Figure 4-5A and B). In fact, mucosal apyrase or hexokinase treatment appeared to stimulate capacitance increases in comparison to pressure treatment alone. These results indicated that ATP released from the serosal surface of the uroepithelium was important in signaling exocytosis.

### ***P2X receptor can modulate pressure-induced exocytosis***

ATP is the physiological ligand for purinergic receptors. To determine whether purinergic receptors were involved in this signaling cascade, the effects of pyridoxalphosphate-6-azophenyl-2',4'-disulfonic acid (PPADS), a general antagonist of the purinergic receptor signaling pathway, was examined. In tissues subjected to increased hydrostatic pressure membrane capacitance increased during the 5 h incubation period (Figure 4-6A). However,

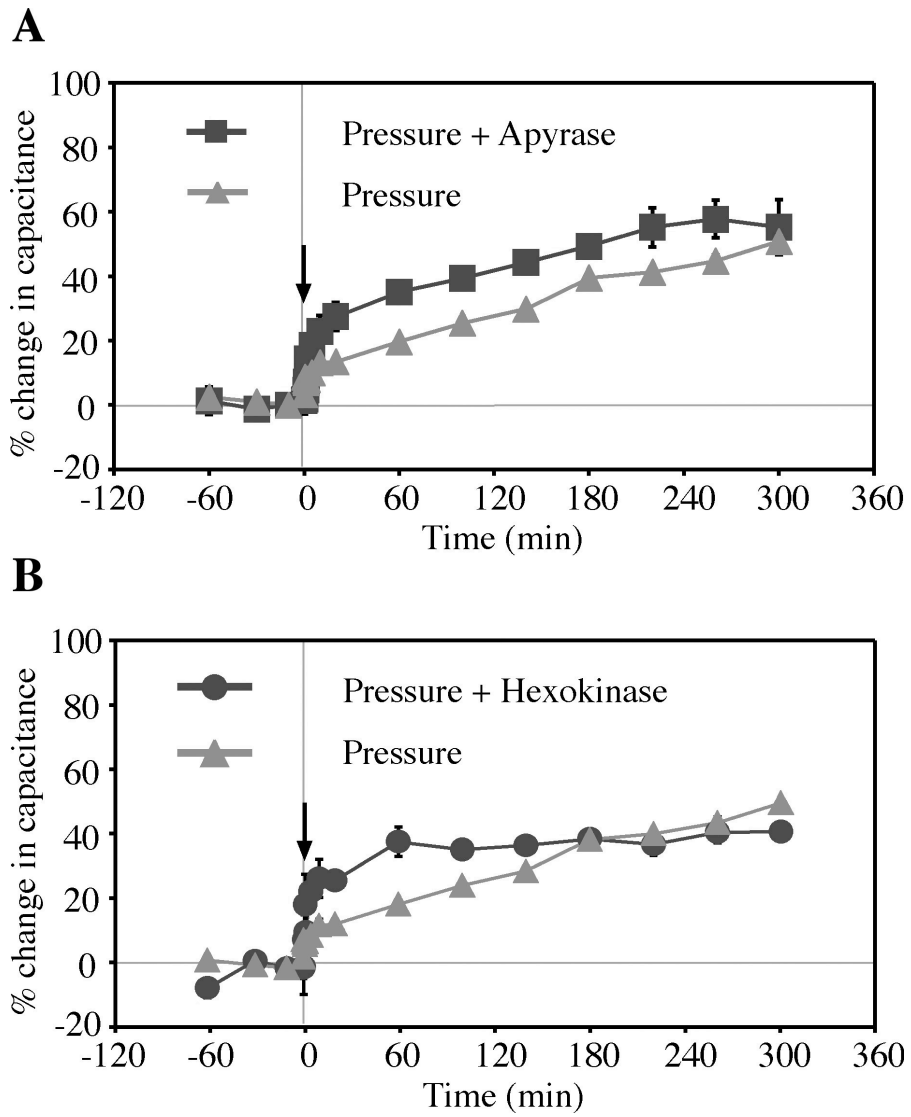


Figure 4-5. Mucosal ATPases have no effect on pressure-induced exocytosis. (A) Effects of 0.4 U/ml mucosal apyrase on membrane capacitance in pressure stimulated tissues. (B) Effects of 3 U/ml hexokinase and 22 mM glucose on membrane capacitance in pressure stimulated tissues. Arrow indicates pressure stimulation. Data is mean  $\pm$  SEM (n=6).

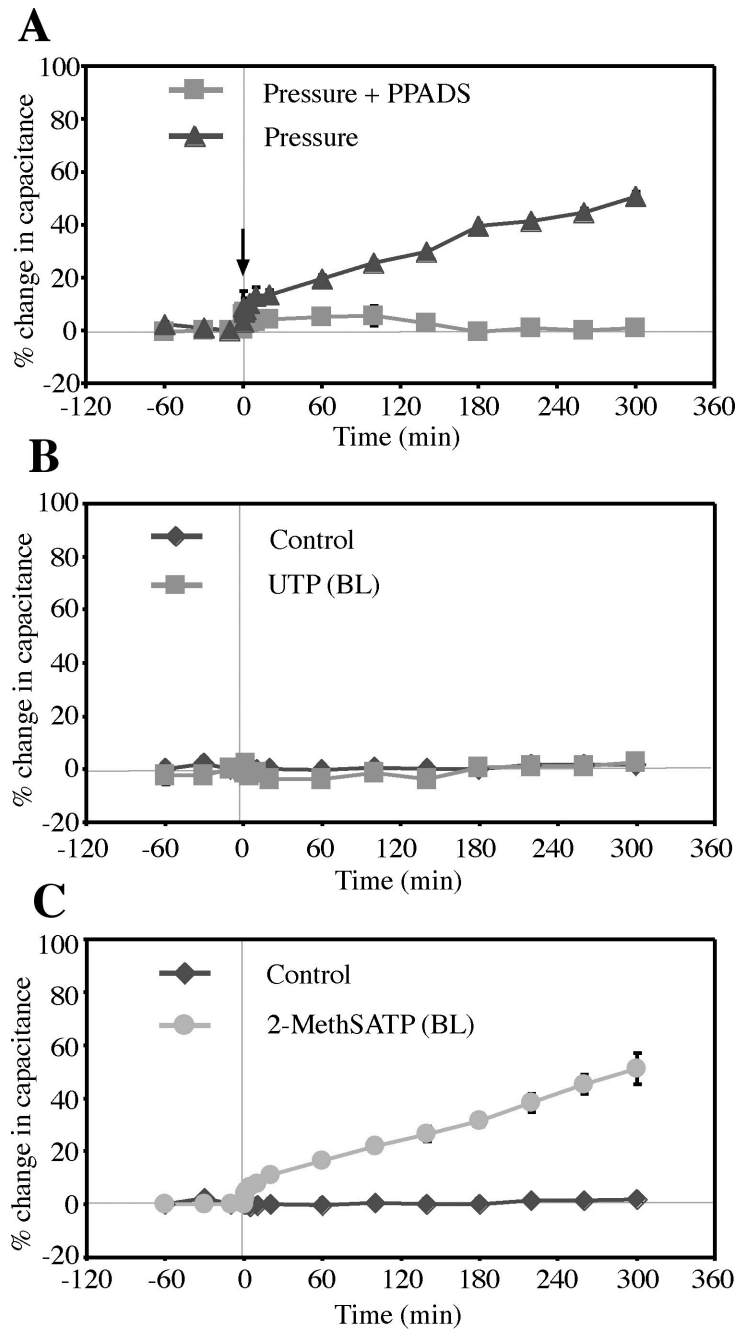


Figure 4-6. P2X receptors can modulate pressure-induced exocytosis. (A) Effects of 100  $\mu$ M PPADS on capacitance in pressure-stimulated uroepithelium. Arrow indicates pressure stimulation. (B) Effects of 50  $\mu$ M serosal UTP on capacitance in non-stimulated tissues. (C) Effects of 50  $\mu$ M serosal 2-MeSATP on capacitance in non-stimulated tissues. Data is mean  $\pm$  SEM (n=6).



when the uroepithelium was treated with PPADS, followed by exposure to hydrostatic pressure, exocytosis was almost completely inhibited (Figure 4-6A). Since PPADS can block both P2X and P2Y receptors the effects of potent P2X or P2Y receptor agonists were examined under pressure stimulation. When nonstimulated tissue was incubated with serosal uridine 5'-triphosphate (UTP) (Figure 4-6B), a potent P2Y receptor agonist, there were no changes in membrane capacitance. In contrast, tissues treated with serosal 2-methylthioadenosine 5'-triphosphate (2-MeSATP), a potent P2X receptor agonist, exocytosis was stimulated by an ~55% increase in membrane capacitance (Figure 4-6C). In the absence of 2-MeSATP, there were no changes in membrane capacitance after a 5-hour incubation period (Figure 4-6C). These data indicated that pressure-induced exocytosis was regulated via P2X receptor-dependent mechanisms.

***P2X<sub>2</sub> and P2X<sub>3</sub> receptors can modulate pressure-induced exocytosis in umbrella cells***

To further examine the importance of P2X receptors in pressure-induced exocytosis a pharmacology approach was used to identify the P2X receptor isoforms that regulate exocytosis. In tissues without pressure stimulation or receptor agonist treatment, membrane capacitance did not exhibit changes over time (Figure 4-4A, 4-6B and 4-6C). In uroepithelium incubated in the presence of P2X receptor agonists, the following rank potency on exocytosis was observed when individual agonist was added serosally and capacitance monitored: ATP[ $\beta$ ] > 2-MeSATP > ATP > BzATP >  $\alpha$ ,  $\beta$ -MeATP (Table 4-1). The pharmacological profiles generated using P2X receptor agonists compared well with known pharmacology of P2X<sub>2</sub> and P2X<sub>3</sub> receptors (Table 4-2).

**Table 4-1**

**Effects of purinergic receptor agonists and antagonists on membrane capacitance**

<b>Agonists*</b>	<b>Serosal treatment (% increase)<sup>a</sup></b>	<b>Mucosal treatment (% increase)<sup>a</sup></b>	<b>Antagonists</b>	<b>[C]f</b>	<b>Serosal treatment (% increase)<sup>b</sup></b>	<b>Mucosal treatment (% increase)<sup>b</sup></b>
<i>No treatment</i>	<b>0%</b>	<b>0%</b>	<i>No treatment</i>	-	<b>55-60%</b>	<b>55-60%</b>
<b>ATP</b>	<b>40%</b>	<b>~20%</b>	<b>Apyrase</b>	<b>0.4U/ml</b>	<b>~5%</b>	<b>~60%<sup>d</sup></b>
<b>ATP<sub>γ</sub>S</b>	<b>60%</b>	<b>0%</b>	<b>Hexokinase</b>	<b>3U/ml<sup>c</sup></b>	<b>~5%</b>	<b>~55%<sup>d</sup></b>
<b>2 MethSATP</b>	<b>~55%</b>	<b>20%</b>	<b>PPADS</b>	<b>100 μM</b>	<b>0%</b>	<b>~50%</b>
<b>BZ ATP</b>	<b>40%</b>	<b>30%</b>	<b>RB-2</b>	<b>50 μM</b>	<b>~55-60%</b>	<b>~55%</b>
<b>α,β-MethylATP</b>	<b>10%</b>	-	<b>PAP</b>	<b>50 μM</b>	<b>~50%</b>	-
<b>ADP</b>	<b>~20%</b>	<b>10%</b>				
<b>AMP</b>	<b>30%</b>	<b>40%</b>				
<b>Adenosine</b>	<b>40%</b>	<b>30%</b>				
<b>UTP</b>	<b>0%</b>	<b>45%</b>				
<b>UDP</b>	<b>30%</b>	<b>40%</b>				
<b>8-Br-ATP</b>	<b>30%</b>	-				

Isolated pieces of uroepithelium were mounted in modified Ussing chambers and equilibrated. Purinergic receptor agonist or antagonist was added into the serosal or mucosal bathing solution, and the effects of drug treatment on membrane capacitance were monitored. \*, Agonists were used at a final concentration of 50μM; <sup>a</sup>, percent increases in capacitance were measured after 5 hours of agonist treatment in the absence of pressure. <sup>b</sup>, percent increases in capacitance were measured after 5 hours of antagonist and pressure treatment. <sup>c</sup>, tissue was treated with hexokinase and 22mM glucose. <sup>d</sup>, initial increases in capacitance were observed (see Figure 4-5B).

## Table 4-2

### P2X Receptor Pharmacology

Our Data:  $\text{ATP}\gamma\text{S} > 2\text{-MeSATP} > \text{ATP} = \text{BzATP} > \alpha,\beta\text{-meATP} > \text{UTP}$

Receptor	Rank order of agonist activity	inhibitors
P2X <sub>1</sub>	$(\text{BzATP}) \geq 2\text{-MeSATP} = \text{ATP} = \alpha,\beta\text{-meATP} > \text{ATP}\gamma\text{S} \gg \text{UTP}$	PPADS, suramin, TNP-ATP
<b>P2X<sub>2</sub></b>	<b><math>\text{ATP}\gamma\text{S} \geq \text{ATP} \geq 2\text{-MeSATP} &gt; \text{BzATP} \gg \alpha,\beta\text{-meATP} &gt; \text{UTP}</math></b>	<b>PPADS, suramin</b>
<b>P2X<sub>3</sub></b>	<b><math>2\text{-MeSATP} \geq \text{ATP} \geq \alpha,\beta\text{-meATP} &gt; \text{ATP}\gamma\text{S} \gg \text{UTP}</math></b>	<b>PPADS, TNP-ATP</b>
P2X <sub>2/3</sub>	$\text{ATP} \geq \text{BzATP} > 2\text{-MeSATP} > \text{ATP}\gamma\text{S} \geq \alpha,\beta\text{-meATP} \gg \text{UTP}$	PPADS, suramin, TNP-ATP
P2X <sub>4</sub>	$\text{ATP} = \text{BzATP} > 2\text{-MeSATP} > \alpha,\beta\text{-meATP} > \text{ATP}\gamma\text{S}$	Weakly-sensitive to PPADS, suramin
P2X <sub>5</sub>	$\text{ATP} > 2\text{-MeSATP} \gg \alpha,\beta\text{-meATP}$	PPADS, suramin
P2X <sub>6</sub>	May not function as homomultimer	—
P2X <sub>7</sub>	$\text{BzATP} > \text{ATP} \geq 2\text{-MeSATP} > \text{ATP}\gamma\text{S} > \alpha,\beta\text{-meATP} > \text{UTP}$	Brilliant blue
P2Y <sub>1</sub>	$2\text{-MeSADP} > \text{ADP} = 2\text{-MeSATP} > \text{ATP}\gamma\text{S} > \text{ATP} \gg \text{UTP}$	PPADS, suramin

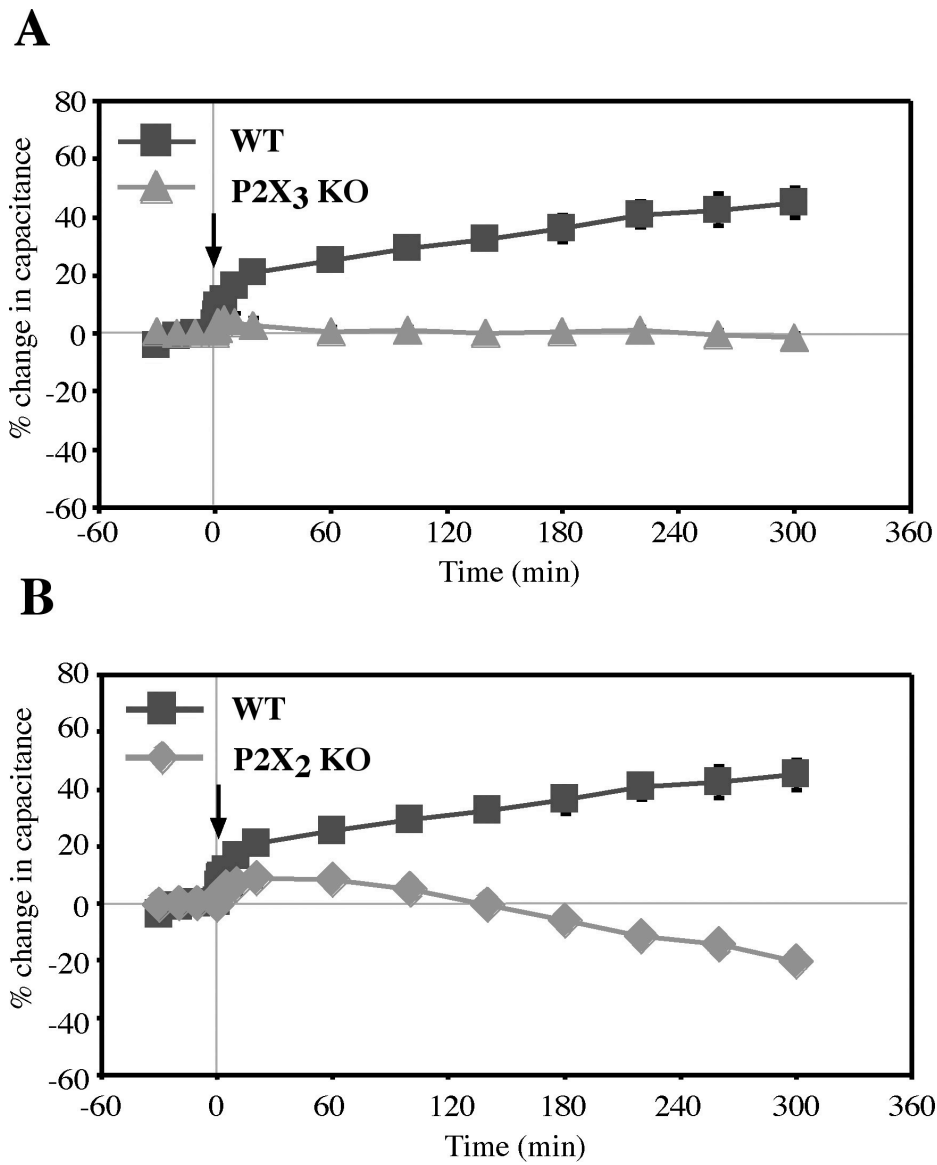


Figure 4-7. *P2X<sub>2</sub>* and *P2X<sub>3</sub>* receptors modulate pressure-induced membrane traffic. (A) Effects of hydrostatic pressure on umbrella cells lacking *P2X<sub>3</sub>* receptors. Uroepithelium from *P2X<sub>2</sub>* KO mice was stimulated with pressure at time = 0 (arrow) and membrane capacitance monitored. WT = wild type mouse bladder. (B) Effects of pressure on membrane capacitance in isolated uroepithelium lacking *P2X<sub>2</sub>* receptors. Data is mean  $\pm$  SEM (n=3).

To confirm that P2X<sub>2</sub> and P2X<sub>3</sub> receptors were indeed modulators of pressure-induced exocytosis, membrane capacitance changes were monitored in both wild type and P2X receptor knockout mice bladders exposed to hydrostatic pressure. Umbrella cells from wild type mice bladders responded to increased pressure with an ~50% increase in membrane capacitance (Figure 4-7A). In knockout mice lacking expression of P2X<sub>3</sub> receptors, membrane capacitance failed to increase when umbrella cells were exposed to hydrostatic pressure for 5 hours (Figure 4-7A). In knockout mice lacking P2X<sub>2</sub> receptors, increased hydrostatic pressure resulted in ~30% decrease in membrane capacitance after 5 hours (Figure 4-7B). These results indicated that P2X<sub>2</sub> and P2X<sub>3</sub> receptors could regulate exocytosis and possibly endocytosis when exposed to increased hydrostatic pressure.

***Expression and localization of P2X<sub>2</sub> and P2X<sub>3</sub> in the uroepithelium***

In the uroepithelium, P2X<sub>2</sub> and P2X<sub>3</sub> receptor expressions were detected by Western blot analysis (Figure 4-8). Several molecular weight species were identified, including the predicted

core protein for P2X<sub>2</sub> receptors (~52 kDa) (Figure 4-8; P2X<sub>2</sub> lane arrowhead) and P2X<sub>3</sub> receptors (~43 kDa) (Figure 4-8; P2X<sub>3</sub> lane arrowhead). To determine the location of P2X<sub>2</sub> and P2X<sub>3</sub> receptor expression in the uroepithelium, antisera against P2X<sub>2</sub> or P2X<sub>3</sub> receptor isoforms

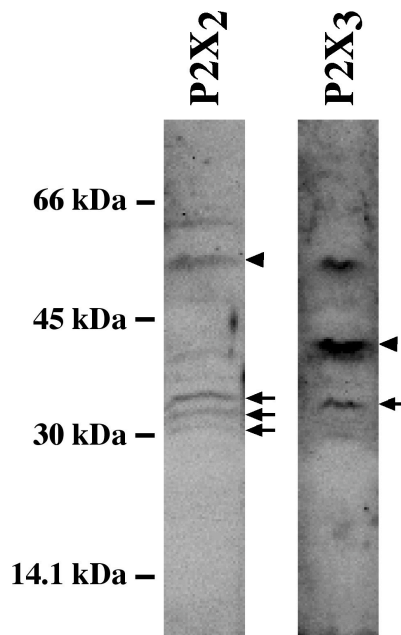


*Figure 4-8. Characterization of the P2X<sub>2</sub> and P2X<sub>3</sub> antisera by Western blotting. Thirty microgram of protein from rat bladder lysate was separated on 10% acrylamide gel, transferred to nitrocellulose, and probed with the rabbit anti-P2X<sub>2</sub> or rabbit anti-P2X<sub>3</sub> antibody. Lane 1, anti-P2X<sub>2</sub> antibody; lane2, anti-P2X<sub>3</sub> antibody. Anti-P2X<sub>2</sub> and anti-P2X<sub>3</sub> were detected by chemiluminescence with peroxidase-conjugated goat anti-rabbit IgG. Arrowheads indicate predicted size of core protein. Arrows indicate possible splice variants.*

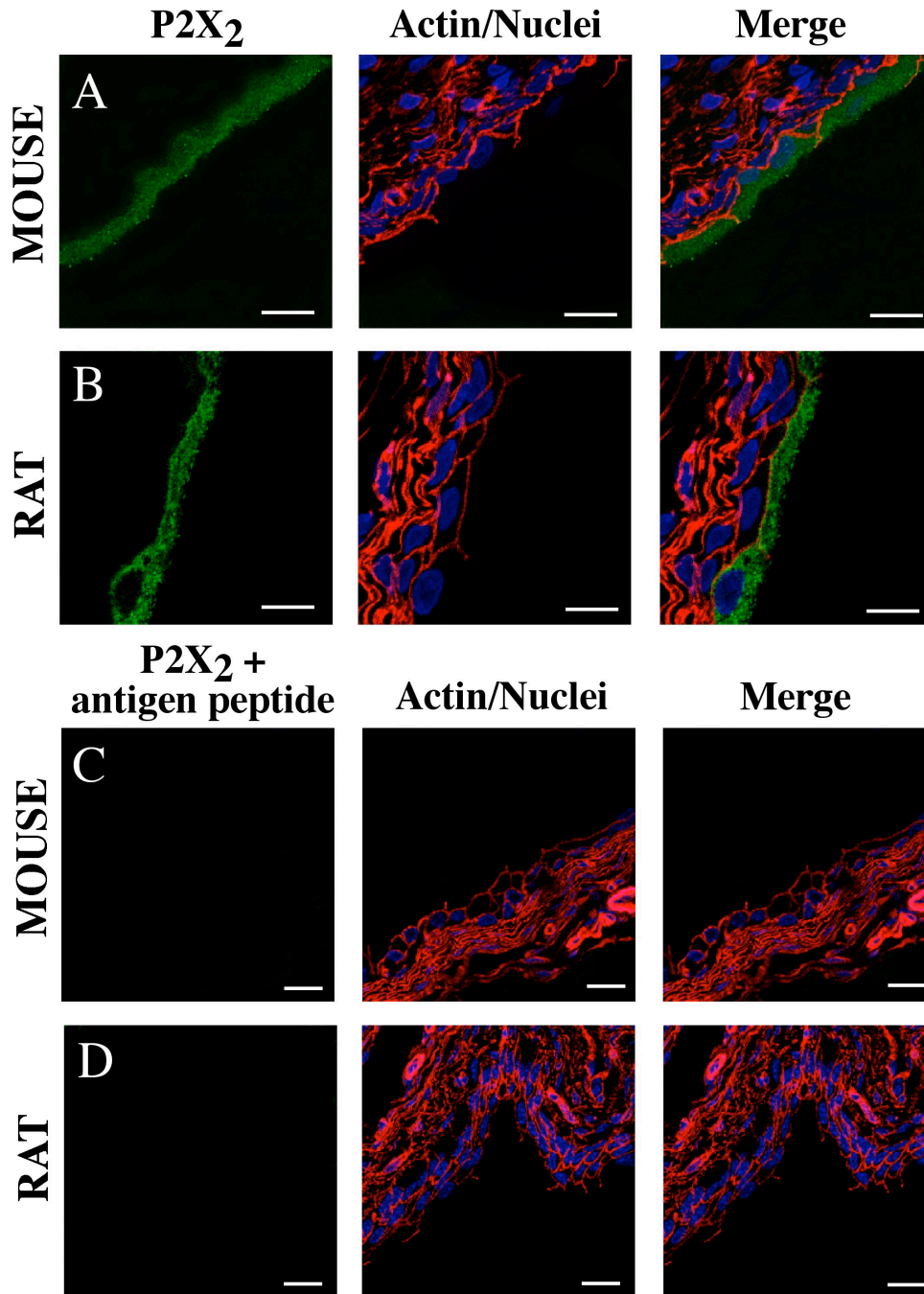


*Figure 4-9. Localization of P2X<sub>2</sub> receptor in the uroepithelium.* Mouse (A and C) and rat (B and D) bladders were fixed with paraformaldehyde and P2X<sub>2</sub> (green), actin (red), and nuclei (purple) were detected by indirect immunofluorescence microscopy with (A and B) and without (C and D) incubation with 1  $\mu$ M P2X<sub>2</sub> competitive antigen peptide. Each image represents a projection of optical sections acquired by a scanning laser confocal microscope. Bar in A and B = 20  $\mu$ m. Bar in C and D = 50  $\mu$ m.

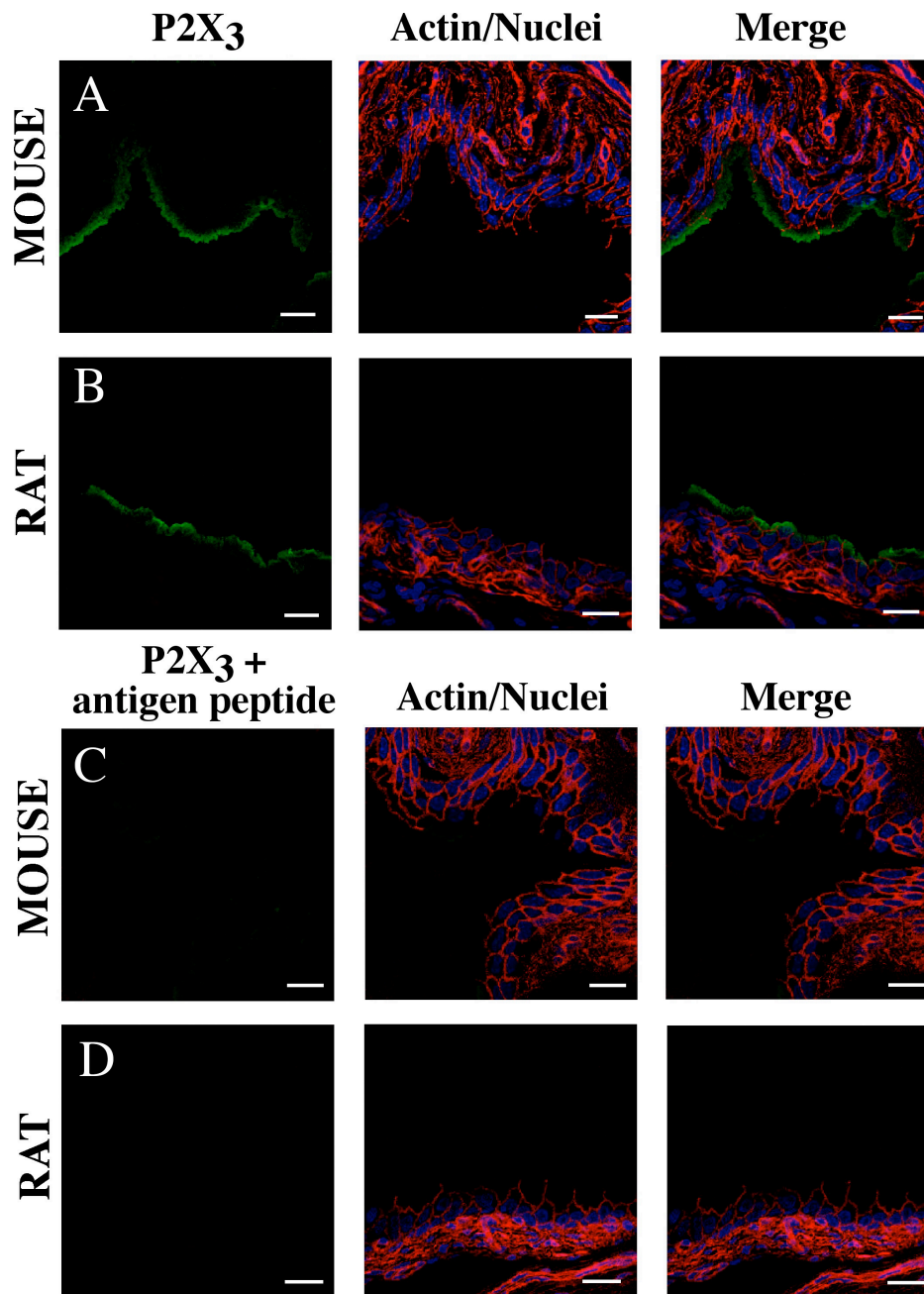


*Figure 4-10. Localization of P2X<sub>3</sub> receptor in the uroepithelium.* Mouse (A and C) and rat (B and D) bladders were fixed with paraformaldehyde and P2X<sub>3</sub> (green), actin (red), and nuclei (purple) were detected by indirect immunofluorescence microscopy with (A and B) and without (C and D) incubation with 1 μM P2X<sub>3</sub> competitive antigen peptide. Each image represents a projection of optical sections acquired by a scanning laser confocal microscope. Bar = 50 μm.

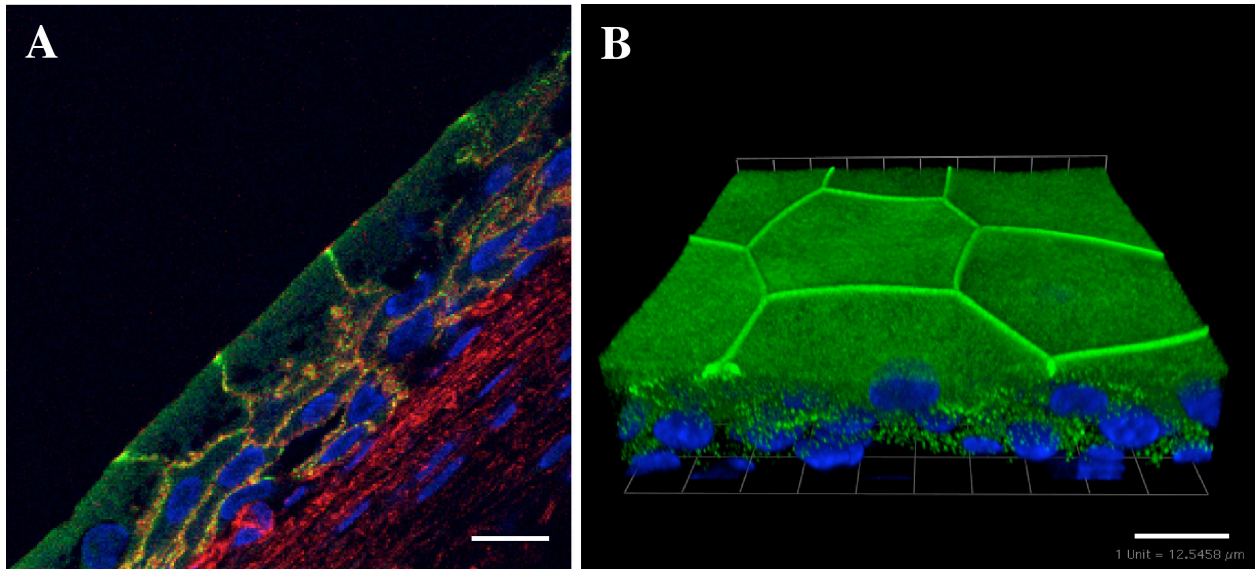


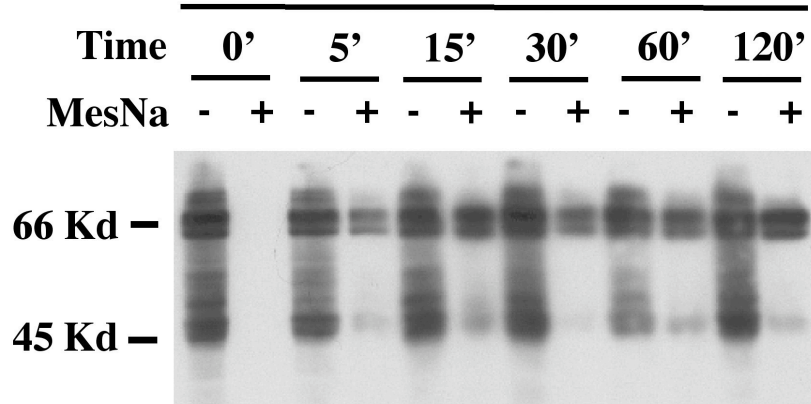
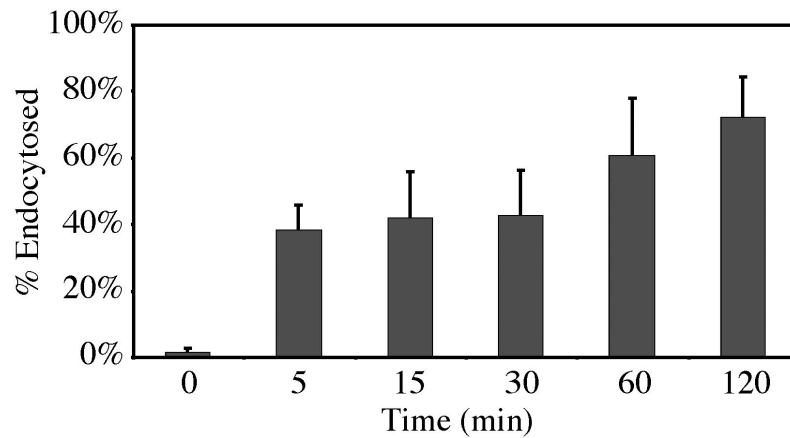
*Figure 4-11. Localization of P2X<sub>3</sub> receptor in the rabbit uroepithelium. (A) Rabbit uroepithelium was fixed with paraformaldehyde and P2X<sub>3</sub> (green), actin (red), and nuclei (purple) were detected by indirect immunofluorescence microscopy. Stacked optical sections of the rabbit uroepithelium. (B) Three-dimensional optical section (0.25 μm step size) reconstruction of rabbit uroepithelium stained with P2X<sub>3</sub> (green) and nuclei (purple). Bar = 20 μM.*



were used in immunohistochemistry. In both rat and mouse uroepithelium, P2X<sub>2</sub> receptors were primarily localized in the umbrella cell layer, with the bulk of the P2X<sub>2</sub> receptor staining found in intracellular compartments and on the basolateral membrane of umbrella cells (Figure 4-9A, 4-9B). Similarly, P2X<sub>3</sub> receptors were predominantly found in the umbrella cell layer of rat and mouse uroepithelium, with staining found in intracellular compartments and the plasma membrane (Figure 4-10A and 4-10B). To control for staining specificity competitive P2X<sub>2</sub> or P2X<sub>3</sub> receptor antigen peptide was preincubated with the appropriate P2X receptor antisera prior to tissue labeling. In the presence of both the control P2X<sub>2</sub> antigen peptide and the P2X<sub>2</sub> antiserum, no receptor staining was observed (Figure 4-9C, 4-9D). Similar results were detected when P2X<sub>3</sub> antigen peptide was preincubated with the P2X<sub>3</sub> receptor antiserum (Figure 4-10C and 4-10D). In rabbit bladder epithelium, a slightly different P2X<sub>3</sub> staining pattern was observed. Punctate P2X<sub>3</sub> staining was observed on basolateral membrane of umbrella cells as well as intermediate and basal cells (Figure 4-11A). P2X<sub>3</sub> stainings were also observed in intracellular compartments directly underneath the apical plasma membrane of umbrella cells (Figure 4-11A and B). Surprisingly, robust P2X<sub>3</sub> receptor staining was observed along the tight junction regions (Figure 4-11B). These data strengthened our hypothesis that P2X<sub>2</sub> and P2X<sub>3</sub> receptors in the umbrella cells could modulate exocytosis of cytoplasmic vesicles and localization of P2X receptors at the tight junctions may modulate tight junction proteins during filling.

### ***ATP[ $\beta$ ] stimulates endocytosis***

In addition to exocytosis, increased hydrostatic pressure stimulated endocytosis in the bladder umbrella cells (see Chapter 2). To test whether ATP could modulate endocytosis apical plasma membrane of the umbrella cell was labeled with biotin and the amount of biotinylated plasma

**A****B**

*Figure 4-12. ATP[S] stimulates endocytosis in bladder umbrella cells. (A) Umbrella cells were surface biotinylated and incubated for time = 0 (cells harvested immediately upon addition of ATP[S]), 5, 15, 30, 60, or 120 minutes in the presence of 50  $\mu$ M serosal ATP[S]. MesNa-protected biotinylated proteins were isolated and Western blots were probed with streptavidin-HRP. Shown is a representative Western blot and location of molecular weight standards (B) Quantification of ATP[S]-induced endocytosis of all biotinylated membrane proteins.*

membrane proteins that internalized upon treatment with serosal ATP[S] was determined (see Materials and Methods). Figure 4-12A is a representative Western blot of multiple experiments. In umbrella cells that were harvested immediately after addition of ATP[S] ( $t = 0$ ) no noticeable internalization of biotinylated membrane proteins was observed (Figure 4-12A, lane 2). However, after 5, 15, 30, 60, and 120 min of incubation with ATP[S], there were significant amounts of internalization for ~66 kDa and ~50 kDa biotinylated membrane proteins (Figure 4-12A, lanes 4, 6, 8, 10, 12). To quantify the amount of internalized biotinylated membrane proteins, the percentage of endocytosed biotin relative to the total amount of cell-associated biotin was determined for each time period (Figure 4-12B). After 5 min of ATP[S] treatment, ~40% of biotinylated membrane protein was internalized. This amount increased up to ~80% after 120 min post ATP[S] treatment (Figure 4-12B). These data indicated that in addition to exocytosis ATP may modulate pressure-induced endocytosis in the bladder umbrella cells as well.

#### ***ATP[S]-mediated exocytosis is $Ca^{2+}$ and PKA-dependent***

Purinergic receptors are important activators of  $Ca^{2+}$  release from intracellular stores. Activation of P2X receptors, which are nonselective cation channels, can transport  $Ca^{2+}$  from the extracellular milieu into the cell, in some cases leading to  $Ca^{2+}$  induced  $Ca^{2+}$  release (CICR) from the ER (17). In contrast, P2Y receptor activation may stimulate phospholipase C (PLC), increase diacylglycerol (DAG) production, inositol 1,4,5-triphosphate ( $IP_3$ ), and activate  $Ca^{2+}$  release from  $IP_3$ -sensitive stores from the ER (17). Increases in intracellular  $Ca^{2+}$  have been shown in this dissertation as well as many other studies to stimulate exocytosis. Increased  $Ca^{2+}$  may activate some isoforms of adenylate cyclase, resulting in increased cAMP production and

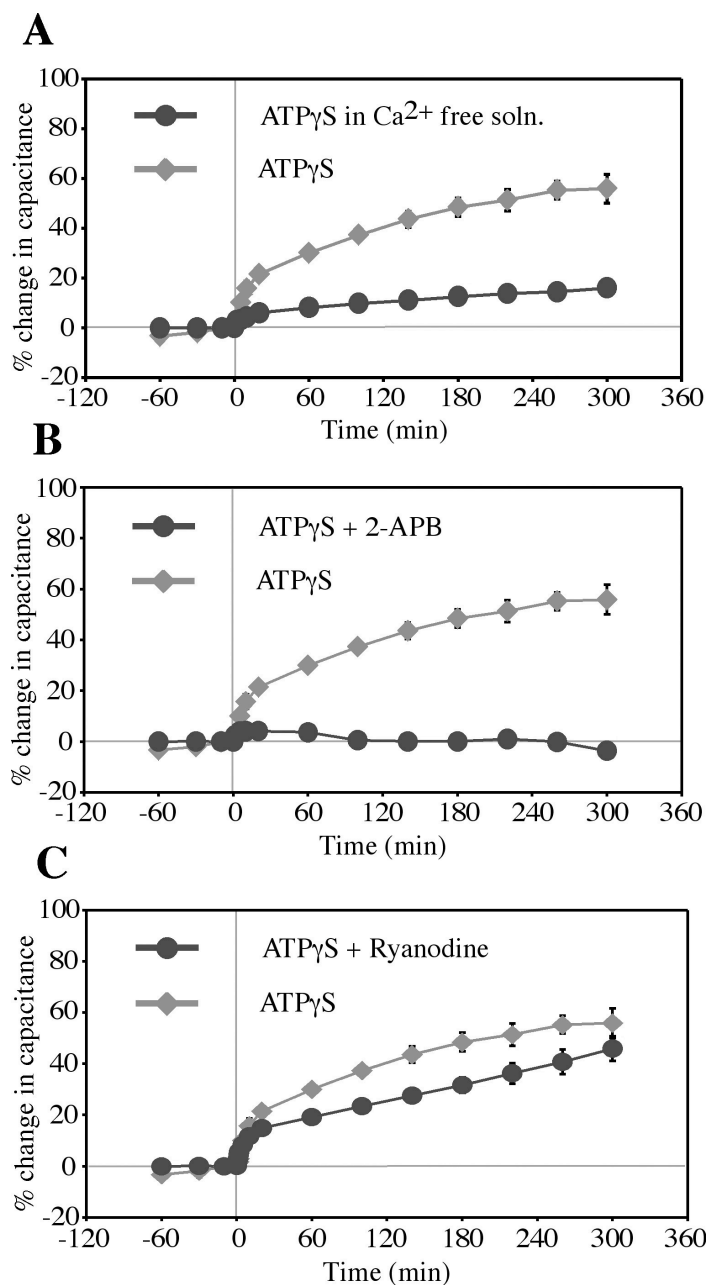


Figure 4-13. Role of  $Ca^{2+}$  on purinergic receptor-mediated exocytosis in umbrella cells. (A) Bladder tissue was mounted in the chamber and allowed to equilibrate. Following equilibration, the normal Krebs solution was isovolumetrically replaced with Krebs solution or Krebs solution lacking  $Ca^{2+}$ . At  $t=0$ , 50  $\mu$ M ATP $\gamma$ S was added into the serosal hemichamber and changes in capacitance were monitored over time. (B) Following equilibration, the tissue was either treated with 50  $\mu$ M serosal ATP $\gamma$ S alone, or treated with both serosal ATP $\gamma$ S and 75  $\mu$ M 2-APB. (C) Mounted bladder was either treated with 50  $\mu$ M serosal ATP $\gamma$ S, or treated with both serosal ATP $\gamma$ S and 50  $\mu$ M ryanodine. Changes in capacitance were monitored over time. Data are means  $\pm$  SEM from 6 separate experiments.

activation of the cAMP effector PKA (17). To determine whether  $\text{Ca}^{2+}$  signaling and PKA activities were important in purinergic receptor-mediated exocytosis in bladder umbrella cells the following experiments were performed.

When isolated uroepithelium was incubated with the nonhydrolyzable ATP analog ATP $\gamma$ S in the absence of hydrostatic pressure, membrane capacitance increased ~60% after the 5-hour incubation period (Figure 4-13A). However, when the tissue was treated with serosal ATP $\gamma$ S in the absence of extracellular  $\text{Ca}^{2+}$  and pressure, capacitance increase was significantly inhibited (Figure 4-13A). Similarly, when the uroepithelium was treated with serosal ATP $\gamma$ S and 75  $\mu\text{M}$  2-aminoethoxydiphenylborate (APB), a drug that inhibited  $\text{Ca}^{2+}$  release from IP $_3$ -dependent stores in the ER, capacitance increase was blocked (Figure 4-13B). When the tissue was incubated with serosal ATP $\gamma$ S and 50  $\mu\text{M}$  ryanodine, a blocker of  $\text{Ca}^{2+}$  release from ryanodine-dependent stores in the ER, membrane capacitance increase was slightly inhibited compared to ATP $\gamma$ S treatment alone (Figure 4-13C). In the presence of serosal ATP $\gamma$ S and the specific PKA inhibitor H89, capacitance increase was inhibited (Figure 4-14). These data indicated that purinergic receptor-mediated exocytosis in bladder umbrella cells may rely on  $\text{Ca}^{2+}$  and PKA-dependent signaling pathways.

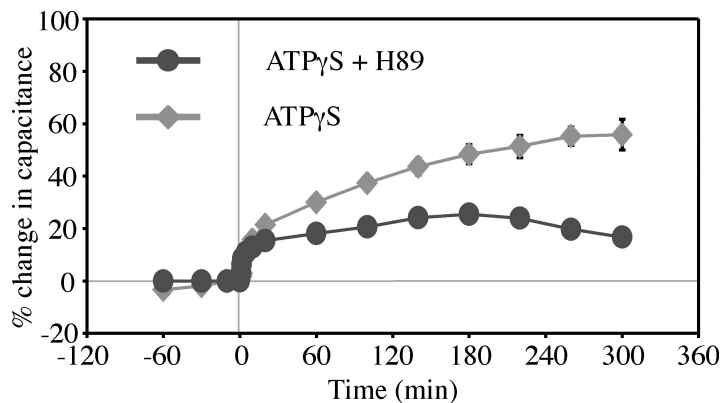


Figure 4-14. Effect of H89 on purinergic receptor-mediated exocytosis in umbrella cells. Bladder tissue was mounted in the chamber and allowed to equilibrate. Following equilibration, the tissue was either treated with 50  $\mu\text{M}$  serosal ATP $\gamma$ S alone, or treated with both serosal ATP $\gamma$ S and 10  $\mu\text{M}$  H-89. Changes in capacitance were monitored over time. Data are means  $\pm$  SEM from 6 separate experiments.

## ***DISCUSSION***

### ***Pressure stimulates ATP release from uroepithelium***

ATP is released from both the serosal and the mucosal surface of the rabbit uroepithelium immediately upon pressure stimulation (Figure 4-15). This is consistent with previous observations where exposing the uroepithelium to hydrostatic pressure caused significant amounts of ATP release (62, 221). However, Ferguson, *et al.* reported that ATP release occurred only from the serosal surface of uroepithelium exposed to hydrostatic pressure, not from the mucosal surface (62). Because the uroepithelium prepared by Ferguson and colleagues did not exhibit high TER ( $\sim 200 \Omega \cdot \text{cm}^2$ ), the integrity of the uroepithelial cells may have been compromised, and as a result ATP was depleted during the washing procedure (62). Also, since uroepithelial ATP release is highly pressure-sensitive, it was possible that the majority of mucosal ATP was depleted during tissue handling. The small amount of serosal ATP detected during pressure stimulation was the residual ATP in uroepithelial cells. Finally, differences in the levels of hydrostatic pressure, 3.5 cmH<sub>2</sub>O (62) versus 8 cmH<sub>2</sub>O (see Chapter 2) may account for differences in ATP release. The minimal amount of hydrostatic pressure required for mucosal ATP release may be greater than 3.5 cmH<sub>2</sub>O.

The extent of ATP release from the mucosal membrane was much greater than ATP released from the serosal membrane. In previous studies, it has been reported that the extracellular ATP concentration required for P2X receptor activation is in the micromolar range (30, 167). Since ATP released from the mucosal membrane is immediately exposed to a large volume of urine, significant ATP release is required to maintain a high local ATP concentration. In addition to the dilution factor, ATP is prone to degradation by ectonucleotidases on the extracellular face of the mucosal membrane and soluble exonucleotidases (168). Releasing large

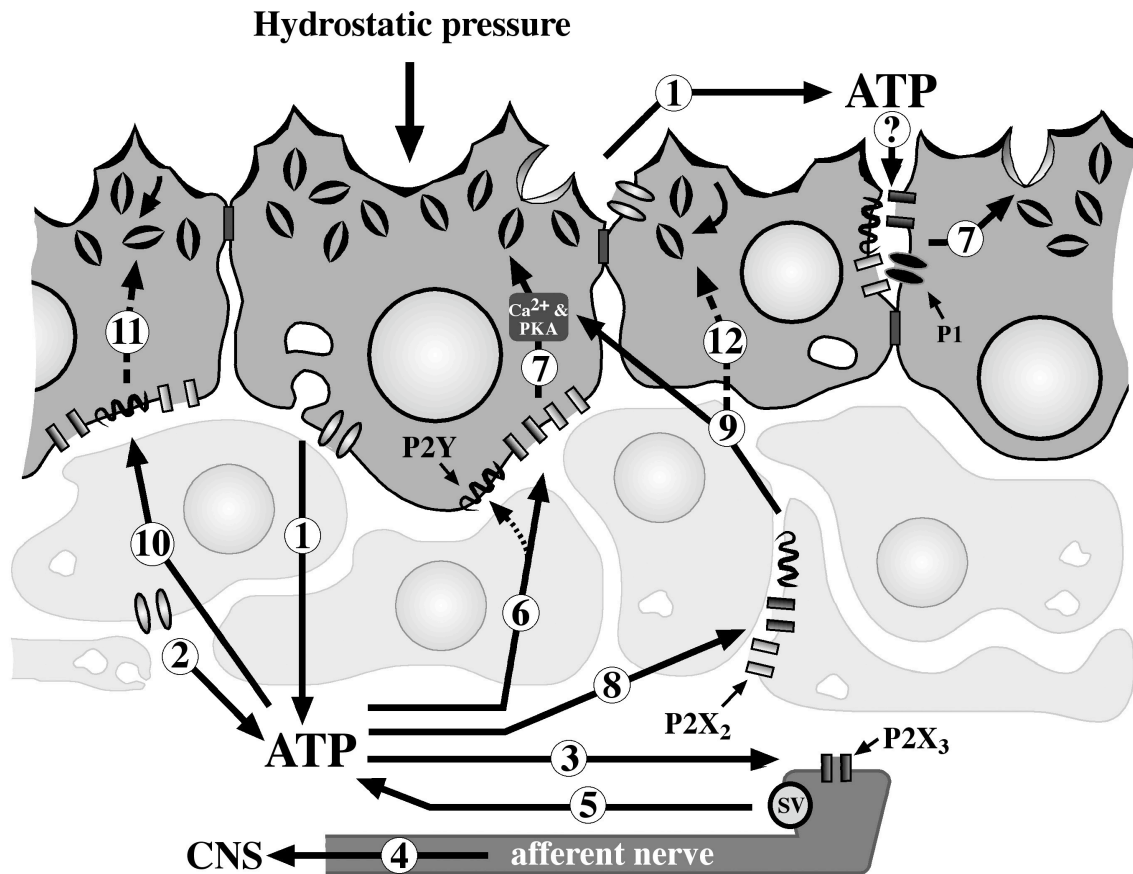


Figure 4-15. Model for ATP and purinergic receptor-regulated exocytosis / endocytosis in bladder umbrella cells. Bladder filling increases hydrostatic pressure, stimulating release of ATP from the uroepithelium via vesicular and connexin hemichannel mechanisms (steps 1 and 2). The released ATP can bind to P2X<sub>3</sub> receptors present on afferent nerve processes (step 3), increasing nerve firing and relaying bladder filling to the central nervous system (CNS) (step 4). Afferent neurons can release ATP through exocytosis of synaptic vesicle (SV) content (step 5). ATP released from either the afferent neurons or the uroepithelium can bind to P2X<sub>2</sub> and/or P2X<sub>3</sub> receptors, and perhaps P2Y receptors, on the umbrella cell (step 6). ATP released from the mucosal membrane may also result in activation of adenosine (P1) receptors. ATP binding stimulates increases in intracellular Ca<sup>2+</sup> (a result of Ca<sup>2+</sup> influx from outside the cell and efflux from IP<sub>3</sub> and ryanodine-dependent intracellular stores). ATP binding also activates PKA, which signals discoidal/fusiform vesicle exocytosis (step 7). ATP may also bind to purinergic receptors on the basal/intermediate cells (step 8), which stimulate release of “secretagogues” that act upon umbrella cells to stimulate vesicle exocytosis (step 9). In addition to exocytosis, ATP released from the uroepithelium and afferent neurons may activate purinergic receptors on umbrella cells and stimulate endocytosis via unknown signaling pathways (step 11, dash line). Umbrella cell endocytosis may also occur indirectly via activation of purinergic receptors on basal/intermediate cells, which stimulate release of “secretagogues” that stimulate umbrella cell endocytosis (step 12, dash line). Dark grey cells indicate umbrella cells. Light grey cells indicate intermediate and basal cells

amounts of ATP into the mucosal media would slow the degradatory process mediated by the extracellular ATPases.

Release of ATP under conditions of increased hydrostatic pressure was measured in the presence of BFA, which completely blocked pressure-induced ATP release. This result indicates that ATP release is via a vesicular-dependent pathway (Figure 4-15) and disagreed with the observations made by Ferguson and colleagues who argued that ATP release is nonvesicular due to calcium independence and lack of ATP-containing neurosecretory-like vesicles in the uroepithelial cells (61, 62). Although I have not directly measured the effect of  $\text{Ca}^{2+}$  depletion on ATP release, it is known that there is a large population of cytoplasmic vesicles in the umbrella cells and intermediate cells. When the umbrella cells are incubated in minimal extracellular  $\text{Ca}^{2+}$  or treated with an intracellular  $\text{Ca}^{2+}$  depleting agent (APB) pressure-induced exocytosis is blocked (see Chapter 2). In the ATP release experiments performed by Ferguson and colleagues, it should be noted that removal of extracellular  $\text{Ca}^{2+}$  from cell bathing media is extremely difficult. Therefore, extracellular  $\text{Ca}^{2+}$  may still be present at a low concentration sufficient for vesicular ATP release.

To further examine whether ATP release is vesicular, I used quinacrine. Because of its high affinity for ATP, quinacrine has been used to locate intracellular stores of ATP (109, 169). In the umbrella cells, quinacrine fluorescence appeared granular and exclusively localized in the cytoplasm. The punctate staining pattern is similar to that observed in other cell types such as endothelial cells and ocular ciliary epithelial cells where mechanically-induced ATP release is via vesicular mechanisms (24, 155). The nature of these quinacrine-positive vesicles in the umbrella cells is currently unknown. However, it is likely that they are discoidal/fusiform vesicles that traffic to and from the apical membrane of the umbrella cells (Figure 4-15). Further,



these vesicles have been shown in previous studies to be storage sites for secretagogue such as growth hormones and urinary proteases (e.g. tissue-type plasminogen activator and urokinase) (48, 113) and therefore may share similar function with neurosecretory vesicles that co-release ATP with neurotransmitters (168).

In addition to vesicular-dependent mechanism of ATP release, nonvesicular-dependent mechanisms are implicated in other cell types (203). To investigate the involvement of connexin hemichannels in pressure-induced ATP release from uroepithelial cells uroepithelium was mounted in Ussing chambers and treated with various inhibitors. In the presence of anandamide, significant amount of ATP release from the uroepithelium was blocked. This indicated that connexin hemichannels are involved in transporting ATP from the cytoplasm to the extracellular milieu (Figure 4-15). However, it should be noted that anandamide could affect other ion channels as well, including the capsaicin-activated ion channel vanilloid receptor (VR1). Alternatively, connexin hemichannels may mediate intercellular  $\text{Ca}^{2+}$  signaling such as propagation of  $\text{Ca}^{2+}$  waves from one cell to another to enhance ATP release (74), or delivery of connexin hemichannels to the plasma membrane may also depend on vesicle exocytosis. Therefore, connexin hemichannels may not be involved in ATP transport, but instead stimulate the propagation of biochemical signals that enhance ATP release. BFA-sensitive ATP release may also reflect a block in delivery of functional connexin hemichannel to the plasma membrane rather than inhibition of ATP transport by the channels. Further studies will need to be performed to address these possibilities.

Glibenclamide, an inhibitor of both the sulfonylurea receptor and CFTR (65, 196), was used to investigate the involvement of ABC proteins in the transport of ATP from the uroepithelial cells. Our results showed that glibenclamide had no effect on the pressure-induced

release of ATP from the uroepithelium. There could be several reasons for this: the role of these ABC proteins in the direct transport of ATP across membrane is still debated and it has been shown that purified CFTR does not function as an ATP transporter (142). ABC proteins may indirectly transport ATP as part of a heterogeneous molecular complex and may not be a vital requirement for ATP transport. Isolating the uroepithelium from its physiological environment (removal of muscle, nerves, and urine) may alter external cues that are required for receptor function. Finally, differences in gene expression (ABC protein) could exist in uroepithelium from rabbits to other animal species.

#### ***ATP stimulates umbrella cell exocytosis***

To examine the role of ATP on umbrella cell exocytosis, the effects of exogenously added ATP, ATP[S], and the ATPase apyrase was examined. My results indicated that not only can endogenous ATP stimulate exocytosis in umbrella cells (Figure 4-15), but exogenously added ATP can stimulate the exocytic response as well. Interestingly, serosal addition of ATP elicited greater exocytic responses than mucosal ATP addition (see Table 4-1). This indicated that different isoforms of ATP-sensitive purinergic receptors may be expressed on the apical and basolateral membrane of the uroepithelial cells. These purinergic receptor isoforms may exhibit slightly different sensitivity to ATP, and as a result, differentially stimulate umbrella cell exocytosis. It should also be noted that under physiological conditions, ATP, once it is released from the uroepithelial cell surfaces are targets of soluble as well as membrane bound nucleotidases. The degraded products of ATP, including ADP, may activate P2X (see Table 4-2) and P2Y receptor isoforms to different degrees of potency. Another degraded product of ATP, adenosine, may stimulate adenosine receptors (18, 66, 187). In fact, when apyrase was incubated

with the mucosal bathing media, a slight stimulatory effect was observed upon pressure stimulation. This could be attributed to activation of adenosine receptors and other purine-activated receptors. Yu, *et al.* has shown that treating isolated pieces of rabbit uroepithelium with mucosal adenosine receptor agonists can stimulate umbrella cell exocytosis in the absence of pressure stimulation (Figure 4-15) (245). Therefore, potential regulatory roles for adenosine receptors on the apical membrane of the umbrella cell cannot be ruled out.

ATP[S]-induced exocytosis was only observed when ATP[S] was added into the serosal bathing media. No changes in membrane capacitance were observed when ATP[S] was administered into the mucosal media. Again, the serosal and mucosal surfaces of the uroepithelium may express different isoforms of purinergic receptors, and as a result, respond differently to ATP[S] (see Table 4-2). It is equally possible that adenosine receptors are the primary regulators of umbrella cell exocytosis via the mucosal surface of the uroepithelium. Therefore, the nonhydrolyzable property of ATP[S] prevented endogenous ATPases from generating adenosine.

### ***P2X receptor can modulate pressure-induced exocytosis***

The effects of ATP released into the extracellular space depend on the specific receptors expressed in the tissue. In previous studies, P2X<sub>2</sub>, P2X<sub>3</sub>, P2X<sub>4</sub>, and P2X<sub>5</sub> were localized to the uroepithelial cells (58, 61, 125). However, the roles of these receptors in the biology of uroepithelial cells are unknown. One important feature of umbrella cells is its ability to commence exocytosis upon exposure to hydrostatic pressure. To determine whether purinergic receptors regulate pressure-induced exocytosis in umbrella cells, isolated uroepithelium was stimulated with the nonselective purinergic receptor antagonist PPADS and the data showed that

pressure-induced exocytosis was blocked. Since there are no selective agonists or antagonists for P2X or P2Y receptors, it was not possible to determine which P2 receptors are involved in modulating pressure-induced exocytosis. However, I saw no effect when the potent P2Y (UTP) or P2X (2-MethSATP) agonist was added into the serosal bathing media indicating that only serosal P2X receptors could modulate pressure-induced exocytosis. This conclusion should be interpreted with caution as P2 receptor agonists (e.g. ATP and 2-MethSATP) can also activate P2Y receptors (29). In a recent study, Jung and colleagues demonstrated that exocytosis in pancreatic duct epithelial cells is dependent on  $Ca^{2+}$ , cAMP, and P2Y receptors (111). Since  $Ca^{2+}$  and cAMP are intracellular modulators of exocytosis in umbrella cells (see Chapter 2) the possibility that P2Y receptors may regulate exocytosis from the apical membrane of umbrella cells cannot be ruled out.

***P2X<sub>2</sub> and P2X<sub>3</sub> receptors can modulate pressure-induced exocytosis in umbrella cells***

To further examine the importance of P2X receptors in pressure-induced exocytosis two different experimental approaches were used. A common, pharmacology approach was used to show that P2X<sub>2</sub> and P2X<sub>3</sub> receptor isoforms on the mucosal membrane of the uroepithelium are important modulators of umbrella cell exocytosis. The rationale for choosing this approach was because no selective agonists or antagonists for different P2X receptor isoforms are currently available, but also because it was relatively easy to generate the pharmacology profile for agonist-induced exocytosis in umbrella cells. Despite the relative ease of this approach, there are several drawbacks. For example, the reported pharmacology profiles for different P2X receptor isoforms in the literature (Table 4-2) were generated using heterologous expression systems such as human embryonic kidney 293 (HEK293) cells and xenopus oocytes (167). When rat or mouse

P2X receptor isoforms are expressed in non-native environments, the receptors may not function in physiological manners. One reason may be because many P2X receptors function in hetero-oligomeric forms (e.g. P2X<sub>1/5</sub>, P2X<sub>2/3</sub>, P2X<sub>2/6</sub>, and P2X<sub>4/6</sub>) (167). Some P2X receptors (e.g. P2X<sub>2</sub>) also have alternative splice variants that exhibit different pharmacology profile from the full-length receptors (see discussion below) (25). Additionally, the uroepithelium may express multiple isoforms of purinergic receptors, complicating the pharmacology results. Any of the aforementioned reasons would obscure the pharmacology data.

To confirm that P2X<sub>2</sub> and P2X<sub>3</sub> receptors are important regulators of umbrella cell exocytosis, P2X receptor null mice were obtained from Roche Bioscience, Palo Alto. In the absence of P2X<sub>3</sub> receptors, pressure-induced exocytosis in umbrella cells was completely blocked. In contrast, when P2X<sub>2</sub> receptor was absent from the mice bladder, there was a net decrease in capacitance after pressure stimulation. One possible explanation for this is that in addition to modulating pressure-induced exocytosis, P2X receptors may modulate pressure-induced endocytosis in umbrella cells (Figure 4-15). The role of P2X receptors in pressure-induced endocytosis will be discussed further below.

### ***Expression and localization of P2X<sub>2</sub> and P2X<sub>3</sub> in the uroepithelium***

The expression of P2X<sub>2</sub> and P2X<sub>3</sub> purinergic receptors in the uroepithelium was examined by Western blot analysis. The predicted core protein for P2X<sub>2</sub> receptors (~53 kDa) was identified in rat uroepithelial cell lysate, indicating that P2X<sub>2</sub> receptors are expressed in the rat uroepithelium. However, Western blot analysis using the polyclonal anti-P2X<sub>2</sub> antisera also detected several smaller molecular weight species ranging from ~30 kDa to ~36 kDa. One potential explanation for the smaller molecular weight species may be due to alternative splicing. In previous studies,

Brandle and colleagues detected several alternative splice variants of P2X<sub>2</sub> receptor in rat tissues using the polymerase chain reaction (PCR) (25). The PCR products resulted in three distinct bands of ~30 kDa, ~33 kDa, and ~36 kDa (25). Two of these PCR products, P2X<sub>2</sub> (~36 kDa) and P2X<sub>2-2</sub> (~30 kDa), yielded functional receptor/channel with significant differences in desensitization time constants and steady-state currents in the continuous presence of ATP. In contrast, the ~33 kDa PCR product was uncharacterized and PCR analysis indicated that it may be an artifact created by the interaction of the P2X<sub>2</sub> splice variant isoforms (25). In addition to the small molecular weight bands, an ~60 kDa band was also detected by Western blot analysis, consistent with the molecular weight of the single or double *N*-linked glycosylated form of P2X<sub>2</sub> receptors (211).

Similar to the expression of P2X<sub>2</sub> receptors, P2X<sub>3</sub> receptors are also detected by Western blot in the rat uroepithelium. Using a polyclonal anti-P2X<sub>3</sub> receptor antiserum, the predicted core protein for P2X<sub>3</sub> receptor (~43 kDa) was observed. Other molecular weight species detected by the P2X<sub>3</sub> antiserum include a high and a low molecular weight band that may correspond to glycosylated form of the P2X<sub>3</sub> receptor and splice variant, respectively. Alternatively, the low molecular weight species may be degraded product of the P2X<sub>3</sub> receptor. The exact identities of the nonpredicted core proteins are currently unknown.

In mouse and rat uroepithelium, P2X<sub>2</sub> and P2X<sub>3</sub> receptor-specific staining were localized to the umbrella cell layer and P2X<sub>2</sub> receptor was also found on the smooth muscles as previously reported (125, 220). While most of the receptors appeared in punctate intracellular structures within the umbrella cells, membrane-bound receptors were hard to distinguish. In contrast, P2X<sub>3</sub> receptor-specific staining was found throughout the rabbit uroepithelium. The basolateral plasma membrane of the umbrella cells and the plasma membrane of the intermediate and basal cells

showed distinct punctate membrane associated P2X<sub>3</sub> staining (Figure 4-15). This is not surprising as pharmacology experiments using P2X receptor agonists or antagonists were most effective when applied from the serosal membrane of the rabbit uroepithelium, indicating that the signaling pathways that stimulated exocytosis occurred via the serosal P2X receptors (Figure 4-15). The more surprising result was the robust localization of P2X<sub>3</sub> receptors at the tight junctions that may regulate the expression of tight junction proteins during filling to accommodate the substantial morphological changes that occur in umbrella cell (214, 225). While the significance of P2X<sub>3</sub> receptors at the tight junctions is unknown, results from current studies underscore the importance of P2X<sub>3</sub> receptors during the filling response.

#### ***ATP[S stimulates apical endocytosis in umbrella cells***

In this study, I have shown that agonist stimulation led to umbrella cell apical plasma membrane internalization (Figure 4-15). Using a biotin protection assay it was estimated that ~80% of a select subset of biotinylated membrane proteins (~66 kDa and ~50 kDa species) was internalized after 2 hours of continued presence of ATP[S. This indicated that ATP[S was able to selectively stimulate certain receptor-mediated endocytic events. Alternatively, the potency of ATP[S on activating internalization of membrane proteins may be diverse. Some membrane proteins may exhibit a rapid internalization kinetic in the presence of ATP[S, while others may exhibit slower kinetics. Regardless, this is the first evidence demonstrating that ATP may be involved in regulation of pressure-induced endocytosis in the bladder umbrella cells.

Under physiological conditions it is known that hydrostatic pressure stimulates endocytosis in the umbrella cells. However, the signaling pathways that regulate endocytosis are unknown. The data from this study indicated that ATP released into the extracellular milieu may

activate purinergic receptors on the serosal membrane of the uroepithelial cells, leading to internalization of apical membrane proteins (Figure 4-15). This is consistent with recent studies where agonist stimulation resulted in internalization of biotinylated P2X<sub>1</sub> receptors (59) and activation of a P2X<sub>7</sub>-like receptor in thyrocytes stimulated exocytosis and endocytosis (119). Similarly, endocytosis of P2Y receptors was stimulated upon uridine nucleotide treatment (27). Results from this study showed that in addition to purinergic receptors, other apical membrane-associated proteins were internalized as well, including uroplakins, albumin, and other unidentified plasma membrane proteins.

#### ***ATP[ $\beta$ ]-activated exocytosis is dependent on Ca<sup>2+</sup> and PKA***

While purinergic receptor activation can induce exocytosis in bladder umbrella cells, the downstream effectors and signaling molecules that can modulate the exocytic event remain unknown. Studies presented in Chapter 2 of this dissertation indicated that Ca<sup>2+</sup> and PKA are important modulators of pressure-induced exocytosis in umbrella cells. However, it is unknown whether Ca<sup>2+</sup> and PKA activities are required for purinergic receptor-induced exocytosis in umbrella cells. By incubating the uroepithelium in minimal Ca<sup>2+</sup> bathing solution, membrane capacitance was inhibited when stimulated with serosal ATP[ $\beta$ ]. Similarly, when release of Ca<sup>2+</sup> from intracellular stores was blocked, capacitance increase was inhibited. These results indicated that purinergic receptor mediated exocytosis is dependent on Ca<sup>2+</sup> entering the cell from extracellular milieu, as well as intracellular release of Ca<sup>2+</sup> from both IP<sub>3</sub>-sensitive and ryanodine-sensitive stores in the ER (Figure 4-15).

Consistent with earlier studies (see Chapter 2), exocytosis in umbrella cells was also PKA-dependent in purinergic receptor activated tissues (Figure 4-15). Although it is unknown



whether PKA activation is dependent on cAMP or increased intracellular  $\text{Ca}^{2+}$ . Previous studies have indicated that PKA can be activated via both mechanisms (cAMP and/or increased  $\text{Ca}^{2+}$ ). Clearly, additional work will be required to elucidate the signaling molecules that function in the purinergic receptor mediated exocytic response. These results are consistent with the functional roles of P2X and P2Y receptors that can stimulate exocytosis in a variety of cell types via increased intracellular  $\text{Ca}^{2+}$  and/or activation of PKA via the adenylate cyclase signaling pathways (29).

## SUMMARY AND CONCLUSIONS

The mammalian urinary bladder was once thought to be a static organ that functioned primarily to store the urine and prevent the toxic components of urine from entering the underlying tissues. However, recent advances in research methods and experimental systems have allowed a closer examination of the urinary bladder, opening up several interesting facets of the bladder that we are only beginning to understand. One interesting feature of the bladder is the presence of various mechanosensitive ion transport pathways. Activation of these pressure-sensitive ion channels may affect uroepithelial cell biology, including release of regulatory factors (e.g. proteases, hormones, and chemical messengers) from the uroepithelium. In addition, the uroepithelium may provide a means of retrieving crucial soluble proteins that are filtered by the kidney (e.g. albumin). Another feature of the bladder is its ability to accommodate large fluctuations in urine volume. This latter feature has important implications as understanding the accommodative responses of the bladder and the effect of filling on uroepithelial cell biology may provide greater insights to how other mechanosensitive cells react to external forces.

In this dissertation, several aspects of the bladder accommodative responses were examined. Using a novel pressure chamber system that mimicked urine filling the effects of hydrostatic pressure on membrane traffic in the bladder umbrella cells were investigated. The signaling mechanisms that modulate the accommodative responses were explored as well, including identification of mechanotransducers such as pressure-activated ion channels and

plasma membrane receptors, and important signaling molecules such as ATP, cAMP, Ca<sup>2+</sup>, and PKA. The following sections will examine how the experiments presented in this dissertation have increased our understanding and opened up future directions in urinary bladder research.

### ***Development of a pressure chamber system***

Examining the adaptive responses of the uroepithelium in the original Ussing chamber system was a major advance in bladder research. The Ussing chambers allowed Lewis and de Moura to make real-time measurements of the bladder luminal surface area in response to osmotic or hydrostatic pressure (135). However, the design of the Ussing chambers only allowed for small increases in hydrostatic pressure, which in turn yielded only modest increases in capacitance (17%). Substantial increases in membrane capacitance were observed when the tissue was subjected to osmotic stress (77%), undermining the physiological significance of the data. To further our understanding of the bladder accommodative responses, steps were taken to improve the design of the existing Ussing chamber system. By closing off the mucosal chamber to the outside air, a physiological pressure could be administered to mimic the filling process in intact bladder while membrane capacitance could be measured to monitor real-time changes in the apical surface area of the umbrella cell.

Using this modified Ussing chamber system, filling responses of the urinary bladder epithelium were investigated. The effect of hydrostatic pressure on the morphology of the umbrella cell and the substantial stimulatory effect on umbrella cell apical membrane surface area were consistent with normal physiological responses during the urine-filling process. These observations demonstrated that the pressure chambers could be powerful tools for examining unanswered questions of bladder biology. Some unexplored aspects of the bladder include, the

transport itinerary of discoidal vesicles during pressure stimulation, effects of mechanical stimuli on tight junction proteins, role of mechanosensors, and the role of potential mechanotransducers (e.g. purinoceptors, integrin receptors, and receptor tyrosine kinases) during the filling process. The pressure chambers can also be used to examine accommodative responses of the bladder during disease states (e.g. interstitial cystitis). With the availability of animal models of cystitis, diseased uroepithelium can be mounted in the pressure chambers, and the effect of physiological pressure stimuli on bladder functions, including barrier, ion transport, and mechanotransduction, can be examined. The following sections will explore the potential future applications of these pressure chambers.

### ***Pressure-induced exocytosis***

Although our data indicated that hydrostatic pressure caused exocytosis of discoidal vesicles at the apical plasma membrane of the umbrella cells, it was unknown whether exocytosis occurred at the basolateral membrane of the umbrella cell as well. Stereological analysis indicated no significant changes in the basolateral membrane surface area after a 5-hour period of pressure stimulation. However, this did not exclude the possibility that fusion of the discoidal vesicles with the basolateral membrane was immediately followed by vesicle internalization. Moreover, since the basolateral surface of the umbrella cells did not contain detectable levels of uroplakin at steady state, recycling of the basolateral membrane cannot be ruled out.

Intermediate cells of the uroepithelium also contain UPIII-positive cytoplasmic vesicles. The role of cytoplasmic vesicles in these cells during the filling response is currently unknown. A recent preliminary experiment performed by Truschel, *et al.* indicated that increased hydrostatic pressure did not stimulate significant changes in intermediate cell surface area

despite disappearance of UPIII-positive vesicles (212). Immuno-EM also did not demonstrate presence of UPIII on intermediate cell plasma membrane (212). These data indicated that the UPIII-positive cytoplasmic vesicles in the intermediate cells may not function akin to discoidal vesicles that fuse with the apical membrane of the umbrella cells. Increased hydrostatic pressure may stimulate rapid UPIII-positive vesicle exocytosis/endocytosis in intermediate cells and delivery to lysosomes for degradation, or the vesicles may be trafficked directly to the lysosomes. However, these ideas are speculative. To further examine whether hydrostatic pressure can stimulate intermediate cell exocytosis, a more thorough stereological analysis of the plasma membrane surface area of intermediate cells will be required. If exocytosis is stimulated, membrane surface area of intermediate cells exposed to hydrostatic pressure will be significantly greater than control, unstimulated cells. The trafficking itinerary of UPIII-positive vesicles in intermediate cells will need to be further elucidated as well. Understanding the dynamics of these vesicles may help us understand how supporting cells of other epithelia respond to mechanical stimuli.

### ***Pressure-induced endocytosis***

Despite the supportive evidence for pressure-induced exocytosis in umbrella cells, our data indicated that other pressure-induced events may be occurring simultaneously. First, stereological analysis indicated that the increase in umbrella cell apical surface area was less than one-third of the decrease in vesicle surface area. Second, the total amount of UPIII decreased significantly after the 5-hour period of pressure stimulation. The reason for these observations was that increased pressure not only stimulated exocytosis, but pressure also stimulated endocytosis and delivery of internalized membrane components to the lysosomes.

I did not explore the molecular mechanisms by which pressure-induced endocytosis occurred. Examination of the umbrella cell apical plasma membrane by electron microscopy did not reveal the presence of clathrin-coated pits nor caveolae (data not shown), indicating that endocytosis may be clathrin- and caveolae-independent. To test this idea in the future, the role of clathrin-mediated endocytosis will be examined during pressure stimulation. Several ways to abate clathrin-mediated internalization include potassium depletion, cytosol acidification, and treating the tissue with hypertonic bathing media (11, 93, 174). If pressure-induced endocytosis is independent of clathrin, these treatments should have no effect. Alternatively, a dominant negative mutant of dynamin, which has been shown previously to inhibit both clathrin- and caveolae-dependent endocytosis (166, 217) could be used since a transfection protocol for bladder uroepithelium is now available (112). The inability of the dynamin mutant to inhibit pressure-induced endocytosis would indicate that clathrin and caveolae are not involved in this membrane internalization.

In contrast to the apical plasma membrane, electron microscopy analysis revealed that the basolateral membrane of the umbrella cells contain clathrin-coated pits (data not shown). The discovery of clathrin-coated invaginations on the basolateral surface indicated that endocytosis from each membrane may be differentially regulated. Whether endocytosis from the basolateral membrane is stimulated by hydrostatic pressure is unknown. However, since stereological analysis did not show statistically significant changes in basolateral membrane surface area, endocytosis from the basolateral surface may be coupled with fusion of discoidal vesicles along the basolateral membrane, resulting in rapid recycling of membrane components. This idea would agree with the lack of steady-state expression of UPIII on the basolateral membrane. A

simple uptake experiment using fluid phase marker incubated in the serosal bathing media can be used to test whether pressure-induced endocytosis occur via the basolateral membrane surface.

The role of pressure-induced endocytosis is still speculative. At first glance, increased endocytosis during pressure stimulation may appear counter-intuitive. However, it can synchronize with exocytosis to fine-tune the addition or retrieval of membrane surface area. Endocytosis may also provide a method for self-repair of damaged membrane components. Interestingly, receptor-mediated reabsorption of important kidney-filtrate may occur in the bladder, including internalization of albumin via the albumin receptor GP60 (210, 222). Resensitization of purinergic receptors after prolonged exposure to its physiological ligand ATP may depend on pressure-activated endocytosis as well. Regardless of its function, endocytosis during filling may play an important role in the normal function of the bladder.

### ***Intracellular modulators of pressure-induced exocytosis***

In isolated uroepithelium, the signaling molecules involved in pressure-induced endocytosis are unknown. However, several important modulators of pressure-induced exocytosis were identified. Similar to other regulated secretory events, extracellular and intracellular  $\text{Ca}^{2+}$  signaling played an important role in modulating exocytosis in umbrella cells (see Chapter 2 and 4). Sources of intracellular  $\text{Ca}^{2+}$  signaling include  $\text{IP}_3$ - and ryanodine-sensitive stores in the ER. To confirm that hydrostatic pressure can stimulate  $\text{Ca}^{2+}$  increase in umbrella cells, live uroepithelium can be mounted in a newly designed pressure chamber (courtesy of Dr. Gerard Apodaca) fitted for the confocal microscope. The effect of pressure on intracellular  $\text{Ca}^{2+}$  concentrations can be assessed in live cells using cell permeable  $\text{Ca}^{2+}$  indicators Fluo-3-acetoxymethyl (Fluo-3-AM) and Fura-Red-acetoxymethyl (Fura-Red-AM). If umbrella cell

exocytosis is  $\text{Ca}^{2+}$ -dependent, then intracellular  $\text{Ca}^{2+}$  concentration should rise when the tissue is exposed to pressure. Alternative possibilities include  $\text{Ca}^{2+}$ -induced release of a secretagogue (e.g. ATP) from intermediate and/or basal cells, which then stimulates umbrella cell exocytosis.

Subsequent downstream  $\text{Ca}^{2+}$  effectors, which include  $\text{Ca}^{2+}$  sensitive isoforms of adenylate cyclase, phospholipase C $\beta$ , and membrane channels, may have profound effects on pressure-induced umbrella cell exocytosis. Numerous blockers and inhibitors that can alter the activities of these  $\text{Ca}^{2+}$  effectors are commercially available. Future studies could include examination of the drug effects on pressure-induced exocytosis. Any deviation from the control response (no drug treatment) would implicate the  $\text{Ca}^{2+}$  effectors in the filling response.

In addition to  $\text{Ca}^{2+}$ , hydrostatic pressure also stimulated cAMP production in the uroepithelium. When isolated uroepithelium was treated with forskolin to artificially raise intracellular levels of cAMP, umbrella cell exocytosis but not endocytosis was dramatically increased. Treating the uroepithelium with forskolin and H89, a specific inhibitor of the cAMP effector PKA, also significantly inhibited umbrella cell exocytosis, indicating that PKA activation is downstream of adenylate cyclase activation. Although adenylate cyclase and PKA are implicated in pressure-induced increases in umbrella cell surface area, the specific adenylate cyclase isoforms and PKA subtypes involved in this process are unknown. Adenylate cyclase enzymes are divided into nine subfamilies based on their regulatory patterns. Group 1 isoforms (I, III, and VIII) are stimulated by calcium/calmodulin. Group 2 isoforms (II, IV, and VII) are regulated by G protein  $\beta\gamma$ -subunits. Group 3 isoforms (V and VI) are regulated by PKA and protein kinase C (PKC), and the group 4 isoform (IX) is characterized by insensitivity to calcium, G-protein  $\beta\gamma$ -subunits, or forskolin. In contrast, PKA is defined by two different subtypes, type I and type II. To further understand the cAMP and PKA-dependent signaling



pathways in the uroepithelium, future investigators can identify the dominant isoforms of adenylate cyclase expressed in the uroepithelium. Antibodies specific for various adenylate cyclase isoforms are commercially available and can be used for immunoblot analysis. In addition, combinations of cAMP analogs that can selectively activate PKA type I (*N*-6-monobutyryl-cAMP and 8-(6-aminohexyl)-amino-cAMP) or PKA type II (*N*-6-monobutyryl-cAMP and 8-(4-chlorophenylthio)-cAMP) can be used in pressure chamber experiments to determine the specific PKA subtypes that can induce umbrella cell exocytosis in the absence of pressure. Understanding the function of these intracellular modulators during the bladder filling process will increase our understanding of mechanotransduction in other cell types. Furthermore, it may improve strategies in designing effective drugs against intracellular molecules that are vital in various bladder ailments.

### **Mechanotransduction in the urinary bladder**

The ability of the bladder to sense cyclical changes in urine volume and initiate the appropriate accommodative responses is an important feature. This depends on the presence of mechanosensors that can detect pressure differences in the lumen space and mechanotransducers that can collaborate the relay of mechanical signals to intracellular components. In the bladder, the mechanosensor that detects urine-induced pressure changes is unknown. However, research presented in this dissertation indicated that pressure-activated ion channels could be ideal candidates. In addition, membrane receptors such as purinergic receptors may play important roles in mechanotransduction. These studies have furthered our understanding of mechanotransduction in the urinary bladder.

### ***Role of ATP***

The bladder uroepithelium released significant amounts of ATP from both the mucosal and serosal membrane when stimulated by hydrostatic pressure. However, the mechanosensor that facilitates ATP release is unknown. One possibility is that ATP release may depend on the activity of the ENaC (62). But this is unlikely as the ENaC blocker amiloride did not block pressure-induced rises in membrane capacitance (data not shown) and increases in membrane capacitance were dependent on ATP release. ATP release may also require expression of vanilloid receptor 1 (VR1), an ion channel expressed by nociceptive afferent neurons and the uroepithelium (20, 21). It is currently unknown how VR1 modulates ATP release from the uroepithelium. Bladder preparations lacking VR1 failed to release ATP in response to hydrostatic pressure, and as a result, membrane capacitance was inhibited as well (21). These observations are worthy of future examination as VR1 may coordinate ATP release by regulating levels of intracellular  $Ca^{2+}$ . This can be tested by measuring intracellular  $Ca^{2+}$  concentrations of uroepithelial cells (see above) in the presence of capsaicin, a potent activator of VR1 receptor. VR1 may also associate with other ion channels or non-ion channel proteins to form mechanosensory complexes to regulate umbrella cell membrane trafficking. It was shown by Guo and colleagues that VR1 receptors colocalized with P2X<sub>3</sub> receptors (88). Future studies using cross-linking agents will allow us to determine whether VR1 receptors are associated with other membrane proteins to form putative mechanosensitive complexes. Examination of P2X receptor activities in VR1 knockout mice bladders will reveal whether expression and function of P2X receptors are VR1-dependent.

While pressure-induced ATP release into mucosal and serosal bathing media can activate membrane receptors, the source of ATP release is currently unknown. Quinacrine staining in the

uroepithelium demonstrated punctate ATP-containing structures in the umbrella cell layer, but punctate staining was observed in the underlining intermediate and basal cell layers as well (data not shown). The observations that ATP-containing vesicles were present throughout the uroepithelial cell layers indicated that ATP release could modulate important cellular functions, not only in bladder umbrella cells, but also in intermediate cells, basal cells, and the smooth muscle cells. The effects of ATP on intermediate and basal cells are currently unknown, but may include alteration in membrane biology and volume regulatory responses. Clearly, smooth musculature surrounding the uroepithelium can respond to ATP as P2X<sub>1</sub> and P2X<sub>2</sub> receptors are localized on the membrane and cytoplasm of the smooth muscle cells, respectively (125). In the future, additional work will be required to examine the functional role of ATP on the biology of the intermediate cells, basal cells, and the smooth muscle cells during the urine-filling process. Stereological analysis of intermediate and basal cells will determine whether ATP stimulation alone can increase membrane surface area and cell volume.

### ***Purinergic receptors***

Another potential mechanotransducer in the bladder uroepithelium is the purinergic (P2) receptor. Several P2X receptor isoforms are expressed on the plasma membrane of uroepithelial cells, including the umbrella cells, but nothing is known about the functional role of P2X receptors in membrane trafficking of umbrella cells. Ferguson and colleagues have proposed that P2X receptors are ideal mechanotransducers in the bladder uroepithelium (62). We observed that general inhibitors of P2 receptors inhibited pressure-induced exocytosis, indicating that P2 receptor activities are required during the filling response. Significantly, pressure-activated exocytosis is blocked in P2X<sub>2</sub> or P2X<sub>3</sub> knockout mice bladder, further implicating P2X<sub>2</sub> and/or

P2X<sub>3</sub> receptor homomers or heteromers in discoidal vesicle exocytosis during filling. Additional studies will be necessary to determine the role of P2X<sub>2/3</sub> heteromer in pressure-stimulated exocytosis. This can be examined by immunofluorescent colocalization studies using commercially available P2X<sub>2</sub> or P2X<sub>3</sub> antibodies in wild type animal bladders.

Hydrostatic pressure also stimulated endocytosis in bladder umbrella cells. Absence of P2X<sub>2</sub> receptors in knockout mice bladders resulted in a net decrease in membrane capacitance, implicating P2X-mediated endocytosis. When isolated uroepithelium was treated with ATP[S], a subset of biotinylated membrane protein was internalized as well, including albumin (~66 kDa) and UPIII (~47 kDa). The observation that ATP[S] could stimulate internalization of some biotinylated membrane proteins indicated that P2X receptors may selectively activate some receptor-mediated endocytic pathways. One potential pathway is the uptake of albumin via the albumin receptor GP60 (210, 222). Other pathways include internalization of uroplakin proteins. Future studies will be required to determine whether the physiological P2X receptor activator ATP can stimulate endocytosis of biotinylated membrane proteins. In addition, pharmacology studies using synthetic P2X receptor agonists can be incubated with the uroepithelium in endocytosis assays to generate the rank potency of agonists for comparison with pharmacology profiles of known P2X receptor isoforms. This will provide clues to which P2X receptor subtypes are modulators of pressure-induced endocytosis in umbrella cells, and possibly increase our understanding of endocytic mechanisms of other mechanosensitive cell types.

At present, any role for P2Y receptors is unclear, although there are preliminary data implicating P2Y receptor in discoidal vesicle exocytosis using potent P2Y receptor agonists (data not shown). Additional pharmacology studies using the pressure chambers will be required to examine the role of specific P2Y receptor isoforms in umbrella cell exocytosis in the future.

### ***Pressure-activated ion channels***

While hydrostatic pressure could stimulate exocytosis in bladder umbrella cells, the mechanosensors that detect pressure changes and initiate the signaling pathways for exocytosis are unknown. One potential mechanosensor is the nonselective cation channel (NSC) on the apical membrane of umbrella cells. Another potential pressure sensor on the umbrella cell apical membrane is the pressure-sensitive Cl<sup>-</sup> channel. Pressure-activated NSC activities in the umbrella cells were sensitive to amiloride, TEA, Ba<sup>2+</sup>, and Gd<sup>3+</sup>. Pressure-regulated Cl<sup>-</sup> transport was confirmed by elevated <sup>36</sup>Cl<sup>-</sup> flux across the uroepithelium during pressure stimulation. Activation of these channels by hydrostatic pressure could alter the membrane biology of the umbrella cells during the accommodative responses. Studies have emerged that mechanosensitive ion channel activities may also play important roles in volume regulatory responses, including pressure sensitive ion channels (NSC and Cl<sup>-</sup> channel) addressed in this dissertation (12, 206).

Whether pressure sensitive ion channels discussed are regulators of membrane traffic in umbrella cells are currently speculative. However, it would not be surprising if NSC and/or Cl<sup>-</sup> channel activities during filling coordinate the accommodative responses. Previous studies indicated that in addition to modulation of membrane potential, activation of NSC and Cl<sup>-</sup> channels could regulate important cellular functions such as Ca<sup>2+</sup> release from intracellular stores, secretion of vasoactive compounds, and cytoskeleton dynamics (16). These studies paralleled with our results where we observed that both intracellular and extracellular Ca<sup>2+</sup> were important modulators of exocytosis in umbrella cells. Similarly, other investigators have demonstrated that exocytosis of discoidal vesicles released secretory proteins (48, 113), and disruption of the microfilament network impaired exocytosis of discoidal vesicles in umbrella

cells (128). To understand the functional roles of these ion channels in  $\text{Ca}^{2+}$  release, protein secretion, and microfilament dynamics, further experiments need to be performed.

The primary advantage of the pressure chambers is that the chambers allow real-time measurement of surface area by monitoring membrane capacitance. The design of the system also allowed manipulation of the bathing media composition so that effects of various drugs and reagents on membrane capacitance can be determined. To this end, the functional roles of pressure-activated ion channels on capacitance increase can be examined by stimulating the uroepithelium in the presence of various ion channel blockers. If NSC activity is essential for exocytosis, the presence of TEA,  $\text{Ba}^{2+}$ ,  $\text{Gd}^{3+}$ , and high concentrations of amiloride should prevent pressure-induced capacitance increase. Other specific ion channel blockers for NSC and  $\text{Cl}^-$  channels are available and similar studies can be performed with ease. Alternatively, membrane capacitance can be monitored in ion substitution experiments as described in Chapter 3 to examine the importance of various pressure-activated channels in umbrella cell exocytosis.

### *Adenosine receptors*

Extracellular ATP is rapidly degraded by ecto- and exonucleotidases into ADP, AMP, and adenosine. While ATP and ADP are potentiators of purinergic receptors, adenosine can activate adenosine receptors. There are at least four different isoforms of adenosine receptors, including  $\text{A}_1$ ,  $\text{A}_{2\text{A}}$ ,  $\text{A}_{2\text{B}}$ , and  $\text{A}_3$  receptors. Their roles on membrane trafficking in the bladder umbrella cells are currently unknown. However there are data to support the stimulatory role of adenosine receptors in umbrella cell exocytosis (245). First, mucosal apyrase treatment stimulated pressure-induced capacitance increase to a greater level than pressure-treatment alone. Second, mucosal adenosine treatment in the absence of pressure resulted in capacitance increase. Third, treating

the uroepithelium with adenosine receptor selective agonist CCPA ( $A_1$  specific), CGS ( $A_{2A}$  specific), or IB-MECA ( $A_3$  specific) stimulated capacitance increase (245). These data support a stimulatory role of adenosine receptor during the filling response. This may occur by regulated coordination between adenosine receptors, purinergic receptors, and ion channels and/or other membrane receptors. Additional studies are underway to elucidate the functional role of adenosine receptors during the filling response in the urinary bladder.

### ***Other mechanotransducers***

Other mechanotransducers, including integrin receptors, tight junction proteins such as occludin and claudins, as well as actin, microtubules and intermediate filaments may play important roles in mechanotransduction during the filling response. Integrins, which link extracellular matrix molecules to the intracellular actin cytoskeleton are capable of transmitting mechanical stress to the underlying cytoskeleton via talin and  $\alpha$ -actinin (6, 31, 226). Tight junctional proteins such as occludin and claudins may relay extracellular stimuli into biochemical signals as well. Both of these proteins form scaffolds that allow communication with intracellular cytoskeletal components (1). During the filling response modification of umbrella cell tight junction is mandatory as it allows expansion of the umbrella cell apical plasma membrane. Adaptive responses of the umbrella cell tight junction to increased hydrostatic pressure and integrin activities during pressure stimulation may transduce extracellular stimuli into biochemical signals. Studies using agents that perturb the activities of integrin or tight junction proteins will provide useful information on the mechanosensory roles of these proteins during the filling response. Any inhibitory effect on pressure-induced exocytosis or endocytosis will implicate integrin and tight junction proteins in membrane traffic in umbrella cells.

Cytoskeletal proteins such as actin, microtubules, and intermediate filaments play important roles in mechanotransduction. They serve as scaffolds that coordinate the organization of signaling complexes that can modulate cellular events such as endocytosis and exocytosis (6, 107). Deformation of the plasma membrane as a result of pressure stimulation is followed by rapid reorganization of the cytoskeleton. Because the cytoskeleton is attached to integrin receptors, tight junction, and other membrane proteins, alterations in membrane tension will affect the activities of the signaling complexes. In umbrella cells, intermediate filaments are required for discoidal vesicle exocytosis (135). Microtubules and actin may also be required for tethering and trafficking of the discoidal vesicles to the periphery of the cell in preparation for exocytosis. Further examination using agents that perturb the normal assembly and turnover of cytoskeleton on pressure-induced membrane traffic will be required to understand the mechanosensory role of cytoskeleton in bladder uroepithelium.

### **Closing comments**

In this dissertation, I presented data to dispel the dogma that the urinary bladder is simply a sac for storage of urine by demonstrating that the bladder is constantly undergoing microscopic and macroscopic changes in response to pressure. These results not only provide greater understanding of how our bladder accommodates increased urine, the studies presented here open new directions in bladder research. It is my hope that future studies will improve our understanding of bladder biology, and help us understand how other mechanosensitive cells respond to external forces.



# **APPENDICES**

## APPENDIX A

### MATERIALS AND METHODS

#### *Materials*

Unless stated otherwise reagents were obtained from Sigma Chemical Co. (St. Louis, MO, USA). Leupeptin and lactacystin were dissolved in DMSO and used at a final concentration of 40  $\mu\text{M}$  and 10  $\mu\text{M}$ , respectively. Stock solution for forskolin was prepared at 10 mM in Krebs solution and used at a final concentration of 10  $\mu\text{M}$ . IBMX was dissolved in Krebs solution to a stock concentration of 500 mM and used at 1:1000. H89 was prepared in DMSO and used at a final concentration of 10  $\mu\text{M}$ . The calcium ionophore calcimycin A23187 was prepared at 1 mM in Krebs buffer and ionomycin was prepared at 2.5 mM in Krebs buffer. Both stock solutions were at 1:1000 to obtain the final concentrations of 1  $\mu\text{M}$  and 2.5 mM, respectively. Intracellular calcium modulator thapsigargin was dissolved in Krebs solution and used at a final concentration of 10  $\mu\text{M}$ . APB was prepared in Krebs solution and used at a final concentration of 75  $\mu\text{M}$ . Stocks of the following ion channel inhibitors were prepared as follows: amiloride was dissolved in water at 10 mM or when used at 500  $\mu\text{M}$  it was dissolved directly into buffer solution; apamin was dissolved in water at 100  $\mu\text{M}$ ;  $\text{BaCl}_2$  was dissolved in  $\text{Na}^+$ ,  $\text{Cl}^-$ -free buffer at 1.5 M;  $\text{GdCl}_3$  was dissolved in  $\text{Na}^+$ ,  $\text{Cl}^-$ -free buffer at 100 mM; glibenclamide was dissolved in DMSO at 50 mM; ouabain was dissolved in water at 13 mM; TEA was dissolved in  $\text{Na}^+$ ,  $\text{Cl}^-$ -free buffer at 1 M. The following  $\text{K}^+$  channel blockers were obtained from Alomone laboratories (Jerusalem,

Israel) and stocks were prepared as follows: charybdotoxin (CTX) was dissolved in water at 100  $\mu\text{M}$ ; iberiotoxin was dissolved in water at 1  $\mu\text{M}$ ; margatoxin was dissolved in water at 10  $\mu\text{M}$ . All inhibitors were freshly prepared prior to use. In ATP depletion experiments, apyrase was used at a final concentration of 0.4 unit/ml, hexokinase and glucose were used at a final concentration of 4 units/ml and 22 mM, respectively. The following purinoceptor agonists were prepared at 50 mM with Krebs buffer and used at a final concentration of 50  $\mu\text{M}$ : ATP, ATP $\beta\text{S}$ , 2-MethSATP, BzATP,  $\alpha$ ,  $\beta$ -MethylATP, ADP, AMP, adenosine, UTP, UDP, and 8-Br-ATP. Stocks of the following P2 receptor antagonists were prepared as follows: PPADS was dissolved in Krebs buffer at 100 mM; reactive blue 2 (RB2) was dissolved in Krebs buffer at 50  $\mu\text{M}$ ; (PAP) was dissolved in Krebs buffer at 50 mM. All stock solutions for P2 antagonists were freshly prepared and used at 1:1000. Polyclonal P2X<sub>2</sub> and P2X<sub>3</sub> antisera were obtained from Neuromics, Inc. (Minneapolis, MN, USA). Rabbit anti-P2X<sub>2</sub> and rabbit anti-P2X<sub>3</sub> antisera were used at 1:1000 for both immunohistochemistry and Western blot analysis. Guinea pig anti-P2X<sub>3</sub> antiserum was used at 1:700 for immunohistochemistry. Antigen peptides for rabbit anti-P2X<sub>2</sub> and rabbit anti-P2X<sub>3</sub> antisera were also obtained from Neuromics and they were used at a final concentration of 1  $\mu\text{g/ml}$ .

### ***Solutions***

Control Krebs solution was prepared by mixing the following (in mM): 110 NaCl, 5.8 KCl, 25 NaHCO<sub>3</sub>, 1.2 KH<sub>2</sub>PO<sub>4</sub>, 2.0 CaCl<sub>2</sub>, 1.2 MgSO<sub>4</sub>, 11.1 glucose. Ca<sup>2+</sup>-free Krebs had the following composition in mM: 113.2 NaCl, 25 NaHCO<sub>3</sub>, 7.8 KCl, 1.2 MgSO<sub>4</sub>, 1.2 K<sub>2</sub>HPO<sub>4</sub>, 11.1 glucose. Na<sup>+</sup>-free Krebs had the following composition in mM: 120 tetramethylammonium (TMA) Cl or N-methyl-D-glucamine (NMDG)-Cl, 3.33 KH<sub>2</sub>PO<sub>4</sub>, 0.83 K<sub>2</sub>HPO<sub>4</sub>, 1.2 CaCl<sub>2</sub>, 1.2 MgCl<sub>2</sub>, 28

choline-HCO<sub>3</sub>, 0.01 atropine, and 2.7 glucose. Na<sup>+</sup>- and Cl<sup>-</sup>-free Krebs had the following composition in mM: 120 NMDG/gluconate buffer (prepared as a stock by adjusting 240 mM NMDG to pH 7.4 with gluconic acid), 3.33 KH<sub>2</sub>PO<sub>4</sub>, 0.83 K<sub>2</sub>HPO<sub>4</sub>, 4 Ca<sup>2+</sup>-gluconate, 4 Mg<sup>2+</sup>-gluconate, 28 choline-HCO<sub>3</sub>, 0.01 atropine, and 2.7 glucose. For Cs<sup>+</sup> transport experiments, NMDG gluconate solution had the following composition in mM: 135 NMDG, 4 hemi-Ca<sup>2+</sup> gluconate, and 10 N-2-hydroxyethylpiperazine-N'-2-ethanesulfonic acid (HEPES). The pH was adjusted to 7.4 with D-gluconic acid. The composition of Cs<sup>+</sup> gluconate solution had the following composition in mM: 135 CsOH, 4 hemi-Ca<sup>2+</sup> gluconate, and 10 Hepes. The pH of the Cs<sup>+</sup> gluconate buffer was adjusted to 7.4 with D-gluconic acid. All the solutions had an osmolarity of 280-300 mOsmol. Solutions that contained bicarbonate were aerated with a 95% O<sub>2</sub>/5% CO<sub>2</sub> mixture and maintained at a pH of 7.4 at 37°C.

### ***Animals***

Urinary bladders were obtained from female New Zealand White rabbits (3-4 kg), female Swiss-Webster mice (3-4 months old) or female Sprague-Dawley rats weighing 275 – 350 g. All animals were fed a standard diet with free access to water prior to euthanization. Rabbits were euthanized by lethal injection of 300 mg sodium pentobarbital into the ear vein. Mice and rats were euthanized by inhalation of 100% CO<sub>2</sub>. Following euthanization and thorocotomy the bladder was rapidly excised and processed as described below. All animal studies were carried out with the approval of the University of Pittsburgh Animal Care and Use Committee and maintained according to the standards set forth in the American Physiological Society's handbook on the care and use of animals.

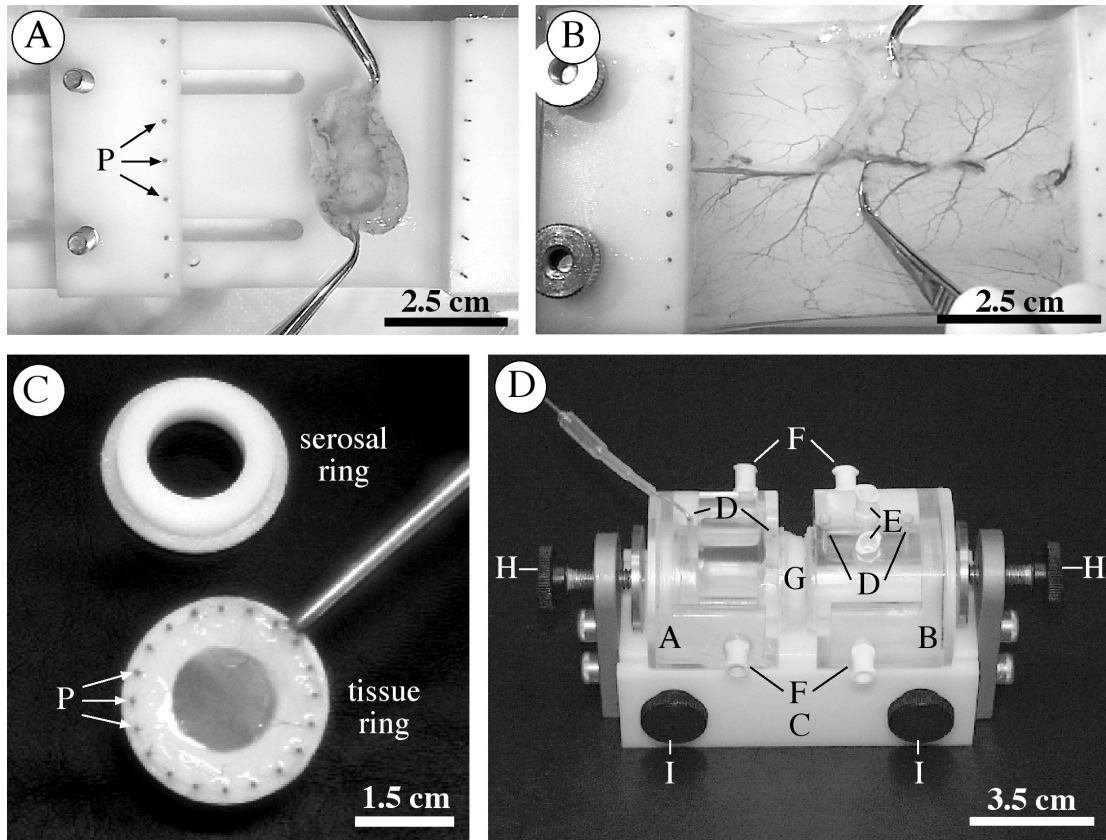


*Figure A-1. Mounting of tissue in pressure chamber. (A) Cut bladder, prior to mounting on Teflon rack. (B) Dissection of smooth muscle layer from overlying mucosa. (C) Serosal ring and tissue ring with uroepithelium attached. (D) Pressure chamber. A, serosal hemichamber; B, mucosal hemichamber; C, chamber base; D, electrode ports; E, Luer ports; F, water jacket ports; G, tissue; H, outside-edge thumb screws; I, parallel alignment thumb screws; P, examples of pins.*

### ***Isolation of uroepithelial tissue***

After the rabbits were euthanized, the rabbits were placed on their back and the bladder was exposed by making an incision from the base of the pelvis toward the midline. The neck region, at the base of the pelvis was clamped with a hemostat and an incision was made along the bladder from the tip of the dome to the neck region, allowing the urine to drain from the organ. The point of connection between the urethra and the bladder was cut and the excised bladder was immediately placed in a 100-ml beaker filled with Krebs solution warmed to 37°C. The bladder was trimmed of excess fat and carefully secured, mucosal side down, onto a custom-made Teflon rack (Figure A-1A, A-1B), sitting in a 150-cm<sup>2</sup> Petri dish containing Krebs solution bubbled with 95% air/5% CO<sub>2</sub> gas. Temperature was maintained at 37°C by placing the Petri dish on a heating place. The smooth muscle layers were removed by dissection with scissors and forceps (Figure A-1B). A custom-made Teflon tissue ring, with an outer diameter of 3 cm and an internal opening of 2 cm<sup>2</sup> (diameter is 1.6 cm) and with 20 sharp pins 2 mm from the edge of the outer ring, was coated with high-vacuum grease (Dow Corning Corp., Midland, MI, USA), placed underneath the tissue, and lifted up, and the tissue was pressed onto the pins with forceps to secure the piece onto the ring (Figure A-1C). Excess tissue surrounding the ring was trimmed with scissors. Normally, each bladder yielded three rings of mounted tissue.

### ***Mounting and equilibration of tissue in pressure chamber***

The tissue, mounted on Teflon tissue ring, was clamped between two halves of a custom-made pressure chamber (Figure A-1D). The serosal hemichamber is similar to that described by Lewis et al. (139). The top of this chamber is open, allowing for aeration lines and inflow and outflow lines. The mucosal hemichamber is essentially a closed system with Luer ports to allow for

addition and removal of Krebs solution, as well as monitoring back pressure (214, 225). Each chamber is jacketed, and the temperature is maintained by circulating water through these jackets.

Both chambers contain a round opening at the side facing the tissue. The opening on the serosal hemichamber is grooved to accept a second Teflon ring (3-cm diameter) that contains an inner raised ring with a 2.6 cm external diameter and an internal opening diameter of 1.6 cm (Figure A-1C). Prior to mounting, a circle of silicon vacuum grease was applied to the inner raised portion of the serosal ring. The vacuum grease serves to cushion the tissue and prevent edge damage as the tissue comes in contact with the ring on the serosal hemichamber. The lower edges of each chamber are grooved to fit into corresponding tracks on a plastic rectangle that abuts the chamber base, maintains the parallel alignment of the two hemichambers, and is held in place by thumb screws. Once placed in the tracks, thumb screws (present on the outside edge of the chamber platform that abut each hemichamber) were tightened to lock the tissue ring between the two hemichambers. It was important to not over tighten the screws or the tissue became damaged.

Finally, other ports are present at the front and rear of each chamber, allowing for the introduction of voltage-measuring Ag/AgCl wires or current-passing Ag/AgCl wires, respectively. The electrodes ports on the mucosal chamber contain a locking mechanism that prevents escape of Krebs solution. The electrodes were connected to a VCC MC6 current/voltage clamp (Physiological Instruments, San Diego, CA, USA), which in turn was connected to a MacLab 8s A/D converter (AD Instruments, Victoria, Australia) interfaced with a 400-MHz PowerPC G3 Macintosh computer (Apple, Cupertino, CA, USA).

Following mounting, each hemichamber (mucosal and serosal) was filled with 12.5 ml Krebs solution, the serosal hemichamber was bubbled with 95% air/5% CO<sub>2</sub> gas, and the tissue was equilibrated for 30-60 min to allow for stabilization of transepithelial resistance (TER; in units of  $\Omega \cdot \text{cm}^2$ ), a measure of the ability of the epithelium to impede transcellular and paracellular ion flow (139), and transepithelial capacitance ( $C_T$ ). The methods for measuring these parameters are given below. As noted previously, TER rose significantly during the equilibration period (139). At the end of the equilibration period, only those preparations that exhibited a TER of  $> 8000 \Omega \cdot \text{cm}^2$  and a capacitance of  $\sim 1.9 - 2.1$  microfarad ( $\mu\text{F}$ ) were used. A high TER is consistent with a functionally intact epithelium. Because the area of the tissue exposed in the tissue chamber is  $2 \text{ cm}^2$ , a capacitance of  $\sim 2 \mu\text{F}$  ensured that the tissue was smooth and free of large folds.

### ***Application of hydrostatic pressure***

To increase hydrostatic pressure, additional Krebs solution was added to the mucosal hemichamber to a volume of 14 ml (hemichamber capacity), and an additional 0.5 ml Krebs was injected by syringe to increase the back pressure in the apical hemichamber to 8 cm H<sub>2</sub>O as measured by a force transducer (AD Instruments, Mountain View, CA, USA) interfaced with a bridge transformer (AD Instruments) to the MacLab device. In rabbit, 8 cm H<sub>2</sub>O is representative of a pressure normally observed during the extended storage phase of bladder filling (127). The force transducer was connected via one arm of a T-fitting to one of the Luer ports of the mucosal hemichamber, and via the other arm to a column of water that was used to calibrate the force transducer. Data were collected using the Scope program (AD Instruments). Alternatively, a slow-filling method was used. Krebs solution was added through the Luer port of the mucosal



hemichamber at a rate of 0.1 ml/min by way of a calibrated syringe injector until a back pressure of 8 cmH<sub>2</sub>O was measured. The chamber was then closed off. Capacitance and TER were measured throughout these experiments.

### *Use of capacitance to estimate umbrella cell surface area*

Capacitance is the ability of two parallel plates (conductors), separated by a dielectric, to store electrical charge. Capacitance ( $C$ ) is defined as (equation 1)

$$C = \frac{\epsilon A}{d} \frac{1}{4\pi k},$$

where  $\epsilon$  is the dielectric constant,  $A$  is the area of each plate,  $d$  is the distance between each plate,  $k$  is a constant ( $9.0 \times 10^{11} \text{ cmF}^{-1}$ ), and  $\epsilon$  has the usual meaning. It should be apparent from this formula that the greater the surface area, the greater the capacitance. Furthermore, capacitance is directly proportional to  $\epsilon$  and inversely proportional to  $d$ . The cell membrane, which is composed of two parallel leaflets, has very high capacitance, which reflects a reasonable  $\epsilon$  of  $\sim 5$  and a very small distance between the leaflets of 3.5 – 7.0 nm (200). It is generally accepted that  $1 \mu\text{F} \approx 1 \text{ cm}^2$  of tissue area (132, 139). The simplest equivalent circuit that describes an epithelium is shown in Figure A-2 (132, 139). The apical and basolateral plasma membranes of the epithelium are each modeled as a resistor and a capacitor in parallel. The resistive pathway reflects ion flow through ion channels, while the capacitive component reflects the ability of the plasma membrane leaflets to store charge. Because the junction has almost no surface area (relative to the surface area of the cell), but does regulate paracellular ion flow, it is modeled simply as a resistor ( $R_j$ ). The bathing solution acts as a pure resistor. Significantly more

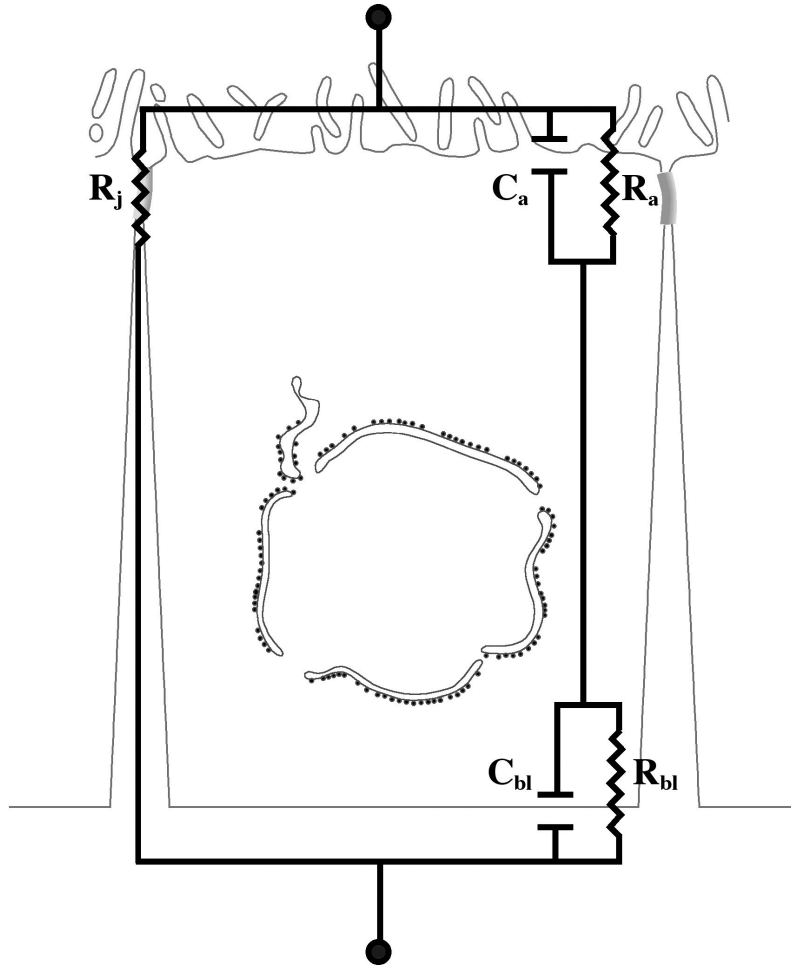


Figure A-2. Equivalent circuit of bladder epithelium.  $C_a$ , apical membrane capacitance;  $C_b$ , basolateral membrane capacitance;  $R_a$ , apical membrane resistance;  $R_b$ , basolateral membrane resistance;  $R_j$ , junctional resistance.

complicated equivalent circuits exist that can be used to model specialized membrane domains of epithelial cells including their lateral membranes (132).

Membrane capacitance is measured by applying a current waveform and then recording the voltage response. Types of current waveforms that have been used to study the bladder epithelium include square current pulses, which are described below and current sinusoids (37, 134, 135). The capacitor values are then determined by fitting the voltage response to that expected for an equivalent circuit. In rabbit bladder, the junctional resistance is greater than the apical membrane resistance of the umbrella cell, and the apical membrane resistance is much greater (up to 50-fold) than the resistance associated with the basolateral membrane. In turn, the resistance associated with the basolateral membrane of the umbrella cells is much greater than the resistance associated with the underlying intermediate and basal cell layers. As such, in rabbit bladder epithelium the voltage response to a square current pulse is determined primarily by the capacitance and resistance of the umbrella cell apical membrane and the parallel junctional resistance (139). Furthermore, as shown in equation 2

$$C_T = \frac{C_a}{(C_a/C_{bl}) + 1},$$

$C_T$  is dependent on the ratio of the apical membrane capacitance  $C_a$  to the basolateral membrane capacitance  $C_{bl}$  (134). If  $C_a$  is much less than  $C_{bl}$  then  $C_T$  is approximately equal to  $C_a$ . This condition is essentially true for the umbrella cell, and the  $\sim C_a/C_{bl}$  ratio is 1:5 results in an underestimation of  $C_a$  by  $\sim 20\%$  (134).

Although significant additional information can be derived using current sinusoids, square current pulses provide a relatively simple method to make estimates of  $C_T$  and apical membrane surface area (134, 135, 139). This method involves applying a square current pulse

and then determining the length of time it takes for the voltage to reach 63% of its steady-state value. Alternatively, one can measure the time it takes for the voltage to decay to 37% of the steady-state value. In either case the measured time constant,  $\tau$  is equal to the product of the resistance across the epithelium ( $R_T$ ) and  $C_T$ . Dividing  $\tau$  (in units of seconds) by  $R_T$  (in units of ohms) yields  $C_T$  (in units of farads). Because the  $\tau$  associated with the apical membrane is much greater than that associated with the basolateral membrane, the estimate of  $C_T$  using this technique provides an estimate of the apical membrane surface area. This has been confirmed under a number of conditions and is independent of spontaneous transepithelial voltage and  $R_T$  (134).

### ***Determination of $C_T$***

Prior to mounting the tissue in the chambers, voltage asymmetry between the voltage-sensing electrodes and the fluid resistance were corrected by positioning the voltage-sensing electrodes in the Ussing chambers and adjusting the potential difference to zero. Following equilibration of the tissue in open-circuit mode, the voltage clamp was switched to current clamp mode. Following a 25 ms delay, a transepithelial square current pulse of 1  $\mu$ A, generated from within the Scope program (AD Instruments) and passed from the MacLab 8s A/D converter to the VCC MC6 current/voltage clamp (Physiological Instruments, San Diego, CA, USA), was applied across the tissue for 200 ms. The voltage response of the tissue was digitized by the MacLab 8s A/D converter and then recorded every 100  $\mu$ s by using the Scope program. An average of eight sweeps were recorded for each current pulse. A sample voltage response is shown in Figure A-3A. The first part of the curve (boxed region in Figure A-3A) shows the “on” voltage response, which increases in a negative exponential manner until the voltage reaches a steady-state peak

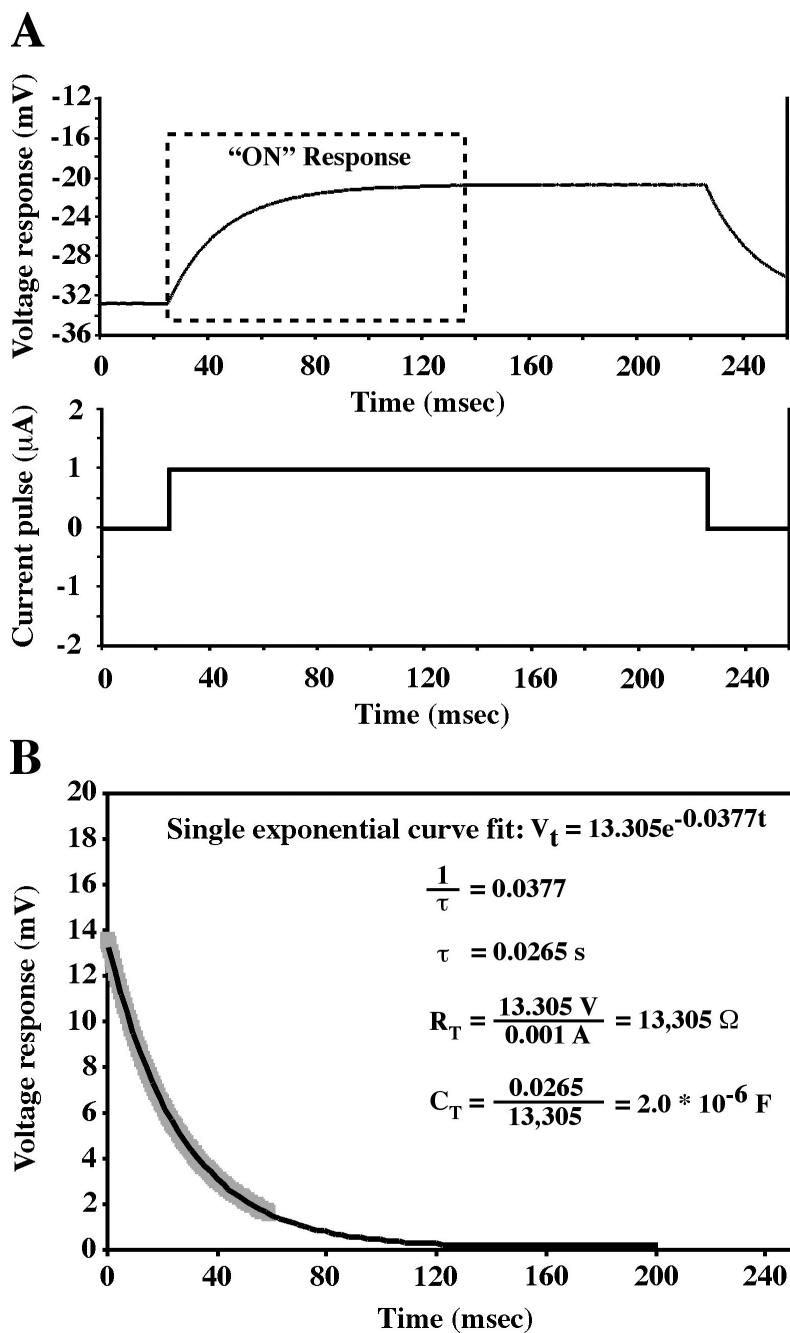


Figure A-3. Voltage response of rabbit bladder epithelium to square current pulse. (A) A  $1 \mu\text{A}$  square current pulse (of 200-msec duration) was delivered to rabbit bladder epithelium and the voltage response was monitored over time. The “on” response to “off” response (black line), curve fitting (gray line), and derivation of  $C_T$  value.

value. The exponential increase in voltage reflects the relatively “slow” charging of the membrane capacitance.

To extract  $C_T$  values from the curve, it was necessary to convert the “on” response to an “off” response by subtracting the steady-state peak value from the prestimulus voltage (the absolute value of which is equal to  $V_{\max}$ ) and from each of the pre-steady-state values. The absolute values of these differences generated a positive exponential curve (Figure A-3B)(134). This transformation was accomplished by copying the data from Data pad in the Scope program to an Excel (Microsoft Corp., Redding, WA, USA) spreadsheet, and performing the necessary data manipulations. Using the build-in curve-fitting function in Excel, the data describing the “off” rate were fit to a single exponential (Figure A-3B) using equation 3:

$$V_t = V_{\max} e^{-t/\tau}.$$

The R values for curve fitting were  $> 0.99$  under all conditions. As described above capacitance was determined using the formula  $C_T = \Delta I / R_T$ . By use of Ohm’s law (where  $\Delta I = \Delta V / \Delta R$ ),  $R_T$  was determined by dividing  $V_{\max}$  (in volts) by the amplitude of the square current pulse (which was 0.001 A in our experiments).

### ***Transmission electron microscopy of uroepithelium***

While tissue was in the pressure chamber, Krebs solution was isovolumetrically replaced with a fixative containing 0.2% (v/v) glutaraldehyde and 2.0% (w/v) paraformaldehyde in 100 mM sodium cacodylate, pH 7.4, 1 mM  $\text{CaCl}_2$ , 0.5 mM  $\text{MgCl}_2$ , for 2 h at room temperature. The fixed tissue was washed 15 min in 100 mM sodium cacodylate, pH 7.4, buffer and treated with 1% (w/v)  $\text{OsO}_4$  in 100 mM sodium cacodylate, pH 7.4, buffer for 60 min at 4°C, and then the tissue

was cut into small pieces. After several water rinses the samples were stained en bloc overnight with 0.5% uranyl acetate in water. Samples were dehydrated in a graded series of ethanol, embedded in the epoxy resin LX-112 (Ladd, VT, USA) and sectioned with a diamond knife (Diatome, PA, USA). Sections, silver to pale gold in color, were mounted on butvar-coated copper grids, contrasted with uranyl acetate and lead citrate, and viewed at 80 kV in a Jeol 100 CX electron microscope. Images were captured on film, scanned on a Linotype-Hell Saphir Ultra II scanner (Eschborn, Germany), contrast corrected in Photoshop 7.0 (Adobe, CA), and assembled in Freehand 10.0 (Macromedia, San Francisco, CA, USA).

### ***Stereological analysis***

Epon blocks were sectioned perpendicular to the length of the epithelium to obtain vertical sections necessary to determine mean cell volume, apical and basolateral surface areas, and discoidal vesicle volume and surface area.

***Mean cell volume.*** The mean umbrella cell volume was estimated in either control or stretched cells by taking a minimum of 50 photographs at 1400 x of randomly chosen umbrella cells, printing an 8 × 10 inch image of each cell and overlaying a cycloid lattice grid on the image (81). When necessary, more than one photograph was taken to include the entire cell and the photographs were overlapped as a montage. The average volume fraction of the nucleus ( $V_{(nuc)}$ ) was determined by point counting and calculating the ratio of counts on the nucleus ( $P_{(nuc)}$ ) relative to counts on the cell ( $P_{(cell)}$ ) as described by the following formula (81):

$$V_{(nuc)} = \frac{\sum_{i=1}^n P_{(nuc)}}{\sum_{i=1}^n P_{(cell)}}$$

In a separate experiment, optical sections through the umbrella cell nuclei were taken by confocal microscopy and the images were projected on to one another to determine the average diameter of the nucleus. The average nuclear volume was calculated using the formula  $4/3\pi r^3$ . Rabbit umbrella cells usually contain 1 nucleus per cell and the nuclei are generally spherical. The mean cell volume was calculated by dividing the volume of the nucleus by  $V_{(nuc)}$  (81).

**Membrane surface areas.** The apical and basolateral membrane surface areas of the umbrella cells were determined by overlaying a cycloid lattice grid as above on the 8 × 10 inch images. Intersections of the cycloids with the apical or basolateral surface domains along with the number of points on the cell were counted. The surface density ( $S_v$ ) was calculated using the following formula (9):

$$S_v = 2(p/l) \frac{\sum_{i=1}^n I_i}{\sum_{i=1}^n P_i}$$

Where (p/l) is the ratio of test points to test curve length and is a function of the cycloid grid, which in this case was 1/4.59 μm. For discoidal vesicle surface area, photographs were taken at 3600 x and overlapping 8 × 10 inch images of the umbrella cells were used to determine  $S_v$ , which was calculated by counting the intersections of the cycloids with the vesicle membrane



domains relative to the points on the cell. The cycloid grid used for this purpose had a p/l ratio of 1:0.87  $\mu\text{m}$ . Surface area was determined by multiplying the membrane surface density by the volume of the cell (9).

**Error analysis.** The standard error of the estimated values was determined by the bootstrap method (55). Briefly, 50 individual geometric parameters (volume or surface area) were obtained for umbrella cells analyzed after point/intersection counting with the cycloid grid as described above. The values were recorded and copied into the Microsoft Excel computer software program (Microsoft Corp.) as a workbook. Using the Resampling Stats Excel add-in (available at [www.resample.com](http://www.resample.com)), the data were resampled, with replacement, to obtain a pseudo-sample of data. The parameter was estimated from the pseudo-data and the value was recorded in a separate column. This process was repeated 50 times to generate a column of 50 bootstrapped parameter estimates. A new mean ( $X_{boot}$ ) and variance ( $s^2_{boot}$ ) were determined for the bootstrapped values and the standard error of the original estimated mean ( $X_{orig}$ ) was determined by the following formula:

$$\text{Standard Error} = \sqrt{(X_{orig} - X_{boot})^2 + s^2_{boot}}$$

Statistical significance was determined by Student's t-test,  $p < 0.05$ .

### ***Immunogold labeling of ultrathin cryosections***

Urinary bladders were isolated and set up in the Krebs bath as described above. Following the experiment cells were fixed 45 min at room temperature with 0.1% (v/v) glutaraldehyde and 2% (w/v) paraformaldehyde in 100 mM cacodylate buffer containing 0.5 mM  $\text{MgCl}_2$  + 1 mM  $\text{CaCl}_2$ ,

and cut into 0.5 - 1.0 mm<sup>2</sup> cubes. The cubes were incubated 30 min at 37°C in 3% (w/v) gelatin and then overnight at 4°C in 1.3 M sucrose and 20% (w/v) polyvinylpyrrolidone (M<sub>r</sub> 10,000). The cubes were mounted on cryo-stubs and frozen in liquid nitrogen. Cryosectioning was performed at -110°C in a Leica (Deerfield, IL) Ultracut E ultramicrotome with an FCS cryochamber attachment. The cryosections were labeled with culture supernatant from the mouse hybridoma cell line K8B12 which produces anti-UPIII antibody (213) and subsequently with goat anti mouse IgG Fc 5 nm gold (Amersham) as described previously (2). Sections were viewed at 80-100 kV in a Jeol 100CX electron microscope (Peabody, MA).

#### ***Biotinylation of apical membrane proteins***

The tissue was mounted and equilibrated as described and then stretched or incubated in the chamber for the indicated amount of time. The tissue was placed on ice and the apical medium was replaced with 10 ml of ice-cold Krebs containing 1 mg/ml of sulfo-N-hydroxysuccinimide (NHS)-disulfo (SS)-biotin (Pierce, Rockford, IL) and incubated for 15 min to biotinylate apical membrane proteins. After incubation, the biotin/Krebs solution was aspirated and fresh biotin in Krebs was added for another 15 min on ice. The reaction was quenched by exchanging the apical solution with ice-cold Minimal Essential Medium (Life Technologies, Inc., Grand Island, N.Y.) + 10% Fetal Bovine Serum (Hyclone, Logan, UT) and washing 3 x 15 min.

#### ***Measurement of uroplakin III at the cell surface***

Following biotinylation, the chamber was disassembled and the epithelial cells were gently scraped and placed in 0.15 ml of 0.5% SDS-lysis buffer (100 mM NaCl, 50 mM TEA, 5 mM EDTA, 0.5% SDS) containing protease inhibitor cocktail (5 µg/ml leupeptin, 5µg/ml of antipain,

5 µg/ml of pepstatin, and 1 mM phenylmethylsulfonyl fluoride). The samples were boiled for 5 min and then shaken in a vortex mixer (Eppendorf) for 15 min at 4°C. Protein lysate, 25 µg, in 500 µl of mixed micelle buffer (150 mM NaCl, 20 mM triethanolamine, 5 mM EDTA, 110 mM sucrose, 1% Triton X-100, and 0.2% SDS), was incubated overnight at 4°C on a rotator with 80 µl of a 50% slurry of streptavidin beads (Pierce) washed prior to use three times with mixed micelle buffer and one time with final wash buffer (150 mM NaCl, 20 mM triethanolamine pH 8.1, 5 mM EDTA). After overnight incubation, the beads were isolated by centrifugation at 14,000 rpm for 10 sec, washed 3 times with mixed micelle buffer and once with final wash buffer. Biotinylated proteins bound to the streptavidin beads were separated by boiling for 5 min in Laemmli sample buffer containing 100 mM DTT. An aliquot of the starting lysate (2.5 µg or 1.25 µg) was similarly boiled in sample buffer. The proteins were resolved on a 15% SDS-polyacrylamide gel and were transferred to Immobilon-P membranes (Millipore, Bedford, MA) for 75 min at 375 mA constant current. The membrane was blocked overnight in 5% (w/v) BSA dissolved in phosphate buffered saline (PBS). The blot was incubated for 2 h at room temperature with rotation with K8B12 antibody diluted 1:1000 in PBS containing 1% dehydrated non-fat milk. The membrane was then washed with TBS-Tween (2.68 mM KCl, 0.5M NaCl, 25mM Tris-HCl, pH 8.0, and 0.05% v/v Tween-20) 2 × 15 min and then 1 × 60 min and incubated in goat anti-mouse antibodies conjugated to HRP (Jackson Immunoresearch Laboratories, Inc., West Grove, PA) diluted 1:25,000 in PBS-milk for 1 h with rotation. The membrane was washed 2 × 15 min and 1 × 60 min in TBS-Tween, incubated for 1 min in Super Signal ECL reagent (Pierce), and exposed to XAR-5 film (Eastman Kodak Company, Rochester, NY). The bands were quantified by densitometry using the Molecular Analyst Program (BioRad, Hercules, CA).

### *Apical secretion*

The tissue was mounted and equilibrated as described and then washed once with PBS (containing 2.0 mM Ca<sup>2+</sup> and 1.0 mM Mg<sup>2+</sup>) and incubated for 30 min in cysteine/methionine-deficient MEM to starve the cells. The basolateral media was removed, the chamber was placed on its side (apical hemi-chamber down) and <sup>35</sup>S cysteine/methionine express labeling mix (taken from a 10 mCi/ml stock, NEN, Boston, MA) diluted in MEM to a final concentration of 0.25 mCi/ml in a volume of 267 µl was added to the basal side of the tissue for 30 min to metabolically label the cells. The tissue was washed 3 times with Krebs and then chased for 60 min in Krebs. After the chase, 500 µl aliquots were taken from the basolateral and apical media to determine background radioactivity, 500 µl Krebs was added back to each hemi-chamber and then the tissue was stretched for 5, 15, 120 or 300 min or incubated without stretch as a control. At the indicated times, 500µl aliquots were taken from the apical and basolateral hemi-chambers and spotted on 1.5 in<sup>2</sup> pieces of filter paper (Whatman International, Maidstone, England) and incubated at room temperature until dry. The pieces were placed in ice-cold 10% (v/v) trichloroacetic acid to precipitate secretory proteins, incubated with shaking at 4°C for 30 min, washed 3 × 5 min with ice-cold 70% (v/v) ethanol at 4°C and then incubated at room temperature until dry. The pieces were placed in 6 ml scintillation vials, the vials were filled with 5 ml Scintisafe scintillation fluid (Fisher Scientific, Pittsburgh, PA) and the radioactivity was determined by counting in a scintillation counter (Wallac, Turku, Finland).

### ***Diffusion of urea across the uroepithelium***

The tissue was mounted and equilibrated as described and the basolateral or apical chamber was incubated with 167  $\mu\text{Ci}$   $^{14}\text{C}$ -urea (taken from a 5 mCi/ml stock diluted in  $\text{H}_2\text{O}$ , American Radiolabeled Chemicals, St. Louis, MO). The tissue was then stretched or incubated without stretch as a control. Duplicate 30  $\mu\text{l}$  aliquots were taken from the basolateral and apical hemichambers at 0, 15, 120, or 300 min and 60  $\mu\text{l}$  of Krebs were replaced to maintain a constant buffer volume. The aliquots were mixed with 10 ml scintillation fluid and the samples were counted in a liquid scintillation counter. The amount of urea that crossed the uroepithelium was expressed as a percentage of the number of counts in the apical medium (or basolateral medium when added apically) divided by the total number of counts in the apical and basolateral media at each time point.

### ***Measurement of endocytosis***

Tissue was mounted, equilibrated, and then biotinylated as described above. After biotinylation, the tissue was warmed to  $37^\circ\text{C}$  in Krebs and stimulated with hydrostatic pressure, or incubated with 10  $\mu\text{M}$  forskolin/500  $\mu\text{M}$  IBMX or 50  $\mu\text{M}$  ATP[S], or the tissue was incubated without pressure stimulation for the indicated amount of time to allow for internalization of the biotinylated proteins. After incubation, the chambers were placed on ice to stop all membrane trafficking. Cell surface biotin was removed by incubating the tissue for 30 min at  $4^\circ\text{C}$  with 17 mg/ml 2-mercaptoethanesulfonic acid (MESNA) in 50 mM Tris pH 8.6, 100 mM NaCl, 0.2% BSA and 1mM EDTA. The buffer was aspirated and the reaction was quenched for 10 min at  $4^\circ\text{C}$  with 25 mg/ml iodoacetic acid diluted in PBS. The iodoacetic acid was removed and the tissue was washed 2 times with ice-cold Krebs buffer. The chamber was disassembled and the

apical surface was gently scraped to remove the uroepithelium. The scraped cells were placed in 150  $\mu$ l of 0.5% SDS-lysis buffer containing a protease inhibitor cocktail (described above). The samples were boiled for 5 min and then vortex shaken for 15 min at 4°C. Protein lysate (5  $\mu$ g) was mixed with sample buffer lacking reducing agent and the proteins were resolved on 15% SDS-polyacrylamide gels and transferred to Immobilon P as described above. To measure endocytosis, the biotinylated proteins were detected by incubating the blots with 0.1  $\mu$ g/ml streptavidin-HRP (Jackson ImmunoResearch Laboratories, Inc.) in PBS containing 1% (w/v) dehydrated non-fat milk for 2 h at room temperature with rotation. The blots were washed and the bands were visualized and quantified by densitometry as described below. The amount of endocytosis was calculated as the quotient of the signal intensity of the MESNA-treated lane and the untreated lane for each time point.

### ***WGA-FITC internalization***

The tissue was mounted and equilibrated as described and then cooled to 4°C. The apical compartment was incubated with 25  $\mu$ g/ml WGA-FITC (Vector, Burlingame, CA) in Krebs, the tissue was warmed and incubated for 15 min with or without pressure. The tissue was then placed on ice and the cell surface WGA-FITC was removed by washing 3  $\times$  30 min with 50 mM *N*-acetyl glucosamine in Krebs buffer on a shaker at 4°C. The tissue was then fixed, stained with DAPI (Molecular Probes, Eugene, OR), and mounted as described (8). Samples were viewed in a TE300 Nikon (Melville, NY) microscope equipped for epifluorescence and outfitted with a Ludl (Electronic Products Ltd., Hawthorne, NY) Z-focus controller. The images were collected and processed by digital deconvolution with Open Lab software (Improvision, Coventry, England). Alternatively, the tissue was stretched for 2 or 5 h, the pressure was released, and WGA-FITC

was added to the apical chamber. The tissue was then re-stretched for 15 min, cooled, and then washed with *N*-acetyl glucosamine at 4°C followed by fixation and mounting as described above. To observe endocytosis in whole bladders, excised bladders were washed with Krebs buffer as described above but otherwise left intact. The contracted bladders were incubated in Krebs buffer (gassed with 95% air/5% CO<sub>2</sub>) for 60 min and then attached to a 60 ml syringe using ligatures. The bladders were filled with 30 ml of Krebs buffer containing WGA-FITC and then incubated for 15 min at 37°C. The bladders were rapidly chilled to 4°C, surface-bound WGA-FITC was removed by treatment with *N*-acetyl glucosamine at 4°C, and the tissue was fixed as described above. Imaging for the latter two experiments was performed on a TCS confocal microscope equipped with krypton, argon, and helium-neon lasers (Leica, Dearfield, IL). Images were acquired using a 40x plan-apochromat objective (zoom = 2) and the appropriate filter combination. The images (1024 x 1024 pixels) were saved in a tag-information-file-format (TIFF) and the contrast levels of the images adjusted in the Photoshop program (Adobe Co.; Mountain View, CA) on a Power PC G-4 Macintosh (Apple; Cupertino, CA). The contrast-corrected images were imported into Freehand (Macromedia; San Francisco, CA) and printed from a Kodak (Rochester, NY) 8650PS dye sublimation printer.

### ***Measurement of intracellular levels of cAMP***

Bladder tissue was mounted and was incubated for 15-300 min in the presence or absence of stretch. After the designated time point, the tissue was removed from the chamber and the mucosal surface was gently scraped with a cell scraper (number 83.1830, Sarstedt, Inc., Newton, NC) to selectively remove the epithelial cells. Intracellular concentrations of cAMP in the

epithelial cells were determined using a Biotrak kit (RPA 538, Amersham Pharmacia, Piscataway, NJ) according to the manufacturer's instructions.

### ***Isc and conductance measurements***

Bladder tissue was mounted as described above and equilibrated with a VCC MC6 current/voltage clamp (Physiological Instruments, San Diego, CA) set to open-circuit mode. Voltage asymmetry between the voltage sensing electrodes and the fluid resistance were corrected as described above. The reference electrode was in the serosal hemichamber. The voltage clamp was switched from the open-circuit mode to the short-circuit mode and the Isc values were recorded with a frequency of 10-Hz, digitized by a MacLab 8s A/D converter (AD Instruments, Mountain View, CA), and then displayed and captured using the Chart program (AD Instruments). Isc data were normalized to the exposed surface area of the tissue ring (2 cm<sup>2</sup>). To measure TER a square voltage pulse, generated by the MacLab 8s A/D converter, was applied with a frequency of 0.1 Hz across the tissue for 500 ms to a new clamp potential of 50 mV. TER was calculated from the change in voltage divided by the change in Isc, where TER = ( $\Delta V / \Delta \text{Isc}$ ) \* exposed surface area of tissue ring (2 cm<sup>2</sup>). Data are expressed in conductance, which is defined as the reciprocal of the TER value. The Isc and conductance values during the 5-min periods of increased hydrostatic pressure were averaged and the standard errors calculated from up to 6 separate experiments. Significant changes in Isc were assessed by t-test.

### ***Unidirectional <sup>36</sup>Cl<sup>-</sup>, <sup>22</sup>Na<sup>+</sup> and <sup>86</sup>Rb<sup>+</sup> flux measurements***

<sup>36</sup>Cl<sup>-</sup>, <sup>22</sup>Na<sup>+</sup> and <sup>86</sup>Rb<sup>+</sup> flux measurements were performed as described previously (26). One set of Ussing chamber setups was used for the mucosal-to-serosal flux (J<sub>MS</sub>) measurements and one



set of Ussing chamber setups was used to measure serosal-to-mucosal flux ( $J_{SM}$ ). Tissue was mounted in standard Krebs solution and when the Isc became stable,  $^{36}\text{Cl}^-$  (specific activity = 3.66 mCi/mg  $^{36}\text{Cl}^-$ , concentration = 20 mCi/ml, Perkin Elmer, Boston, MA),  $^{22}\text{Na}^+$  (specific activity = 100 mCi/mg  $^{22}\text{Na}^+$ , concentration = 2 mCi/ml, Amersham, Piscataway, NJ), or  $^{86}\text{Rb}^+$  (specific activity = 1.53 mCi/mg  $^{86}\text{Rb}^+$ , concentration = 20 mCi/ml, NEM Life Sciences, Boston, MA) was added to the serosal or mucosal side of the chamber at a final concentration of 1  $\mu\text{Ci/ml}$  and sampling was performed as previously described (26). Unidirectional fluxes ( $J_{\text{net}}$ ) were calculated using standard equations and all fluxes were corrected for the exposed surface area of the tissue ring (26). Isc values were averaged and converted to  $\mu\text{Eq}\cdot\text{cm}^{-2}\cdot\text{h}^{-1}$  using the following formula:  $1\ \mu\text{A}\cdot\text{cm}^{-2} = 3.736 \times 10^{-2}\ \mu\text{Eq}\cdot\text{cm}^{-2}\cdot\text{h}^{-1}$  (26).

### ***Western blot analysis of P2X receptors***

Freshly-isolated bladders from rats were placed in 100  $\mu\text{l}$  of 0.5% SDS-lysis buffer containing protease inhibitors cocktail (see above). The samples were boiled for 5 min and then shaken in an eppendorf vortex mixer (Eppendorf – 543□ mixer, Boulder, CO, USA) for 15 min at 4°C. An aliquot of the rat bladder lysate (30  $\mu\text{g}$ ) was dissolved in Laemmli sample buffer containing 100 mM DTT, heated to 37°C for 5 min, and then resolved by SDS-PAGE on 10% (w/v) polyacrylamide gels. The proteins were transferred to Immobilon-P membrane (Millipore, Bedford, MA, USA) for 75 min at 375 mAmps and the membrane was blocked overnight in 5% (w/v) BSA dissolved in PBS. The blotted proteins were reacted with primary antibodies (diluted in PBS containing 1% dehydrated non-fat milk) for 2 h at room temperature with rotation. The membrane was then washed with TBS-Tween (see above) three times 30 min and then incubated in the appropriate secondary antibody conjugated to HRP diluted 1:25,000 in PBS-milk for 1 h

with rotation. The membrane was washed with 3 changes of TBS-Tween over 3 h and then incubated for 1 min in Super Signal (Pierce, Rockford, IL, USA) and exposed to XAR-5 film (Eastman Kodak, Rochester, NY, USA). The bands were quantified by densitometry using the Quantity One Program (Bio-Rad, Hercules, CA, USA).

### ***Immunofluorescence labeling of bladder cryosections***

Bladders from mice or rats were fixed in 4% paraformaldehyde, 100 mM sodium cacodylate buffer, pH 7.4 for 2 h at room temperature, and then cryoprotected by incubation in phosphate buffered saline (PBS) containing 30% (w/w) sucrose overnight at 4°C on a rotator. Tissue was then placed in OCT compound (Tissue-Tek, Torrance CA, USA) and frozen in molds placed on dry ice blocks. Blocks were stored at -70°C. Sections were cut at a thickness of 4 µM using a CM 1900 cryostat machine (Leica, Bannockburn, IL), collected on Fisherbrand Superfrost/Plus slides (Fisher, Pittsburgh, PA), and then dehydrated by incubating the slides for 1 min at room temperature. After washing the sections three times with PBS for 5 min, the paraformaldehyde was quenched and the cells permeabilized with PBS containing 20 mM glycine, pH 8.0, 75 mM ammonium chloride, and 0.1% (v/v) Triton X-100 for 10 min at room temperature. The cells were washed with block solution (PBS containing 0.7% [w/v] fish skin gelatin and 0.025% [w/v] saponin) and then incubated in block solution containing 10% (v/v) new born calf serum and 100 µg/ml boiled RNase A for 15 min at ambient temperature. Sections were subsequently washed in block solution three times over 15 min and then incubated for 60 min at ambient temperature with primary antibody diluted in block solution. Following incubation with the primary antibody, the sections were washed three times with block solution over a 15 min period of time. The sections were then incubated with the secondary antibody for 60 min at ambient temperature, and

then washed 3 times with block solution over a 15-min time period. Following 3 washes with PBS, the tissue was postfixed for 10 min in 4% paraformaldehyde in 100 mM sodium cacodylate, pH 7.4. Following a final wash with PBS coverslips were placed over the stained tissue using p-diaminobenzidine-containing mounting medium (8).

### ***Immunodepletion of P2X receptor-specific antisera***

P2X<sub>2</sub> and P2X<sub>3</sub>-specific tissue staining were blocked with competitive antigen peptides. Rabbit anti-P2X<sub>2</sub> or P2X<sub>3</sub> antisera was preincubated with its respective antigen peptide in block solution 1 h prior to tissue labeling in 4°C on rotator. After the 1 h incubation period, the anti-P2X antibody/antigen peptide cocktail was incubated with the tissue as described above in the immunohistochemistry protocol.

### ***Scanning laser confocal analysis of fluorescently-labeled cell***

Imaging was performed on a TCS-SL confocal microscope equipped with argon-, and green and red helium-neon lasers (Leica, Dearfield, IL, USA). Images were acquired with the use of a 100x plan-apochromat oil objective (1.4 numerical aperture) and the appropriate filter combination. Settings were as follows: photomultipliers set to 600-800 V, 1.0 µm pinhole, and Kalman filter (n=4). Serial (Z) sections were captured with a 0.5 µm step size. The images (512 x 512 pixels) were saved as TIFF files. The OpenLab program (Improvision, Lexington, MA) was used to project the serial sections into one image. The contrast level of the images was then adjusted in the Photoshop program (Adobe, Mountain View, CA, USA), and the contrast-corrected images were imported into FreeHand (Macromedia, San Francisco, CA, USA).

## APPENDIX B

### ABBREVIATIONS

ABC	adenosine triphosphate binding cassette
ADP	adenosine diphosphate
AM	acetoxymethyl
AMP	adenosine monophosphate
cAMP	cyclic adenosine monophosphate
ANF	atrial natriuretic factor
APB	2-aminoethoxydiphenylborate
ATP	adenosine triphosphate
ATP[S	adenosine 5'-[S-thio]triphosphate
AUM	asymmetric unit membrane
BFA	brefeldin A
BSA	bovine serum albumin
BZATP	2',3'-(4-benzoyl)-benzoyl-adenosine triphosphate
C	capacitance
CCPA	2-chloro N <sup>6</sup> -cyclopentyladenosine
CFTR	cystic fibrosis transmembrane conductance regulator
CGS21680	2-[ <i>p</i> -(2-carbonyl-ethyl)-phenylethylamino]-5'- <i>N</i> -ethylcarboxamidoadenosine
CICR	Ca <sup>2+</sup> induced Ca <sup>2+</sup> release
CPM	counts per minute
DAG	diacylglycerol
DIDS	4,4'-diisothiocyanostilbene-2,2'-disulfonic acid
DMSO	dimethyl sulfoxide
DTT	Dithiothreitol
EDTA	ethylenediaminetetraacetic acid
EGTA	ethylene glyco-bis(aminoethylether) <i>N,N,N',N'</i> -tetraacetic acid

ENaC	epithelial sodium channel
ER	endoplasmic reticulum
FITC	fluorescein isothiocyanate
GAG	glycosaminoglycan
GFP	green fluorescent protein
HEK293	human embryonic kidney 293
HEPES	<i>N</i> -2-hydroxyethylpiperazine- <i>N'</i> -2-ethanesulfonic acid
HRP	horse radish peroxidase
I	current
IB-MECA	<i>N</i> <sup>6</sup> -(3-iodobenzyl)adenosine-5'- <i>N</i> -methyluronamide
IBMX	3-isobutyl-1-methylxanthine
IG	immunoglobulin
IP <sub>3</sub>	inositol 1,4,5-triphosphate
Isc	short circuit current
LDH	lactate dehydrogenase
MDCK	Madin-Darby canine kidney
□, □-MeATP	□, □-methylene adenosine triphosphate
MEM	minimal essential medium
MESNA	2-mercaptoethanesulfonic acid
2-MethSATP	2-(Methylthio) adenosine triphosphate
NHS	<i>N</i> -hydroxysuccinimide
NMDG	<i>N</i> -methyl- <i>D</i> -glucamine
NO	nitric oxide
NSC	nonselective cation channel
P1	adenosine receptor
P2	purinergic receptor
P2X	purinergic receptor type X
P2Y	purinergic receptor type Y
PAGE	polyacrylamide gel electrophoresis
PAP	adenosine 3,5-diphosphate
PBS	phosphate buffered saline
PCR	polymerase chain reaction
PKA	protein kinase A

PKC	protein kinase C
PLC	phospholipase C
PPADS	pyridoxalphosphate-6-azophenyl-2',4'-disulfonic acid
R	resistance
RB2	reactive blue-2
SDS	sodium dodecyl sulphate
SEM	standard error of the mean
TBS	tris buffer solution
TEA	tetraethylammonium
TEM	transmission electron microscopy
TER	transepithelial resistance
TIFF	tag-information-file-format
TMA	tetramethylammonium
TNP-ATP	2',3'- <i>O</i> -(2,4,6-trinitrophenyl) adenosine 5'-triphosphate
UP	uroplakin
UTP	uridine 5'-triphosphate
V	voltage
VR1	vanilloid receptor
VR-OAC	vanilloid receptor-related osmotically activated channel
WGA	wheat germ agglutinin
ZO-1	zona occludin-1

## BIBLIOGRAPHY

1. **Acharya P, Beckel J, Wang E, Ruiz W, Rojas R, and Apodaca G.** Distribution of the tight junction proteins ZO-1, occludins, and claudin-4, -8, and -12 in bladder epithelium. *in press*, 2003.
2. **Altschuler Y, Kinlough C, Poland P, Apodaca G, Weisz O, and Hughey R.** Clathrin-mediated endocytosis of MUC1 is regulated by glycosylation. *Mol Biol Cell* 11: 819-831, 2000.
3. **Alves D and Duarte I.** Involvement of ATP-sensitive K<sup>+</sup> channels in the peripheral antinociceptive effect induced by dipyrrone. *Eur J Pharmacol* 24: 47-52, 2002.
4. **Amano O, Kataoka S, and Yamamoto T.** Turnover of Asymmetric Unit Membranes in the Transitional Epithelial Superficial Cells of the Rat Urinary Bladder. *Anat Rec* 229: 9-15, 1991.
5. **Andersson K.** Bladder activation: afferent mechanisms. *Urology* 59: 43-50, 2002.
6. **Apodaca G.** Modulation of membrane traffic by mechanical stimuli. *Am J Physiol* 282: F179-F190, 2002.
7. **Apodaca G.** The uroepithelium: not just a passive barrier. *in press*, 2003.
8. **Apodaca G, Katz L, and Mostov K.** Receptor-mediated transcytosis of IgA in MDCK cells is via apical recycling endosomes. *J Cell Biol* 125: 67-86, 1994.
9. **Baddeley A, Gunderson H, and Cruz-Orive L.** Estimation of surface area from vertical sections. *J Microscopy* 142: 259-276, 1986.
10. **Banes AJ, Tsuzaki M, and Yamamoto J.** Mechanoreception at the cellular level: the detection, interpretation, and diversity of responses to mechanical signals. *Biochem Cell Biol* 73: 349-365, 1995.

11. **Bayer N, Schober D, Huttinger M, Blaas D, and Fuchs R.** Inhibition of clathrin-dependent endocytosis has multiple effects on human rhinovirus serotype 2 cell entry. *J Biol Chem* 276: 3952-3962, 2001.
12. **Bear CE.** A nonselective cation channel in rat liver cells is activated by membrane stretch. *Am J Physiol* 258: C421-C428, 1990.
13. **Beardmore J, Howell KE, Miller K, and Hopkins CR.** Isolation of an endocytic compartment from A431 cells using a density modification procedure employing a receptor-specific monoclonal antibody. *J Cell Sci* 87: 495-506, 1987.
14. **Belousov LV, Dorfman JG, and Cherdantzev J.** Mechanical stresses and morphological patterns in amphibian embryos. *J Embryol Exp Morphol* 34: 559-574, 1975.
15. **Belousov LV, Kazakova NI, Luchinskaia NN, and Novoselov VV.** Studies in developmental cytomechanic. *Int J Dev Biol* 41: 793-799, 1997.
16. **Bernd N.** Ion channels and their functional role in vascular endothelium. *Physiol Rev* 81: 1415-1459, 2001.
17. **Berridge MJ, Lipp P, and Bootman MD.** The versatility and universality of calcium signalling. *Nat Rev Mol Cell Biol* 1: 11-21, 2000.
18. **Bianchi BR, Lynch KJ, Touma E, Niforatos W, Burgard EC, Alexander KM, Park HS, Yu H, Metzger R, Kowaluk E, Jarvis M, and Biesen T.** Pharmacological characterization of recombinant human and rat P2X receptor subtypes. *Eur J Pharmacol* 376: 127-138, 1999.
19. **Birder L, Apodaca G, De Groat W, and Kanai A.** Adrenergic- and capsaicin-evoked nitric oxide release from urothelium and afferent nerves in urinary bladder. *Am J Physiol* 275: F226-F229, 1998.
20. **Birder LA, Kanai AJ, de Groat WC, Kiss S, Nealen ML, Burke NE, Dineley KE, Watkins S, Reynolds IJ, and Caterina MJ.** Vanilloid receptor expression suggests a sensory role for urinary bladder epithelial cells. *PNAS* 98: 13396-13401, 2001.
21. **Birder LA, Nakamura Y, Kiss S, Nealen ML, Barrick S, Kanai AJ, Wang E, Ruiz G, de Groat WC, Apodaca G, Watkins S, and Caterina MJ.** Altered urinary bladder function in mice lacking the vanilloid receptor TRPV1. *Nature Neurosci* 5: 856-860, 2002.



22. **Blokkebak-Poulsen M, Sheikh I, and Jacobsen C.** Non-selective cation channels in basolateral-membrane vesicles from pars recta of rabbit kidney proximal tubule. *Biochem J* 272: 839-842, 1990.
23. **Bloom W and Fawcett D.** *A textbook of histology*. New York: Chapman & Hall, 1994.
24. **Bodin P and Burnstock G.** Evidence that release of adenosine triphosphate from endothelial cells during increased shear stress is vesicular. *J Cardio Pharm* 38: 900-908, 2001.
25. **Brandle U, Spielmanns P, Osteroth R, Sim J, Surprenant A, Buell G, Ruppertsberg JP, Plinkert PK, Zenner H-P, and Glowatzki E.** Desensitization of the P2X<sub>2</sub> receptor controlled by alternative splicing. *FEBS Lett* 404: 294-298, 1997.
26. **Bridges RJ.** Transepithelial measurements of bicarbonate secretion in calu-3 cells. *Meth Mol Med* 70: 111-128, 2002.
27. **Brinson AE and Harden TK.** Differential regulation of the uridine nucleotide-activated P2Y<sub>4</sub> and P2Y<sub>6</sub> receptors. *J Biol Chem* 276: 11939-11948, 2001.
28. **Burnstock G.** P2X receptors in sensory neurons. *Br J Anaesthes* 84: 476-488, 2000.
29. **Burnstock G.** Purine-mediated signalling in pain and visceral perception. *Trends in Pharm Sci* 22: 182-188, 2001.
30. **Burnstock G and Williams M.** P2 purinergic receptors: modulation of cell function and therapeutic potential. *J Pharmacol Exp Ther* 295: 862-869, 2000.
31. **Burridge K and Chrzanowska-Wodnicka M.** Focal adhesions, contractility, and signaling. *Annu Rev Cell Dev Biol* 12: 463-519, 1996.
32. **Burridge MJ, Lipp P, and Bootman MD.** The versatility and universality of calcium signalling. *Nature Rev Mol Cell Biol* 1: 11-21, 2000.
33. **Chang A, Hammond T, Sun T, and Zeidel M.** Permeability properties of the mammalian bladder apical membrane. *Am J Physiol* 267: C1483-C1492, 1994.
34. **Chen BM and Grinnell AD.** Integrins and modulation of transmitter release from motor nerve terminals by stretch. *Science* 269: 1578-1580, 1995.
35. **Chepilko S, Zhou H, Sackin H, and Palmer L.** Permeation and gating properties of a cloned renal K<sup>+</sup> channel. *Am J Physiol* 268: C389-C401, 1995.
36. **Chiba T and Marcus D.** Nonselective cation and BK channels in apical membrane of outer sulcus epithelial cells. *J Membr Biol* 174: 167-179, 2000.

37. **Clausen C, Lewis SA, and Diamond JM.** Impedance analysis of a tight epithelium using a distributed resistance model. *Biophys J* 26: 291-318, 1979.
38. **Clemow D, Steers W, and Tuttle J.** Stretch-Activated Signaling of Nerve Growth Factor Secretion in Bladder and Vascular Smooth Muscle Cells From Hypertensive and Hyperactive Rats. *J Cell Physiol* 183: 289-300, 2000.
39. **Cockayne DA, Hamilton SG, Zhu Q, Dunn PM, Zhong Y, Novakovic S, Malmberg AB, Cain G, Berson A, Kassotakis L, Hedley L, Lachnit WG, Burnstock G, McMahon SB, and Ford A.** Urinary bladder hyporeflexia and reduced pain-related behaviour in P2X3-deficient mice. *Nature* 407: 1011-1015, 2000.
40. **Coco S, Calegari F, Pravettoni E, Pozzi D, Taverna E, Rosa P, Matteoli M, and Verderio C.** Storage and release of ATP from astrocytes in culture. *J Biol Chem* 278: 1354-1362, 2003.
41. **Cook SP and McCleskey EW.** ATP, pain and a full bladder. *Nature* 407: 951-952, 2000.
42. **Cooke HJ, Wunderlich J, and Christofi FL.** "The force be with you": ATP in mechanosensory transduction. *NIPS* 18: 43-49, 2003.
43. **Dai J and Sheetz MP.** Regulation of endocytosis, exocytosis, and shape by membrane tension. *Cold Spring Harbor Symp Quant Biol* 60: 567-571, 1995.
44. **Dai J, Ting-Beall P, and Sheetz M.** The Secretion-coupled Endocytosis Correlates with Membrane Tension Changes in RBL 2H3 Cell. *J Gen Physiol* 110: 1-10, 1997.
45. **Davies PF and Tripathi SC.** Mechanical stress mechanisms and the cell. *Cir Res* 72: 239-245, 1993.
46. **Davis CW, Dowell ML, Lethem M, and van Scott M.** Goblet cell degranulation in isolated canine tracheal epithelium: response to exogenous ATP, ADP, and adenosine. *Am J Physiol Cell Physiol* 262: C1313-C1323, 1992.
47. **de Groat WC and Yoshimura N.** Pharmacology of the lower urinary tract. *Annu Rev Pharmacol Toxicol* 41: 691-721, 2001.
48. **Deng F, Ding M, Lavker R, and Sun T-T.** Urothelial function reconsidered: A role in urinary protein secretion. *PNAS* 98: 154-159, 2001.
49. **Deng F, Liang F, Tu L, Resing KA, Hu P, Supino M, Hu C, Zhou G, Ding M, Kreibich G, and Sun TT.** Uroplakin IIIb, a urothelial differentiation marker, dimerizes

- with uroplakin Ib as an early step of urothelial plaque assembly. *J Cell Biol* 159: 685-694, 2002.
50. **Devor DC and Pilewski JM.** UTP inhibits sodium absorption in wild-type and delF508 CFTR-expressing human bronchial epithelia. *Am J Physiol Cell Physiol* 276: C827-C837, 1999.
  51. **Dietz J.** Release of atrial natriuretic factor from heart-lung preparation by atrial distension. *Am J Physiol* 247: R1093-1096, 1988.
  52. **Donaldson P and Lewis SA.** Effect of hyperosmotic challenge on basolateral membrane potential in rabbit urinary bladder. *Am J Physiol Cell Physiol* 264: C248-C257, 1993.
  53. **Eaton DC, Hamilton KL, and Johnson KE.** Intracellular acidosis blocks the basolateral Na-K pump in rabbit urinary bladder. *Am J Physiol* 247: F946-F954, 1984.
  54. **Edward YS.** Stretch stimulation: its effects on alveolar type II cell function in the lung. *Comp Biochem Physiol A Physiol* 129: 245-260, 2001.
  55. **Efron B and Tibshirani R.** *Introduction to the Bootstrap*: CRC Press, 1993.
  56. **Egee S, Lapaix F, Cossins AR, and Thomas S.** The role of anion and cation channels in volume regulatory responses in trout red blood cells. *Bioelectrochemistry* 52: 133-149, 2000.
  57. **El-Sherif Y, Weiraszko A, Banerjee P, and Penington NJ.** ATP modulates Na<sup>+</sup> channel gating and induces a non-selective cation current in a neuronal hippocampal cell line. *Brain Res* 904: 307-317, 2001.
  58. **Elneil S, Skepper JN, Kidd EJ, Williamson JG, and Ferguson DR.** Distribution of P2X(1) and P2X(3) receptors in the rat and human urinary bladder. *Pharmacology* 63: 120-128, 2001.
  59. **Ennion SJ and Evans RJ.** Agonist-stimulated internalization of the ligand-gated ion channel P2X<sub>1</sub> in rat vas deferens. *FEBS Lett* 489: 154-158, 2001.
  60. **Fenteany G, Standaert R, Lane W, Choi S, Corey E, and Schreiber S.** Inhibition of proteasome activities and subunit-specific amino-terminal threonine modification by lactacystin. *Science* 268: 726-731, 1995.
  61. **Ferguson DR.** Urothelial function. *B J Urol Int* 84: 235-242, 1999.

62. **Ferguson DR, Kennedy I, and Burton TJ.** ATP is released from rabbit urinary bladder epithelial cells by hydrostatic pressure changes - a possible sensory mechanism. *J Physiol* 505: 503-511, 1997.
63. **Filipovic D and Sackin H.** Stretch- and volume-activated channels in isolated proximal tubule cells. *Am J Physiol* 22: F1253-F1262, 1992.
64. **Fink R and Cooper M.** Apical membrane Turnover is accelerated near cell-cell contacts in an embryonic epithelium. *Dev Biol* 174: 180-189, 1996.
65. **Fosset M, de Weille JR, and Green RD.** Antidiabetic sulfonylureas control action potential properties in heart cells via high affinity receptors that are linked to ATP-dependent K<sup>+</sup> channels. *J Biol Chem* 263, 1988.
66. **Fredholm BB, Ijzerman AP, Jacobson KA, Klotz K, and Linden J.** International union of pharmacology. XXV. Nomenclature and classification of adenosine receptors. *Pharmacol Rev* 53: 527-552, 2001.
67. **Fuchs PA.** Synaptic transmission at vertebrate hair cells. *Curr Op Neurobiol* 6: 514-519, 1996.
68. **Fujihara M, Muroi M, Muroi Y, Ito N, and Suzuki T.** Mechanism of lipopolysaccharide-triggered junB activation in a mouse macrophage-like cell line. *J Biol Chem* 268: 14898-14905, 1993.
69. **Fujiwara T, Oda K, Yokota S, Takatsuki A, and Ikehara Y.** Brefeldin A causes disassembly of the Golgi complex and accumulation of secretory proteins in the endoplasmic reticulum. *J Biol Chem* 263: 18545-18552, 1988.
70. **Fujiyama C, Masake Z, and Sugihara H.** Reconstruction of the urinary bladder mucosa in three-dimensional collagen gel culture: fibroblast-extracellular matrix interactions on the differentiation of transitional epithelial cells. *J Urol* 153: 2060-2067, 1995.
71. **Furuse M, Fujita K, Hiiragi T, Fujimoto K, and Tsukita S.** Claudin-1 and -2: novel integral membrane proteins localizing at tight junctions with no sequence similarity to occludin. *J Cell Biol* 141: 1539-1550, 1998.
72. **Furuse M, Hirase T, Itoh M, Nagafuchi A, Yonemura S, and Tsukita S.** Occludin: a novel integral membrane protein localizing at tight junctions. *J Cell Biol* 123: 1777-1788, 1993.

73. **Gabella G and Davis C.** Distribution of afferent axons in the bladder of rats. *J of Neurocytology* 27: 141-155, 1998.
74. **Gallagher CJ and Salter MW.** Differential properties of astrocyte calcium waves mediated by P2Y1 and P2Y2 receptors. *J of Neurosci* 23: 6728-6739, 2003.
75. **Gargus JF, Frace AM, and Jung F.** The role of a PDGF-activated nonselective cation channel in the proliferative response. *Experientia Supplementum* 66: 289-295, 1993.
76. **Gillis K.** Techniques for membrane capacitance measurements. In: *Single Channel Recording* (2nd ed.), edited by Sakman B and Neher E. New York: Plenum, 1995, p. 155-198.
77. **Gonzales-Mariscal L, Betanzo A, Nava P, and Jaramillo BE.** Tight junction proteins. *Progress Biophys Mol Biol* 81: 1-44, 2003.
78. **Gonzalez-Perrett S, Kim K, Ibarra C, Damiano AE, Zotta E, Batelli M, Harris PC, Reisin IL, Arnaut MA, and Cantiello HF.** Polycystin-2, the protein mutated in autosomal dominant polycystic kidney disease (ADPKD) is a Ca<sup>2+</sup>-permeable nonselective cation channel. *Proc Natl Acad Sci* 98: 1182-1187, 2001.
79. **Gordon JL.** Extracellular ATP: effects, sources, and fate. *Biochem J* 233: 309-319, 1986.
80. **Gray H.** *Anatomy of the human body.* Philadelphia: Lea & Febiger, 2000.
81. **Griffiths G.** *Fine Structure Immuno-cytochemistry.* Berlin: Springer-Verlag, 1993.
82. **Griffiths G, Back R, and Marsh M.** A quantitative analysis of the endocytic pathway in baby hamster kidney cells. *J Cell Biol* 109: 2703-2720, 1989.
83. **Griffiths G and Simons K.** The trans Golgi network: sorting at the exit site of the Golgi complex. *Science* 234: 4381-4443, 1986.
84. **Gruden G, Thomas S, Burt D, Lane S, Chusney G, Sacks S, and Viberti G.** Mechanical stretch induces vascular permeability factor in human mesangial cells: Mechanisms of signal transduction. *PNAS* 94: 12112-12116, 1997.
85. **Grygorczyk R and Hanrahan JW.** CFTR-independent ATP release from epithelial cells triggered by mechanical stimuli. *Am J Physiol Cell Physiol* 272: C1058-C1066, 1997.
86. **Guan X, Cravatt BF, Ehring GR, Hall JE, Boger DL, Lerner RA, and Gilula N.** The sleep-inducing lipid oleamide deconvolutes gap junction communication and calcium wave transmission in glial cells. *J Cell Biol* 139: 1785-1792, 1997.

87. **Guerineau NC, Bossu JL, Gahwiler BH, and Gerber U.** Activation of a nonselective cationic conductance by metabotropic glutamatergic and muscarinic agonists in CA3 pyramidal neurons of the rat hippocampus. *J Neurosci* 15: 4395-4407, 1995.
88. **Guo A, Vulchanova L, Wang J, Li X, and Elde R.** Immunocytochemical localization of the vanilloid receptor (VR1): Relationship to neuropeptides, the P2X<sub>3</sub> purinoceptor and IB4 binding sites. *Eur J Neurosci* 11: 946-958, 1999.
89. **Hamill OP and Martinac B.** Molecular basis of mechanotransduction in living cells. *Physiol Rev* 81: 685-740, 2001.
90. **Hamill OP and McBride DW.** The pharmacology of mechanogated membrane ion channels. *Pharmacol Rev* 48: 231-252, 1996.
91. **Harter C and Wieland F.** The secretory pathway: mechanisms of protein sorting and transport. *Biochim Biophys Acta* 1286: 75-93, 1996.
92. **Hayat M.** *Principles and Techniques of Electron Microscopy*. Boca Raton: CRC Press, Inc., 1989.
93. **Heuser JE and Anderson RG.** Hypertonic media inhibit receptor-mediated endocytosis by blocking clathrin-coated pit formation. *J Cell Biol* 108: 389-400, 1989.
94. **Hicks R.** The fine structure of the transitional epithelium of rat ureter. *J Cell Biol* 26: 25-48, 1965.
95. **Hicks R.** The function of the Golgi complex in transitional epithelium. *J Cell Biol* 30: 623-644, 1966.
96. **Hicks RM.** The mammalian urinary bladder: an accommodating organ. *Biol Rev* 50: 215-246, 1975.
97. **Higuchi T, Xin P, Buckley M, Erickson D, and Bhavanandan VP.** Characterization of the rabbit homolog of human MUC1 glycoprotein isolated from bladder by affinity chromatography on immobilized jacalin. *Glycobiology* 10: 659-667, 2000.
98. **Hill AE and Hill BS.** Transcellular sodium fluxes and pump activity in *Necturus* gall-bladder epithelial cells. *J Physiol* 382: 35-49, 1987.
99. **Hille B.** *Ion channels of excitable membranes, Third Edition*. Sunderland, MA: Sinauer Associates, 2001.

100. **Hoger U, Torkkeli PH, Seyfarth E, and French AS.** Ionic selectivity of mechanically activated channels in spider mechanoreceptor neurons. *J Neurophysiol* 78: 2079-2085, 1997.
101. **Homann U.** Fusion and fission of plasma-membrane material accommodates for osmotically induced changes in the surface area of guard-cell protoplasts. *Planta* 206: 329-333, 1998.
102. **Howard CV and Reed MG.** *Unbiased stereology: three dimensional measurement in microscopy.* New York: Springer-Verlag, 1998.
103. **Howard J, Roberts WM, and Hudspeth AJ.** Mechanoelectrical transduction by hair cells. *Annu Rev Biophys Biophys Chem* 17: 99-124, 1988.
104. **Hu P, Deng F-M, Liang F-X, Hu C-M, Auerbach A, Shapiro E, Wu X-R, Kachlar B, and Sun T-T.** Ablation of Uroplakin III Gene Results in Small Urothelial Plaques, Urothelial Leakage, and Vesicoureteral Reflux. *J Cell Biol* 151: 961-971, 2000.
105. **Hunziker W, Male P, and Mellman I.** Differential microtubule requirements for transcytosis in MDCK cells. *EMBO J* 9: 3515-3525, 1990.
106. **Ihrke G, Martin G, Shanks M, Schrader M, Schroer T, and Hubbard A.** Apical Plasma Membrane Proteins and Endolyn-78 Travel through a Subapical Compartment in Polarized WIF-B hepatocytes. *J Cell Biol* 141: 115-133, 1998.
107. **Ingber DE.** Tensegrity: the architectural basis of cellular mechanotransduction. *Annu Rev Physiol* 59: 575-599, 1997.
108. **Insel PA.** ATP-and nucleotide-mediated signaling via multiple P2Y receptors in renal epithelial cells. *Clin Exp Pharm and Physiol*, In press.
109. **Irvin JL and Irvin EM.** The interaction of quinacrine with adenine nucleotides. *J Biol Chem* 210: 45-56, 1954.
110. **Iwase N, Sasaki T, Shimura S, Yamamoto M, Suzuki S, and Sharito K.** ATP-induced chloride secretion with suppressed sodium absorption in rabbit tracheal epithelium. *Respir Physiol* 107: 173-180, 1997.
111. **Jung S-R, Kim M-H, Hille B, Nguyen TD, and Koh D-S.** Regulation of exocytosis by purinergic receptors in pancreatic duct epithelial cells. *Am J Physiol Cell Physiol* (in press), 2003.

112. **Kanai AJ, Zeidel ML, Lavelle JP, Greenberger JS, Birder LA, de Groat WC, Apodaca GL, Meyers SA, Ramage R, and Epperly MW.** Manganese superoxide dismutase gene therapy protects against irradiation-induced cystitis. *Am J Physiol Renal Physiol* 283: F1304-F1312, 2002.
113. **Kerr D, Liang F, Bondioli K, Zhao H, Kreibich G, Wall R, and Sun T-T.** The bladder as a bioreactor: Urothelium production and secretion of growth hormone into urine. *Nature Biotech* 16: 75-79, 1997.
114. **Kim SH, Cho KW, Chang SH, Kim SZ, and Chae SW.** Glibenclamide suppresses stretch-activated ANP secretion: involvements of K<sup>+</sup> ATP channels and L-type Ca<sup>2+</sup> channel modulation. *Pflugers Arch* 434: 362-372, 1997.
115. **Kitano I, Doi K, N. M, and Matsunaga T.** Involvement of Cl<sup>-</sup> transport in forskolin-induced elevation of endocochlear potential. *Hearing Res* 71: 23-27, 1993.
116. **Kleyman TR and Cragoe EJJ.** Amiloride and its analogs as tools in the study of ion transport. *J Membr Biol* 105: 1-21, 1988.
117. **Kleyman TR and Cragoe EJJ.** Cation transport probes: the amiloride series. *Methods Enzymol* 191: 739-755, 1990.
118. **Knight GE, Bodin P, W.C. dG, and Burnstock G.** ATP is released from guinea pig ureter epithelium on distention. *Am J Physiol* 282: F281-F288, 2002.
119. **Kochukov MY and Ritchie AK.** ATP stimulation of membrane trafficking in FRTL thyrocytes is mediated by a P2X<sub>7</sub>-like receptor. *Mol Biol Cell* 14: 76a, 2003.
120. **Koss L.** The Asymmetric Unit Membranes of the Epithelium of the Urinary Bladder of the Rat: an electron microscopic study of a mechanism of epithelial maturation and function. *Lab Invest* 21: 154-168, 1969.
121. **Laine M, Arjamaa O, Voulteenaho O, Ruskoaho H, and Weckstrom M.** Block of stretch-activated atrial natriuretic peptide secretion by gadolinium in isolated rat atrium. *J Phys (London)* 480: 553-561, 1994.
122. **Lang R, Tholken H, Ganten F, Luft F, Ruskoaho H, and Unger T.** Atrial natriuretic factor-a circulating hormone stimulated by volume loading. *Nature* 314: 264-266, 1985.
123. **Lavelle J, Meyers S, Ramage R, Bastacky S, Doty D, Apodaca G, and Zeidel M.** Bladder permeability barrier: recovery from selective injury of surface epithelial cells. *Am J Physiol* 283: F242-F253, 2002.



124. **Lavelle JP, Apodaca G, Meyers SA, Ruiz WG, and Zeidel ML.** Disruption of the guinea pig urinary bladder permeability barrier in noninfectious cystitis. *Am J Physiol* 274: F205-F214, 1998.
125. **Lee HY, Bardini M, and Burnstock G.** Distribution of P2X receptors in the urinary bladder and the ureter of the rat. *J Urol* 163: 2002-2007, 2000.
126. **Levin R, Longhurst P, Monson F, Haugaard N, and Wein A.** Experimental studies on bladder outlet obstruction. In: *Prostate Diseases*, edited by Lepor H and Lawson RK. Philadelphia: W.B. Saunders, Co., 1993, p. 119-130.
127. **Levin R and Wein A.** Response of the in vitro whole bladder (rabbit) preparation to autonomic agonists. *J Urol* 128: 1087-1090, 1982.
128. **Lewis SA.** Everything you wanted to know about the bladder epithelium but were afraid to ask. *Am J Physiol* 278: F867-F874, 2000.
129. **Lewis SA.** The mammalian urinary bladder: it's more than accommodating. *News in Physiol Sci* 1: 61-65, 1986.
130. **Lewis SA and Alles WP.** Urinary kallikrein: a physiological regulator of epithelial Na<sup>+</sup> absorption. *Proc Natl Acad Sci* 83: 5345-5348, 1986.
131. **Lewis SA, Berg JR, and Kleine TJ.** Modulation of epithelial permeability by extracellular macromolecules. *Physiol Rev* 75: 561-589, 1995.
132. **Lewis SA and Clausen C.** A guide to methods and experimental analysis. edited by Wills NK, Reuss L and Lewis SA. London: Chapman & Hall, 1996, p. 118-145.
133. **Lewis SA and Clausen C.** Urinary proteases degrade epithelial sodium channels. *J Membr Biol* 122: 77-88, 1991.
134. **Lewis SA and de Moura JL.** Apical membrane area of rabbit urinary bladder increases by fusion of intracellular vesicles: an electrophysiological study. *J Membr Biol* 82: 123-136, 1984.
135. **Lewis SA and de Moura JLC.** Incorporation of cytoplasmic vesicles into the apical membrane of rabbit urinary bladder epithelium. *Nature* 297: 685-688, 1982.
136. **Lewis SA and Diamond JM.** Active sodium transport by mammalian urinary bladder. *Nature* 253: 747-748, 1975.
137. **Lewis SA and Diamond JM.** Na<sup>+</sup> transport by rabbit urinary bladder, a tight epithelium. *J Membr Biol* 28: 35-40, 1976.

138. **Lewis SA, Eaton DC, and Damiano AE.** The mechanism of Na<sup>+</sup> transport by rabbit urinary bladder. *J Membr Biol* 28: 41-70, 1976.
139. **Lewis SA and Hanrahan J.** Physiological approaches for studying mammalian urinary bladder epithelium. *Methods Enzymol* 192: 632-650, 1990.
140. **Lewis SA and Hanrahan JW.** Apical and basolateral membrane ionic channels in rabbit urinary bladder epithelium. *Pflugers Arch* 405: S83-S88, 1985.
141. **Lewis SA, Ifshin MS, Loo DDF, and Diamond JM.** Studies of sodium channels in rabbit urinary bladder by noise analysis. *J Membr Biol* 80: 135-151, 1984.
142. **Li C, Ramjeesingh M, and Bear CE.** Purified cystic fibrosis transmembrane conductance regulator (CFTR) does not function as an ATP channel. *J Biol Chem* 271: 11623-11626, 1996.
143. **Liang F-X, Riedel I, Deng F-M, Zhou G, Xu C, Wu X-R, Kong X-P, Moll R, and Sun T-T.** Organization of uroplakin subunits: transmembrane topology, pair formation and plaque composition. *Bioch J* 355: 13-18, 2001.
144. **Liedtke W, Choe Y, Marti-Renom MA, Bell AM, Denis CS, Sali A, Hudspeth AJ, Friedman JM, and Heller S.** Vanilloid receptor-related osmotically activated channel (VR-OAC), a candidate vertebrate osmoreceptor. *Cell* 103: 525-535, 2000.
145. **Light DB, Schwiebert EM, Fejes-Toth G, Naray-Fejes-Toth A, Karlson KH, McCann FV, and Stanton BA.** Chloride channels in the apical membrane of cortical collecting duct cells. *Am J Physiol* 258: F273-F280, 1990.
146. **Lindinger MI, Hawke TJ, Vickery L, Bradford L, and Lipskie SL.** An integrative, in situ approach to examining K<sup>+</sup> flux in resting skeletal muscle. *Can J Physiol Pharmacol* 79: 996-1006, 2001.
147. **Liu M, Liu J, Buch S, Tanswell AK, and Post M.** Mechanical strain induces pp60<sup>src</sup> activation and translocation to cytoskeleton in fetal rat lung cells. *J Biol Chem* 271: 7066-7071, 1996.
148. **Luo X, Zheng W, Yan M, Lee G, and Muallem S.** Multiple functional P2X and P2Y receptors in the luminal and basolateral membrane of pancreatic duct cells. *Am J Physiol Cell Physiol* 277: C205-C215, 1999.

149. **Magner and Papagiannes.** Blockage by brefeldin A of intracellular transport of secretory proteins in mouse pituitary cells: effects on the biosynthesis of thyrotropin and free alpha-subunits. *Endocrinology* 122: 912-920, 1988.
150. **Maroto R and Hamill OP.** Brefeldin A block of integrin-dependent mechanosensitive ATP release from *Xenopus* oocytes reveals a novel mechanism of mechanotransduction. *J Biol Chem* 276: 23867-23872, 2001.
151. **Martin-Padura I, Lostaglio S, Schneemann M, Williams L, Romano M, Fruscella P, Panzeri C, Stoppacciaro A, Ruco L, Villa A, Simmons D, and Dejana E.** Junctional adhesion molecule, a novel member of the immunoglobulin superfamily that distributes at intercellular junctions and modulates monocyte transmigration. *J Cell Biol* 142: 117-127, 1998.
152. **Matter K and Balda MS.** Signaling to and from tight junctions. *Nat Rev Mol Cell Biol* 4: 225-236, 2003.
153. **Minsky BD and Chlapowski FJ.** Morphometric analysis of the translocation of luminal membrane between cytoplasm and cell surface of transitional cells during the expansion-contraction cycles of mammalian urinary bladder. *J Cell Biol* 77: 685-697, 1978.
154. **Misumi Y, Misumi Y, Miki K, Takatsuki A, Tamura G, and Ikehara Y.** Novel blockade by brefeldin A of intracellular transport of secretory proteins in cultured rat hepatocytes. *J Biol Chem* 261: 11398-11403, 1986.
155. **Mitchell CH, Carre DA, and McGlenn AM.** A release mechanism for stored ATP in ocular ciliary epithelial cells. *Proc Natl Acad Sci* 95: 7174-7178, 1998.
156. **Mitic LL and Anderson JM.** Molecular architecture of tight junctions. *Annu Rev Physiol* 60: 121-142, 1998.
157. **Molnar J and L. L.** Studies on apyrases. *Arch Biochem and Biophysics* 93: 353-363, 1961.
158. **Morris C and Homann U.** Cell Surface Area Regulation and Membrane Tension. *J Memb Biol* 179: 79-102, 2001.
159. **Morris CE.** Mechanosensitive ion channels. *J Membr Biol* 113: 93-107, 1990.
160. **Mukherjee S, Ghosh RN, and Maxfield FR.** Endocytosis. *Physiol Rev* 77, 1997.

161. **Mulvey MA, Lopez-Boado YS, Wilson CL, Roth R, Parks WC, Heuser J, and Hultgren SJ.** Induction and evasion of host defenses by type 1-piliated uropathogenic *Escherichia coli*. *Science* 282: 1494-1497, 1998.
162. **Namasivayam S, Eardley I, and Morrison JFB.** Purinergic sensory neurotransmission in the urinary bladder: an in vitro study in rat. *Br J Urol Intl* 84: 854-860, 1999.
163. **Nasdala I, Wolburg-Buchholz K, Wolburg H, Huhn A, Ebnet K, Brachtendorf G, Samulowitz U, Kuster B, Engelhardt B, Vestweber D, and Butz S.** A transmembrane tight junction protein selectively expressed on endothelial cells and platelets. *J Biol Chem* 277: 17294-16303, 2002.
164. **Negrete HO, Lavelle JP, Berg J, Lewis SA, and Zeidel M.** Permeability properties of the intact mammalian bladder epithelium. *Am J Physiol* 271: F886-F894, 1996.
165. **Nelson J and Yeaman C.** Protein trafficking in the exocytic pathway of polarized epithelial cells. *Trends in Cell Biol* 11: 483-486, 2001.
166. **Nichols B.** Caveosomes and endocytosis of lipid rafts. *J Cell Sci* 116: 4707-4714, 2003.
167. **North RA.** Molecular physiology of P2X receptors. *Physiol Rev* 82: 1013-1067, 2002.
168. **Novak I.** ATP as a signaling molecule: the exocrine focus. *News Physiol Sci* 18: 12-17, 2003.
169. **Olson L, Alund M, and Norberg KA.** Fluorescence-microscopical demonstration of a population of gastrointestinal nerve fibers with a selective affinity for quinacrine. *Cell Tissue Res* 171: 407-423, 1976.
170. **Pappone PA and Lee SC.** Purinergic receptor stimulation increases membrane trafficking in brown adipocytes. *J Gen Physiol* 108: 393-404, 1996.
171. **Paradiso AM, Mason SJ, Lazarowski ER, and Boucher RC.** Membrane-restricted regulation of calcium release and influx in polarized epithelia. *Nature* 377: 643-646, 1995.
172. **Parsons CL, Boychuk D, Jones S, Hurst R, and Callahan H.** Bladder surface glycosaminoglycans: an epithelial permeability barrier. *J Urol* 143: 139-142, 1990.
173. **Parsons CL, Greenspan C, Moore SW, and Mulholland SG.** Role of surface mucin in primary antibacterial defense of bladder. *Urology* 9: 48-52, 1977.
174. **Paterson S and Morgan EH.** Effect of changes in the ionic environment of reticulocytes on the uptake of transferrin-bound iron. *J Cell Physiol* 105: 489-502, 1980.

175. **Porter K, Kenyon K, and Badenhausen S.** Specializations of the unit membrane. *Protoplasma* 63: 262-274, 1967.
176. **Raucher D and Sheetz M.** Membrane Expansion Increases Endocytosis rate during Mitosis. *J Cell Biol* 144: 497-506, 1999.
177. **Redman JF.** *Anatomy of the urogenital tract.* New York: McGraw-Hill, 2001.
178. **Reisin IL, Prat AG, Abraham EH, Amara JF, Gregory RJ, Ausiello DA, and Cantiello HF.** The cystic fibrosis transmembrane conductance regulator is a dual ATP and chloride channel. *J Biol Chem* 269: 20584-20591, 1994.
179. **Rice WR.** Effects of extracellular ATP on surfactant secretion. *Annu NY Acad Sci* 603: 64-74, 1990.
180. **Ross MH, Romrell LJ, and Kaye GI.** *Histology: a text and atlas.* Baltimore: Williams & Wilkins, 1995.
181. **Rusch A, Kros CJ, and Richardson GP.** Block by amiloride and its derivatives of mechano-electrical transduction in outer hair cells of mouse cochlear cultures. *J Physiol* 474: 75-86, 1994.
182. **Russo L, Rannels S, Laslow K, and Rannels D.** Stretch-related changes in lung cAMP after partial pneumonectomy. *Am J Physiol* 257: E261-E268, 1989.
183. **Sackin H.** Stretch-activated ion channels. *Kidney Intl* 48: 1134-1147, 1995.
184. **Sadoshima J and Izumo S.** The cellular and molecular response of cardiac myocytes to mechanical stress. *Annu Rev Physiol* 59: 551-571, 1997.
185. **Sadoshima J and Izumo S.** Mechanical stretch rapidly activates multiple signal transduction pathways in cardiac myocytes: potential involvement of an autocrine/paracrine mechanism. *EMBO* 12: 1681-1692, 1993.
186. **Sadoshima J, Xu Y, Slayter H, and Izumo S.** Autocrine release of angiotensin II mediates stretch-induced hypertrophy of cardiac myocytes in vitro. *Cell* 75: 977-984, 1993.
187. **Sak K and Webb TE.** A retrospective of recombinant P2Y receptor subtypes and their pharmacology. *Arch Biochem and Biophysics* 397: 131-136, 2002.
188. **Sandy J, Meghji S, Farndale R, and Meikle M.** Dual elevation of cyclic AMP and inositol phosphates in response to mechanical deformation of murine osteoblasts. *Biochim Biophys Acta* 1010: 265-269, 1989.

189. **Satlin LM, Sheng S, Woda CB, and Kleyman TR.** Epithelial Na<sup>+</sup> channels are regulated by flow. *Am J Physiol* 280: F1010-F1018, 2001.
190. **Schweibert E and Kishore BK.** Extracellular nucleotide signaling along the renal epithelium. *Am J Physiol* 280: F945-F963, 2001.
191. **Schweibert E, Mills JW, and Stanton BA.** Actin-based cytoskeleton regulates a chloride channel and cell volume in a renal cortical collecting duct cell line. *J Biol Chem* 269: 7081-7089, 1994.
192. **Schweibert EM, Egan ME, Hwang T-H, Fulmer SB, Allen SS, Cutting GR, and Guggino WB.** CFTR regulates outwardly rectifying chloride channels through an autocrine mechanism involving ATP. *Cell* 81: 1063-1073, 1995.
193. **Schwiebert EM.** ATP release mechanisms, ATP receptors and purinergic signalling along the nephron. *Clin Exp Pharm and Physiol* 28: 340-350, 2001.
194. **Seabra MC, Mules EH, and Hume AN.** Rab GTPases, intracellular traffic and disease. *T Mol Med* 8: 23-30, 2002.
195. **Sheetz MP.** Cell control by membrane-cytoskeleton adhesion. *Nature Rev Mol Cell Biol* 2: 392-396, 2001.
196. **Sheppard DN and Welsh MJ.** Effect of ATP-sensitive K<sup>+</sup> channel regulators on cystic fibrosis transmembrane conductance regulator chloride currents. *J Gen Physiol* 100: 573-591, 1992.
197. **Smith PR, Mackler SA, Weiser PC, Brooker DR, Ahn YJ, Harte BJ, McNulty KA, and Kleyman TR.** Expression and localization of epithelial sodium channel in mammalian urinary bladder. *Am J Physiol* 274: F91-F96, 1998.
198. **Smith RM, Bailbakov B, Ikebuchi Y, White BH, and Lambert NA.** Exocytotic insertion of calcium channels constrains compensatory endocytosis to sites of exocytosis. *J Cell Biol* 148: 755-767, 2000.
199. **Sorensen CE and Novak I.** Visualization of ATP release in pancreatic acini in response to cholinergic stimulus. Use of fluorescent probes and confocal microscopy. *J Biol Chem* 276: 32925-32932, 2001.
200. **Sperelakis N.** Cell physiology source book. edited by Sperelakis N. San Diego: Academic press, 1998, p. 1061-1075.

201. **Stachelin L, Chlapowski F, and Bonneville M.** Lumenal plasma membrane of the urinary bladder. *J Cell Biol* 53: 73-91, 1972.
202. **Steers W, Broder S, Persson K, Bruns D, Ferguson II J, Bruns M, and Tuttle J.** Mechanical stretch increases secretion of parathyroid hormone-related protein by cultured bladder smooth muscle cells. *J Urol* 160: 908-912, 1998.
203. **Stout CE, Costantin JL, Naus CCG, and Charles AC.** Intercellular calcium signaling in astrocytes via ATP release through connexin hemichannels. *J Biol Chem* 277: 10482-10488, 2002.
204. **Sun Y, Keay S, De Deyne P, and Chai TC.** Augmented stretch activated adenosine triphosphate release from bladder uroepithelial cells in patients with interstitial cystitis. *J Urol* 166: 1951-1956, 2001.
205. **Takeuchi S, Ando M, Kozakura K, Saito H, and Irimajiri A.** Ion channels in basolateral membrane of marginal cells dissociated from gerbil stria vascularis. *Hearing Res* 83: 89-100, 1995.
206. **Takeuchi S, Marcus D, and Wangemann P.** Ca<sup>2+</sup> activated nonselective cation, maxi K<sup>+</sup> and Cl<sup>-</sup> channels in apical membrane of marginal cells of stria vascularis. *Hearing Res* 61: 86-96, 1992.
207. **Takeuchi S, Marcus D, and Wangemann P.** Maxi-K<sup>+</sup> channel in apical membrane of vestibular dark cells. *Am J Physiol* 262: C1430-C1436, 1992.
208. **Taniguchi J and Imai M.** Flow-dependent activation of maxi-K<sup>+</sup> channels in apical membrane of rabbit connecting tubule. *J Membr Biol* 164: 35-45, 1998.
209. **Taskinen P, Toth M, Vuolteenaho O, Magga J, and Ruskoaho H.** Inhibition of atrial wall stretch-induced cardiac hormone secretion by lavendustin A, a potent tyrosine kinase inhibitor. *Endocrinology* 140: 4198-4207, 1999.
210. **Tiruppathi C, Finnegan A, and Malik AB.** Isolation and characterization of a cell surface albumin-binding protein from vascular endothelial cells. *Proc Natl Acad Sci* 93: 250-254, 1996.
211. **Torres GE, Egan TM, and Voigt MM.** N-linked glycosylation is essential for the functional expression of the recombinant P2X<sub>2</sub> receptor. *Biochemistry* 37: 14845-14851, 1998.

212. **Truschel S.** *Stretch-regulated adaptations in urinary bladder epithelium.* Pittsburgh: University of Pittsburgh, 2003.
213. **Truschel S, Ruiz W, Shulman T, Pilewski J, Sun T, Zeidel M, and Apodaca G.** Primary uroepithelial cultures. *J Biol Chem* 274: 15020-15029, 1999.
214. **Truschel S, Wang EC, Ruiz W, Leung S, Rojas R, Lavelle J, Stoffer D, and Apodaca G.** Stretch-regulated exocytosis/endocytosis in bladder umbrella cells. *Mol Biol Cell* 13: 830-846, 2002.
215. **Tsukita S and Furuse M.** Claudin-based barrier in simple and stratified cellular sheets. *Curr Opin Cell Biol* 14: 531-536, 2002.
216. **Vaca L and Kunze DL.** Anion and cation permeability of a large conductance anion channel in the T84 human colonic cell line. *J Membr Biol* 130: 241-249, 1992.
217. **van Dam EM and Stoorvogel W.** Dynamin-dependent transferrin receptor recycling by endosome-derived clathrin-coated vesicles. *Mol Biol Cell* 13: 169-182, 2002.
218. **Vandeburgh H.** Mechanical forces and their second messengers in stimulating cell growth in vitro. *Am J Physiol* 262: R350-R355, 1992.
219. **Vanoye CG and Reuss L.** Stretch-activated single K<sup>+</sup> channels account for whole-cell currents elicited by swelling. *Proc Natl Acad Sci* 96: 6511-6516, 1999.
220. **Vial C and Evans RJ.** P2X receptor expression in mouse urinary bladder and the requirement of P2X<sub>1</sub> receptors for functional P2X receptor responses in the mouse urinary bladder smooth muscle. *B J Pharm* 131: 1489-1495, 2000.
221. **Vlaskovska M, Kasakov L, Rong W, Bodin P, Bardini M, Cockayne DA, Ford A, and Burnstock G.** P2X<sub>3</sub> knock-out mice reveal a major sensory role for urothelially released ATP. *J Neurosci* 21: 5670-5677, 2001.
222. **Vogel SM, Minshall RD, Pilipovic M, Tiruppathi C, and Malik AB.** Albumin uptake and transcytosis in endothelial cells in vivo induced by albumin-binding protein. *Am J Physiol Lung Cell Mol Physiol* 281: L1512-L1522, 2001.
223. **Walz T, Haner M, Wu XR, Henn C, Engel A, Sun T, and Aebi U.** Towards the molecular architecture of the asymmetric unit membrane of the mammalian urinary bladder epithelium: a closed twisted ribbon structure. *J Mol Biol* 248: 887-900, 1995.



224. **Wang E, Lee JM, Johnson J, Kleyman T, Bridges R, and Apodaca G.** Hydrostatic pressure-regulated ion transport in bladder uroepithelium. *Am J Physiol Renal Physiol* 285: F651-F663, 2003.
225. **Wang E, Truschel S, and Apodaca G.** Analysis of hydrostatic pressure-induced changes in umbrella cell surface area. *Methods* 30: 207-217, 2003.
226. **Wang N, Butler JP, and Ingber DE.** Mechanotransduction across the cell surface and through the cytoskeleton. *Science* 260: 1124-1127, 1993.
227. **Watson P, Haneda T, and Morgan H.** Effect of higher aortic pressure on ribosome formation and cAMP content in rat heart. *Am J Physiol* 256: C1257-C1261, 1989.
228. **Watson PA.** Function follows form: generation of intracellular signals by cell deformation. *FASEB J* 5: 2013-2019, 1991.
229. **Watt WC, Lazarowski ER, and Boucher RC.** Cystic fibrosis transmembrane regulator-independent release of ATP. *J Biol Chem* 273: 14053-14058, 1998.
230. **Wickham JEA.** Active transport of sodium ion by the mammalian bladder epithelium. *Invest Urol* 2: 145-153, 1964.
231. **Williamson-Kirkland.** Neurological aspect of rehabilitation. In: *University of Washington orthopaedic resident lecture series*. Seattle: University of Washington, 1980.
232. **Wirtz HRW and Dobbs LG.** Calcium mobilization and exocytosis after one mechanical stretch of lung epithelial cells. *Science* 250: 1266-1269, 1990.
233. **Woda CB, Bragin A, Kleyman TR, and Satlin LM.** Flow-dependent K<sub>+</sub> secretion in the cortical collecting duct is mediated by a maxi-K channel. *Am J Physiol* 49: F786-F793, 2001.
234. **Wu ER, Manabe M, Yu J, and Sun TT.** Large scale purification and immunolocalization of bovine uroplakins I, II and III. *J Biol Chem* 265: 19170-19179, 1990.
235. **Wu X-R, Lin J-H, Walz T, Haner M, Yu J, Aebi U, and Sun T-T.** Mammalian Uroplakins. *J Biol Chem* 269: 13716-13724, 1994.
236. **Wu X-R and Sun T-T.** Molecular cloning of a 47 kDa tissue-specific and differentiation-dependent urothelial cell surface glycoprotein. *J Cell Sci* 106: 31-43, 1993.

237. **Wu XR, Medina J, and Sun TT.** Selective interactions of UPLa and UPLb, two members of the transmembrane 4 superfamily, with distinct single transmembrane-domained proteins in differentiated urothelial cells. *J Biol Chem* 270: 29752-29759, 1995.
238. **Xu J, Liu M, Liu J, Caniggia I, and Post M.** Mechanical strain induces constitutive and regulated secretion of glycosaminoglycans and proteoglycans in fetal lung cells. *J Cell Sci* 109: 1605-1613, 1996.
239. **Yang CM, Tsai YJ, Pan SL, Tsai CT, Wu WB, Chiu CT, Luo SF, and Ou JT.** Purinoceptor-mediated phosphoinositide hydrolysis in Madin-Darby canine kidney (MDCK) cells. *Naunyn Schmeidebergs Arch Pharm* 356: 1-7, 1997.
240. **Yang X and Sach F.** Mechanically sensitive, nonselective cation channels. In: *Nonselective cation channels: pharmacology, physiology and biophysics*, edited by Siemen D and Hescheler J. Boston: Birkhauser, 1993, p. 79-92.
241. **Yeaman C, Grindstaff K, and Nelson J.** New Perspectives on mechanisms involved in generating epithelial cell polarity. *Physiol Rev* 79: 73-98, 1999.
242. **Yeh T, Tsai M, Lee S, Hsu M, and Huy P.** Stretch-activated nonselective cation, Cl<sup>-</sup> and K<sup>+</sup> channels in apical membrane of epithelial cells of Reissner's membrane. *Hearing Res* 109: 1-10, 1997.
243. **Yu J, Lin JH, Wu XR, and Sun TT.** Uroplakins Ia and Ib, two major differentiation products of bladder epithelium, belong to a family of four transmembrane domain (4TM) proteins. *J Cell Biol* 125: 171-182, 1994.
244. **Yu J, Manabe M, and Sun T.** Identification of an 85-100 kDa glycoprotein as a cell surface marker for an advanced stage of urothelial differentiation: association with the inter-plaque (hinge) area. *Epithel Cell Biol* 1: 4-12, 1992.
245. **Yu W, Wang E, and Apodaca G.** Adenosine receptor-dependent modulation of bladder umbrella cell surface area. *Mol Biol Cell* 14: 355a, 2003.
246. **Zegarra-Moran O, Romeo G, and Galletta LJ.** Regulation of transepithelial ion transport by two different purinoceptors in the apical membrane of canine kidney (MDCK) cells. *Br J Pharm* 114: 1052-1056, 1995.
247. **Zerial M and McBride H.** Rab proteins as membrane organizers. *Nature Rev Mol Cell Biol* 2: 107-117, 2001.

248. **Zhang WH, Skerrett M, Walker NA, Patrick JW, and Tyerman SD.** Nonselective currents and channels in plasma membranes of protoplasts from coats of developing seeds of bean. *Plant Physiol* 128: 388-399, 2002.
249. **Zweifach A and Lewis SA.** Characterization of a partially degraded Na<sup>+</sup> channel from urinary tract epithelium. *J Membr Biol* 101: 49-56, 1988.
250. **Buckley M, Xin P, Washington S, Herb N, Erickson D, Bhavanandan VP.** Lectin histochemical examination of rabbit bladder glycoproteins and characterization of a mucin isolated from the bladder mucosa. *Arch Biochem Biophys* 375: 270-277, 2000.